Proteins at Charged Interfaces

by

Ganesh Venkataraman

Submitted to the Department of Chemical Engineering
in partial fulfilment of the requirements for the degree of

Doctor of Philosophy
in
Chemical Engineering

at the

MASSACHUSETTS INSTITUTE OF TECHNOLOGY
February 1993

Author _____
Department of Chemical Engineering

Certified by _____
Prof. T. Alan Hatton
Thesis Supervisor, Department of Chemical Engineering

Certified by _____
Prof. Karen K. Gleason
Thesis Supervisor, Department of Chemical Engineering

Accepted by _____
Prof. Robert E. Cohen
Chairman, Committee for Graduate Students

Proteins at Charged Interfaces

by

Ganesh Venkataraman

Submitted to the Department of Chemical Engineering
on September 28,1991
in partial fulfillment of the requirements for the degree of

Doctor of Philosophy in Chemical Engineering

ABSTRACT

The three dimensional structure of a protein, the result of an intricate balance between hydrophilic and hydrophobic forces, is important in maintaining its biological function. The effect of an interfacial environment on protein structure was studied using two systems: cytochrome-c in AOT-isooctane reversed micelles and peptides binding to heparin. Amide proton exchange and 2-D NMR, coupled with other spectroscopic techniques, indicated that the solvent accessibility of the N-terminal helix of cytochrome-c is increased in a reversed micellar environment. The amide proton exchange rates of residues in the C-terminal helix increased dramatically in the reversed micelle indicating significant structural changes. The helical content of cytochrome-c inside the reversed micelle changed as a function of time, as evidenced by circular dichroism spectroscopy. Absorption spectroscopy of the heme confirmed the change in protein conformation in the vicinity of the heme group. Molecular modeling of the C-terminal helical peptide indicated that electrostatic interactions play a dominant role in disrupting the hydrogen bonded structure of the C-terminal helix.

Heparin and related glycosaminoglycans modulate a variety of biological functions, both at the cellular and tissue levels, by interacting with proteins in a specific manner. The interaction between heparin and proteins was studied using two heparin binding systems: (i) heparinase-I, an enzyme that binds and specifically cleaves heparin and (ii) HBEGF, a cytokine that binds to heparin. Peptides representing the heparin binding domains of these two

proteins were isolated and characterized. The effect of these peptides on the degradation of heparin by heparinase-I was investigated. HBP, the peptide derived from heparinase-I, competed with the enzyme slowing the initial reaction rate but over long times facilitated the degradation of smaller oligosaccharides. Peptide P13, from HBEGF, did not affect the degradation reaction rate or the product profiles. Peptide P21, also from HBEGF, potentiated the heparinase-I degradation of heparin. The amount of products obtained in the presence of P21 was much higher than in the control reaction, although the product distribution remained the same. The dimeric form of P21 formed through the disulfide linkage of cysteine-17 bound to heparin with much higher affinity. The degradation reaction in the absence of peptides did not go to completion, although the enzyme activity was unaffected. It is proposed that the enzyme recognizes a particular heparin conformation that is lost below a critical heparin fragment length.

The heparin binding peptides do not exhibit any regular secondary structure. Circular dichroism and 2-D NMR studies indicated that these peptides exist predominantly in a random coil, and heparin or heparin fragments did not induce any regular secondary structure. Capillary electrophoresis and fluorescence spectroscopic methods were developed to quantify heparin binding affinities of these peptides. Molecular modeling studies on heparin binding peptides also confirmed the absence of any regular secondary structure in these peptides. The specificity of the interaction seems to be mediated through a unique heparin conformation, which depends on the sugar pucker and the ϕ and ψ torsion angles of the linkage. The allowed region of the conformational space for a heparin disaccharide was found to be less than 10% of the total conformational space. Starting structures from these allowed regions can then be used in conjunction with experimental data to elucidate the heparin conformation.

Thesis Supervisors: Prof. T. Alan Hatton
Prof. Karen K. Gleason

Acknowledgements

Thank you, Alan Hatton, for being my mentor and friend, and for providing me with the necessary scientific freedom, support and encouragement to pursue vastly different things - I am indebted to you. Thank you, Karen Gleason, for sharing your insights and experiences with NMR spectroscopy.

Charles Cooney, I would like to extend my sincere gratitude for your interest and for the numerous discussions. Your encouragement and enthusiasm for experiments in insulin purification have been invaluable. Dr. P. S. Kim and Dr. D. I. C. Wang, I would like to express my appreciation for helpful suggestions as members of my thesis committee. I would like to thank Bob Langer and Noubar Afeyan for their help and interest.

Cheryl Boyer, and John Rhee, your long patient hours at the spec. and the BIOCAD are greatly appreciated. To my colleagues in Bldg 66, for the friendly atmosphere, and, especially to Costas and Gerald, for answering the innumerable phone calls, and to my colleagues in E-17, for putting up with the mess (?) - *Graci.* Carol ("Mom"), you made my stay not just comfortable, but most enjoyable - I shall always cherish your love and affection. Jeff, Marcy, Aparna and the Practice School group - Phew ! it was actually enjoyable because of you. Keith and Sissy - I think my stint at Merck was well worth it!

Words cannot express my gratitude to RamP, Ramanth, Yekkoi Gai, LL, and Rat for everything, including educating me all about unselfish affection. I am glad our paths crossed, Ramnath and RamP, but for which I would be somebody very different. Varada, I shall always remember your tips on *Succeeding in the US,* back in '87, and the experiences we shared. (P)ski and Anu, Chinnster, Chandru, Mama, Manya and Shampaji, Porikki Mulari, Preeti and Ben, Le' Ramar, Shanti and Ravi - you made life outside MIT exciting and fun-filled. You made Boston my second home - so much so that I decided to continue staying here inspite of the KK cold. Atre, Tuffs, Butch, and Sundi - you helped me learn a lot about life and the little I know of ChemE. Vishak, Bhavik and Suresh have been ever willing for a game of tennis or squash so that I could get all my research frustrations out on the ball.

My family on the other side of the planet have made innumerable sacrifices so I could be here today. Nagu, Lakshmi, Radha, and Mahadevan - I am indebted to you. Amma, Appa, I could not ever ask for more than your being there for me always. All my uncles, aunts and cousins back home - you have played a significant role in my life - *Nandri!*

Dedicated with love to

Amma, Appa,
Nagu, Lakshmi, Radha & Mahadevan.

Table of Contents

List of Figures

Chapter 1

Chapter 2

Chapter 3

Chapter 4

List Of Tables

Chapter 2

Chapter 3

Chapter 4

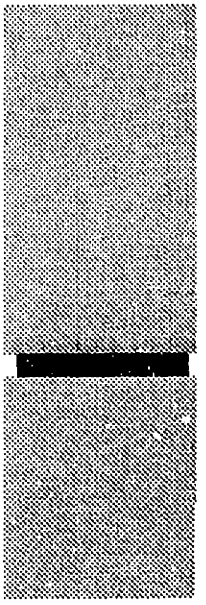

Chapter 1

Introduction

The concept of molecular recognition and its importance in chemical engineering and biological sciences is introduced. The importance of the three dimensional structure of the protein in molecular recognition in its biological function is illustrated with examples. The motivation for the study of protein structure-function relationship at two different charged interfaces - reversed micelles and glycosaminoglycans, is provided.

Interaction between two entities can be viewed as chemical recognition. There are three fundamental principles that govern chemical recognition: ***molecular structure***, which defines the geometric shape and form of the interacting entities, ***chemical thermodynamics***, which determines the energy state of all entities, and finally ***chemical kinetics***, which decides the time scale of interaction of the two entities. At the turn of the century, classicial physicists focussed primarily on thermodynamics. However, with the advent of quantum mechanics, the chemistry of the atoms which make up the macromolecules that are the keys to life, has been understood. Quantum mechanical approaches, coupled with thermodynamics, helped in understanding the structure of various molecules, and this contributed to the progress in the synthesis and alteration of macromolecules. Our understanding of chemical kinetics, however, has been limited by the ability of the experimental techniques to observe these fast interactions. It is the belief that in the decades to come advances in *chemical kinetics* will match those in *molecular structure*.

1.1 Chemical Recognition

Progress in the field of molecular recognition has been exponential in the last couple of decades. Advances in techniques that help elucidate molecular structure, in conjunction with streochemistry and thermodynamics, have been instrumental in the development of this field. Recognition at atomic level is best exemplified by metal surfaces. The atoms at the metal surface have unsatisfied bonding in at least one direction. This results in unusual

properties that are recognized by complementary agents. The importance of this behavior can be seen in corrosion of iron surfaces. This surface property costs the U. S billions of dollars annually - be it the Statue of Liberty or be it an iron nut holding the Tobin bridge. The reactive surface of iron is recognized and attacked by the complementary oxygen molecule causing corrosion. On the other hand, specific metal surfaces are capable of restructuring hydrocarbons to produce gasoline, which is of significant commercial value. Determination of atomic structure and composition of surfaces is basic to our understanding of surface properties and mechanisms and to advances in corrosion sciences, lubrication, adhesion, heterogeneous catalysis and production of new surfaces with novel electronic properties.

Instrumentation has played an important role in our understanding of atomic recognition. Figure 1.1 describes the different surface phenomena and the techniques that one can use to gain information about various atomic recognitions. The real challenge of understanding and manipulating molecular behavior on a surface has driven the field of surface chemistry to the forefront of modern chemistry and chemical engineering.

1.2 Biological Recognition

"Structure-function" relationship of macromolecules is recognition at a biological level which play a key role in elucidating various biological phenomena.

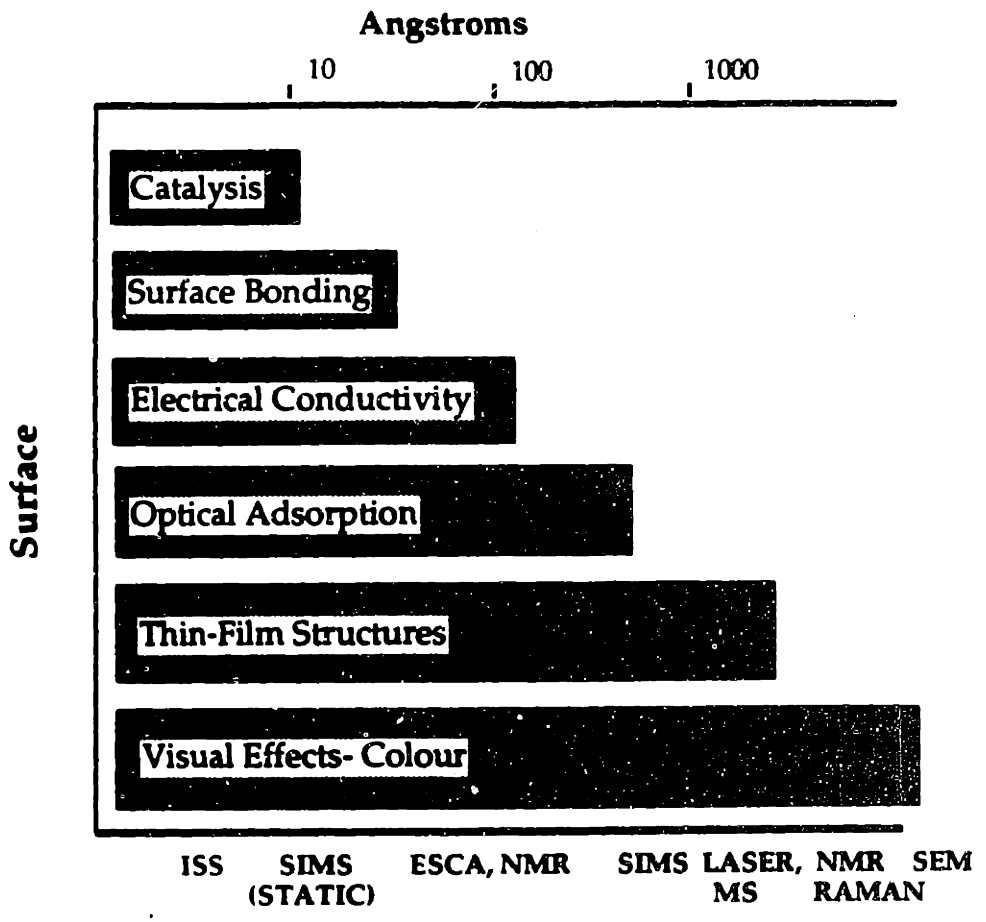

[from Pimental and Coonrod, 1987]

Figure 1.1 Surface properties and commonly used techniques for their characterization.

1.2.1 Chemical Engineer's eye view of a living cell

Each living organism can be pictured as a chemical factory, which, with the help of its chemical work force - enzymes and other molecules - efficiently makes numerous products from the raw materials (glucose and other nutrients) that it takes in. The important thing is that this chemical factory is state run, i.e., it makes numerous products for its own maintenance and self subsistence, and not with capitalistic intentions to make profit - unless it is a parasite which lives off another organsim. The main function of the chemical factory is to make several factories like itself, a process called reproduction. The living organism carries out this process by transmitting the essential blue prints that contain the necessary information for the organism to become an independent factory capable of propagating itself.

The chemical blue prints of a living cell are the Deoxyribo Nucleic Acid (DNA) which have the unique capacity to make several copies of themselves. The structural units of the chemical factory are large macromolecules called carbohydrates. These molecules range from simple chemical units, used as fuel, to complex structures which provide structural integrity to the factory. DNA, or the blue print, carries all the information necessary to create a work force called the proteins. The most important battalion of this work force is a group called the enzymes. Enzymes are the chemical engineers of the factory and guide the construction of every part of this chemical factory with dexterity. The enzymes are very specific and selective in using raw or processed material to manufacture products. The enzyme, like a lock, has the right design and shape into which the raw materials key into.

Biotechnology attempts to adapt a specific natural process of this chemical factory to produce a product that mankind desires. Enzymatic conversion of starch to bread by and of sugar to either vinegar or wine are examples of early biotechnology. Modern biotechnology is far more ambitious, as the important properties of the chemical blue print (DNA) have been understood. It is possible to alter the blueprint into something which did not previously exist in nature's product line. Complete understanding of the events in an organism can then help in designing factories with the blueprints necessary to produce products for human consumption.

As modern science got a better insight into several events taking place in the factory, it has become evident that there is close interaction and orchestration of events between the different chemical entities. A strategic game plan for the success of any chemical plant is proper communication between the players of the game. Communication in living organisms is mediated through **recognition**.

1.2.2 More about the polymers biologists call Proteins, DNA and Carbohydrates

The structures of nucleic acids (the blueprints), proteins (the workforce) and carbohydrates (the structural units) play a key role in molecular recognition in a biological system. The three dimensional structure of a protein molecule is important for the specific biological function of that protein. A protein or ***polypeptide*** chain is made up of many amino acid units linked through an

amide bond. This chain folds into a three dimensional architecture or *conformation* which is dependent on its primary amino acid sequence. Certain spatial arrangements of these amino acids can act as catalysts in converting some substrates to products. Such proteins, called enzymes, specifically recognize a substrate at their *active site.* The conformation of the enzyme is critical for its activity. Structural studies indicate that proteins are highly dynamic molecules. Proteins sometimes change their structure while performing their function. A fascinating example is that of rhodopsin, a protein of the retina involved in the first few steps of vision. This protein undergoes structural changes in less than a billionth of a second, registering all the changes in the visual signal to our eye.

One of the important areas of development in enzymology has been that of enzyme inhibitors, substances that interfere in the action of an enzyme. Availability of structural information at the molecular level has helped in the design of inhibitors. Experimental techniques such as X-ray crystallography, Nuclear Magnetic Resonance and other kinds of spectroscopy have greatly helped in understanding protein conformation and folding. Combining structural knowledge with the mechanisms of enzyme action, through sophisticated computation has helped in rationale drug design - a novel and powerful field of modern biotechnology. Approaches to design an enzyme inhibitor take advantage of both, enzyme surface and catalytic properties. Enzymes are believed to stabilize a transition or intermediate form of the substrate molecule. A compound called *enzyme blocker* is designed to mimic this intermediate structure, and to occupy the active site of the enzyme. Alternatively, chemical compounds that structurally resemble the substrate, but with surface properties that inactivate the enzyme, have

also been used as inhibitors. These are the so-called *suicide* or mechanism based inhibitors. Enzyme inhibition has been successful in numerous therapies for auto immune diseases, asthma etc.

A related surface phenomenon involving proteins has been receptors. Receptors are important protein molecules in cell surfaces that mediate a wide range of function, including cell-cell communication, cell migration and cell recognition. Cell recognition is fundamental to the immune system, which discriminates between *self* and *non-self* and eliminates the *non-self*. The immune system uses two sets of highly polymorphic protein molecules, called Class I and Class II molecules to perform this function. These molecules belong to the major histo-compatibility complex (MHC) and are found on the surface of all cells. The T-cell receptor, a membrane protein on a immune cell, is used by the immune system in differentiating between *self* or *non-self*. An invading organism (antigen) is processed and recognized as *non-self* by the T cell receptor in the context of Class I or Class II molecules. The immune system then mounts a response to the antigen. The enormous complexity in the interaction and the importance of protein conformation in its function in a biological system is evident.

The information required for synthesis of a protein is stored in the DNA. DNA is a long polymeric structure made up of a base, sugar and phosphate, repeating linearly in a duplex fashion. The DNA molecules appear as a ladder when flattened. It carries volumes of genetic information using a combination of just four bases. It encodes for protein molecules and protein molecules regulate DNA structure, replication and modification. Thus, life

depends upon the interplay of these two classes of molecules that interact through specific structures.

The third class of biological macromolecules, carbohydrates, are complex. Until recently their functional role was thought to be merely providing structural integrity to living organisms. Carbohydrates seem to protect, solubilize, and target proteins. An area of focus of this thesis is the characterization of a class of carbohydrates called acidic polysaccharides. These complex carbohydrates are the constituents of the extracellular matrix. Acidic polysaccharides provide compositional and structural properties of the matrix. In the extracellular matrix acidic polysaccharides hydrate the interface and act as roller coasters for different messengers involved in cell growth and function.

1.2.3 Importance of 3-D structure in biological recognition:

A fascinating study that has helped unravel the importance of *proper structure* in recognition is the example of the enzyme dihydrofolate reductase (DHFR), which is involved in the biosynthesis of DNA. Folic acid was found to enhance tumor growth in animals by stimulating the production of DHFR, which in turn was responsible for the dramatic increase in cell growth and division. A DHFR antagonist would prove to be a potent anti-cancer drug, and a search was on for an *antifolate* molecule. Methotrexate, a molecule very similar to folic acid was found to irreversibly inactivate DHFR. Incredibly, the only difference between folic acid and methotrexate was the substitution of the folate's 4-hydroxyl group by a 4-amino group. Such a subtle change resulted in a covalent amide bond between DHFR and

methotrexate instead of the weak hydrogen bond between folate and DHFR. It was subsequently established that methotrexate inhibited the enzyme DHFR by covalently binding to the same site as that of folic acid, in an irreversible manner. Today, methotrexate has proved to be effective in slowing tumor cells, and is a used in treating several cancers, like leukemia.

Further development in this field was in solving the three dimensional structure of DHFR using x-ray crystallography. This really paid off as several analogs which would target species specific DHFR could be designed. An *E.coli* specific DHFR antagonist - trimethoprim, was designed which has proved to be a potent antibiotic not toxic to the human DHFR. This site-specific targeting of DHFR antagonist is one of the most dramatic achievements in 'structure-function' relationships of proteins.

1.3 Proteins at Interfaces:

Chemical recognition with biological significance - a theme for this thesis

As seen from the previous section, proteins play an important role in regulating several biological processes. One fundamental aspect of protein structure is the manner in which they are folded: all the hydrophobic amino acids of the protein are buried inside while the charged amino acids are exposed to the environment. This is not surprising considering the protein surface interacts with the outside largely with water molecules, i.e., a

hydrophillic interaction. Preserving this hydrophobic core is crucial in maintaining the correct structure of the protein and hence, its function.

Aspects of the surface property of the protein, like an acitive site cleft, or charges on the protein that *see* complementary residues on a substrate or other proteins are important for its function. What controls the intricate balance, between the charge on the surface and hydrophobic forces inside, which maintains the crucial structure and hence the protein function, is poorly understood. This question has obviously some fundamental implications in understanding of protein structure and hence its relevance to function. Once one brings charged forces versus hydrophobic forces one automatically brings an ***interface*** ! There are several examples of interfacial protein functions, like receptors and actions of the enzyme phopholipase A_2 in degrading hydrophobic substrates.

This thesis has focused on two kinds of interfaces:

1) a charged hydrophilic-hydrophobic interface as seen in a reversed micellar system, to understand the properties of an interfacial protein - cytochrome-c, a key protein involved in the electron transfer in the respiratory pathway, in 'pseudo-natural' environment.

2) a highly charged interface, involving nature's most acidic biopolymer, - heparin and the proteins which interact with this acidic polysaccharide. When heparin acts as a charged surface, the proteins seem to recognize this surface through an intricate balance

between their hydrophilic and hydrophobic residues, and that creates a necessary interface.

1.3.1 Reversed - micellar system

Micellar systems are fundamental in several fields. They have been used in physics to understand the interplay of hydrophobic and hydrophilic forces. In chemical engineering, they play an important role in tertiary oil recovery. Micelles are structures formed by assembly of surfactant molecules and water. The surfactant, or detergent, molecules have a hydrophilic head group attached to a hydrophobic tail group. In water, the hydrophobic tail groups align together, while the polar head groups shield them from water. Oil and other non polar compounds can be solubilized in the hydrophobic core, hence micelles are gaining increasing importance in waste water treatment.

When the bulk medium is hydrophobic, the surfactants align in such a way that the hydrophilic head groups are buried inside, protected by the tail groups. These surfactant aggregates, called reversed micelles, are capable of solubilizing water and other hydrophilic compounds. Reversed micelles are capable of selectively solubilizing certain proteins, and hence have been used as protein extractants. In addition, they have been used as membrane-mimetic systems as they provide an interface which can be easily controlled.

1.3.2 Protein - Carbohydrate interaction

Heparin, a complex carbohydrate, is a fundamentally important biological macromolecule. It binds to several important proteins in the body and modulates their functions, which could range from cell growth to tissue differentiation. However, very little is known about the nature of the protein-heparin interaction, i.e., the biochemical and biophysical basis of this interaction, and the different parameters that govern it.

This thesis outlines a strategy to address the nature of heparin-protein interaction from a biochemical and biophysical point of view. The theme to the study of heparin-protein interaction is to understand the structural basis of this interaction. There are two issues -

1) The primary sequence/domain of the protein and of heparin.

2) The conformation of the two interacting units.

Heparinase is used in this study as a model protein, chosen because of its unique capacity to not just bind but also cleave heparin. On one hand this provides us with structural information on the polysaccharide, and, on the other, it defines the elements of protein-heparin interaction. Heparin Binding Epidermal Growth Factor (HB-EGF), is the other model protein in this study. HB-EGF is novel and important growth factor controlling physiological events at the extracellular matrix, mediated primarily through the cell surface heparan sulfate molecules.

1.4 Scope of the Thesis

This thesis has four main divisions. An introduction to the overall concept forms the first division. At the heart of the first chapter is the fundamental concept of molecular recognition and its implication in chemical engineering and biological sciences. The chapter focuses on the role of protein structure in molecular recognition, and in its biological function. A motivation for the study of structure-function relationship of proteins at two different kinds of interfaces 1) reversed micellar system and 2) Glycosaminoglycans is also provided.

Chapter II outlines the different experimental procedures that have been carried out during the course of this study and is divided into biochemical and structural characterization techniques. These techniques are further elaborated in the different sections of the thesis, where relevant, in order to bring out the significance of a given procedure or method to a specific problem or application.

Chapter III details the work carried out on cytochrome-c in an AOT-isooctane reversed micellar system. This chapter introduces the model - the protein and the interface following which is a background description on the structure of proteins in reverse micelle. The results from this work are divided into three main sections. The first section summarizes the results from amide proton exchange experiments, using 1-D NMR. Following this, site specific information on the N- terminal and the C- terminal helix obtained from a 2-

D NMR study are discussed. The second section discusses the CD studies that were performed to corroborate the overall structural changes in the protein. The third section wraps up the study on the cytochrome-c structure, by giving a structural meaning to all the observed effects. Molecular modeling work was performed to translate the characterized biochemical effects into a physical picture.

Chapter IV is devoted to the heparin-protein interaction studies. This chapter introduces the fundamental significance of the acidic polysaccharide heparin. Following the discussion on chemical and structural properties of heparin, the biological role of heparin binding to at least five classes of proteins is described. Also, the current understanding of heparin-protein interaction is summarized. There were two heparin binding systems chosen for this study. 1) heparinase I and 2) HB-EGF. Heparin binding domains for these two proteins were mapped. Following this, effect of the heparin binding peptides on the degradation of heparin by heparinase was investigated. The heparin binding specificity of the different peptides was investigated by different chromatographic techniques. Structural characterization of the peptides was performed using CD and NMR. Conformational analysis and molecular modeling studies were carried out in order to gain molecular details of heparin-peptide interaction.

The thesis concludes with an overall significance of this study.

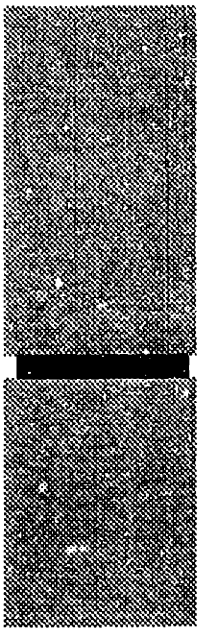

Chapter 2

Materials and Methods

The experimental procedures used in this study have been divided into biochemical and structural characterization techniques. A brief background on some of these techniques is provided. Protocol and recipes for the experiments are outlined in this chapter

2.1 Materials and Experimental Protocol

2.1.1 Cytochrome - c in Reversed Micelles

Horse heart cytochrome-c was obtained from Sigma Chemical Company in the purest available form (TYPE VI) and used directly. Aerosol OT (99%) from Sigma was used without any further purification. Isooctane (analytical grade) was obtained from Mallinckrodt Inc. Deuterium oxide (99.9% D_2O) from Cambridge Isotopes was used directly for the NMR studies.

2.1.1.1 Proton Exchange In Reversed Micelles

The protonated protein was solubilized in the reversed micellar phase by transfer from a bulk aqueous solution containing a sodium salt, typically sodium ascorbate. Three different reversed micellar sizes were studied. By using 350mM ascorbate for the forward transfer, a reversed micelle of W_o 20 was formed. Use of 200mM and 50mM ascorbate in the forward transfer buffer resulted in a reversed micelle with W_o of 30 and 50 respectively. Equal volumes of the aqueous phase and the organic phase containing the surfactant were contacted by vortexing for a couple of minutes. The two phase mixture was then centrifuged for about 5 minutes to get a clear phase boundary. The amide protons of the protein were then allowed to exchange with deuterium inside the reversed micellar phase. After varying exchange times, the protein was back-extracted to the aqueous phase by changing the

salt concentration or the pD* and the exchange quenched by the addition of DCl to a final pD* of about 5.6. The back extracted protein solution was then concentrated for detection of the remaining amide protons.

2.1.1.2 W_o measurements

The amount of water solubilized in the reversed micelle was measured using a Karl-Fisher titration using a Mettler #DL18 automatic titrator. The titrator determines the water content of the organic phase based on potentiometric measurements of the solution as it is titrated with iodine.

2.1.1.3 UV - VISIBLE Spectroscopy

The UV-Visible spectra were collected in a Perkin Elmer double beam spectrophotometer (Lambda 3B). The samples were prepared as described in 4.1.1 and the absorbance between 350 and 700nm was recorded. A 2mm path-length quartz cell was used for the concentrated protein samples (10 mg/ml) and a 1cm path-length quartz cell was used for the dilute protein samples.

2.1.1.4 IR Spectroscopy

The infrared spectra were collected in a Perkin Elmer dual beam infrared spectrometer. Reversed micellar samples were prepared as described previously and loaded between 2 NaCl windows. FTIR spectra were obtained on the Perkin Elmer double beam instrument at the Polymer and Surface Analysis Lab at MIT. The signal was averaged over 16 acquisitions to

improve the signal to noise ratio for the FTIR runs prior to Fourier transformation.

2.1.1.5 Circular Dichroism

CD spectra were obtained in an AVIV-60 instrument in the Department of Biology at MIT. Cytochrome-c in reversed micelles were analyzed using a 0.1mm path length quartz cell. The spectra were collected between 200 to 260nm in intervals of 0.5nm with a 3sec averaging. The temperature was controlled at 27°C.

2.1.1.6 NMR Acquisition

NMR spectra were acquired in the 500 MHz proton NMR spectrometer at the Francis Bitter National Magnet Laboratory at MIT. Amide proton exchange of cytochrome-c was followed using a 2-D phase-sensitive coherence transfer (COSY) experiment. A standard COSY pulse sequence of - (t_0-90°-t_1-90°-t_2)- with phase cycling and quadrature detection was used. 2048 data points were acquired in t_2 from 0 to 257ms and 512 data points in t_1 from 0 to 67 ms which were zero filled to 2048 points. A recycle delay of 1 second was used to obtain the z measurements for each point. The residual HDO peak was suppressed by a weak irradiation at all times except during acquisition. The data were acquired at 40°C.

2-D NOESY (nuclear overhauser effect spectroscopy) spectra were collected with the pulse sequence of t_0-90°-t_1-90°-t_m-90°-t_2- with phase cycling and quadrature detection. A mixing time of 150ms, comprising of 145ms without

homospoil and 5ms with homospoil was used. The t_1 and t_2 conditions were the same as in the COSY experiment above. Data were acquired at 40°C.

2.1.1.7 Data Processing

A convolution difference window function was used for the data analysis. The cytochrome-c COSY spectra were scaled with a non-exchanging peak to normalize for the protein concentration. Data were referenced to an internal trimethylsilyl propionic acid (TSP) standard set at 0 ppm. For the COSY experiments, the amide region of the spectra (6 to 10 ppm) was used to determine the intensity of the cross peaks of the amide protons with the C_α protons (0-6 ppm). The amide region was subdivided into four regions and proton peaks were identified based on previous assignments (Wand et al., 1989 and Feng et al., 1989). The intensities of the assigned peaks were then estimated from the peak heights, and normalized using the C_5H-C_6H and the C_6H-C_7H cross peak intensities of Trp-59 to account for minor variations in the protein concentrations between samples.

2.1.2 Heparin - Peptide Interaction

The Peptides HBP and P21 were synthesized using solid state synthesis at the Biopolymer Laboratory at the Center for Cancer Research at MIT. Heparin (Porcine mucosa) with an number average molecular weight of 10,000 was obtained from HEPAR Inc.

2.1.2.1 SDS - PAGE and protein transfer

Sodium dodecylsulfate polyacrylamide gel electrophoresis (SDS-PAGE) of heparinase was carried out according to the method of Laemmli (1970) with a Mini Protean II electrophoresis apparatus (BioRad). Visualization of proteins in gels was accomplished with 0.1% Coomassie Brilliant Blue stain or by silver staining (BioRad). The gels were dried with a gel dryer (BioRad) on transparent cellophane backing (BioRad). Proteins were blotted onto nitrocellulose sheets (Millipore, Corp.) according to the method of Matsudaira (1987). Transfer was carried out by use of the following amperage sequence: 30 min at 50 mA, 30 min at 100 mA, and 60 min at 275 mA. Proteins were visualized with a 0.1% Coomassie Brilliant Blue R-250 solution followed by destaining with a 40% (v/v) methanol/10% (v/v) acetic acid aqueous solution. The membrane was blocked with 1% BSA and then probed with ^{125}I heparin, at a concentration of 10^6 c.p.m/ml. The membrane was dried and autoradiographed.

2.1.2.2 HPLC Competition experiments

A nanomole (~ 45 µg) of the purified/ modified enzyme was denatured in 50 µl (8 M urea, 0.4 M ammonium carbonate) solution and reduced with 5 mM DTT at 50° C cooled to room temperature and alkylated with 10 mM iodoacetamide for 15 min in the dark. The total reaction volume was 200 µl. To this 1/25 th w/w of trypsin was added and digestion was carried out at 37° C for 24 h. The reaction was terminated by heating the sample at 65° C for 2 min. The digest was separated using a gradient reverse phase HPLC (0 to 80 % acetoniltile). The tryptic peptides were monitored at 210 and 277 nm. For the competition experiments, 1: 1, 10 , 50 , 100 and 200 heparinase to heparin or

chondroitin sulfate was added in a mole: mole ratio, after the tryptic digest, before the HPLC step. The tryptic peaks were collected in Eppendorff tubes. The tryptic peaks were sequenced using an Applied Biosystems sequencer model 477 with on line model 120 PTH amino acid analyzer (The Biopolymers lab, Center for Cancer Research, MIT).

2.1.2.3 Heparin Degradation Assay:

The degradation of Heparin was followed at 232 nm. Heparin (0.1mg/ml) in 100mM MOPS with 5mM Calcium Acetate along with 20ul of peptide (1mg/ml) was incubated in a 1cm path length quartz cuvette at 37°C for a few minutes. The peptide was replaced with buffer for the control runs. 5 µl of Heparinase I (1nM) was added to the cuvette. The absorbance at 232 nm was recorded as a function of time until saturation. The reaction was then quenched by heating the sample to 80°C and frozen for subsequent analysis.

2.1.2.4 Degradation Product Analysis

The Products from the heparin degradation was analyzed using a POROS®-Q strong anion exchange column. A salt gradient of 0 to 1M NaCl in 5 minutes was used for the elution. The product profiles from the reactions with different peptides was compared.

2.1.2.5 Homogeneous Heparin fragment Isolation

Heparin (25mg/ml) in 100mM MOPS, 5mM Calcium acetate buffer was exhaustively digested by heparinase. The products were then separated using

an POROS-Q anion exchange chromatography column. The collected peaks were then pooled and desalted using a Biogel P-50 fine desalting column. The desalted fractions were then lyophilized and recharacterized on the ion-exchange column to check for the purity of the fraction. The peaks were also analyzed using a capillary electrophoresis to determine the homogeneity of the collected fractions.

2.1.2.6 Chromatographic Characterization of Heparin Binding Peptides

The peptides were characterized using a POROS® C-18 reversed phase column with a gradient of 0.1%TFA to 0.085% TFA, 80% acetonitrile in water over 5 minutes. A Heparin POROS® column was used to determine the binding affinities of the different peptides to heparin. A 100µl column with a gradient of 0 to 1 M NaCl in 5 minutes was used. Typically 50 µg of the peptides was used for the characterization runs. Peptide specificity to heparin was analyzed by competition binding to heparin column with 1mg/ml of chondroitin sulfates A and C, dextran sulfate and heparin.

2.1.2.7 Capillary Electrophoresis Experiments

An Applied Biosystems capillary electrophoresis unit was used with a system Gold data acquisition routine. A 50 micron ID capillary with a sample to detector length of 25cm was used. a field strength of 30kV/50cm. was applied and the detector set at 210nm. The buffer used was a 10mM MOPS, 5mM Calcium acetate with different amounts of substrate (heparin or chondroitin sulfate). 100µM of the peptide was injected using vacuum injection. Mesityl Oxide (MO) was used as the neutral marker.

2.1.2.8 CD Spectroscopy

CD spectra on the peptide samples were collected between 180nm and 260nm using a 0.5mm path length quartz cell. The spectra from five acquisitions were averaged to improve the signal to noise. The temperature was controlled at 27°C. PROSEC was used as a deconvolution routine to determine the relative amounts of different secondary structures in the peptides.

2.1.2.9 Fluorescence Measurements

Fluorescence spectra were measured on a Perkin Elmer DM-60 instrument, The peptide samples were loaded on a 50µl quartz cuvette. The sample compartment was held at 27°C. The peptide samples were excited at 278nm and the fluorescence emission between 300 to 360nm was recorded.

2.1.2.10 Molecular Modeling

The simulations were performed on a IRIS Indigo workstation using the software QUANTA (Polygen Inc, MA). Energy minimizations and other energy calculations were performed using CHARMM. A 500 step adopted basis Newton Raphson method was generally used. The peptide was built using the sequence builder program supplied with QUANTA.

2.2 Techniques for Characterization

2.2.1 Amide Proton Exchange

The backbone of a protein molecule is held together by amide bonds between the carbonyl carbon and the nitrogen. The polar nature of the nitrogen in the peptide backbone makes the hydrogen attached to it (amide proton) labile. As a result, the amide proton can exchange with other protons in the vicinity. The rate of this proton exchange depends on temperature, pH and the location of the proton. The exchange behavior of these amide protons in poly-amino acids have been previously characterized. The exchange rate of amide protons in poly alanine increases exponentially with temperature with an activation energy of about 20KCal/mol. The exchange mechanism seems to be both acid and base catalyzed with a minimum exchange at about a pH of 3.0 (Perrin et al., 1990, Englander et al., 1972).

The important property of the proton exchange is its dependence on the location of the proton. Any proton involved in hydrogen bonding is less labile compared to a free proton and hence exchanges less readily. Depending on the strength of the hydrogen bond, the rate of proton exchange decreases. In addition, accessibility to other protons in the viscinity is an important criterion for the exchange to occur. Normally, the amide proton of a surface residue of the protein is in close contact with the solvent molecules, usually water and hence can readily exchange with the protons of the water.

However, the hydrophobic core of the protein has solvent molecules excluded and hence there is a scarcity of protons in the viscinity of the amide protons. As a result the amide protons of the residues in the hydrophobic core are conserved for extended periods of time. However, they do eventually exchange out, possibly because of the small fluctuations in the protein structure, termed as "Breathing".

Amide proton exchange studies have been used to characterize folding pathways of different proteins. The folding pathway of BPTI has been studied using this technique. The amide protons of a fully unfolded protein is allowed to exchange with deuterium. The protein is then allowed to fold and the exchange is quenched after different folding times. A subsequent NMR of the protein reveals the number of protons that are hydrogen bonded or solvent excluded.

A more recent application of amide proton exchange has been to look at binding sites of proteins to substrates, other proteins or nucleic acids. The antibody binding site of cytochrome-c has been mapped using this technique (Paterson et al., 1990). Protons at the binding site exchange extremely slowly when the protein ligand is bound to the protein. Comparing exchange rates of different protons in the presence and absence of ligands can therefore provide specific information about the location of the binding site.

The molecular level detail provided by this technique can be exploited to determine small perturbations in protein conformations. Changes in the three dimensional structure of a protein under different environments can be followed in a site-specific manner by observing the amide proton exchange

rates. By using deuterated solvents, the exchanging amide protons can be labeled with deuterium. The proton exchange can then be quenched and a subsequent NMR experiment can then reveal the number and location of the amide protons that have been labeled. Disruption of hydrogen bonded structure in the protein causes a dramatic increase in the exchange rate. In addition, changes in the solvent accessibility due to partial or complete unfolding of the protein can cause dramatic increase in the exchange rate. This site-specific information can then be used in conjunction with the protein's three dimensional structure to gain a better understanding of the forces that operate in the protein structure. More importantly, one can gather information about interacting surfaces in the protein and the ligand or the environment. Moreover, conventional structure measurement techniques measure the average conformation of the molecule and seldom can measure fluctuations or dynamics about this average. Amide proton exchange rates depend strongly on the fluctuation dynamics in the protein backbone. Changes in this fluctuation dynamics will cause large changes in the amide proton exchange rates.

A limitation of this technique, however, is that the proton NMR resonances of the native protein be assigned. Assignment strategies for small peptides and proteins have been well worked out. However for large proteins, the slow tumbling rate in solutions causes line broadening. This, taken together with the high overlap of peaks, complicates peak assignments. A second limitation of this technique is that protons whose exchange rates are slow compared to the experimental time scale (12 hours for a 2-D COSY) can only be observed. Protons at the surface of the proteins that are not hydrogen

bonded exchange fast, even at a low pH and hence cannot be followed by this technique.

2.2.2 UV - VIS Absorption Spectroscopy

A quantum mechanical treatment of the energy states available to a molecule indicates that, in addition to the lowest occupied molecular orbitals, there are higher energy states that can be occupied by the electrons. The energy difference between these states is quite small and the electron can be excited by providing it with this energy. For most atoms, this energy is within the UV region of the spectrum. The energy difference between the orbitals depends strongly on the electronic environment around the atom or group of atoms, and hence the absorption energy and wavelength also depend on the environment.

The heme group of cytochrome-c consists of an iron atom in the center of a porphyrin structure (Figure 2.1). This structure absorbs in the visible range (520 to 550 nm) in addition to UV absorption. The Soret bands of the heme group are sensitive to the location of the heme group and its environment. Perturbations in the local structure around the heme can hence be followed by monitoring its absorption spectrum.

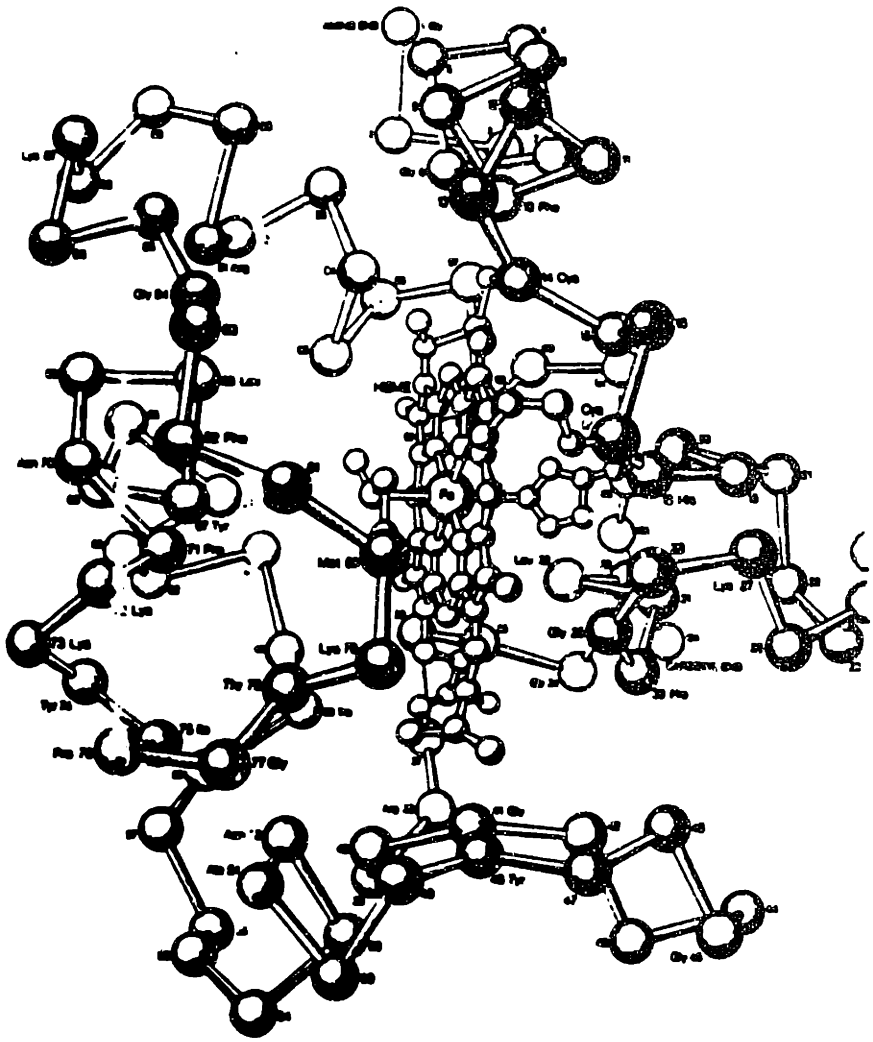

[Adapted from Dickerson and Geis, 1975]

Figure 2.1 Conformation of horse heart cytochrome-c
The main chain atoms and the heme group are shown.

2.2.3 Fluorescence Spectroscopy

Fluorescence emission is observed when an excited electron returns from the first excited state to the ground state. As some energy is always lost by non-radiative processes, such as vibrational transitions, the energy of the emitted light is always less than that of the absorbed light. Hence, the fluorescence emission is always shifted towards longer wavelength compared to the absorption of the respective chromophore. Fluorescence emission is much more sensitive to changes in the environment of the chromophore than light absorption. Fluorescence is thus an excellent spectroscopic probe to investigate conformational changes of proteins.

Fluorescence of proteins originate from phenylalanine, tyrosine, and tryptophan residues. The absorption and emission wavelengths for these amino acids in solution are shown in Table 2.1. Also indicated is the sensitivity factor, which is a measure of the fluorescence efficiency. Tryptophan fluorescence is dominant in proteins because of the high sensitivity factor. In addition, transfer of energy from the tyrosine and phenylalanine residues to the tryptophan, especially in a folded protein molecule, makes it difficult to monitor the fluorescence of phenylalanine and tyrosine.

The emission intensity as well as the wavelength of maximum emission depends on the environment around the fluorescing moieties. Changes in the three dimensional structure of the protein lead to changes in the fluorescence properties.

Table 2.1: *Absorbance and Flourescence Properties of Aromatic Amino Acids .*
[in water at neutral pH (12)]

	Absorbance		Flourescence		
Compound	λ_{max} nm	ε_{max} $M^{-1} cm^{-1}$	λ_{max} nm	ϕ_F [b]	Sensitivity $\varepsilon_{max} \phi_F$
Tryptophan	280	5600	348	0.20	1100
Tyrosine	274	1400	303	0.14	200
Phenylalanine	257	200	282	0.04	8

Adapted from Creighton, 1989

ϕ_F = flourescence quantum yield.

2.2.4 IR Spectroscopy

The vibrational, bending and rotational motions of a molecule are associated with discrete energy values. The frequency of vibration can be determined using a classical representation of the atom as two point masses connected by a spring. The frequency of vibration of this system is given by:

$$\nu = (1/2\pi)\,\mathrm{Sqrt}\,(k/n)$$

where n represents the reduced mass ($1/n = 1/m_1 + 1/m_2$) and k the spring constant of the bond. This frequency of vibration for bonds between most atoms lies in the infra-red region. As a result, energy from the infra-red light can be absorbed by the molecule as an increase in the vibrational or the rotational motion of the molecule. The actual frequency of energy absorption

depend on the nature of the bond, and the atoms connected by the bond. Infra-red spectra peaks corresponding to vibrations of hydrogen be easily assigned by specifically replacing the hydrogen with deuterium.

Infra-red spectroscopy can be used to predict secondary structures of peptide and proteins. The peptide bond absorbs around 1650 cm^{-1}, called the amide-I region of the spectrum. An α-helix absorbs at 1652 cm^{-1}, while a β-sheet exhibits a peak at 1632 cm^{-1}. Random coils absorb light at 1642 cm^{-1}. Based on the amide-I region of the IR spectra, the secondary structure of the protein or peptide can be determined.

2.2.5 Capillary Electrophoresis

The migration of a molecule under the influence of a electric field depends on its charge and size, and hence can be used to separate small quantities of sample. In CZE, a fused silical capillary column is filled with an electrolytic buffer and placed between two buffer reservoirs. High voltage is then applied across the capillary. The sample, introduced at one end of the capillary, migrates to the other end at a velocity that is a combination of its electrophoretic velocity and the bulk endoosmotic velocity of the buffer (Chien and Burgi, 1992). The migration of a negative charged species would require a large endoosmotic velocity. The migrating molecule is detected, usually using a UV-visible detector fixed on-line to the capillary.

2.2.6 Circular Dichroism

Circular Dichroism and Optical Rotary Dispersion are two interrelated phenomena that are used to measure the optical activity of asymmetric molecules in solution. ORD is the ability of the molecule to rotate the plane of linearly polarized light as a function of the wavelength. CD gives information on the unequal absorption of left- and right-handed circularly polarized light by optically active molecules.

CD bands of proteins occur in two spectral regions: the far UV or amide region (170-250nm) and the near-UV region (250-300nm). The amide region is dominated by contributions of the peptide bonds and hence, contain information regarding the secondary structure of the molecule. In particular, the α-helix displays a strong and characteristic CD spectrum in the far-UV region (Figure 2.2). The spectral contributions of other structural elements of a protein are less well defined.

The CD spectrum of a protein can be deconvoluted into the individual contributions using upto 6 basis spectra. Standard algorithms that predict the amount of secondary structure based on the CD profile are accurate for α-helices. However, β-sheets and β-turns do not have a very characteristic spectra and hence their estimations are not as accurate.

The CD profile can be a very good indicator of changes in the secondary structure of the protein in non-native environments. Information regarding the actual site of secondary structure cannot be derived from CD spectra for most proteins. However, a qualitative picture of the changes in secondary

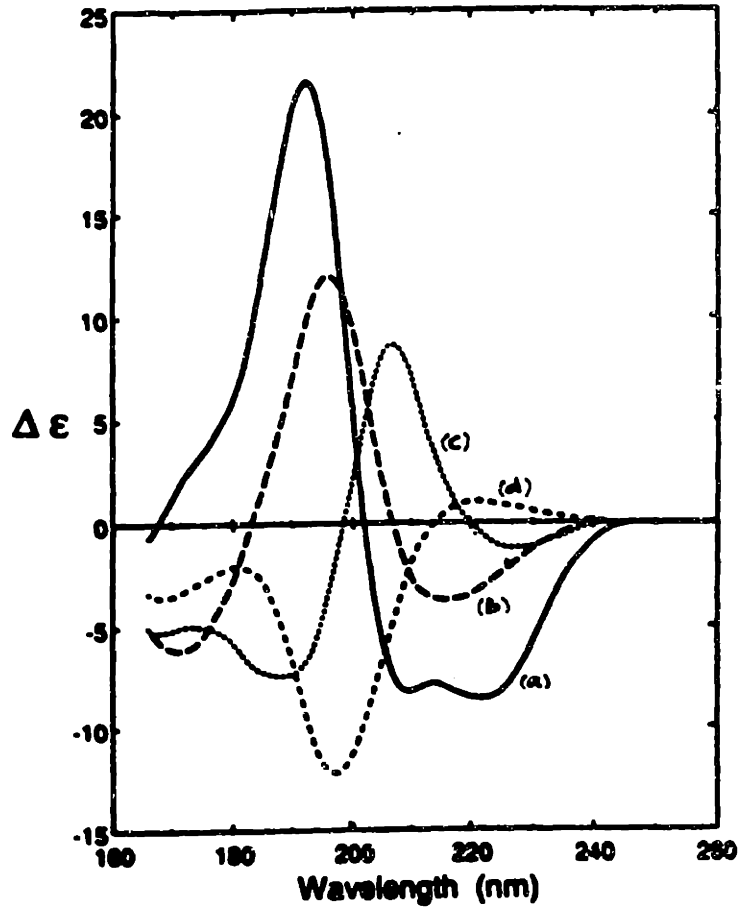

[from Brahms and Brahms, 1980]

Figure 2.2 Circular Dichroism spectra of regular secondary structures
(a) α-helix, (b) anti-parallel β-sheet, (c) β-turn, and (d) random coil

structure under the influence of different forces can be determined using CD spectroscopy.

2.2.7 NMR

Nuclear Magnetic resonance is a very powerful technique invented about 45 years ago. Although NMR is a quantum mechanical phenomenon, a classical vector picture can provide much insight. The macroscopic nuclear magnetization (M_o) of the sample, at thermal equilibrium precesses about the large external magnetic field, which defines the Z axis of the coordinate system. The magnetization precesses at the resonance or larmor frequency, which depends on the static magnetic field and the gyromagnetic ratio. In a frame of reference rotating at a frequency of ω, the Z magnetization of the sample is static. An RF pulse, at the larmor frequency is applied to rotate the magnetization away from the Z axis (Figure 2.3). When the RF pulse is turned off, the X,Y component of the magnetization will precess at the offset frequency, defined as the difference between the frequency of the rotating frame and the Larmor frequency. The precession of the magnetization along the x-y direction induces a current in the detection coil. The signal decays as a result of relaxation processes and hence is called the free induction decay or the FID. A Fourier transformation of this signal results in a spectrum with resonance lines corresponding to the observed nucleus.

The resonance frequency of a particular nucleus depends on its chemical environment. The relatively small chemical shift in the resonances of different protons, expressed as parts per million or ppm, reflects the chemical

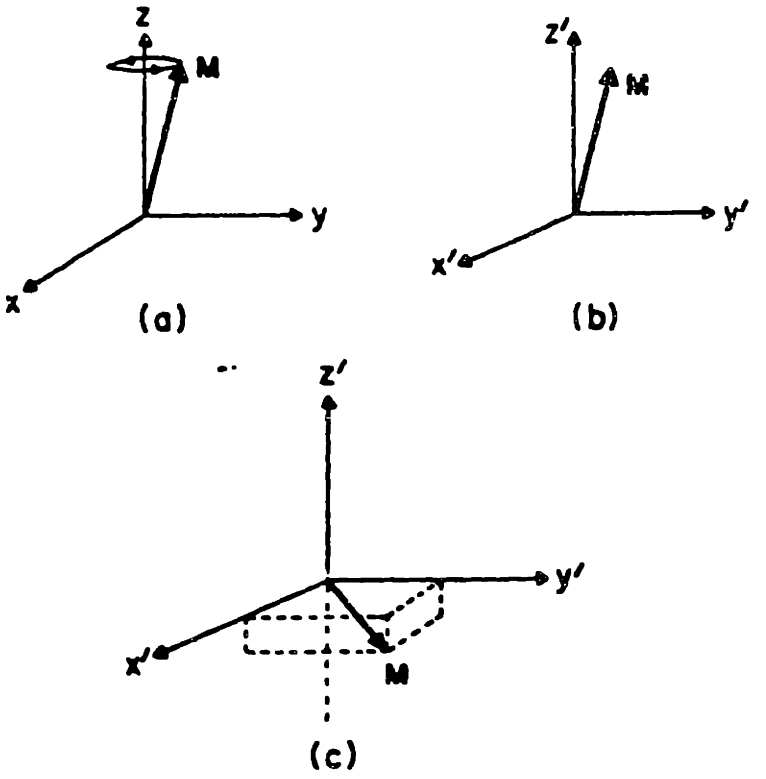

Figure 2.3 Schematic representation of an NMR experiment
(a) Labcratory frame of reference, M precesses about Z axis.
(b) Rotating frame of reference with frequency ω.
(c) M perturbed to a position along the x-y axis.

environment around that proton. NMR therefore, provides a wealth of information regarding the local environments around the protons and hence the structure of the molecule. The overlapping of spectral lines makes it difficult to assign the resonances, especially in a large molecule like a protein. The ability of 2-D NMR to resolve overlapping spectral lines and enhance sensitivity makes it possible to determine solution structures of large molecules using NMR. In addition, internuclear distances and scalar coupling constants can be easily measured using 2-D NMR techniques.

The transfer of magnetization to the nearby nuclei can be either through covalent bond or through space. A coherence transfer spectroscopy experiment give information on through bond magnetization transfer and hence the J coupling between two protons. A COSY experiment gives rise to cross peaks between atoms that are connected by 3 bonds or less. The typical pulse sequence for a COSY experiment is shown in Figure 2.4. The NOESY (Nuclear Overhauser effect Spectroscopy) determines through space interactions between protons that are close in space. NOESY cross peaks can be used effectively to determine distance constraints between atoms not connected though bonds, and hence is useful for solution structure determination. Different pulse sequences can be designed depending on the kind of information sought.

The assignment of the individual resonance peaks to the residues in a peptide starts with a COSY experiment in D_2O. The side chain resonances of the residues are assigned by identifying standard patterns of the spin systems. For example, the cross peaks of a leucine residue are shown in Figure 2.5. A COSY experiment in H_2O is then used to assign the amide protons of these

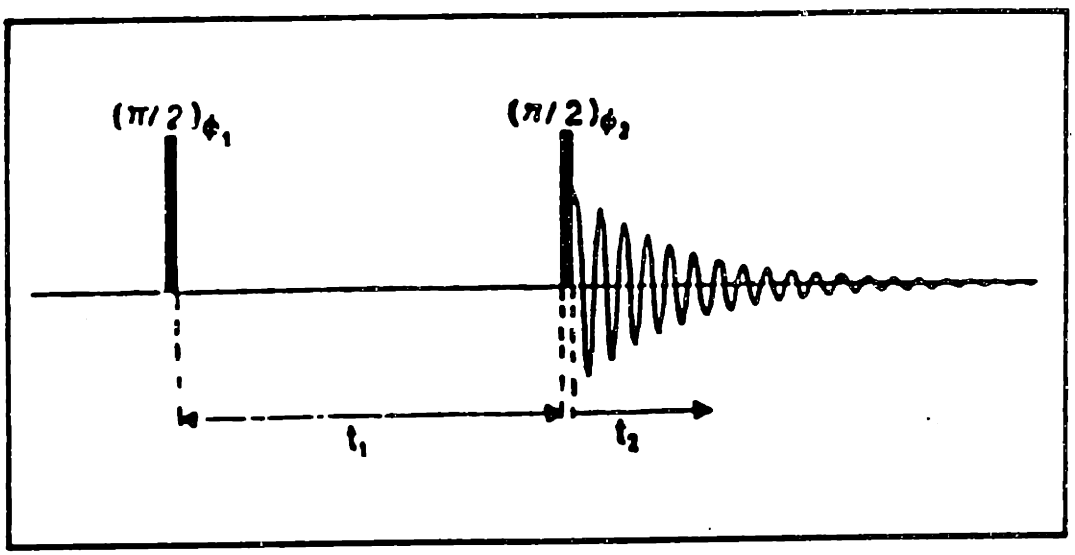

Figure 2.4 Pulse sequence for a Coherence Transfer Experiment (COSY)

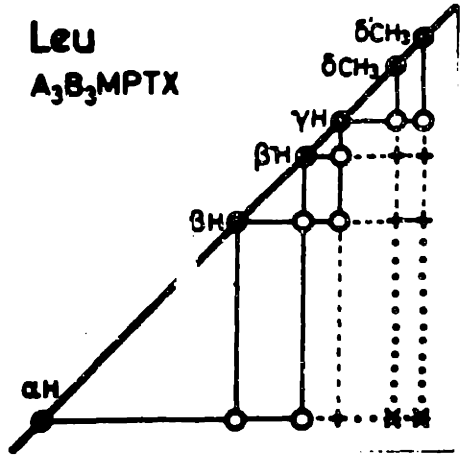

Figure 2.5 NMR Cross peaks from amino acid - Leucine.
The cross peaks from COSY (O), Relayed COSY (+) and Double-relayed COSY (°).

residues. Information from TOCSY experiments also aid in the side chain assignments. The sequential information is then derived from an appropriate ROESY or NOESY experiment. The ROESY or NOESY experiment provides cross peaks between the C_α proton and the amide proton of the next amino acid. Once the resonances are fully assigned, ROESY can be used to generate distance constraints between the different residues. The distances can then be used in a molecular modeling program to determine the solution structure of the protein.

2.2.8 Molecular Modeling

The conformation of molecules is a result of a balance between the different energy contributions. The internal energy of a molecule is made up of contributions from bond energy, angle energy, energy of dihedral angles and energy from improper torsion angles. In addition, van der Waals energy and electrostatic energy dictate the position of the atoms relative to one another and hence determine the conformation of the molecule.

The internal energies for most molecules can be approximated by a simple mathematical function. The parameters for these energy equations have been investigated extensively for proteins, nucleic acids and organic molecules. However, the energy parameters for carbohydrates have not been determined and a part of section 4.2.5 will be devoted to this issue.

The bond energy is calculated by approximating the covalent bond as a spring connecting two masses:

$$E_b = \Sigma K_b(X - X_o)^2$$

where X_o is the equilibrium bond distance and K_b is the spring constant or the bond energy parameter. Similarly the angle energy is defined as:

$$E_\theta = \Sigma K_\theta (\theta - \theta_o)^2$$

where θ_o is the equilibrium bond angle. The dihedral and the improper torsion terms are calculated as:

$$E_\phi = \Sigma k_\phi [1 + \cos(n\phi - \delta)]$$

$$E_\tau = \Sigma k_\tau (\tau - \tau_o)^2$$

Various mathematical forms have been proposed for the van der Waals force between a pair of atoms. The Lennard-Jones 6-12 potential has been used to calculate near neighbor interactions. Electrostatic interactions are calculated using Coulomb's law for the pair-wise interaction between two charges. The surface of the protein is in contact with solvent molecules and hence an invariant dielectric constant can be used. However, the core of the protein excludes the solvent and an estimate of the dielectric constant here is not easy. It has been found that a distance dependent dielectric constant best describes the electrostatic interactions between amino acid residues of a protein.

At any particular conformation, the energy of the molecule can be calculated taking two atoms at a time. The long-range energy terms decay rapidly after a particular cut-off distance and hence it would be a waste to calculate all pair-wise interactions. To reduce the computational intensity, the electrostatic and van der Waals energy terms are calculated only for atoms that are within the cutoff distance specified.

For minimizations, the coordinates of the molecule are incremented by a small amount and the energy calculated again. The coordinate increment is adjusted based on the direction and magnitude of the energy change and the process repeated until convergence. This minimum energy, however, need not be the lowest energy (global minimum) but a local energy well in which the molecule is trapped. The energy minimization calculations are usually done at absolute zero and hence thermal energy cannot bounce the molecule out of the energy well. Hence this low energy conformer will depend very much on the starting conformation. Therefore, the choice of an appropriate starting conformer for the molecule is critical before energy minimization studies are initiated. X-ray crystal structures prove to be very useful starting structures as in the case of cytochrome-c. However, if little is known about the structure of the molecule, as in case of the heparin binding peptides, then an exhaustive search of all the local conformations should be done to locate the global minimum.

Dynamics simulations help to reach the global minimum by imparting kinetic energy to the molecule so that it is able to jump out of the potential wells. The molecule is heated to either 300 or 600K and the force on each atom is then calculated. Newton's laws of motions are used to move the

atoms to the new coordinates and the energy is calculated. This process is repeated until the potential energy of the molecule does not change any further. This conformation is likely to be the global minimum. However, it is important to check that the same minimum is reached from a different starting point.

The central dogma of molecular modeling is that the global minimum conformation is the physically existing conformer. However, in reality, conformers with higher potential energy (the workable minimum) sometimes fit the experimental data much better. This could be either because the energy contributions are weighted wrongly or because there are additional contributions to the energy that are not included in the problem formulation. Hence, it is imperative that the molecular modeling results are interpreted with care, particularly if apriori predictions of molecular properties are to be made. However, the modeling studies are excellent guides to help understand the physics behind experimental observations.

Chapter 3

Cytochrome-c in reversed micelles

Cytochrome-c is an key protein in the respiratory pathway that functions as an electron transporter between integral membrane proteins The interaction of cytochrome-c with a membrane-mimetic system is considered. Amide proton exchange, coupled with 2-D NMR and other spectroscopic techniques are used to determine changes in cytochrome-c conformation in a reversed micellar environment.

3.1 Background

3.1.1 Introduction

3.1.1.1 The Protein

Cytochrome-c is an essential component of the mitochondrial respiratory chain (Dickerson and Timkovich, 1975). It acts as an electron transporter between the membrane bound enzymes cytochrome reductase and cytochrome oxidase (Figure 3.1). Cytochrome oxidase utilises four electrons to reduce oxygen to water and this reaction is coupled to the synthesis of ATP, the ultimate source of metabolic energy.

The detailed mechanism of the electron transfer reactions of cytochrome-c and its redox partners is not fully understood, but electrostatic interactions seem to dominate. In addition, components of the mitochondrial membrane play an important role in this electron transport process. For example, cardiolipin, an anioinic diphosphoglyceride, facilitates the binding of cytochrome-c to cytochrome oxidase (Vik et al., 1981, Marsh and Powell, 1988). In anionic lipid bilayers, especially cardiolipin bilayers, cytochrome-c interacts strongly with the lipids (Demel et al., 1989, Kimberberg and Lee, 1969). There is evidence that in addition to the electrostatic interactions between the surface lysines of the protein, cytochrome-c can penetrate into the bilayers of cardiolipin to interact hydrophobically with the membrane interior (Brown and Wuthrich, 1977, Szerbeni and Tollin, 1988). The

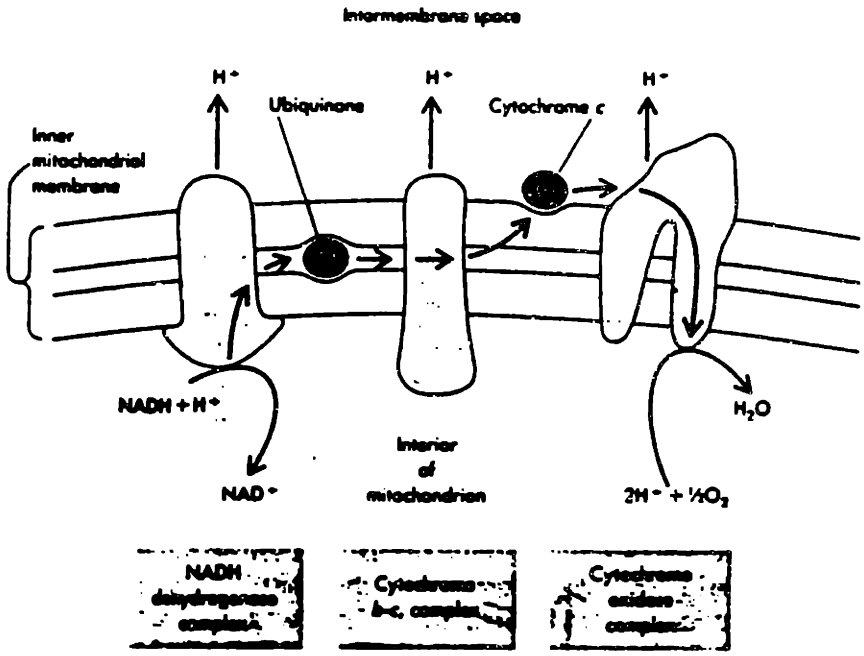

Figure 3.1 Electron transport role of cytochrome-c in mitochondrial membrane

redox potential of the protein when bound to cardiolipin is lower and exhibits some physical characteristics of the mitochondrial protein (Huang and Kimura, 1984).

Studies on the interaction of cytochrome-c with lipids mostly focus on the lipid component while assuming that the protein retains its water soluble structure. Spooner and Watts (1990) used deuterium NMR and ^{31}P NMR to determine the influence of cardiolipin binding on the structure and the motional behavior of cytochrome-c. They found that the surface lysine groups interact with the lipid so very strongly that some of the backbone α-helical structure is destroyed. Raman resonance study of the cardiolipin-cytochrome-c complex indicated that the protein exists in the reduced state despite the absence of a chemical reducing agent (Vincent and Levin, 1986). Interaction of the protein with the cardiolipin appears to change both the porphyrin ring conformation and the heme coordination to mimic Raman spectra of reduced cytochrome-c; however, no electron transfer occurs and the iron atom remains in the ferric state.

The relationship between protein structure and protein interaction with the membrane was considered an important factor in processing, targeting and compartmentalizing the mitochondrial cytochrome proteins (Demel et al., 1989). Cytochrome-c may lose its well defined hydrated structure in order to penetrate the lipid bilayer of the mitochondrial membrane. It is important to establish whether the changes at the reaction center of cytochrome-c and the lower oxidation potential are a consequence of some specific perturbation at the active site or are related to more general changes in the backbone structure.

In this study we looked at the effect of a membrane mimetic environment on the structure of cytochrome-c. Perturbations in the structure of the protein at a

molecular level were addressed by following the amide proton exchange rates. The technique is discussed in greater detail in the following chapter. The water-restricted membrane-like environment in this study was provided by an AOT-isooctane reversed micelle.

3.1.1.2 The Interface

Reversed micelles are spheroidal aggregates formed by certain surfactants in apolar media. The surfactant molecule consists of a polar head group attached to a hydrophobic tail group, usually a nonpolar hydrocarbon or fluorocarbon. In reversed micelles the polar head groups of the surfactant molecules are directed towards the interior of the aggregates which entrap a small amount of water, shielding it from the apolar bulk solvent (Figure 3.2). This provides a stable aqueous phase in a bulk organic medium. The water pool of the reversed micelles can solubilize inorganic ions, amino acids, proteins and peptides in organic solvents under a variety of conditions (Luisi and Magid, 1986, Luisi et al., 1988, Leodidis and Hatton, 1989). The water inside the reversed micelle interacts strongly with the head groups and shows unusual properties relative to bulk water, at low water contents (Wong, 1976, Wong 1977). The reversed micellar system has gained a great deal of attention in recent years as a protein extractant, a microreactor for enzyme kinetic studies and a membrane mimetic system and has aided in a better understanding of the function and mechanism of membrane proteins.

The surfactants that are capable of forming reversed micelles form two broad categories: those that require a cosurfactant to form a stable microemulsion, and those that do not. CTAB (cetyltrimethylammonium bromide), will form stable reversed micelles only in the presence of a medium length alcohol like hexanol.

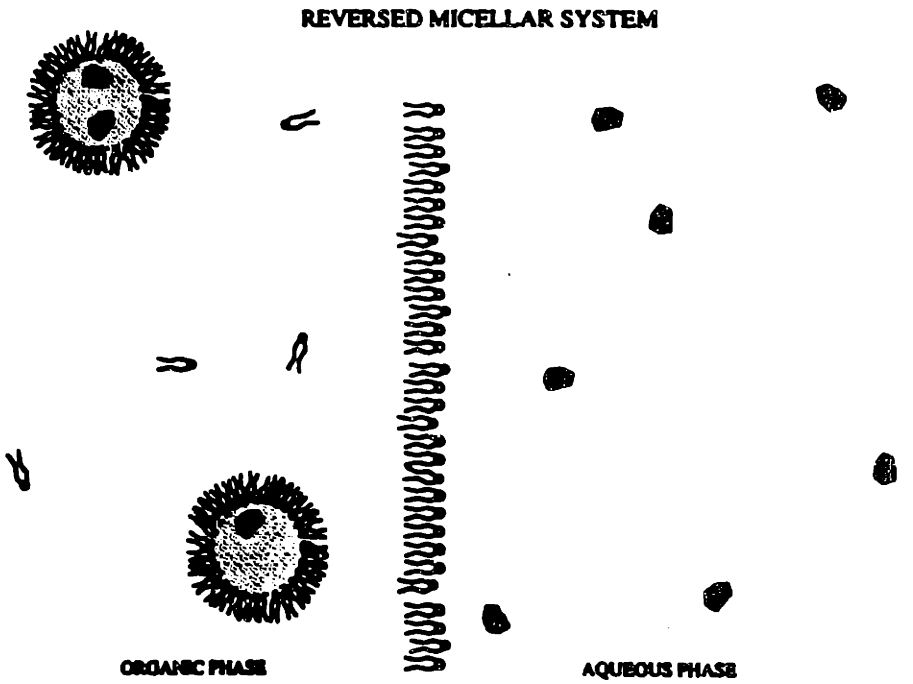

Figure 3.2 Schematic of a reversed micelle

However, the commonly used surfactant Aerosol OT (sodium bis-2-ethylhexyl sulfosuccinate) in isooctane does not require a cosurfactant and is stable over a wide range of surfactant and water concentrations. The AOT-isooctane reversed micellar system was chosen for its stability over a range of surfactant and salt concentrations and easy control of its size.

Two different methods are used in forming reversed micelles. In the injection method water and the solutes are injected into the organic phase containing the surfactants. The injected solutes are forced into the reversed micellar phase causing rearragements of the surfactant molecules sometimes to form more complex aggregates. Very large, multi-subunit proteins and even kilobases of DNA have been solubilized in the reversed micelle by this technique (Imre and Luisi, 1987). The other method of forming reversed micelles, the phase transfer technique, involves transfer of solute by contacting an aqueous phase with the reversed micellar phase. The aqueous and the reversed micellar phases are assumed to be in equilibrium with each other. The solute can be transferred back to the aqueous phase by adjusting the salinity or the pH conditions.

The amount of water transferred to the organic phase depends on the ionic strength of the aqueous phase and also the surfactant concentration in the organic phase. The water content of the reversed micelle can be characterized using the variable W_o which is defined by

$$W_o = [H_2O]_{rm} / [\text{Surfactant}]$$

It has been shown that W_o is linearly proportional to the size of the water pool (Day et al.,1978). This has also been confirmed by neutron scattering data (Luisi and

Magid, 1986, Fletcher et al., 1986). The equilibrium phase transfer approach was used for solubilizing protein in reversed micelles in this study.

It is important to study the effect of these water restricted and charged environments on the structure of proteins. The three dimensional structure of a protein is stabilized by an intricate balance between the hydrophilic and hydrophobic forces. The reversed micellar environment can alter the balance between these weak forces and cause some changes in the structure of the solubilized proteins. This structural change can vary from a reversible temporary perturbation to complete unfolding of the protein. Understanding the effect of this charged interface on the structure of proteins can help us better understand the forces behind protein structure stability and give some insight into protein folding.

3.1.2 Protein Structure in Reversed Micelles

The effect of the charged interfaces on the structure of the protein solubilized has been studied using different techniques. The optical transparency of the reversed micellar solutions allows a wide range of spectroscopic studies essential for monitoring conformations, dynamics, and reactivities (Waks, 1986). Moreover, one can precisely control the range of water microenvironments (interfacial to bulk) and the size of the micelles as well by varying the surfactant-to-water ratio. The highly organized water present in the core of the reversed micelles brings about intramolecular hydrogen bonding that would have otherwise been disrupted by the solute-water interactions. In addition to the unusual nature of the water, the charge on the surfactant head group as well as the concentration and nature of the counter ions in the micellar water pool can be important factors in bringing about a

conformational change. Protein conformation in reversed micelles has been studied using a variety of spectroscopic studies such as circular dichroism (CD), UV absorption, fluorescence and phosphorescence, enzyme activity measurements, NMR etc.

Grandi et al. (1981) found that the activity of lysozyme in AOT-isooctane reversed micelles depends on both the pH and W_0. The pH optimum was shifted by about 2-3 pH units in the reversed micelle, possibly due to the differential partitioning of the hydrogen ions within the reversed micelle. Circular dicroism spectra of lysozyme solubilized in AOT-isooctane reversed micelles showed an increase in the amount of helical structure in the protein. The molar helicity increased with a decrease in the water content of the reversed micelle. The protein seemed to have acquired greater structural rigidity in the reversed micelle as the secondary structure did not change when the temperature was lowered to -30°C or when the pH of the stock solution was changed. This higher stability of the enzyme in reversed micelles was also supported by the change in the melting temperature determined using flourescence measurements.

Fluoresecence spectra of lysozyme in AOT-isooctane reversed micelles with W_0 3.3 showed a blue shift of Lmax and a marked increase in the quantum yield (Grandi et al., 1981, Luisi et al., 1984) possibly due to a local conformational change near the fluorescing moities. Upon increasing W_0 to about 33, the fluorescence spectrum of lysozyme became similar to that observed in aqueous solution. It was later shown that this change in protein structure at low W_0 values was observed only in the absence of substrate or inhibitors to the enzyme (Luisi, 1985). The UV absorption spectra in the presence of a substrate, however, in this range of W_0 was identical to that in water (Luisi et al., 1984).

Enzyme kinetics studies on trypsin in reversed micelles indicate that the pH profile for the enzyme is not significantly altered with respect to aqueous solutions (Walde et al., 1988). The maximum activity, however seems to depend strongly on W_0 and seemed to peak at W_0 of 12, suggesting that the enzyme is most active when there is a small layer of water sorrounding it. The enzyme was almost completely inactive in an AOT-heptane reversed micelle W_0 of 20 (Martinek et al., 1981). Fluorescence data on trypsin in AOT-isooctane reversed micelles showed that the emission properties of the protein in aqueous solution matched those of the protein in reversed micelles at W_0 13 (Walde et al., 1988). The λ_{max}, however shifts towards the red upon increasing W_0 indicating an exposure of the tryptophan residues, and maybe even partial unfolding. CD spectra of trypsin in AOT-isooctane reversed micelles indicated a slight unfolding of the protein (Walde et al., 1988). This unfolding has been attributed to loss of calcium ions inside the reversed micelles. Injection of trypsin solutions with an excess of calcium resulted in practically no change in CD profiles. The effects of other surfactant systems on trypsin conformation and activity are summarised in Table 3.1.

Table 3.1: *Trypsin in Reversed Micelles*

Protein	System	UV[b]	Flourescence	CD	Activity
Trypsin (EC 3.4.21.4)	Methyltrioctyl ammonium chloride/CH*	Red shift of 4 nm	Blue shift of 3 nm; Q.Y. much higher.	Smaller intensity especially in near UV.	No activity
	CTAB/$CHCl_3$ /O** 1:1:W_0 25				Less active than in water.
	AOT/heptane: W_0 20				Almost no activity.

** CH: Cyclohexane; ** O: Octane*

from Luisi and Steinmann-Hoffmann 1987

There have been contradicting reports on the activity of α-chymotrypsin in reversed micelles. Martinek et al., (1981) observed that the activity of α-chymotrypsin in AOT-octane reversed micelles at W_o 20, pH 8 was lower than in water. Kumar and Balasubramanium (1982) observed that at low water contents (1-5%) the helical content and the enzyme activity were lower in reversed micelles. In an AOT-Heptane reversed micelle, however, at a Wo of 25, Menger and Yamada (1979) found that the activity was higher than in water and the pH optimum was shifted by 1.5 pH units. Belongava et al. (1983) investigated α-chymotrypsin spin labelled at the active site, in AOT reversed micelles in octane. The mobility of the label decreased first and then increased with increasing W_o. The catalytic activity of chymotrypsin reached its optimum at W_o values when maximum rigidity of the active site was detected. Barbaric and Luisi (1981) studied the CD spectrum of α-chymotrypsin in AOT-isooctane reversed micelles and found that the far UV region of the spectrum was significantly different from the bulk aqueous spectrum while the near UV spectrum was not altered. This represented a change in the main chain conformation of the molecule while the aromatic side-chains were not affected. Decreasing W_o increased the amount of enzyme activity and also the molar helicity. However, UV absorption experiments of α-chymotrypsin in AOT-octane reversed micelles at W_o of 5 to 25 indicated that perturbations in structure are larger at smaller W_o. A blue shift in the fluorescence of chymotrypsin in revesed micelles, with quantum yield similar to that in water, has also been observed (Barbaric and Luisi (1981)). The effect of other reversed micellar surfactant systems on α-chymotrypsin structure and activity is summarised in Table 3.2.

Table 3.2: *α - Chymotrypsins in Reversed Micelles*

Protein	System	UV[b]	Flourescence	CD	Activity
α-Chymotrypsin (EC 3.4.21.1)	Methyltrioctyl ammonium chloride/CH*	Red shift of 2 nm	Red shift of 12 nm; incr. of Q.Y.	Similar to that in water	No activity
	CTAB/$CHCl_3$ /O** 1:1:W_0 25				Almost no activity
	Triton X-100/CH/ n-hexanol (4%); 1-13% water				Max. 49 % of water activity; opt water content 5%
	SDS/CH/ n-hexanol (10%); 2-5% water			As in water	Max. 85% of water activity; opt water content 5%

** CH: Cyclohexane; ** O: Octane*
from Luisi and Steinmann-Hoffmann, 1987

Schomaecker et al. (1988) showed that although AOT interacts strongly with α-chymotrypsin, the stability of the enzyme in aqueous solutions is not affected. The surfactant acts as a competitive inhibitor to the enzyme both in aqueous solutions and in reversed micelles. This could also be the reason for the earlier observed drop in enzyme activity.

Pancreatic ribonuclease exhibits almost no change in both UV absorption and CD measurement in AOT-isooctane reversed micelles (W_o 18) (Wolf and Luisi, 1979). The enzyme activity was observed to be higher in reversed micelles with a shift in the pH optimum of about 1.5 pH units.

The activity of horse liver alcohol dehydrogenase in AOT-isooctane reversed micelles was found to be slightly lower than the activity in water (Meier and Luisi,

1980). Although there was very little change in the CD and UV spectra of the protein, flourescence studies indicated a slight blue shift and a decrease in quantum yield. This change in flourescence has been attributed to changes in the side chain orientation rather than a change in protein structure (Vos et al., 1987). However, time resolved fluoresecence anisotropy experiments indicate that horse liver alcohol dehydrogenase interacts strongly with the surfactant layer, and this interaction is largely electrostatic in nature (Vos et al. 1987).

Time resolved flourescence experiments with porphyrin (heme iron removed) and Zn porphyrin (heme iron replaced with zinc) cytochrome-c in reversed micelles showed that AOT interacts very strongly with the protein (Vos et al., 1987). This interaction seems to be predominantly electrostatic, between the positively charged cytochrome-c and the negatively charged AOT. This was supported by the very weak interaction between the protein and negatively charged CTAB surfactant. Porphyrin cytochromes were used in this study to improve the quantum yield of flourescence. CD studies on these cytochromes indicated that there was a small change in the structure of the cytochrome-c in aqueous solution as a result of replacing the heme iron with zinc (Table 3.3). More importantly, the helical content of the protein was lower at higher W_o in AOT-isooctane reversed micelles. The structure of the protein, however, is relatively unaffected in CTAB isooctane hexanol reversed micelles.

Table 3.3 *Circular Dichroism of porphyrin cytochrome-c and Zn porphyrin cytochrome-c in different solutions at 25 °C*

Solution	W_o	θ_{222} porphyrin cytochrome-c	θ_{222} Zn - porphyrin cytochrome-c
		deg cm^2 dmol^{-1}	
20mM KP_i pH 7.0	-	-14100	-10400
0.2M AOT/isooctane	5	-12800	-8500
	10	-10700	-6500
	40	-6700	-3800
0.2 M CTAB/isooctane /hexanol	10	-12100	-10200
	40	-11900	-10100

adapted from Vos et al., 1987

The loss of protein structure at high W_o values as evidenced by CD measurements could be ascribed to the association of the protein at the AOT interface. Small angle X-ray scattering studies of the protein in AOT-isooctane reversed micelles indicate that cytochrome-c is strongly associated with the AOT interface (Brochette et al., 1988). This interfacial activity of cytochrome-c also explains the slight increase in the water solubilized in the presence of protein.

The dependence of the cytochrome-c structure upon the size of the reversed micelle is evident from flourescence studies of a single tryptophan residue buried close to the heme group. The very low quantum yield of this tryptophan residue in aqueous solution is ascribed to the quenching by the heme group. In reversed micelles, the tryptophan emmission undergoes a large increase as well as a small blue shift (Erjomin and Metelitza, 1984). This was interpreted as an increased polarity and decreased viscosity in the proximity of the tryptophan residue and hence a change in the protein conformation upon incorporation into an AOT reversed micelle. The emission intensity, however, seems to depend strongly on the water content of the

reversed micelles (Brochette et al., 1988). At a W_0 of about 10, the emission intensity of the protein in reversed micelles seems to be close to that in aqueous solution (Figure 3.3).

The reduction of the heme group with sodium ascorbate is regioselective (Castro, 1971) and is dependent on the conformation of the residues around the exposed edge of the heme group. Reduction of cytochrome-c in AOT-isooctane reversed micelles is most efficient at low water contents (Figure 3.4), with a maximum reduction at a W_0 of about 10 (Brochette et al., 1989). The kinetics of the reduction in reversed micelles (Figure 3.4) also imply that cytochrome-c is closest to native structure when W_0 is about 10. The potency of the ascorbate as a reducing agent in the reversed micelles was also tested using potassium hexacyanoferrate.

In neutral pH aqueous solutions, cytochrome-c is characterized by a weak absorption band at 695 nm, the Q bands of the heme (520-550nm), and the 406nm Soret band. In microemulsions, at short times after the protein is incorporated in the reversed micelle, the Q bands do not change. There is a slight increase in the Soret intensity along with a small red shift.

Erjomin and Metelitza (1983) observed changes in the helicities of heme proteins after incorporation in reversed micelles. This perturbation of structure increases with decrease of Wo. The decrease in the intensity of the Soret band indicates a change in the heme pocket at the same time as the unfolding occurs (Craik et al., 1980).

The effect of a reversed micellar environment on the conformation of small peptides has been studied. Waks (1986) noticed a secondary structure

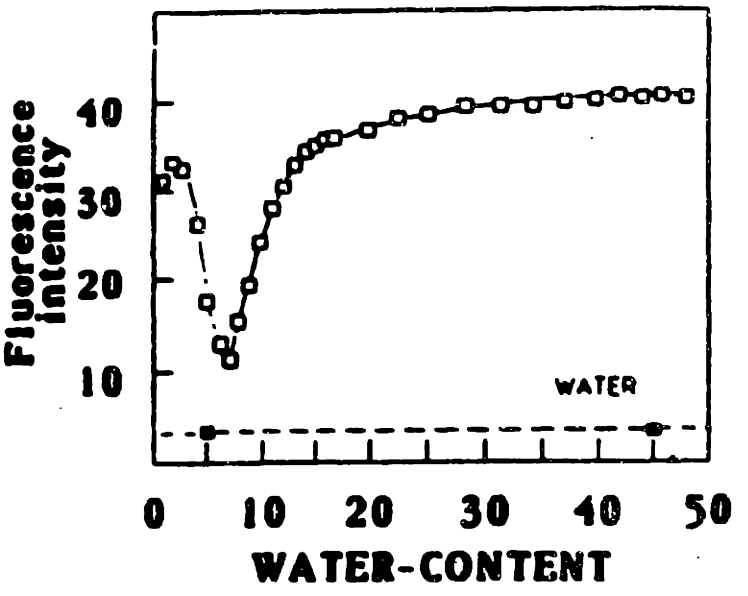

[Adapted from Brochette et al., 1988]

Figure 3.3 Fluorescence of cytochrome-c in Reversed Micelles
The emission intensity of Trp-59 as a function of water content in the revesred micelle. Shown also is the emission intensity in neutral pH aqueous solution. [cyt-c] = 10^{-5} M, excitation at 280nm, emission at 330nm.

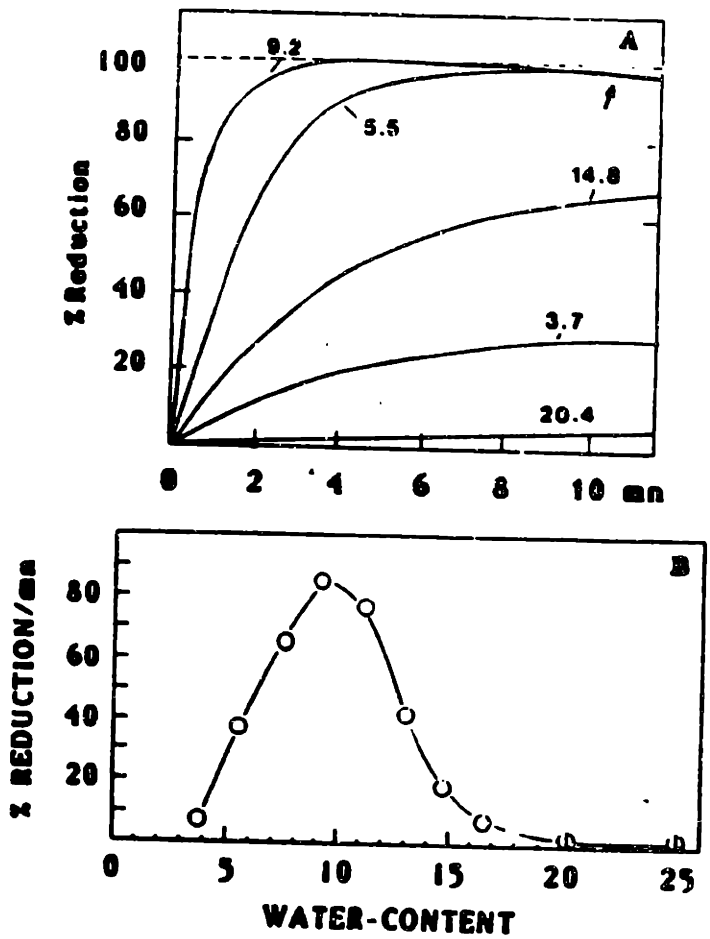

[Adapted from Brochette et al., 1988]

Figure 3.4 Kinetics of Cytochrome-c reduction in reversed micelle
(a) Reduction kinetics of water-pool entrapped cytochrome-c by sodium ascorbate at various water contents. 100% reduction refers to the total reduction obtained in aqueous solution under the same concentration conditions. (b) Initial reduction rate as a function of the water content

induction/stabilization effect with myelin basic protein in reversed micelles. Although MBP is an extended polyampholyte in aqueous solution, in reversed micelles it undergoes folding and exhibits dichroic activity. The dichroic activity was however not a function of the water content or the surfactant concentration. Additional evidence for this change in conformation is provided by flourescence studies. Nicot et al. (1985) found that the maximum emission wavelength of MBP in AOT-isooctane reversed micelles shifted from 357nm in aqueous solution to 334nm in reversed micelles. These values were not affected by increasing the water content of the reversed micelles.

CD spectra of Folch-Pi proteolipid complex, the second major myelin protein exhibit a decrease in the amount of helical structure upon insertion into reversed micelles (Delahodde et al., 1984). This decrease however is questionable as the initial experiments were performed in organic solvent mixtures that have been shown to promote an artificially high helical content. The measured helical content in reversed micelles of 55%, however, is comparable to models of the protein with four major helices penetrating the myelin bilayer (Laursen et al., 1984)

The effect of reversed micellar environments on model basic homopolyaminoacids in reversed micelles has been investigated by Seno et al., (1984). Poly L-Lysine, poly L-Arginine and poly L-ornithine undergo a conformational transition from coil in water to β structure in reversed micelles. The β sheet inducing effect is more prominent at low W_o values than at high water content. A leucine rich copolymer of L-Lysine and Leucine forms a highly stable α helix, possibly due to the hydrophobic interactions between the Leucine side chains. In reversed micelles, these helices are disrupted due to the non-polar environment provided by the reversed micelle. The disruption is higher at lower water contents.

Gierasch et al. (1982) studied tripeptides and other small peptides in AOT reversed micelles using CD. The CD spectrum of Gly-Pro-Gly was found to be the same in both aqueous solution and in reversed micelles. However, for Gly-Gly-Tyr, Lys-Asp, Grammicidin-S and cyclo-Gly·Pro-Gly-D-Ala-Pro, the CD spectra in reversed micelles were considerably different from in bulk aqueous solution. Increasing the water content of the reversed micelles caused the spectra to approach those of bulk water. It is potulated that the change in the conformation of the peptides is caused by the highly ordered arrangement of the interfacial water, especially at low W_o values.

The influence of the counterion concentration on a cyclic pentapeptide solubilized in AOT-isooctane reversed micelle has been investigated by Thompson and Gierasch (1984). CD spectra for various W_o values had qualitatively similar profiles to those obtained in water with varying sodium ion concentration. Similar correlations were also obtained from carbon-13 NMR. The changes in the carbon atom chemical shifts have been correlated to the sodium ion concentrations. However, there has been no quantitative correlation, suggesting that the counterion is just one of the many factors that affect the conformation.

DeMarco et al. (1986) studied the interaction of three peptides; Met-enkephalin, Pancreatic secretory trypsin inhibitor (PSTI), and Epidermal growth factor (EGF), with AOT reversed micelles. Using Lanthanide shift reagents, it was shown that while Met-enkephalin exists as a random coil in aqueous solution, it adapts a folded conformation in the reversed micelles. PSTI, on the other hand appears to become highly flexible suggesting a non-specific interaction between the protein and the surfactants. In addition, there is a overall loss of conformation of the polypeptide in

the reversed micelles as compared to bulk water. The disulfide bridges in the peptide however, seem to be unaffected in the reversed micelle (Masson and Wuthrich, 1973).

The NMR spectrum of EGF indicates that the overall globular conformation of the protein is retained in the reversed micelle (De Morco et al., 1986). The tyrosines in the C-terminal fragment, however, exhibit large shifts, suggesting a rearranged conformation for this region inside the reversed micelle.

Reversed micelles are also capable of solubilizing nucleic acids, which undergo structural changes as evidenced by changes in the spectroscopic properties of these molecules. For example, low molecular weight DNA exhibits a decrease in the absorbance at 260nm accompanied by an increase in the molar ellipticity. This effect is more pronounced at low water concentrations in the reversed micelles and has been ascribed to an increased base stacking as a result of increased hydrogen bonding. This increased conformational rigidity is more pronounced for RNA than for the already stable double stranded DNA.

The techniques used to characterize the protein in reversed micelles do not provide detailed site-specific information. The measured property in these techniques is averaged over the entire molecule and hence specific information is lost, and sometimes even misleading. Large perturbations at specific sites can be averaged out to be insignificant changes. To study the interaction of proteins with a charged interface, it is important to use some technique that provides site-specific information. Amide proton exchange coupled with NMR proved to be an extremely powerful technique to characterize protein structural changes at a site-specific level.

3.2 Results

3.2.1 1 - D NMR Experiments

The 1-D proton NMR spectrum of cytochrome-c in D_2O is shown in Figure 3.5. The protons of the side chains (β, γ, δ etc) are far upfield of the spectrum. The protons of the α carbon fall close to the residual water peak, which in this case is suppressed by a weak irradiation during mixing. The amide region and the aromatic side chains fall in the region between 6 and 10 ppm of the NMR spectrum. The number and intensity of the peaks in this region have been used as indicators of the extent of amide proton exchange and therefore of the integrity of the protein structure. Since the number of amide protons that are well resolved to be assigned in a 1-D NMR spectrum is limited (Patel and Canuel, 1976), site specific information on the proton exchange will be obtained at a later stage using 2-D NMR.

3.2.1.1 Surfactant Contamination

Previous assignments of the 2-D COSY spectrum of cytochrome-c has been done in aqueous solution (Feng et al., 1989). In order to use these assignments, it is important to show that there is no surfactant contamination in the back transferred aqueous phase. The solubility of AOT in aqueous solutions decreases rapidly as the concentration of salt is increased (Ayeyard et al. 1986). At 1M salt, the solubility of AOT in water is negligible, and, therefore, we can expect the back transfer solution to

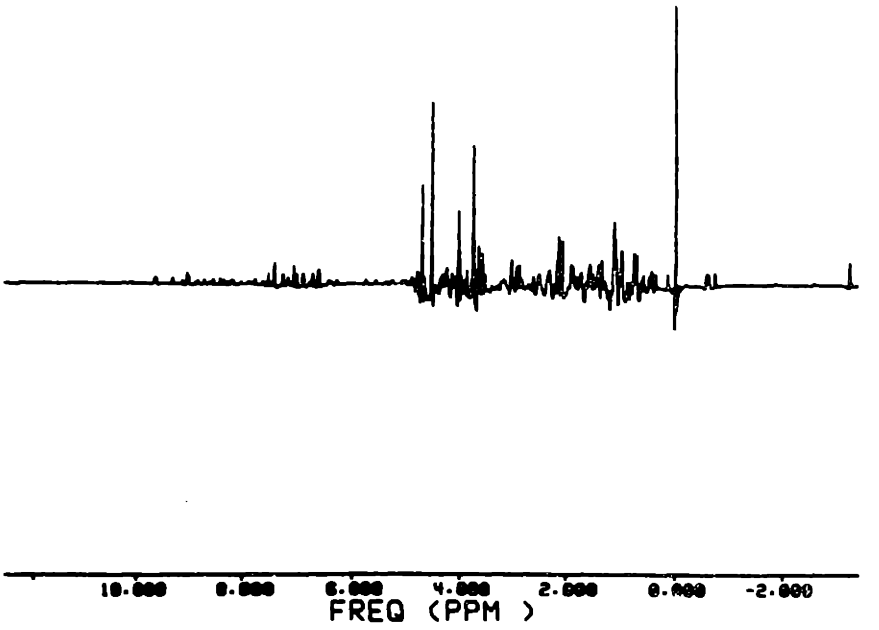

Figure 3.5 1-D proton NMR of Cytochrome-c
Cytochrome-c (1mM) in D_2O, NMR spectrum collected in a 500MHz. proton NMR spectrometer.

have negligible AOT contamination. However, cytochrome-c interacts strongly with the AOT interface (Brochette et al., 1988) through a combination of ionic and hydrophobic forces. The hydrophobic interaction might not be disrupted at high salt concentrations and hence it is possible that some AOT molecules accompany cytochrome-c into the back transfer buffer.

The 1-D proton NMR spectrum of AOT in water is shown in Figure 3.6. The resonance peaks from the methyl and the methylene groups of AOT can be easily detected at very low concentrations of AOT, on the order of a few ppm. Figure 3.7 shows the NMR spectrum of cytochrome-c back-transferred from an AOT reversed micellar phase. The absence of any of the AOT proton peaks suggests that no AOT is back-transferred to the aqueous phase along with the protein. The 1-D NMR spectrum of a back transfer solution in the absence of cytochrome-c also shows no AOT resonances. However, with some other proteins, e.g. BSA, significant amount of AOT is transferred back to the aqueous phase.

3.2.1.2 Back Transfer Buffer

The efficiency of recovering the protein back to the aqueous phase depends on the salt type, salt concentration and the pH of the back extraction buffer. A potassium carbonate buffer pH 10.8 provided the most efficient back-extraction. The back-extraction efficiency was comparable to that obtained using a 1M KCl buffer; with sodium and potassium phosphate buffers at a pH of 7.0, it was slightly lower. However, since the amide proton exchange rate is a strong function of pH, use of a high pH during the back extraction step could cause labelling of all the amides with deuterium. In addition, it is important to maintain the structural integrity of the

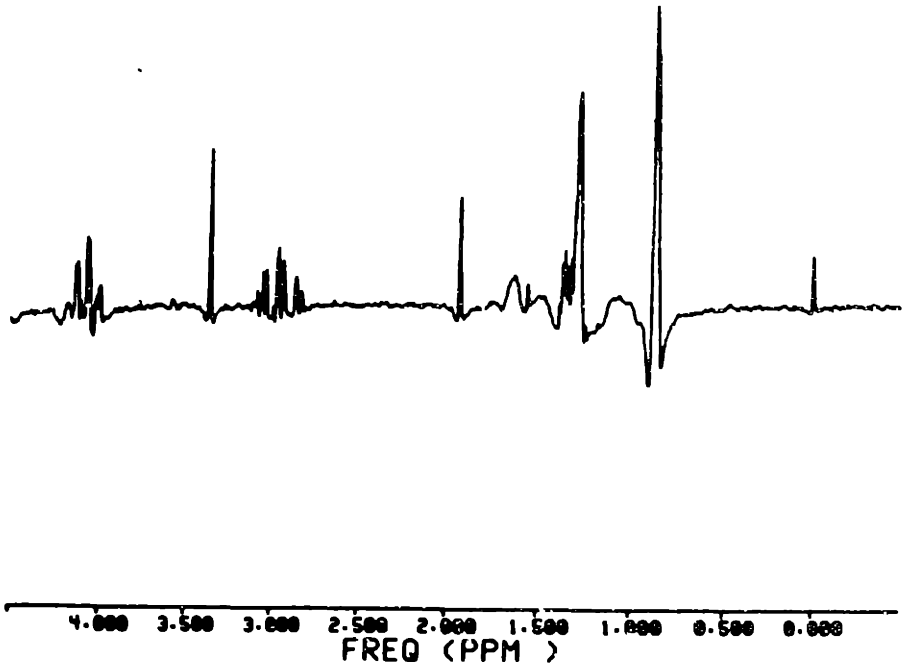

Figure 3.6 1-D proton NMR Aerosol OT (AOT)
NMR spectrum of AOT dissolved in D_2O collected in a 500MHz. proton NMR spectrometer.

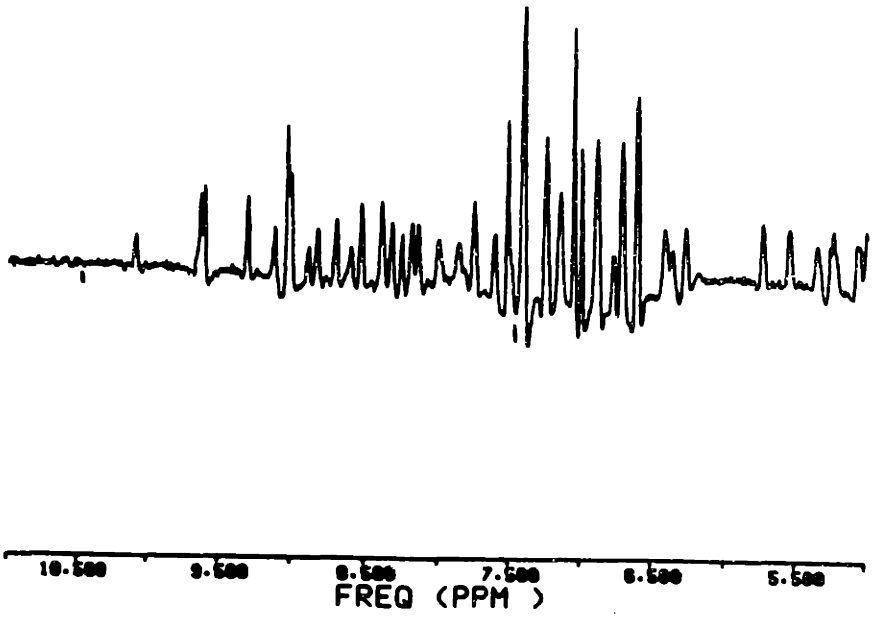

Figure 3.7 Cytochrome-c Back transferred from an AOT-isooctane reversed micelle

Amide region of cytochrome-c after back extraction to aqueous phase (D_2O). The peaks between 6.5 and 7.5 ppm (referenced to a TSP standard at 0 ppm) belong to aromatic side chains of the protein. The exchanging amide protons fall predominantly between 7.5 to 9 ppm.

protein during contact with the organic phase when transferring to and from the reversed micelle.

Figure 3.8 shows the amide region of the 1-D proton NMR spectrum of cytochrome-c in four different back transfer buffers, contacted with the organic phase containing the surfactant. Under these conditions, the protein will not transfer into the reversed micellar phase but will remain in the aqueous phase. The amide protons are completely exchanged in the carbonate buffer. This increased exchange is probably due to the high pH coupled with a small change in conformation due to the contact with organic phase. With the phosphate buffer of the same concentration (sodium or potassium), most of the amide protons are conserved indicating no drastic change in structure of the protein upon contact with the organic phase. However, the least change in exchange behavior seems to be with KCl. With KCl, different contact times and different contacting modes (vortexing vs gentle mixing) did not result in any change in the amide region of the spectrum. In addition, the amide proton exchange peaks at very short times in the reversed micelles are exactly the same as in bulk aqueous solution (section 3.2.5). Therefore, the protein can be transferred into and out of the reversed micelle without any significant change in conformation, allowing us to monitor changes in the protein structure as a result of the reversed micellar environment. The high degree of superimposability of the two spectra also indicates that the protein does not bind to AOT under these conditions.

3.2.1.3 Protein Concentration

Protein-protein interactions within the reversed micelle can also cause changes in the protein structure. The interaction of protein molecules due to proximity at high

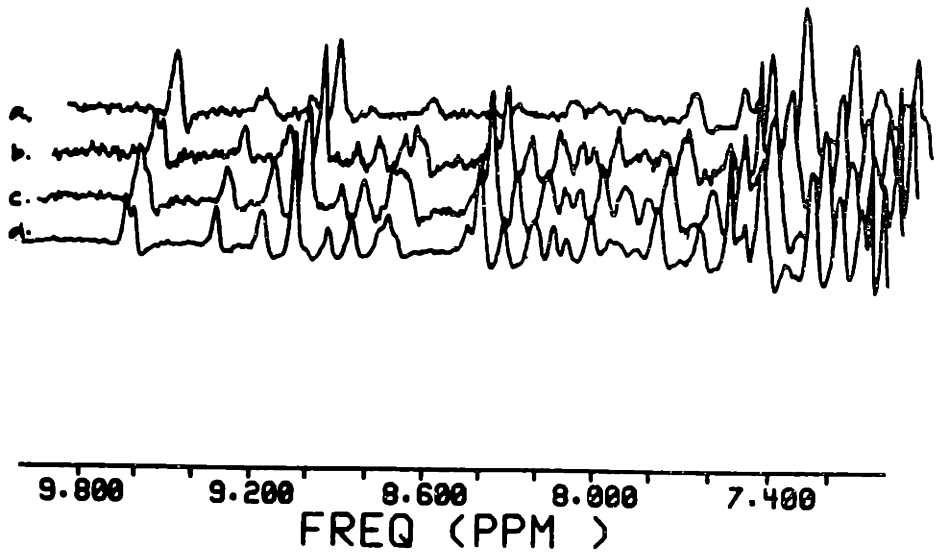

Figure 3.8 Effect of organic phase contact on cytochrome-c
Amide proton region of cytochrome-c when contacted with AOT-isooctane phase. conditions adjusted such that the protein remains in the aqueous phase after contact. (a) KCarb, (b) NaPhos, (c) KPhos, (d) KCl.

concentrations can cause large and irreversible changes in the protein structure. At low protein loadings, single occupancy of the reversed micelle can be expected. However, for NMR and other spectroscopic techniques, high protein concentrations are essential to achieve good signal intensity. As a result, very high protein loadings are required.

With NaCl as the forward transfer salt, protein at four different concentrations was solubilized in the reversed micelles, and amide proton exchange carried out for 1 hour. The amide region of the NMR spectra of the back transferred solutions are plotted in Figure 3.9. The almost complete loss of amide proton at very high protein concentrations indicates a significant loss of protein conformation. Assuming that a micelle is made of about 400 surfactant molecules, a protein concentration of 10mg/ml in the aqueous phase translates to an average of four protein molecules in each reversed micelle. This high protein loading causes changes in the micellar structure to accommodate the protein molecules, and hence changes the protein conformation. Figure 3.9 also shows that at lower protein concentrations, the amide protons are conserved and there is little or no change in the protein secondary structure. However, when reversed micelles are formed with sodium ascorbate, the protein structure is conserved even as high as 10 mg/ml in the aqueous phase (Figure 3.10).

Sodium ascorbate is a effective reducing agent for the heme group of the cytochrome-c. The stabilization effect of ascorbate for cytochrome-c can be viewed as a substrate protection that has been previously reported for other enzymes in reversed micelles (Luisi et al., 1985). The binding of the substrate to the protein increases the rigidity of the protein, reducing large scale changes in the structure.

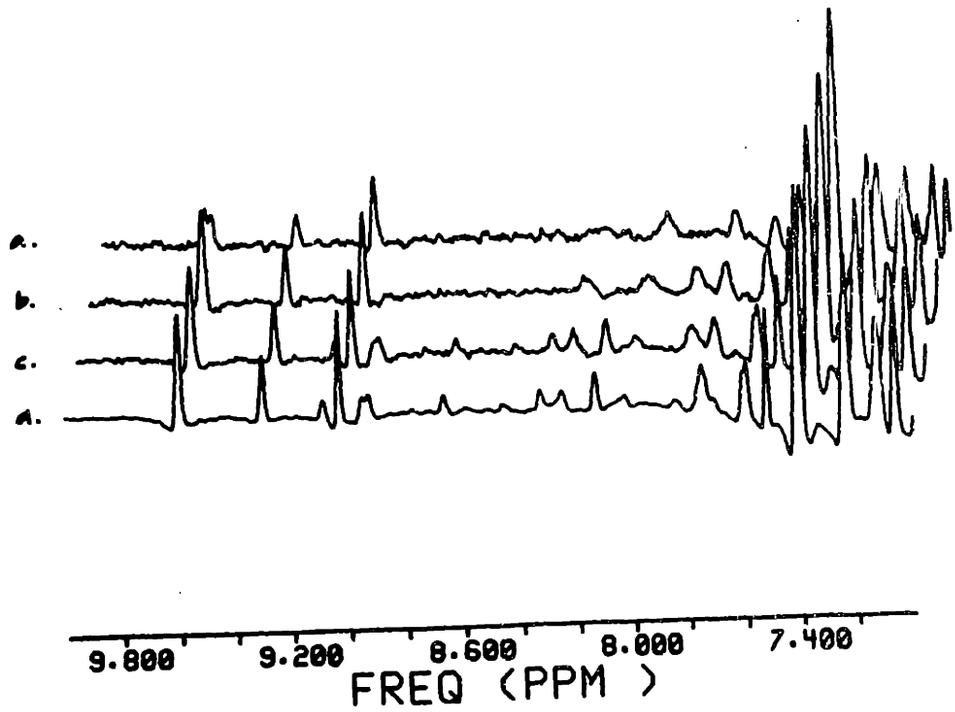

Figure 3.9 Effect of Protein concentration
Amide proton region of cytochrome-c after back extraction from AOT-isooctane reversed micelles. Initial protein concentration in aqueous phase containing 200mM NaCl: (a) 10mg/ml, (b) 5 mg/ml, (c) 2 mg/ml, (d) 1mg/ml.

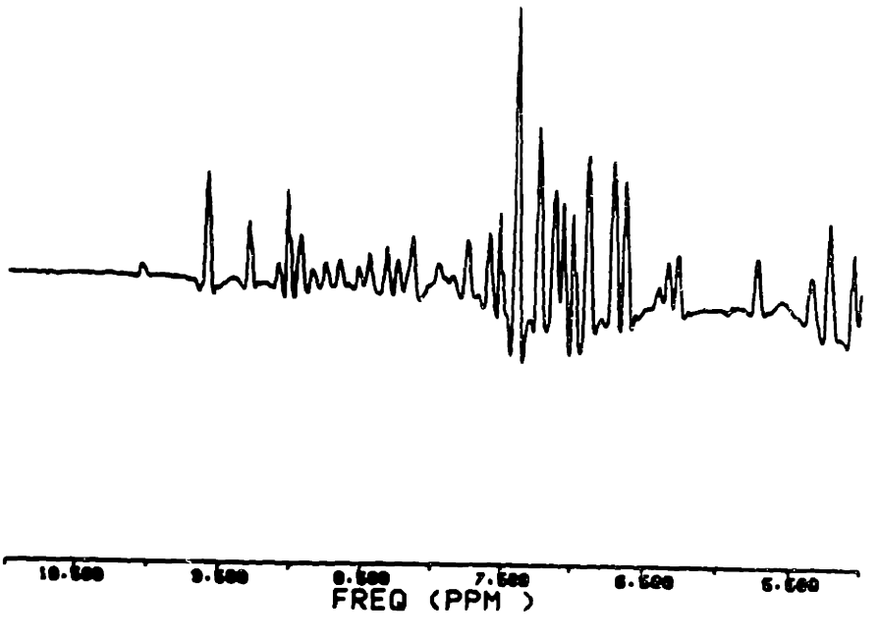

Figure 3.10 Effect of Protein concentration - FT with sodium ascorbate
Amide proton region of cytochrome-c after back extraction from AOT-isooctane reversed micelles. Initial protein concentration in aqueous phase containing 200mM Sodium ascorbate was 10mg/ml.

3.2.1.4 Forward Transfer Buffer

The salt used for the forward transfer seems to play a critical role in the stabilization of the protein structure inside the reversed micelle. The effect of different cations on the size of reversed micelles has been investigated in detail previously (Leodidis and Hatton, 1989). In this work, the anion used seems to have a significant effect on the protein structure. Three different salts were considered: Sodium monobasic and dibasic phosphate buffer, sodium chloride, and sodium ascorbate. The concentration and the pH of these buffers were adjusted to be identical. When sodium phosphate buffer was used for the forward transfer, the protein seemed to undergo large changes in structure inside the reversed micelle; the amide protons were all exchanged within an hour (Figure 3.11). Visible absorption spectra also indicate that the change in the heme environment is pronounced in the presence of phosphate. From Figure 3.11, it is also apparent that the change in protein structure is much less pronounced with sodium chloride, and even less so with sodium ascorbate. The amide region of the spectrum with ascorbate as the transfer buffer is exactly superimposable with the spectrum in aqueous solution.

The rapid exchange of all the amide protons in the presence of phosphate buffer could be due to an uneven partitioning of the buffer salts into the reversed micelles causing local pH changes. Thus, reversed micelles formed with sodium chloride in the presence of different commercial buffers were investigated. Figure 3.12 shows the amide region of cytochrome-c after proton exchange for 1 hour in the reversed micelle with different buffers. All these buffers show no large scale disruption of protein structure, in contrast to observations with phosphate buffer.

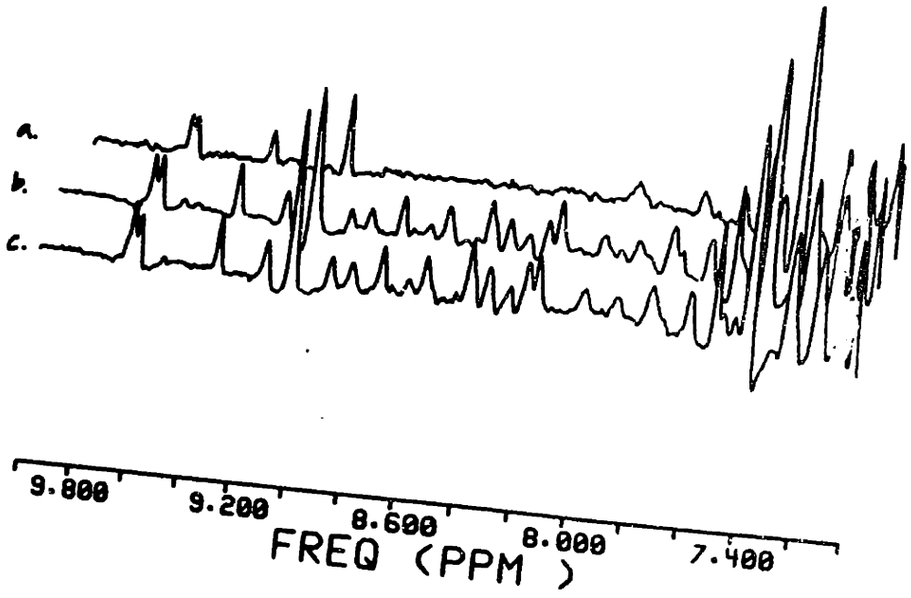

Figure 3.11 Effect of Forward transfer salt
Amide proton region of cytochrome-c after back extraction from AOT-isooctane reversed micelles. The protein was incorporated into the reversed micelle using (a) 200mM sodium phosphate buffer (b) 200mM sodium chloride, and (c) 200mM sodium ascorbate.

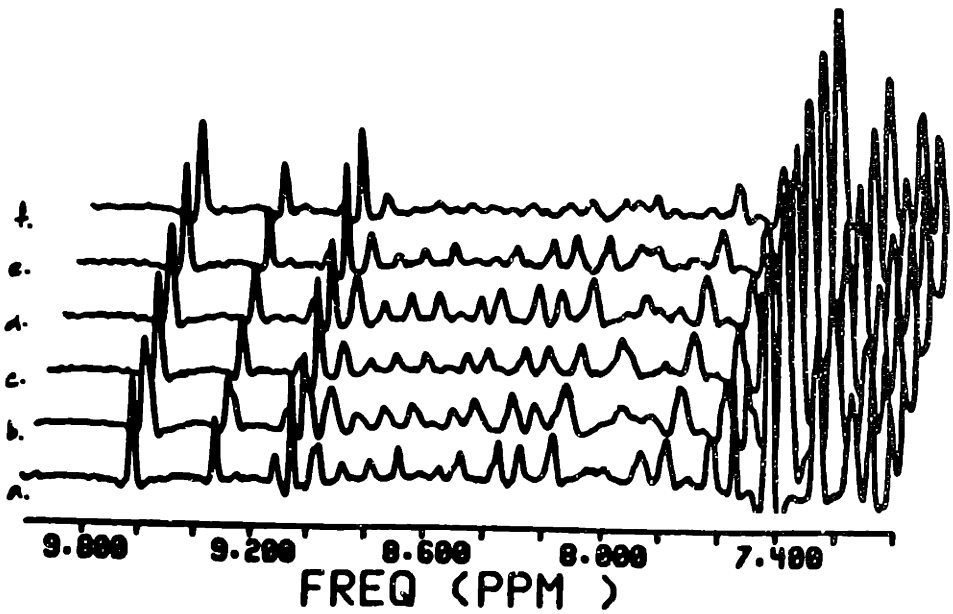

Figure 3.12 Effect of Buffer salts on proton exchange
Amide proton region of cytochrome-c after back extraction from AOT-isooctane reversed micelles. [Cyt-c] = 10mg/ml. Forward Transfer was with 200mM NaCl buffered with (a) TAPS, pH 8.5, (b) EPPS, pH 7.2, (c) Hepes pH 7.2, (d) GlyGly, pH 7.5, (e) Tris pH 8.2, (f) Tris pH 8.2, 20mg/ml [cyt-c].

The stabilization of the cytochrome-c in the presence of ascorbate is not totally due to the change in the oxidation state of the heme. When reduced cytochrome-c is solubilized in AOT-isooctane reversed micelles with NaCl buffer, the amide protons are conserved only for small exchange times in the reversed micelle (Figure 3.13a). The protons of the amide region are completely labelled by two hours in the reversed micelle. When NaCl is substituted with increasing amounts of ascorbate, the stability of the protein increases, as evidenced by conserved amide protons at longer exchange times (Figure 3.13b to d). The ascorbate concentration required for the stability of the protein is far in excess of the stoichiometric requirement. The possibility of an oxidizing contaminant in the surfactant was ruled out by treating the AOT with a reducing agent prior to reversed micelle formation. Hence, cytochrome-c seems to be stabilized by the 'substrate' ascorbate inside the reversed micelles.

3.2.1.5 Size of Reversed Micelle

The concentration of the forward transfer buffer determines the size of the reversed micelle. The W_o is related to the cation type and for a protein free reversed micelle (Figure 3.14). Three different reversed micellar sizes were studied. Transfer of protein from an aqueous phase containing 200mM salt resulted in a W_o of about 30. In the absence of cytochrome-c, the W_o was 28. This increase in W_o is due to the interfacial activity of cytochrome-c. Earlier studies (Brochette et al., 1988) using x-ray scattering confirm the interfacial association of cytochrome-c in AOT-isooctane reversed micelles. In effect, the protein acts like an additional surfactant molecule. This same trend of higher water uptake in the presence of cytochrome-c exist for the other reversed micellar sizes as well: W_o of 50 and W_o 20 (salt concentration of 50mM and 350mM). Changing the size of a reversed micelle changes the curvature

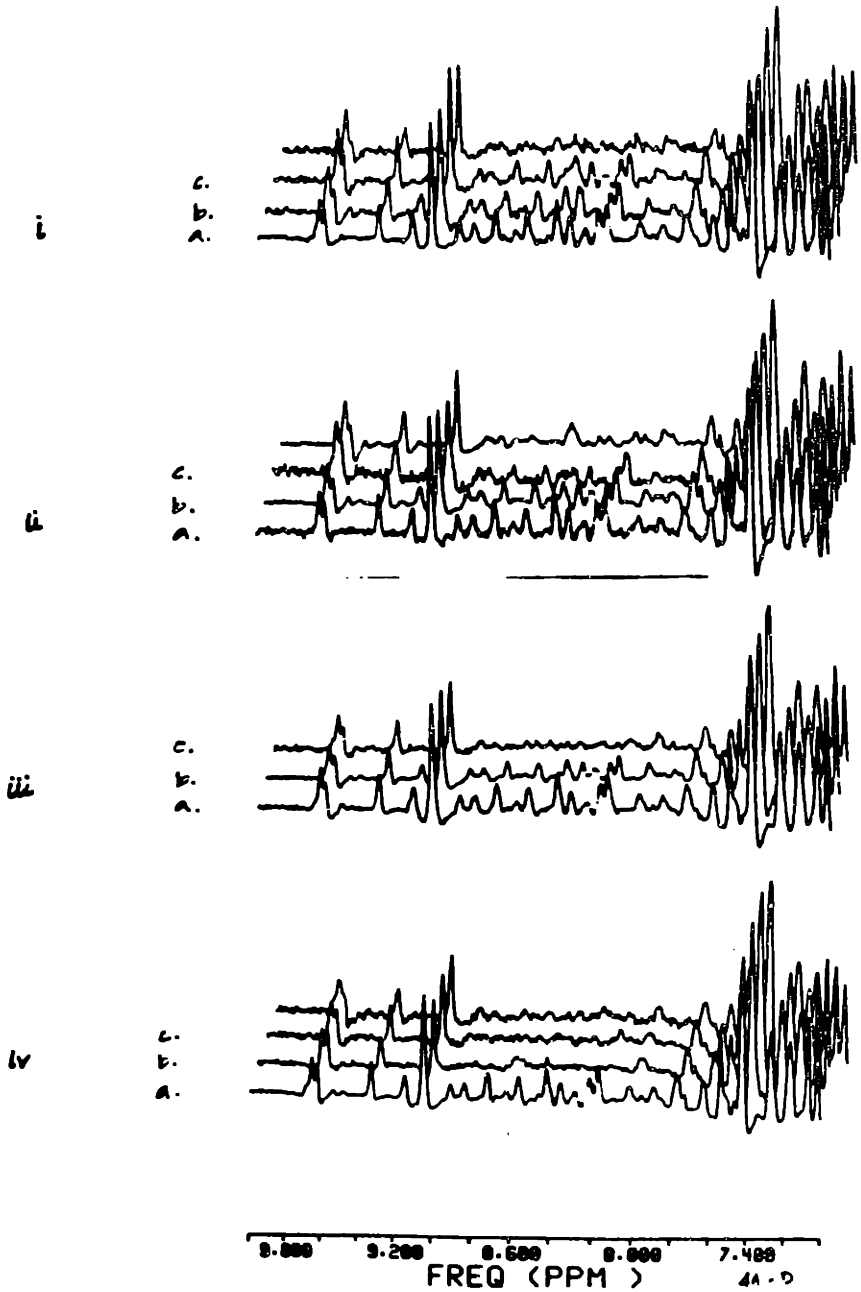

Figure 3.13 Forward Transfer Anion - ascorbate vs. chloride
Amide proton region of cytochrome-c after back extraction from AOT-isooctane reversed micelles, exchange time of (a) 30min, (b) 60 min, (c) 120 min. Forward transfer salt: (i) 200mM NaCl, (ii) 150mM NaCl, 50mM NaAsc, (iii) 100mM NaCl, 100mM NaAsc, (iv) 200mM NaAsc.

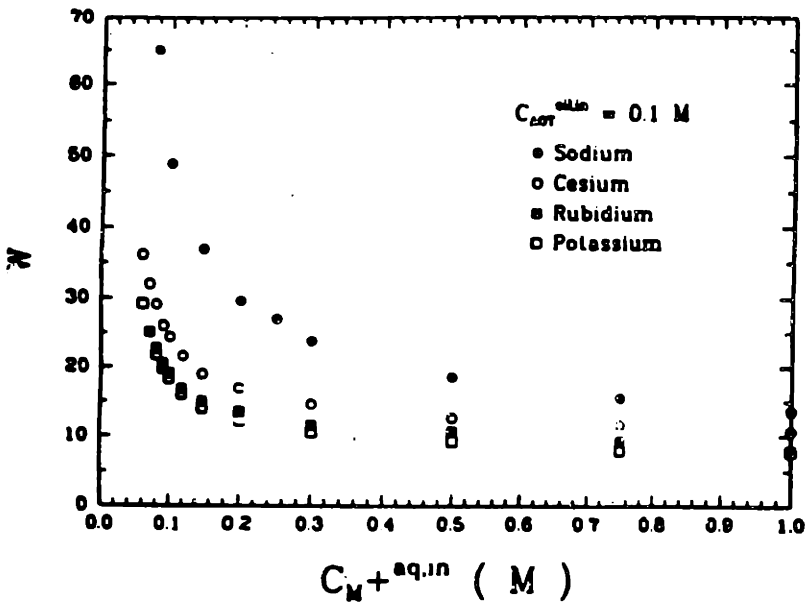

[Adapted from Leodidis , 1990]

Figure 3.14 W_0 as a function of salt concentration

of the interface and hence can induce some stress on an interfacial protein, causing structural perturbations. On the other hand, a hydrophilic protein is expected to be at the core of the micelle surrounded by a water pool. These proteins exhibit properties as in bulk water as the size (W_o) of the micelle is increased (Waks, 1986).

The charged head group of the surfactant also interacts with the charges on the protein. Under our experimental conditions, cytochrome-c is positively charged with a predominance of surface lysines. These lysines are important for the protein interaction with cytochrome-oxidase or reductase and hence for its physiological function. The heme group is buried in a hydrophobic core, flanked on three of the sides by the peptide chain (Figure 3.15). It is likely that the tail groups of AOT interact with the heme, causing structural perturbations in the protein. This change in structure might reflect on the physiological structure of cytochome-c in the mitochondrial membrane.

3.2.2 Amide Proton Exchange Experiments : 2-D NMR

The cytochrome-c molecule comprises of 5 helices: the N-terminal helix, the 50s helix, 60's helix, 70's helix and the C-terminal helix. The porphyrin of the heme group is held in place by covalent linkages to Cys-14 and Cys-17. In addition, His-18 and Met-80 provide two axial ligands to the iron. Hydrogen bonding between Trp-48, Trp-59 and the porphyrin group also help in the stabilization of the heme pocket.

In aqueous solution, the amide proton exchange rates of the residues in the 5 helices are quite low, especially the residues of the C-terminal helix. The tight hydrogen bonding coupled with the amphipathic nature of the C-terminal helix make the

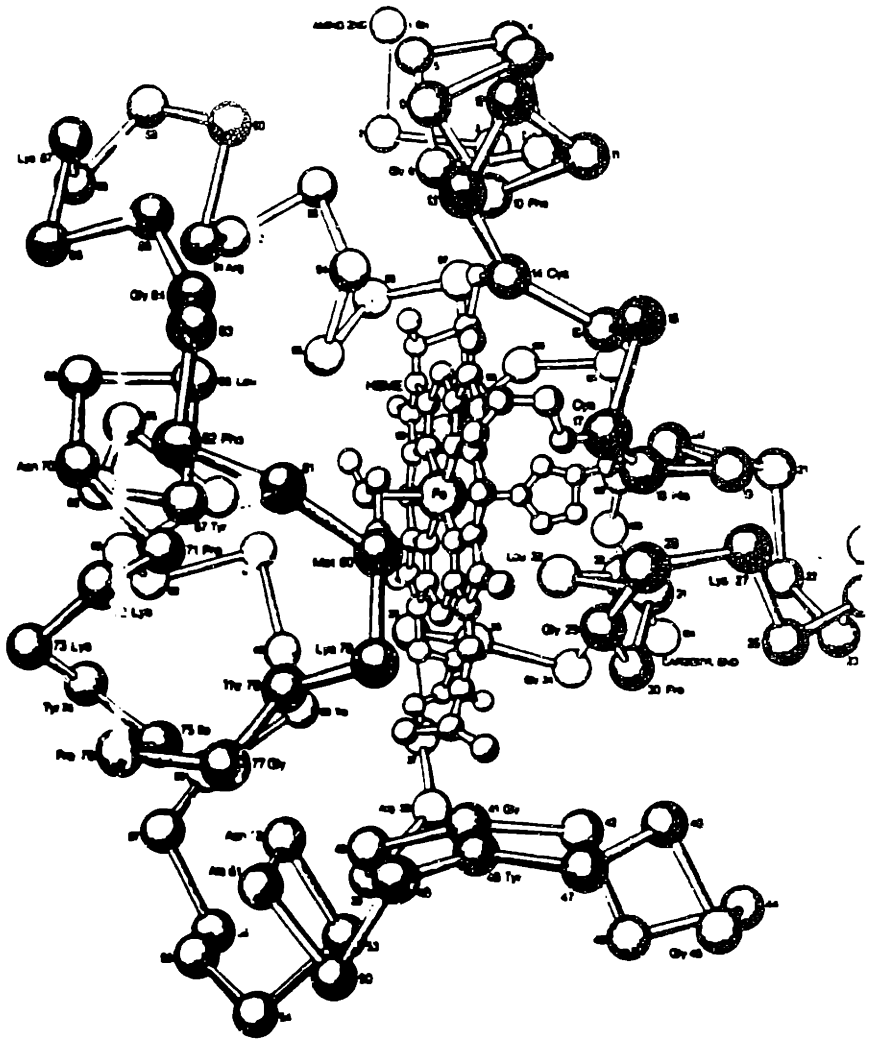

[Adapted from Dickerson and Geis, 1975]

Figure 3.15 Molecular Structure of horse heart cytochrome-c
The main chain atoms and the heme group are shown.

amide protons less labile. Of the 104 amino acids, about 65 exchange rapidly at physiological pH. The remaining 39 exchange at a very slow rate and hence can be used as markers for structural change.

3.2.2.1 C - Terminal Helix

The effect of the reversed micellar environment on the C-terminal helix will be considered first. Residues 88-101 of horse heart cytochrome form a tight right handed α-helical structure. The first few residues of the α-helix exchange out rapidly even in aqueous solution. The hydrogen bonds in the end of the helix can be broken very easily as the chain is very flexible. The exchange characteristics of residues in the center of the helix (93 to 99) inside the reversed micelles (W_o 20, W_o 30, and W_o 50) are shown in Figures 3.16 I, II, and III. The exchange in bulk aqueous solution (D_2O) for the same time period is also plotted on the same graph. Although the noise in the data for the protein in D_2O is quite high, long time exchange experiments confirm that the exchange rates of these protons are indeed very slow (Figure 3.17). The proton peak intensities at short times in the reversed micelles are almost equal to the peak intensities in aqueous solution, thereby confirming that there is no large-scale damage to the protein structure during the transfer process.

The exchange rates of the amide protons for these residues are increased dramatically under the reversed micellar environment. At the end of about 6 hours incubation in the reversed micelle the amide proton intensity falls off to almost zero in these residues. Increasing the size of the reversed micelle seems to increase the rate of amide proton exchange, although the high scatter in the data makes it difficult to correlate structural changes quantitatively to the size of the micelle. The

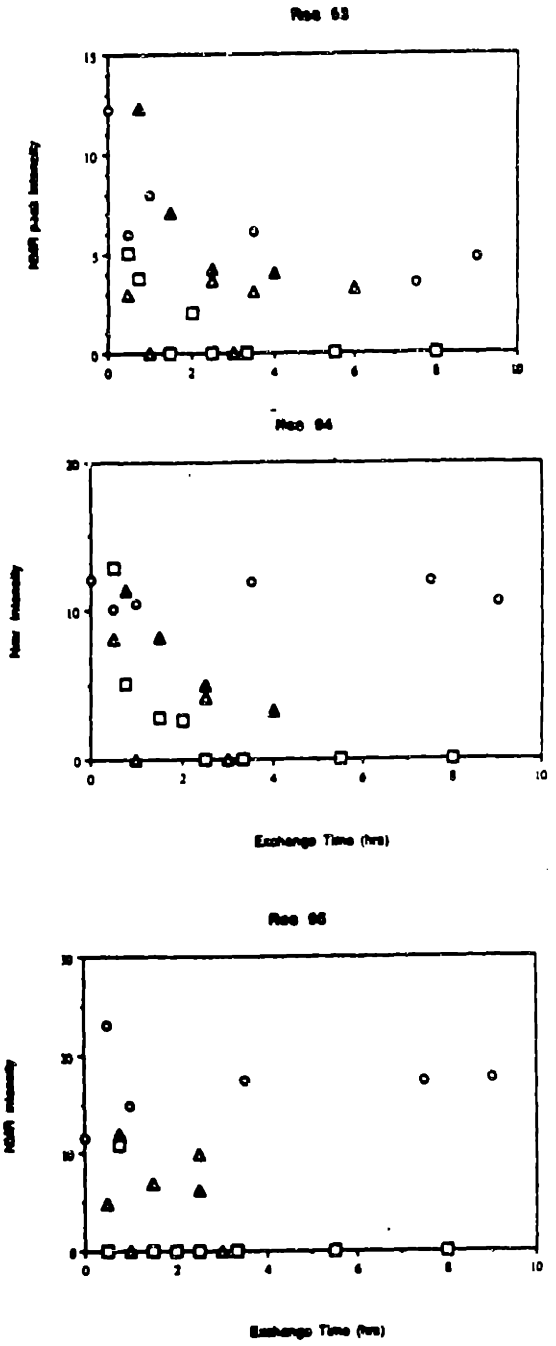

Figure 3.16 - I Amide proton exchange of C-terminal helical region
Amide proton peak intensity of (a) Asp-93, (b) Leu-94, (c) Ile-95 as a function of exchange time in aqueous solution (○), and in reversed micelle of Wo 50, (□) Wo 30 and (△) Wo 20 (▲)

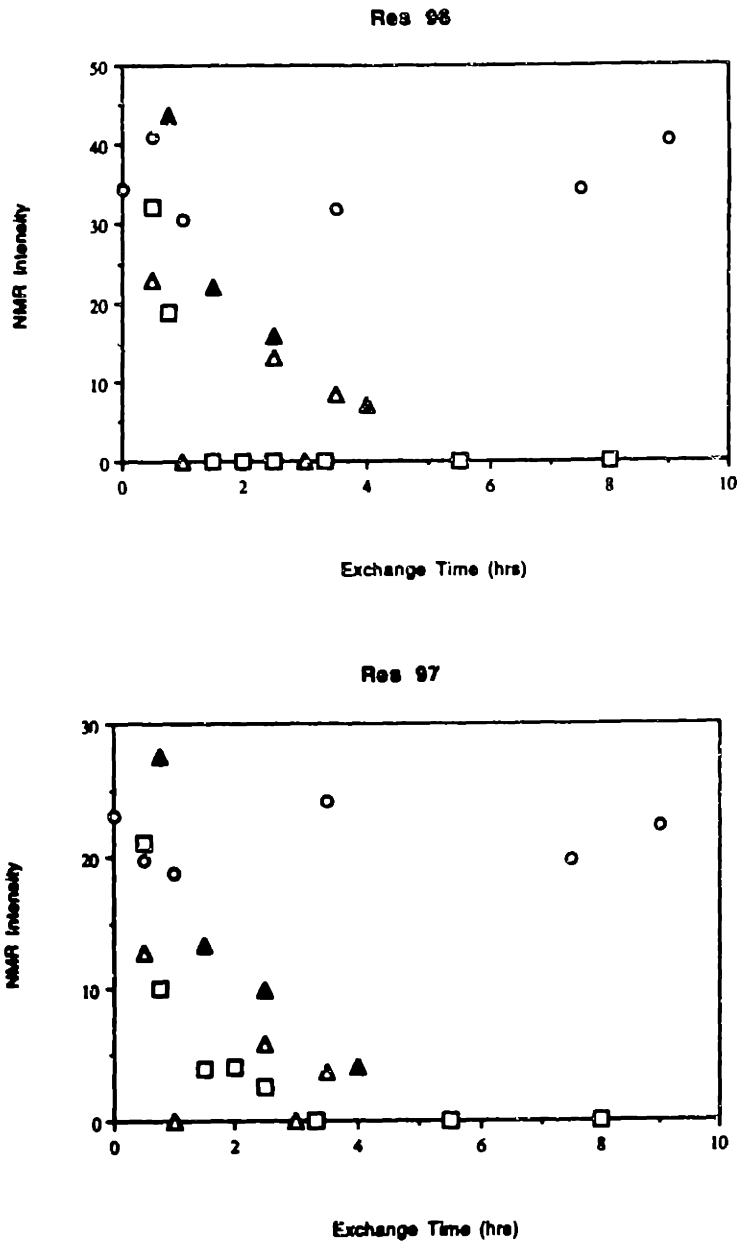

Figure 3.16 - II Amide proton exchange of C-terminal helical region
Amide proton peak intensity of (a) Ala-96, (b) Tyr-97 as a function of exchange time in aqueous solution (O), and in reversed micelle of Wo 50, (□) Wo 30 and (Δ) Wo 20 (▲)

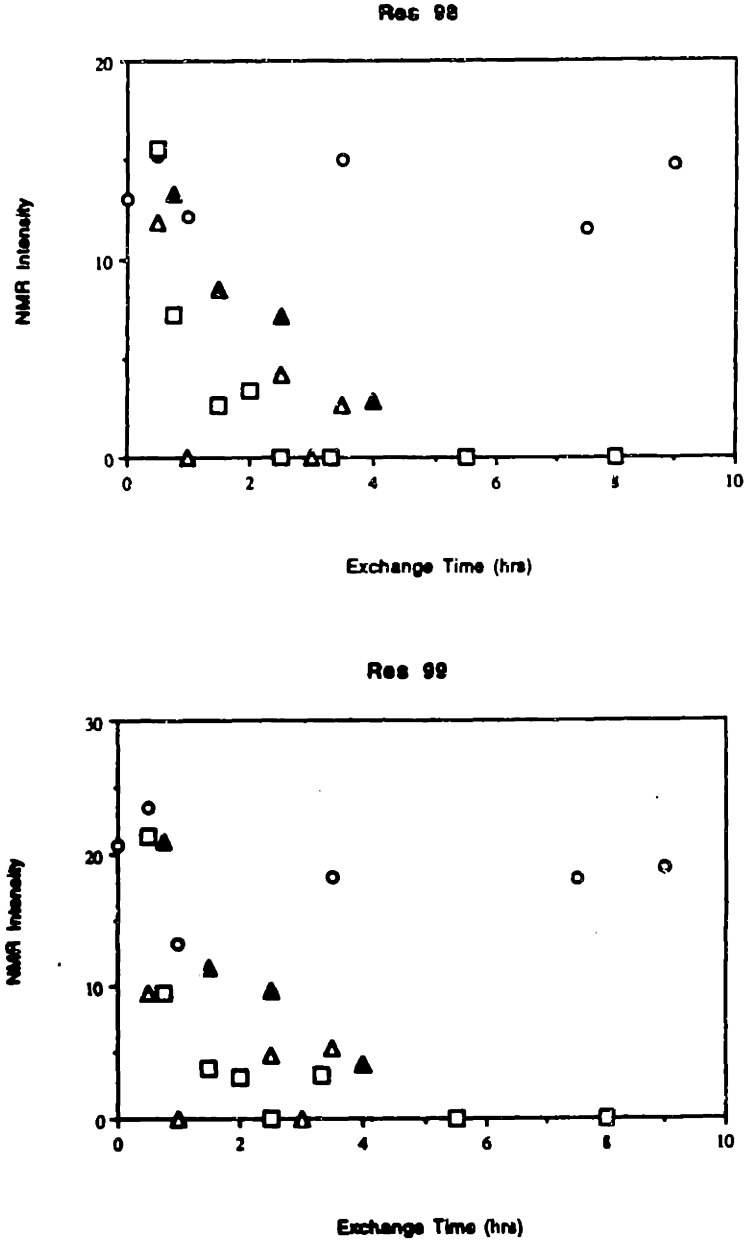

Figure 3.16 - III Amide proton exchange of C-terminal helical region
Amide proton peak intensity of (a) Leu-98, (b) Lys-99 as a function of exchange time in aqueous solution (O), and in reversed micelle of Wo 50, (□) Wo 30 and (Δ) Wo 20 (▲)

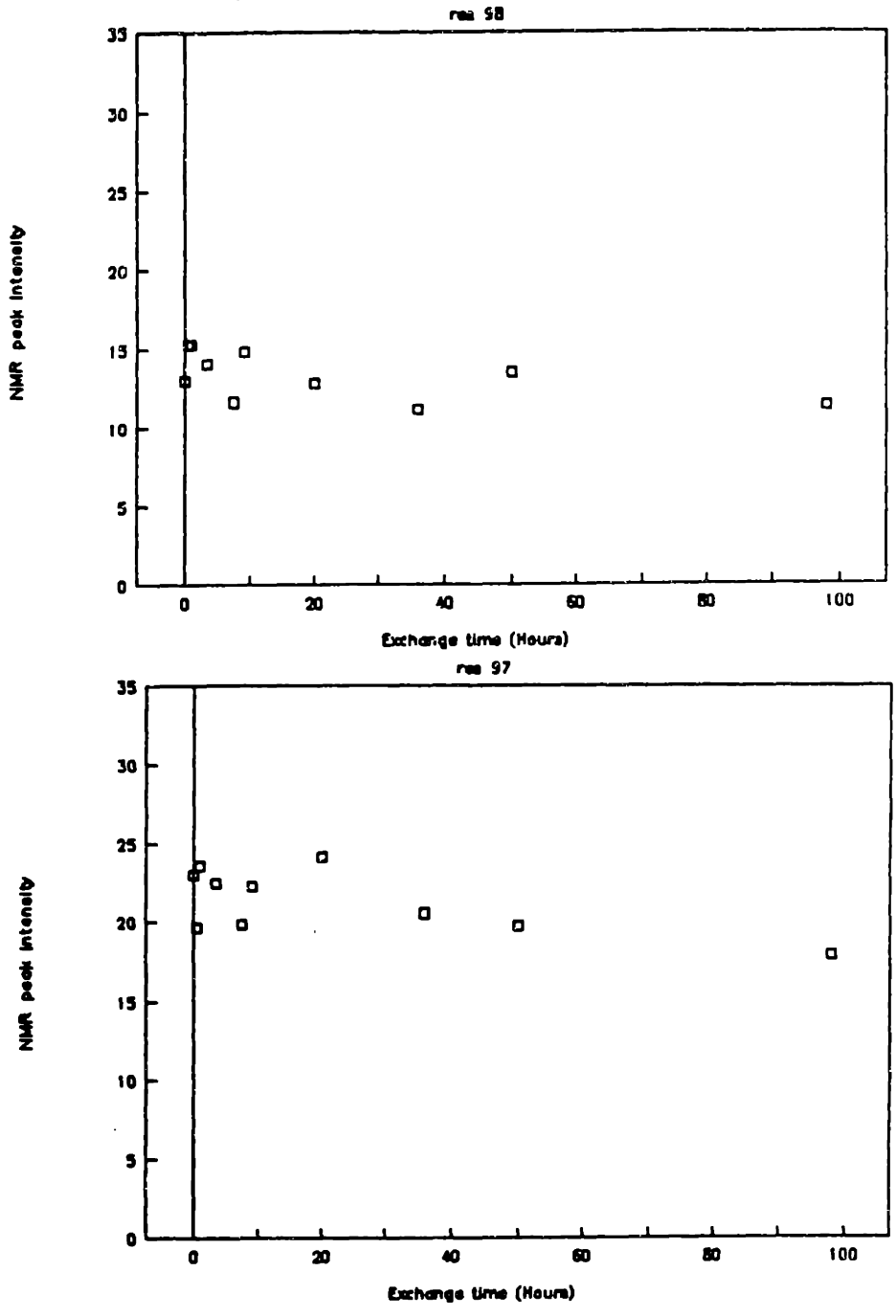

Figure 3.17 Amide proton exchange in D_2O

Amide proton peak intensity of (a) Leu-98, (b) Tyr-97, as a function of exchange time in aqueous solution.

trends, however, clearly indicate a higher proton exchange rate for the larger micelle, consistent with earlier observations of cytochrome-c structure in reversed micelles.

For a fixed protein conformation, the amide proton exchange kinetics is expected to be first order. The experimental data, however, indicate more complex behaviour, possibly due to chenges in the protein structure with time, which leads to changes in the hydrogen bonding and/or solvent accesibility of the monitored amide protons. This is confirmed by CD experiments below.

This increase in the exchange rate in the reversed micelle can be explained by a change in the conformation of the molecule or by an extremely high dynamic flexibility of the molecule about its native conformation. However the conformational change was not complete unfolding since the protein would exchange extremely rapidly (on the order of few seconds) and would give no observable amide proton peaks. In addition, the exact value of the pH inside the reversed micelle is unknown as the charged interface causes an uneven distribution of ions. Near the negatively charged surfactant layer, the pH is expected to be lower than in the bulk aqueous solution, resulting in a reduction in the amide proton exchange rate. Since the observed effect here was an increase in the exchange rate, the hydrogen bonds in the C-terminal helical region must have been weakened due to presence of the charged interface causing perturbations in the local structure.

The last four residues of the C-terminus displayed an increase in the amide proton peak intensity after being incorporated inside the reversed micelle (Figure 3.18). In aqueous solution, the amide protons of Lys-100 and Ala-101 are hydrogen-bonded to Asn-103 and Glu-104, as a part of the helical structure. The amide protons of 102-104

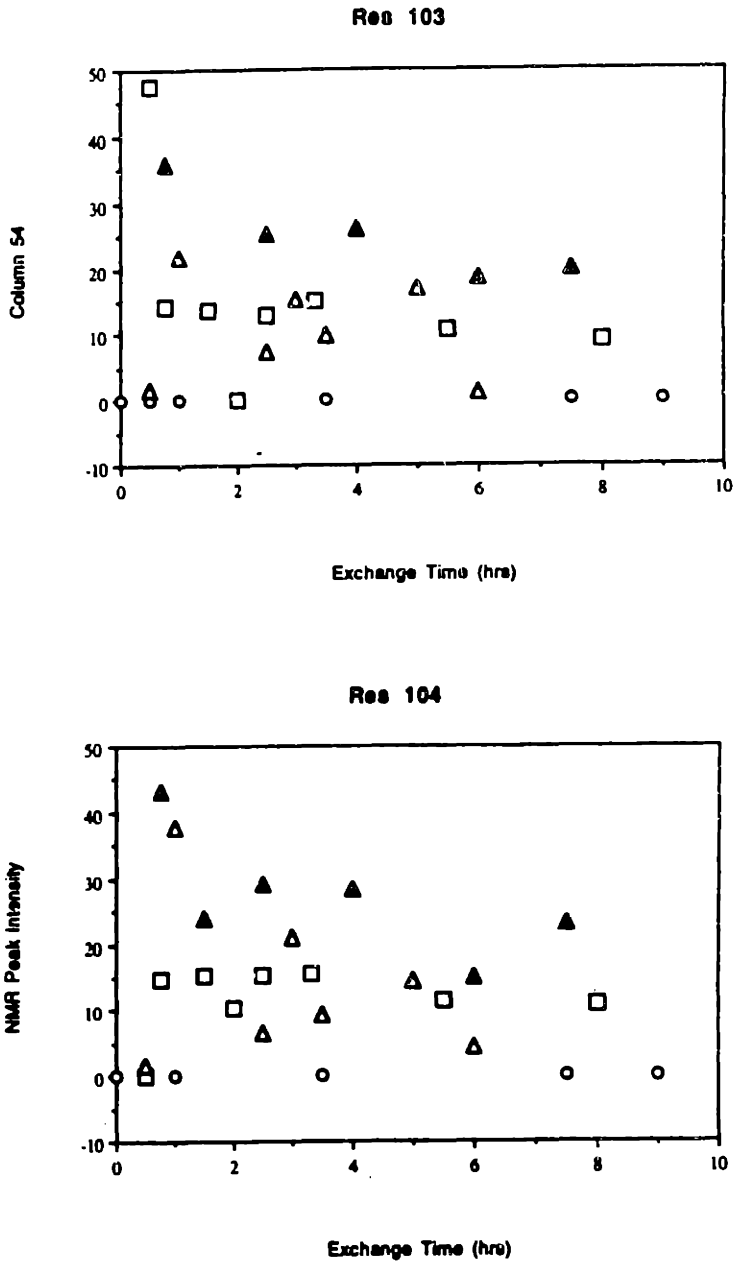

Figure 3.18 Amide proton exchange of C-terminal helix
Amide proton peak intensity of (a) Asn-103, (b) Glu-104 as a function of exchange time in aqueous solution (O), and in reversed micelle of Wo 50, (□) Wo 30 and (Δ) Wo 20 (▲)

exchange rapidly as they are not involved in any hydrogen bonding. Tertiary interactions between the helices and other parts of the structure could result in the formation of hydrogen bonds and hence of a more rigid C-terminal end, thus lowering the exchange rate inside the reversed micelle. The x-ray crystal structure of the protein in aqueous solution shows that these residues are spatially close to the irregular loops (the region at the bottom of Figure 3.15) and could form some hydrogen bonds with the carbonyl groups of these residues. However, upon back-extraction to the aqueous phase, the protein returns to its native conformation as evidenced by the invariance of the C_α - C_β cross peaks and also visible absorption spectrum of the heme. This would then result in a fast exchange of these protons and hence any reduction in the exchange rate in the reversed micelle would not be detected.

The increase in the amide proton intensity of these residues could be due to exchange of these protons with other protons rather than with deuterium. The water of hydration of AOT or the salt used for transfer could be the source of these protons. IR spectra on these samples indicate the presence of appreciable quantities of protons bound to the sodium ascorbate used for the forward transfer. Subsequent experiments using ascorbate whose labile protons were replaced with deuterium indicated that this abnormal proton exchange behavior of these residues was indeed because of the protons associated with the ascorbate.

The protons transferred into the reversed micelle along with the ascorbate were expected to alter the baseline of the exchange profiles by a uniform amount. The solvent protons associated with the ascorbate would exchange rapidly with the deuterium and hence this would be equivalent to carrying out an amide proton exchange experiment using D_2O of slightly lower purity (e. g., 98% D). Therefore,

instead of all the protons being completely labelled with deuterium, there should be an equilibrium distribution of protonated and deuterated amide protons. However, the exchange behavior of residues in the middle of the C-terminal helix was quite different from that of the last few residues, implying an uneven distribution of protons in the vicinity of these groups inside the reversed micelles. The amide protons of residues 93 to 99 seemed to exchange with a im rich solvent while the protons of the last four residues appear to have been exposed to a high proton concentration.

3.2.2.2 N - Terminal Helix

Glu-4 and Lys-5 exchange extremely rapidly in aqueous solution as their amide protons do not participate in any hydrogen bonding. In reversed micelles, particularly, W_o 30 micelles, the peak intensity increased and then droped with increasing exchange time (Figure 3.19). This behavior was similar to that for the residues in the C-terminal end of the protein. X-ray crystal structure indicates a close proximity between these residues and the last few residues of the C-terminal helix, suggesting an abundance of protons near specific sites in the protein. The abnormal behavior was also exhibited by residues Lys-79 and Met-80 (Figure 3.20), which are far removed from the C-terminus of the protein.

Met-80 forms a rather weak ligand to the heme and absorbs at 695nm. At pH above 8, it has been shown that this bond is replaced by Lys-79 and hence the Met-80 absorption band disappears. The amide proton of Lys-79 is hydrogen bonded to the propionic acid in the heme and Met-80 to the O of Thr-78. All the residues in this region show a monotonic decrease in the peak intensity in a W_o 50 reversed micelle. However, the amide proton intensity increases first and then drops for Lys-79, Met-

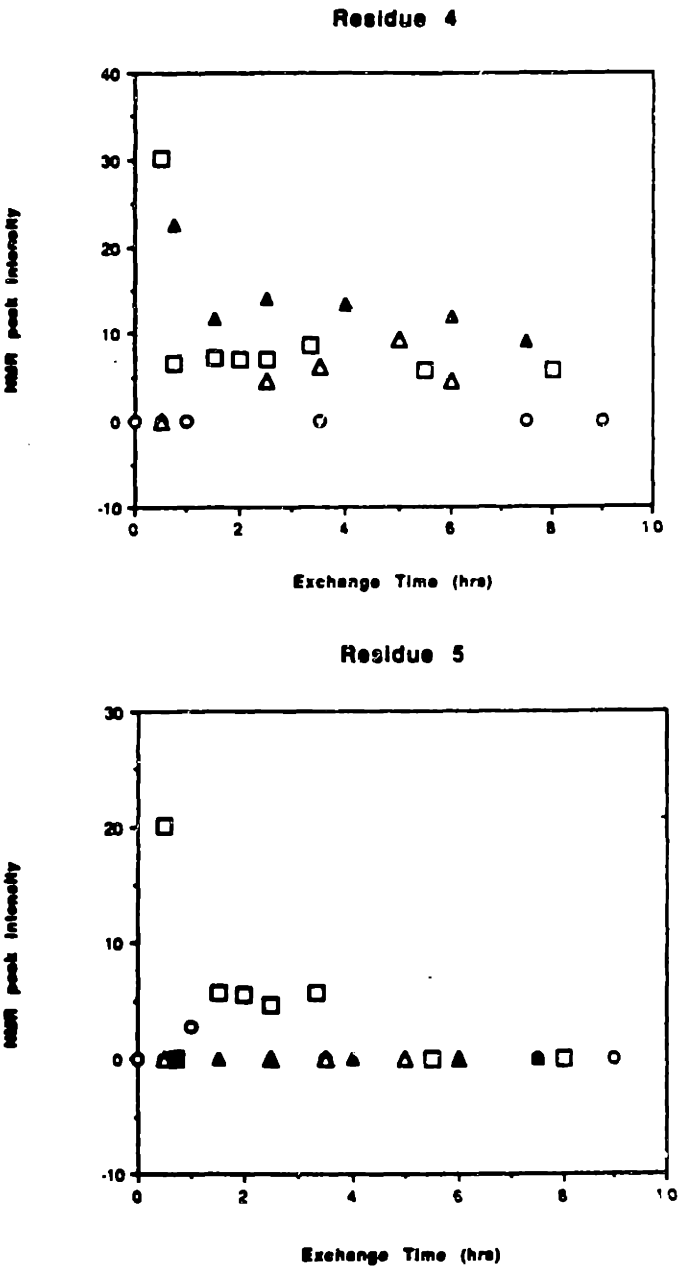

Figure 3.19 Amide proton exchange of N-terminal helix
Amide proton peak intensity of (a) Glu-4, (b) Lys-5, as a function of exchange time in aqueous solution (O), and in reversed micelle of Wo 50, (□) Wo 30 and (Δ) Wo 20 (▲).

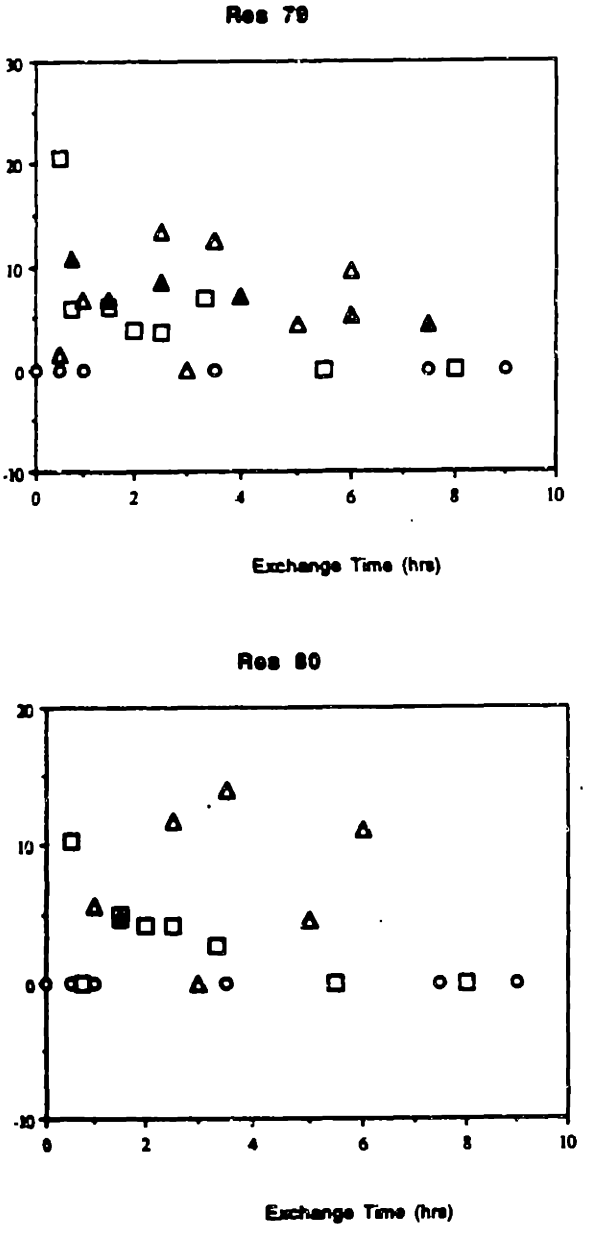

Figure 3.20 Amide proton exchange of Heme Ligand.
Amide proton peak intensity of (a) Lys-79, (b) Met-80, as a function of exchange time in aqueous solution (O), and in reversed micelle of Wo 50, (□) Wo 30 and (Δ) Wo 20 (▲).

80, Ile-85 and Lys-87 in the smaller reversed micelles. The high proton concentration in this region close to the heme pocket suggests a strong interaction between the heme and the ascorbate.

3.2.3 Source of Protons

3.2.3.1 IR Studies

The unusual proton exchange behavior suggests a source of protons inside the reversed micelle in the proximity the protein. The protons could come from water adsorbed by the hygroscopic AOT or from the hydrates of salts used for transfer. IR absorption was used to determine the presence of H_2O in the reversed micellar samples.

Figure 3.21 shows the IR spectrum of AOT-isooctane solution that is normally used for the NMR experiments. The C-H vibrational and rotational absorptions are clearly seen. There is however, no significant absorption in the H-O vibrational frequency indicating that the amount of H2O in the AOT-isooctane solution is very low. Figure 3.21 shows the IR spectrum of a reversed micellar sample formed using sodium ascorbate in D_2O. The H-O vibrational bands (3450 cm-1) are quite significant. The reversed micelles therefore contain significant amounts of H_2O. Proton exchange rate measurements through NMR could now be skewed because of the exchange of protons with other protons (from the H_2O). IR experiments using dry sodium chloride as the forward transfer buffer did not have significant H-O vibration band. This indicates that the source of protons is the ascorbate used for the

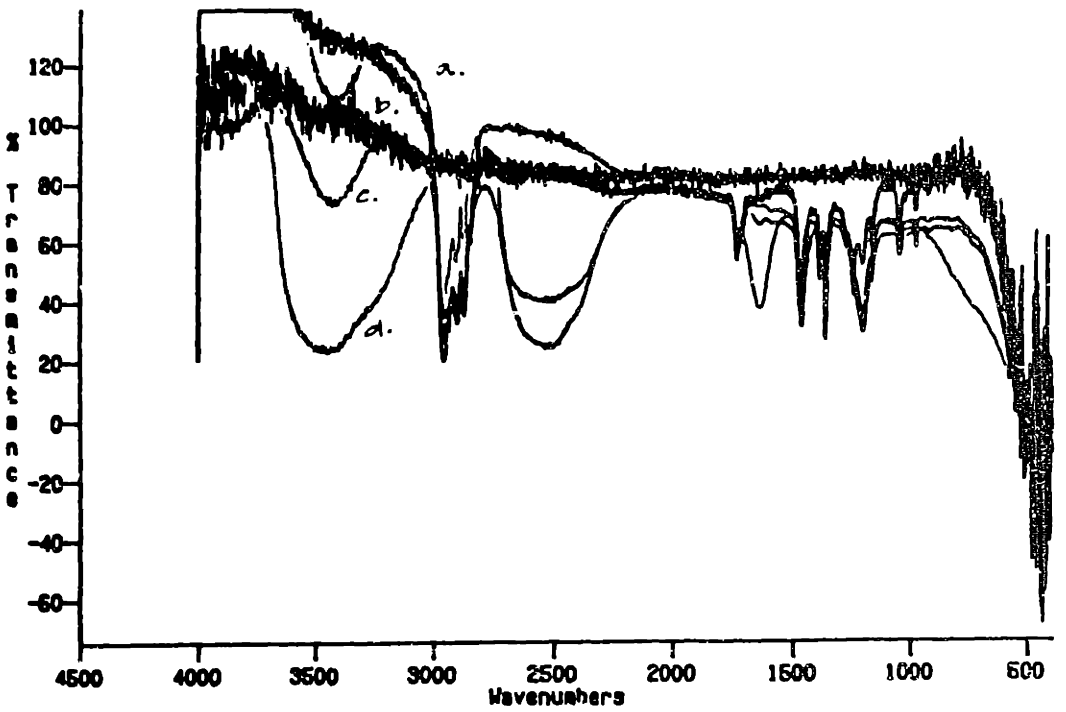

Figure 3.21 IR spectrum of AOT-isooctane reversed micelles
IR spectrum of AOT-isooctane reversed micelles with (a) no water transfer (b) D2O transferred, (c) Protein and D2O transferred, (d) H2O transferred.

forward transfer. Further NMR study confirmed the source of protons to be the hygroscopic ascorbate.

3.2.3.2 NMR Study

The D_2O used for the samples contained about 0.1% protons according to the manufacturer. Proton NMR spectra on D_2O indicated small amounts of the HDO peak. The HDO peak did not increase in intensity upon addition of more D_2O to the sample. A 2M ascorbate solution was then prepared in D_2O and added in 10μL increments. The HDO peak at 4.632 increased almost directly with the amount of ascorbate added. A plot of the area of the HDO peak with the area of the ascorbate peak at 4.2 showed a 1:1 correlation (Figure 3.22). This clearly indicates that the H_2O was transferred into the reversed micelle along with the salt used for transfer. It is also interesting to note that the presence of hydrogen atoms inside the reversed micelle did not affect the exchange kinetics of all the residues equally, indicating a spatial polarization of the H atoms inside the reversed micelles, possibly due to the charged interface.

The difference in the proton distribution within the reversed micelle could be used to gain some insight into the ascorbate binding site of cytochrome-c. If the protons were tightly bound to the ascorbate there would have been an excess of protons in the proximity of the ascorbate binding site. Further investigations in this direction could give biophysical correlation of the ascorbate binding site to physiological mechanism of cytochrome-c function at the mitochondrial membrane. This was beyond the scope of the present study, however. Our interest was in conducting the amide proton experiments using a proton free sodium ascorbate as the forward

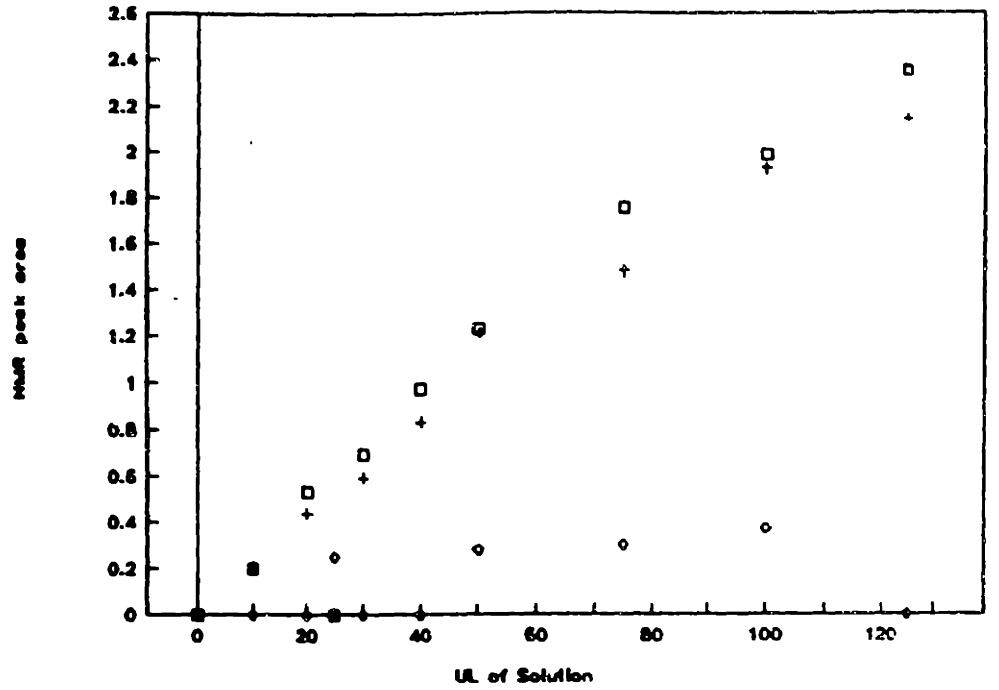

Figure 3.22 NMR peak intensity of HDO peak
Peak intensity of HDO peak (4.63 ppm) by addition of different amounts of concentrated ascorbate solution (+) and different amounts of D2O (◇).

transfer buffer, so as to avoid the complications introduced by the uneven distribution of protons.

3.2.4 Ascorbate Dehydration

The proton exchange kinetics in the reversed micelle were distorted by the presence of protons from the water molecules of the hygroscopic sodium ascorbate. The labile protons associated with the ascorbate were replaced with deuterium by repeated cycles of dissolving in D_2O and lyophilization. This process replaced almost all the exchangeable protons from the ascorbate with deuterium. It is this sodium ascorbate that will henceforth be referred to as "dry ascorbate". There was no change in the properties of the salt including its capacity as a reducing agent, as a result of this drying process. The dried salt was used subsequently in the transfer of cytochrome-c into the reversed micelles.

3.2.5 Proton Exchange with Dehydrated Ascorbate

As described earlier, amide proton exchange experiments were carried out in the reversed micelle for three different W_o. The unusual behavior of peaks was no longer observed. These protons exchanged rapidly in both aqueous solution and in reversed micelles. This suggests that the cause of the unusual exchange behavior was indeed the presence of protons inside the reversed micelles.

3.2.5.1 C_α - C_β Connectivities

In order to assign the amide proton peaks in the NMR spectrum using previous assignments, it was important to check for gross structural changes in the protein subsequent to back-extraction. Changes in the structure of the protein inside reversed micelles were expected to be reversible and hence the protein should have recovered its aqueous phase conformation upon back-extraction. Permanent changes in the protein structure would be reflected in shifted C_α-C_β connectivities of the protein backbone.

The chemical shift of the backbone protons depended to a large extent on the environment around it, which affected their resonance frequencies. If, subsequent to the back-transfer, the protein assumed a non-native conformation, the C_α region of the NMR spectrum would be altered compared to the native spectrum. The backbone C_α and C_β protons for cytochrome-c appear in the -3 to 5 ppm range. Figure-3.23a shows a typical protein spectrum in bulk aqueous (D_2O) solution. The resonance frequencies for the cytochrome-c protons were assigned at pH of 5.6 and 40°C by Wand et al., (1989).

Figure-3.23b shows the same region of the spectrum for a protein back-extracted from a reversed micellar phase. Most of the cross peaks of this spectrum are exactly superimposable over the D_2O spectrum. This indicates that there was no large scale conformational change in the back-extracted protein. Any changes in the protein structure inside reversed micelles must have been reversible, with the protein returning to almost native conformation after the back-transfer step. This was verified using UV-visible spectroscopy of the heme as discussed below. The amide protons associated with the missing or altered peaks are identified (Table 3.4) from the assigned resonances. It is interesting to note that all the edited peaks were those

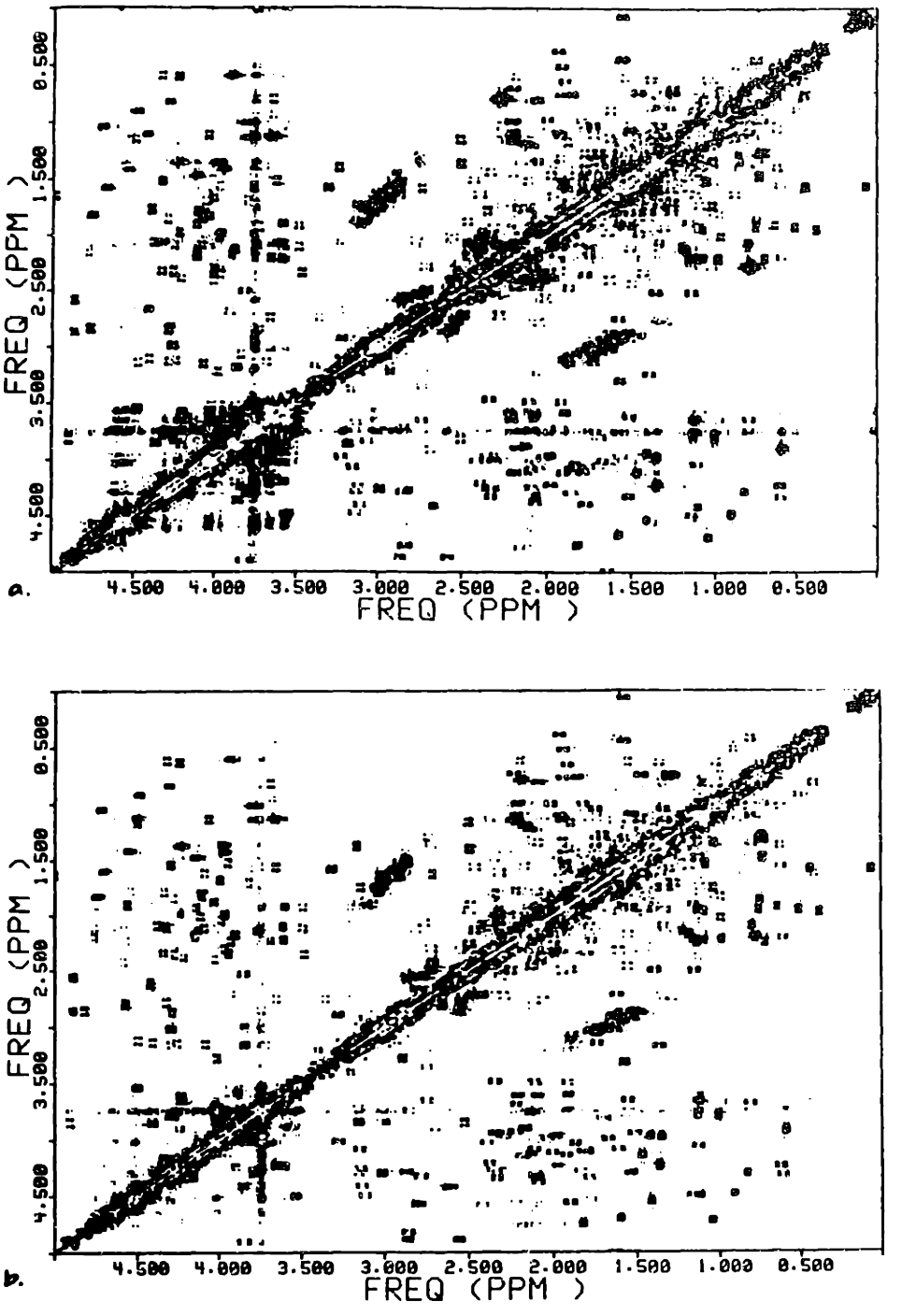

Figure 3.23 C_α-C_β connectivities of cytochrome-c
(a) in aqueous solution (b) in reversed micelle Wo 30.

for positively charged residues, and they belonged to the region where the secondary protein structure is low. Based on x-ray crystal structure, this region seems to have a random coil conformation which can be easily perturbed. The shift in the resonance frequency can also be caused by changes in the net charge in the region. The ionization of side chains, or surfactant binding, can alter the environment around these residues. It is unlikely that the charge on the side chain was different from in bulk aqueous solution as the pH of the solutions were fairly close. Surfactant binding to the positively charged side chains could change both the charge and the hydrophobicity around the residues.

Table 3.4 *Edited peaks in $C\alpha$–$C\beta$ connectivity*

Peak ID	Freq (t_1)	Freq (t_2)	Possible Peaks
G	4.570	2.812	Asn-54
F	4.421	2.450	Lys-60
J	4.324	2.786	Asn-70, Gly-84, Asp-96
H	3.841	2.997	His-33
K	3.278	2.891	Phe-36
I	3.164	1.371	Lys-22
E	4.561	1.898	Gln-42

AOT contamination of the back-extracted protein can also be assessed based on the C_α-C_β connectivity information. The surfactant molecule (AOT) has a large number of CH_2 and CH_3 groups, the resonance frequencies of which fall in the 0-5 ppm region. Very small concentrations of the surfactant (about 1 surfactant in 10 protein molecules) can be detected from the crosspeaks in this region. Figure 3.23b shows no AOT peaks at all, indicating that the surfactant concentration in the solution was extremely low. This is consistent with the extremely low solubility of AOT under

high salt concentrations (1M). It can be concluded that no surfactant molecules were back extracted along with the protein.

The conservation of most of these connectivities suggest that the conformation of the protein molecule is regained upon back extraction. Additional evidence is provided by CD and visible spectra of the heme group after back extraction. Therefore, changes in the proton exchange rate must now directly reflect on the protein structure within the reversed micelle.

3.2.5.2 Proton Exchange

The intensity of the amide protons of the different residues has been followed as a function of time, both in aqueous solution and in reversed micelles of 3 different sizes. The amide proton exchange behavior of the different residues will be discussed in the sections to follow.

3.2.5.2.1 *N - Terminal Helical Region*

Residues 7 to 15 form the N-terminal helix. Ile-9, Phe-10 and Val-11 are hydrogen bonded to Gly-6, Lys-7, Lys-8 respectively. The exchange rates of Ile-9 in aqueous solution and in the reversed micelles are almost identical (Figure 3.24a). The amide proton of Val-11 exchanges slightly faster in reversed micelles (all W_os) but there is no dramatic change in the exchange rate (Figure 3.24b). However Phe-10 which is on the hydrophobic face of the N-terminal helix displays a dramatic increase in exchange rate (Figure 3.25). In aqueous solution, Phe-10 is one of the extremely slow exchanging amide protons. However, in the reversed micelle, the exchange rate is increased by about three orders of magnitude. It is unlikely that the conformation of the helix is altered in such a way that only the hydrogen bonding between Phe-10

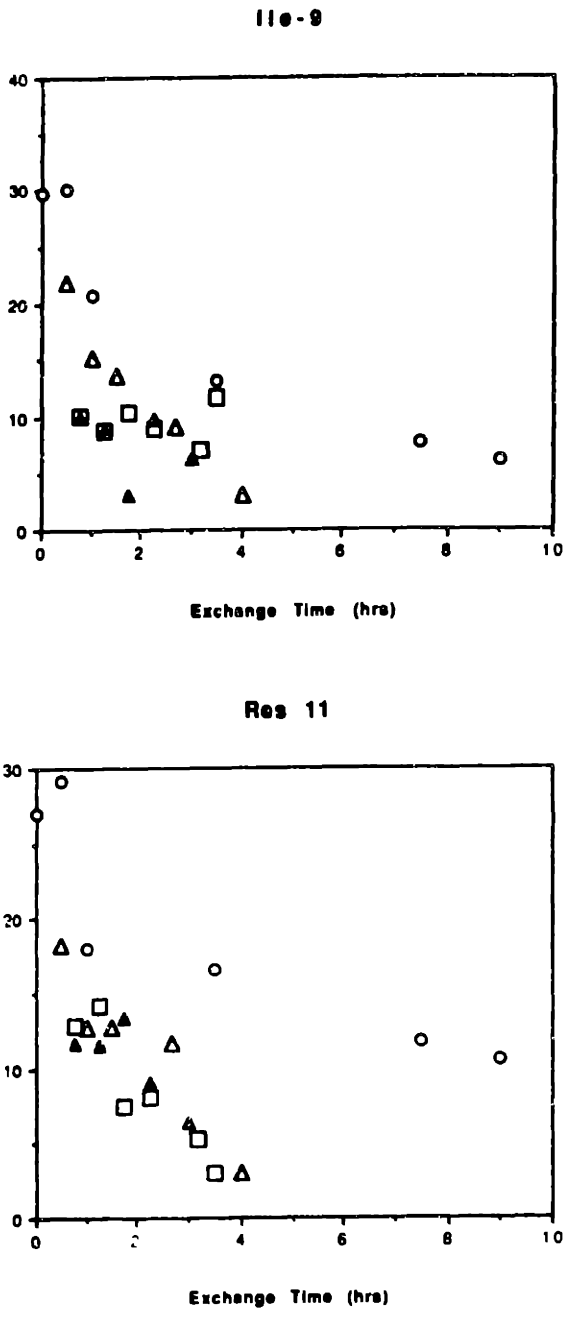

Figure 3.24 Amide proton exchange in reversed micelle - I
NMR peak intensity of (a) Ile-9, (b) Val-11, as a function of exchange time in aqueous solution (O), and in reversed micelle of Wo 50, (□) Wo 30 and (Δ) Wo 20 (▲).

and Lys-7 is broken with the other hydrogen bonds intact. Increase in solvent accessibility of the otherwise buried Phe-10 can however, explain this behavior. This suggests that the helical structure is not disrupted, but the orientation of the helix is altered, thereby changing the solvent accessibility. This in turn causes a increase in the exchange rate to match the exchange rate of other exposed surface residues in this region.

The size of the reversed micelle does not affect the exchange rates significantly, although previous studies (Vos et al., 1987) and CD data (section 3.2.6) indicate that the structure of cytochrome-c is dependent on the reversed micellar size. The experimental scatter on the amide proton data make it difficult to interpret the effect of reversed micellar sizes on cytochrome-c structure.

The exchange rate of Lys-13 in reversed micellar solutions is almost exactly identical to the exchange rate in aqueous solution (Figure 3.26a). However, the amide protons of Cys-14, one of the heme ligand, exchanges more rapidly in reversed micelles compared to aqueous solutions (Figure 3.26b). The increase in the exchange rate is of similar magnitude to that of Phe-10. The exchange behavior of the amide protons coincides with the periodicity of the helix, of about 4 residues. Residues 9 and 13 are unaffected in reversed micelle, while residues 10 and 14 demonstrate a increase in exchange rate. The porphyrin group of the heme is covalently attached to cysteines 14 and 17. In addition His-18 and Met-80 donate a lone pair of electron to the iron. The exchange rate of Cys-17 in aqueous solution is extremely fast and hence this residue is not a good structural probe. However, His-18 exchanges slowly in aqueous solution and the exchange rate is increased in the reversed micellar solution (Figure 3.26c). This clearly indicates that the hydrogen bonds in the N-

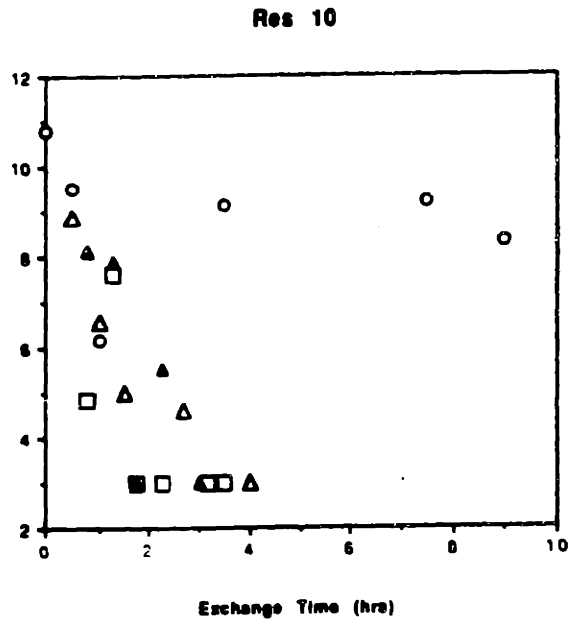

Figure 3.25 Amide proton exchange in reversed micelle - II
NMR peak intensity of Phe-10 as a function of exchange time in aqueous solution (O), and in reversed micelle of Wo 50, (□) Wo 30 and (Δ) Wo 20 (▲).

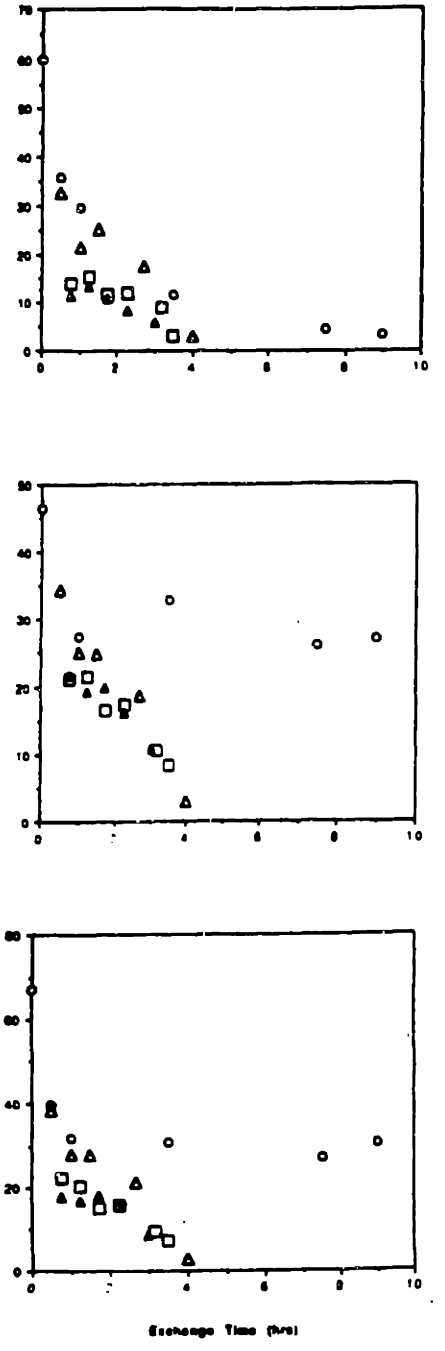

Figure 3.26 Amide proton exchange in reversed micelle - III
NMR peak intensity of (a) Lys-13, (b) Cys-14, (c) His-18 as a function of exchange time in aqueous solution (O), and in reversed micelle of Wo 50, (□) Wo 30 and (Δ) Wo 20 (▲).

terminal helix are not broken but the solvent accessibility of the hydrophobic face of the helix is altered.

This change in the environment of the helix is probably due to the interaction of the tail groups of the surfactant with the hydrophobic core of the heme. The hydrophobic interaction between the tail group of AOT and the heme could cause a reorientation of the N-terminal helix to provide greater solvent accessibility. This change in the heme environment is clearly reflected in the changes in the absorption spectra of the heme group. The slow time scales for these changes might be due to the covalent linkage between the heme and Cys-14 holding the n-terminal helix in place.

This increase in the amide proton exchange rates is consistent with the change in the solvent accessibility of the N-terminal helical region. Since Phe-10, Cys-14 and His-18 fall on the same side of the α-helix, they are also hydrogen bonded to each other. Disruption of structure in this region could break all these hydrogen bonds and cause increase in exchange rate. However the exchange rates of residues on the other side of the helix do not change in reversed micelles suggesting no change in overall hydrogen bonding network. It can therefore be concluded that the solvent accessibility of the N-terminal helix is increased inside the reversed micelle.

3.2.5.2.2 *Other Residues*

The 60s helix extends between 60 to 69 and runs along a face of the heme group. The shortness of this helix makes it very easy for the end to unwind due to thermal motion. This helix is very flexible and hence most of the amide protons exchange out in aqueous solution. Residues Leu-68 and Glu-69 exchange slowly in bulk aqueous solution. In reversed micelles, residues 68 and 69 exchange much faster

than in bulk aqueous solution. The exchange rate in all the three reversed micelles seems to be increased by about two orders of magnitude (Figure 3.27). This increase in exchange rate could be a result of the increased solvent accessibility in the residues close to the heme or due to disruptions in the hydrogen bonding. As before, the size of the reversed micelles does not play a role in determining the exchange behavior. The 50s helix and the 70s helix are very small and dynamic. The amide protons of these residues are completely labelled in bulk aqueous solution and hence it is not possible to monitor changes in their conformations.

3.2.5.2.3 *C - Terminal Helix*

The residues of the C-terminal helical region of the protein form a very tight right handed α-helical structure. The helix extends form Residue 88 to 101. The amide protons in the beginning and the end of the helix exchange out rapidly because of the high flexibility of these residues. The middle section of the helix, however, is extremely rigid and tightly hydrogen bonded in aqueous solution. These amide protons (Res 94 to Res 99) exchange very slowly with a time constant in excess of 100 hours. In reversed micelles, these protons, however are completely labelled with deuterium in a much shorter time. Figures 3.28A to C show the exchange behavior of these amide protons. It can be seen that the exchange rates of all the amide protons of the C-terminal helix are enhanced by more than 3 fold and the protons are completely labelled within the first 6 hours. Unlike the N-terminal helix, there is no difference in the exchange behavior between the hydrophobic and the exposed face of the C-terminal helix. Hence, the hydrogen bonds that stabilize this helix must be broken in a reversed micellar environment, leading to unfolding of the helical structure.

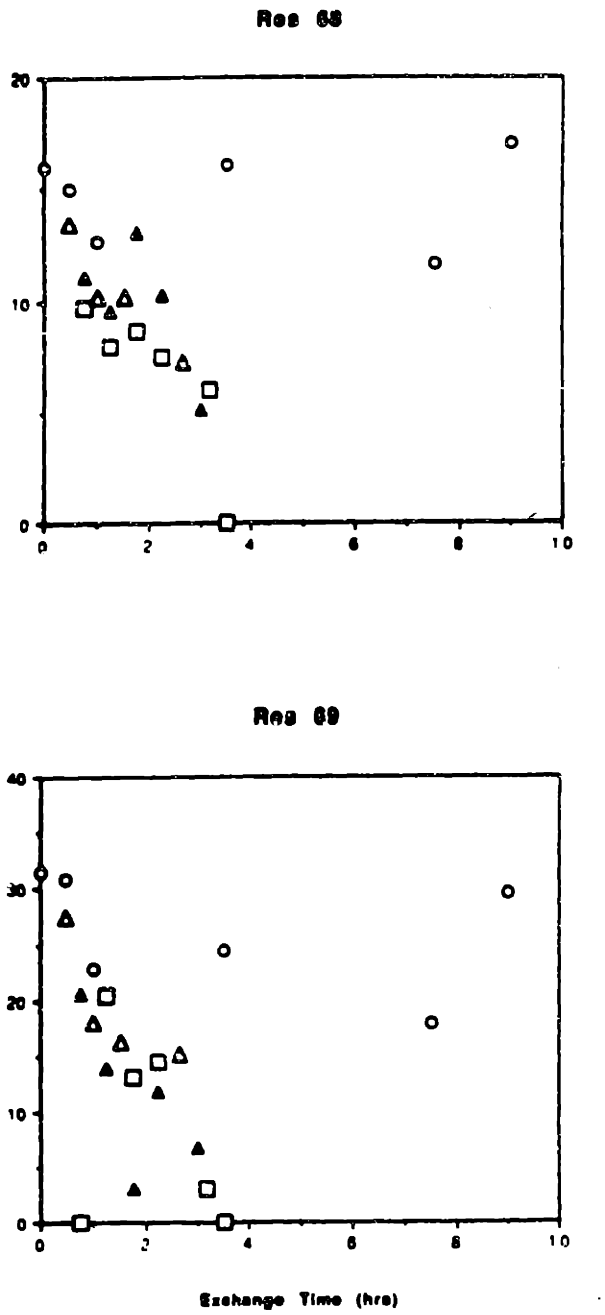

Figure 3.27 Amide proton exchange in reversed micelle - IV
NMR peak intensity of (a) Leu-68, (b) Glu-69, as a function of exchange time in aqueous solution (O), and in reversed micelle of Wo 50, (□) Wo 30 and (Δ) Wo 20 (▲).

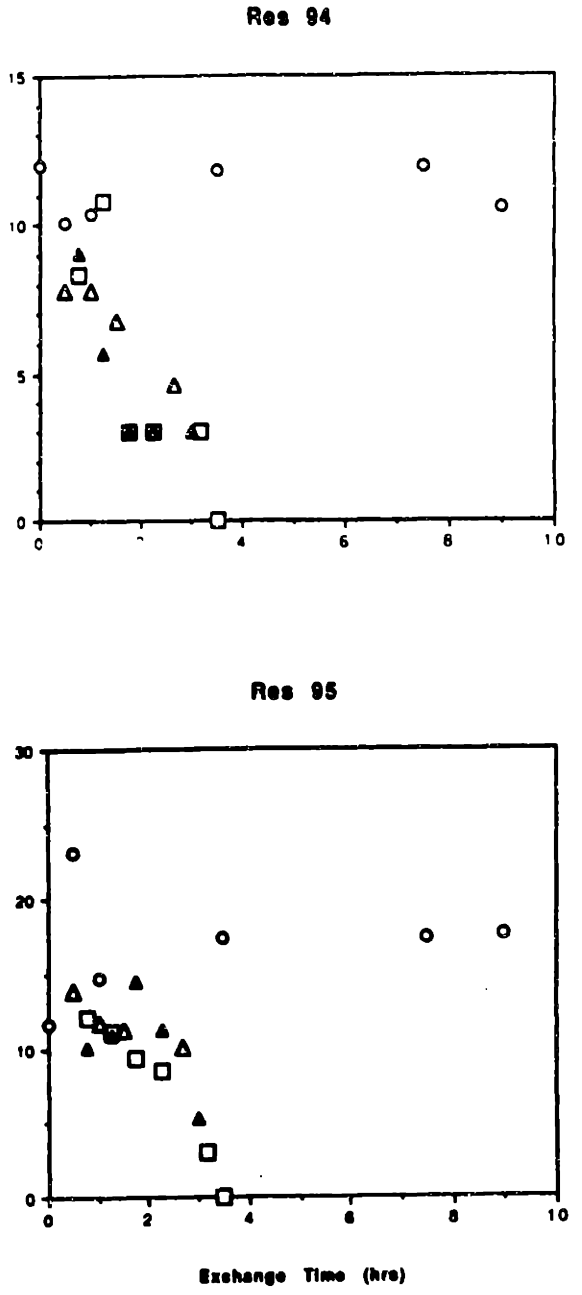

Figure 3.28 A Amide proton exchange in reversed micelle: C-terminal helix
NMR peak intensity of (a) Leu-94, (b) Ile-95, as a function of exchange time in aqueous solution (O), and in reversed micelle of Wo 50, (□) Wo 30 and (Δ) Wo 20 (▲).

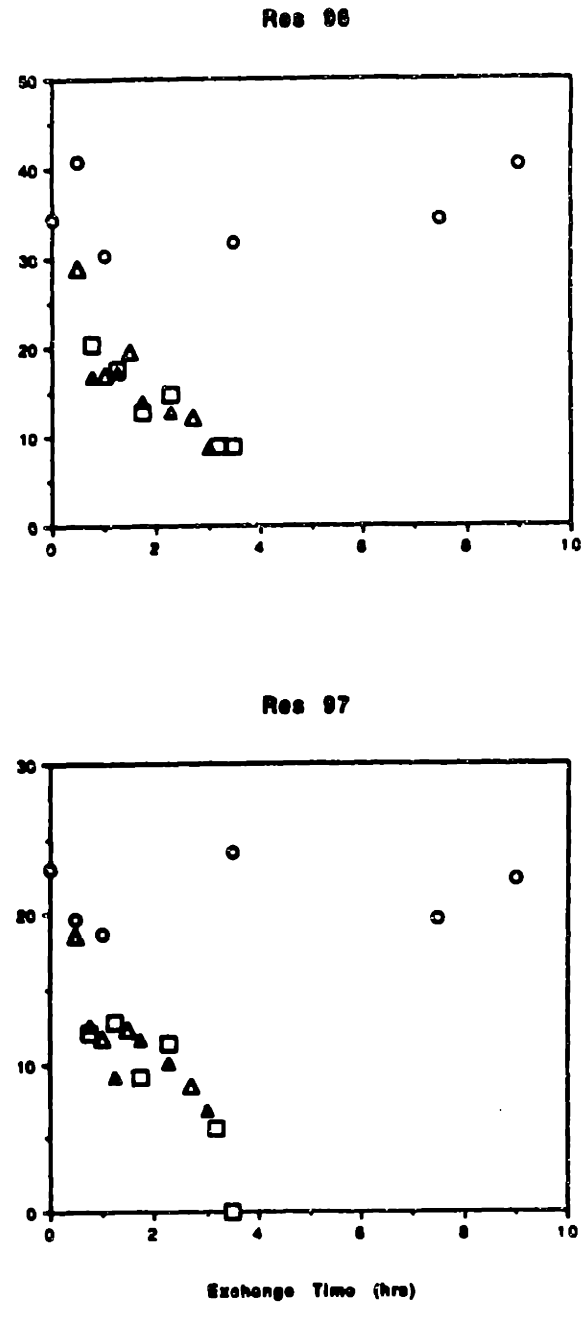

Figure 3.28 B Amide proton exchange in reversed micelle: C-terminal helix
NMR peak intensity of (a) Ala-96, (b) Tyr-97, as a function of exchange time in aqueous solution (O), and in reversed micelle of Wo 50, (□) Wo 30 and (Δ) Wo 20 (▲).

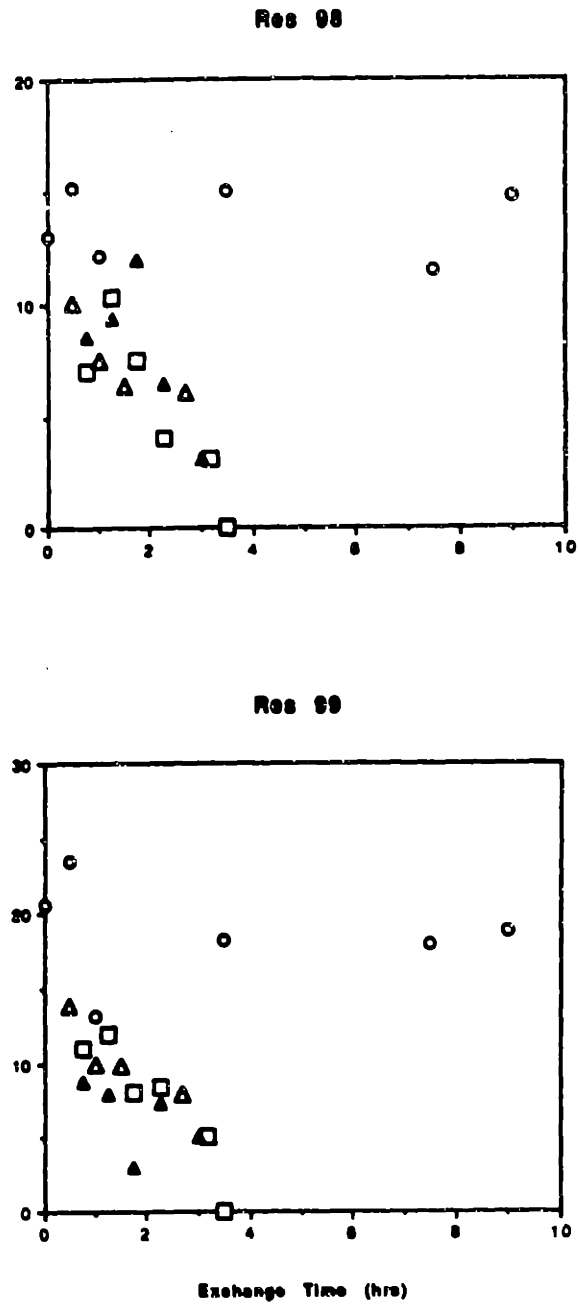

Figure 3.28 C Amide proton exchange in reversed micelle: C-terminal helix
NMR peak intensity of (a) Leu-98, (b) Lys-99, as a function of exchange time in aqueous solution (O), and in reversed micelle of Wo 50, (□) Wo 30 and (Δ) Wo 20 (▲).

The amide proton intensity, as a function of time is almost identical in the C-terminal and the N-terminal regions of the protein inside the reversed micelle. The three dimensional structure of cytochrome-c inside reversed micelle is disrupted, as evidenced by CD studies. The helical content in the protein decreases dramatically within six hours in the reversed micelle. Almost all the amide protons, would therefore have exchanged by this time. The NMR proton peak intensities therefore approach zero by the end of six hours in the reversed micelle. Therefore, the actual proton peak intensities or the exchange rates should not be compared. The ratio of the exchange rate in reversed micelle to that in aqueous solution would therefore indicate that in the N-terminal helical region, one face of the helix exchanges almost as in aqueous solution, while the hydrophobic face of the helix has a dramatically increased exchnage rate. However, for the C-terminal helix, the ratio of exchange rates is very high for all the residues here, indicating disruption of structure. Molecular modelling studies (section 3.2.8) suggest that the electrostatic interactions with the micellar wall can cause unfolding of the C-terminal helical region.

The amide proton exchange results suggest that the C-terminal helical region is the one that interacts strongly with the micellar wall. The other side of the protein comprising the N-terminal helix does not undergo large disruption in structure and seems to be immersed in the solvent. The orientation of the protein within the reversed micelle can then be inferred from this data. The C-terminal face of the cytochrome-c is oriented towards the interface, with the N-terminal region towards the core of the micelle. In addition, hydrophobic interactions between the surfactant molecule and the heme group probably disrupt the non polar packing around the heme group, leading to denaturation of the protein over long time periods.

3.2.6 CD Studies

Amide proton exchange studies indicate that the conformation of the protein is significantly altered in the reversed micellar state. The heme group of the protein is stabilized by 5 α-helices surrounding it. The absence of any secondary structure in the protein other than α-helix makes it feasible to use circular dichroism to monitor the change in the protein structure within the reversed micelle.

The UV region of the circular dichroism spectrum of cytochrome-c in aqueous solution exhibits the characteristic a-helical spectrum (Figure 3.29). The negative ellipticity bands at 222 and 231 nm are characteristic of the α-helical structure (Chapter 2). Figure 3.30 shows the CD spectrum of cytochrome-c in AOT-isooctane reversed micelle with W_o of 50. The CD profile of the protein at short times (30 min.) in the reversed micelle is identical to the spectrum in aqueous solution. This would suggest that the conformational changes in the protein are minimal in the reversed micellar environment and hence, the amide proton exchange rates should not be affected. However, amide proton exchange rates indicate that the protein structure is altered significantly inside the reversed micelle, leading to complete exchange by about 6 hours. This suggests a change in the protein structure at longer times in the reversed micelles. CD spectra of the protein solubilized in reversed micelles for longer times (> 30 min) indicate that the secondary structure of the protein is altered as a function of time. The helical content of the protein seems to decrease with increasing residence times in the reversed micelle. When the protein is solubilized in the reversed micelles for about 6 hours, there is almost a total loss of secondary structure.

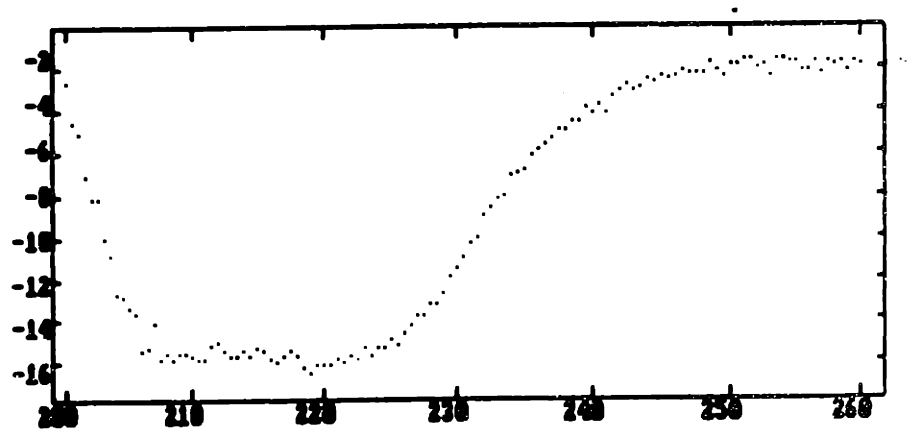

Figure 3.29 Circular Dichrosim of Cytochrome-c in aqueous solution

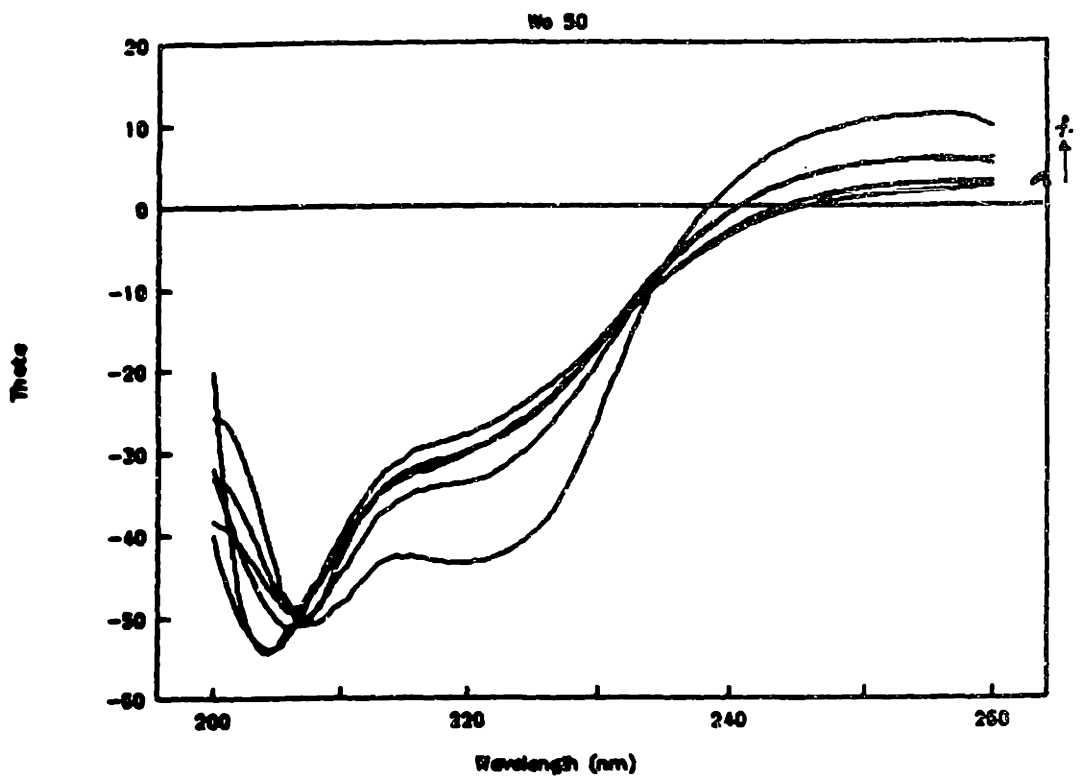

Figure 3.30 Circular Dichrosim of Cytochrome-c in Reversed Micelle
Helical content of protein measured as a function of time in
AOT-isooctane reversed micelle of Wo 50, (a) 15 min to (f) 375 min in intervals of 60 min.

This slow transition of the protein conformation with time in reversed micelle is unexpected. When exposed to the reversed micellar environment, the protein should adopt a new conformation extremely rapidly as the time scales for molecular motions are of the order of femtoseconds. Protein dynamics studies indicate that the protein achieves an equilibrium conformation within about 100 picoseconds when exposed to a non-native environment. One would therefore expect the protein to reach an equilibrium conformation within the reversed micelle rapidly and the amide proton exchange would then be a simple exponential with a rate constant as defined by the new conformation.

When the protein is solubilized in a smaller reversed micelles, the conformational change that the protein undergoes seems to be less drastic. Figure 3.31 shows the CD spectra of cytochrome-c in AOT-isooctane reversed micelle with W_o of 30 and 20. The deviation of the protein from its aqueous structure is much less pronounced for a smaller micelle. This is in agreement with earlier observation on the structure of Zn porphyrin cytochrome-c in AOT-isooctane reversed micelles (Vos et al., 1987) and the ascorbate reducibility experiments (Brochette et al., 1988). Enzymes have also been observed to exhibit aqueous conformations at smaller reversed micelles (section 3.1) although the properties of the solubilized water are closer to bulk water properties at large W_o. For an interfacially active protein like cytochrome-c, this might be due to the change in the curvature of the interface. A larger reversed micelle has a correspondingly larger radius of curvature. A protein buried in the interface, therefore experiences stress from packing of the tail groups with this large radius of curvature. It is possible that these stresses disrupt the balance of forces in the protein molecule causing it to unfold.

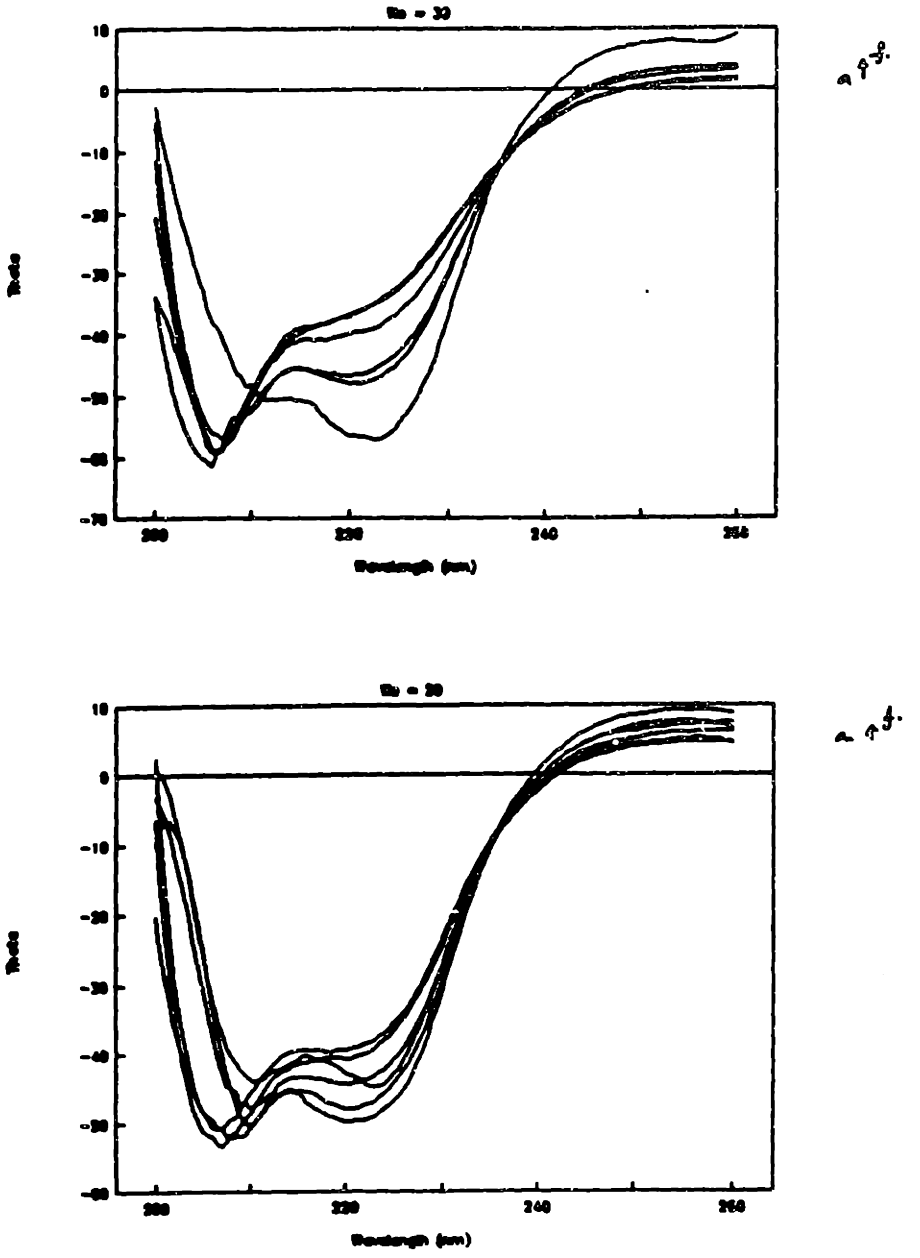

Figure 3.31 Circular Dichrosim of Cytochrome-c in Reversed Micelle
Helical content of protein measured as a function of time in
AOT-isooctane reversed micelle of (i)Wo 30 and (ii) Wo 20,
(a) 15 min to (f) 375 min in intervals of 60 min.

3.2.7 UV / Visible Spectroscopy

In neutral pH aqueous solutions, cytochrome-c is characterized by a weak absorption band at 695nm, the Q bands of the heme (520-550 nm) and the 406nm Soret band (Figure 3.32). The Soret bands of the reduced protein is a doublet at 519 and 549nm. The oxidized protein shows a strong absorption at 539nm. AOT or isooctane do not show any absorption bands in the visible region and sodium ascorbate does not absorb in the region of the heme absorption.

The absorption spectra of cytochrome-c in AOT-isooctane reversed micelles at short times after transfer into reversed micelles is identical to the spectrum in aqueous solution (Figure 3.33). However, as the time in the reversed micelles increase, the intensity of the peaks decrease and the peaks start to merge. The absorption spectrum changes from a doublet to a single peak of much less intensity centered at 439nm. It is tempting to attribute this spectral decay to a change in the heme oxidation state from the reduced to the oxidized state. However, the 695nm absorption band that is characteristic of the oxidized protein is absent in the reversed micellar case. The electronic environment around the heme seems to be altered in a dynamic fashion, with almost a total denaturation after about 6 hours. This time scale of denaturation is in agreement with the time scale obtained from both CD measurements and proton exchange data.

The change in the structure of the protein around the heme group seems to be reversible. Figure 3.34 shows the Soret bands of the protein after back extraction to the aqueous phase. There is a loss in the intensity of the peaks but they exhibit no shift in the absorption maxima. This indicates that the conformation in the

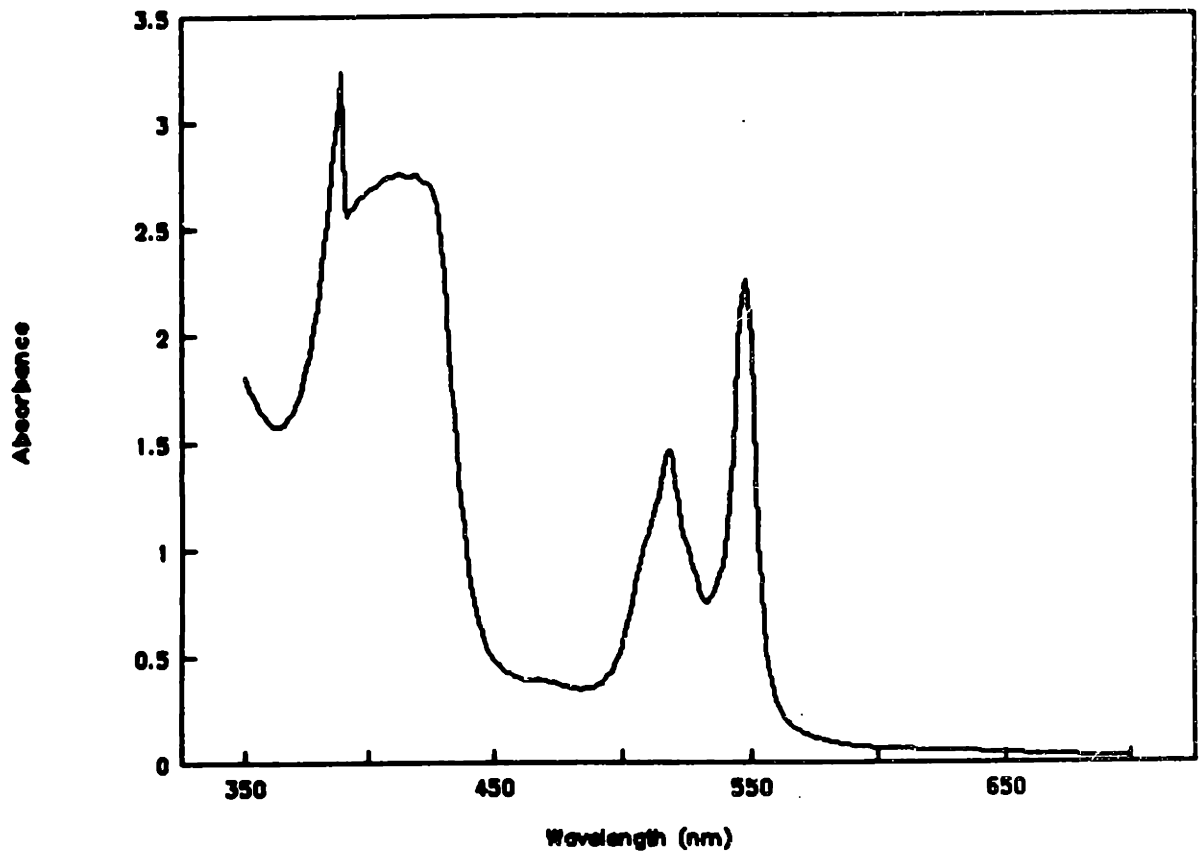

Figure 3.32 Absorption spectrum of Cytochrome-c in Aqueous solution

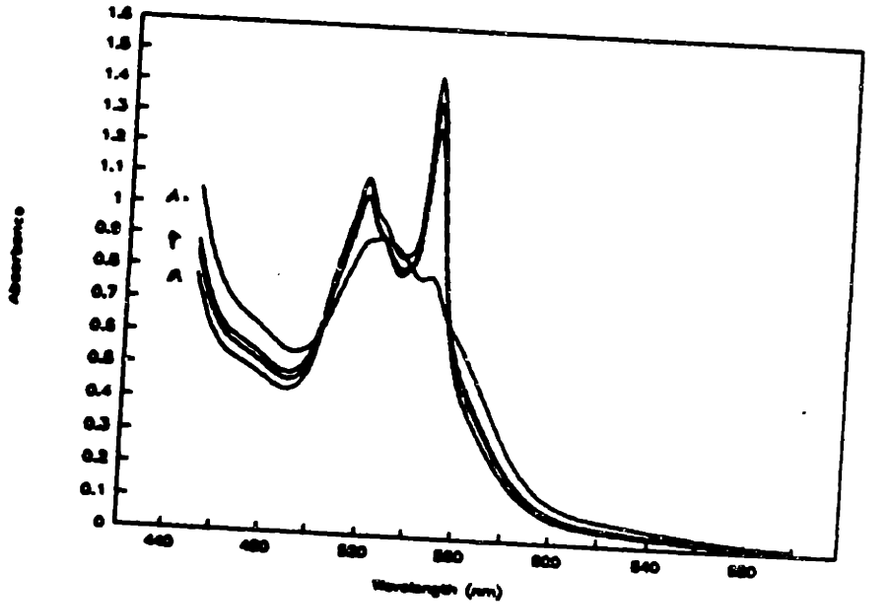

Figure 3.33 Absorption spectrum of Cytochrome-c in Reversed Micelle
Visible absorption spectra of cytochrome-c for different times in AOT-isooctane reversed micelle. (a) 30 min, (b) 60 min, (c) 180 min, (d) 360 min.

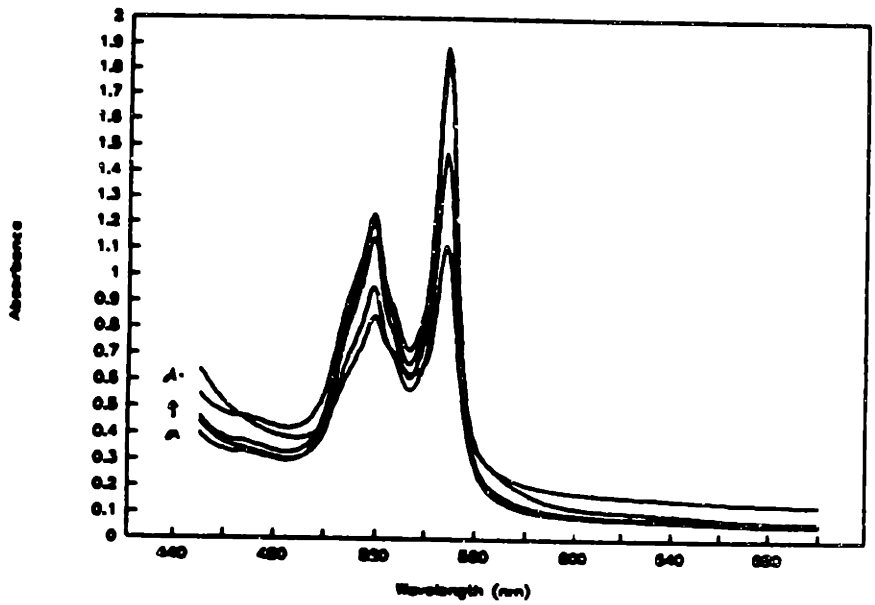

Figure 3.34 Absorption spectrum of Cytochrome-c after back extraction
Visible absorption spectra of cytochrome-c after back extraction from AOT-isooctane reversed micelle of Wo 30. Residence times in the reversed micelle: (a) 30 min, (b) 60 min, (c) 180 min, (d) 360 min.

proximity of the heme group is almost completely restored upon back extraction to the aqueous phase. The loss in intensity can be attributed to a loss in the amount of protein back extracted from the reversed micelles with increasing residence time.

The protein conformation inside the reversed micelle seems to be altered extensively, especially at longer residence times in the reversed micelles. However, cytochrome-c seems to regain its native structure upon back extraction to the aqueous phase indicating that the changes in conformation inside the reversed micelle are temporary and reversible. The nature of the protein and the time it spent inside the reversed micelle determine the extent of reversibility of conformation change. Cytochrome-c, at very long times in the reversed micelle (~ 24 hours) is completely denatured and bound tightly to the reversed micellar phase. The amount of protein extracted back to the aqueous phase with a 1M salt buffer is negligible. This indicates that the ionic interactions between the head group of the surfactant and the protein are no longer important. Instead, the hydrophobic interaction between the surfactant tails and the heme group in the core of the protein seems to dominate.

3.2.8 Molecular Model

The interaction between cytochrome-c and AOT-isooctane reversed micelles seems to be governed by a combination of forces. Although ionic interactions between the head group of the surfactant and the surface lysines of the protein are important, hydrophobic interactions also seem to play an crucial role in stabilizing the protein in the reversed micelle. The interplay between these forces determines the three dimensional structure of the protein and hence its function.

Molecular modelling studies can be used to understand the effects of the non-aqueous environments on the structure of the protein. By a combination of energy minimizations and simple dynamics studies, the structure of the protein under the influence of different force fields can be calculated. The force fields can either be incorporated into the energy equation as an additional energy term or can be mimicked using poly amino acids.

The computational intensity of these calculations depends exponentially on the number of atoms used in the simulation. The three dimensional structure of the protein is stabilized by interaction between all the residues of the protein. However, it is possible to simulate the specific effects at different sites of the protein by considering the amino acids that directly interact with this site. Using peptides that represent the site of interest in the protein, therefore, is a very good first approximation to study the effect of non-native environments on the protein conformation.

The starting point for these calculations is the coordinates from the three dimensional structure of the protein. When the crystal structure is not available, it

is possible to guess a possible conformation and then using energy minimizations and dynamics, arrive at a low energy conformer (Chapter 2). The crystal coordinates for atoms of cytochrome-c have been solved to a resolution of within 2 A (Takano and Dickerson, 1981). The entire protein was used to visualize the effects of the reversed micellar environment on the different sites of the protein. Information on the proximity of residues in the folded structure of the protein can help in the interpretation of the proton exchange data. In addition, energy calculations can be used to understand the effects of ionic forces on the protein structure. Hydrophobic forces, however are more difficult to quantify by a simple mathematical equation. They can be accounted by solvating the entire molecule and then minimizing the interaction energies of the side chains with water. The number of atoms involved in the calculation when the protein molecule is solvated becomes prohibitively high.

The C-terminal peptide of cytochrome-c was used for the calculations in this study. The residues from 88 to 101 form a tight α helix as seen from the crystal structure. The energy of the peptide was minimized starting from an α-helical structure. The peptide conformation did not deviate from the starting α-helical structure (Figure 3.35). AOT molecule was built using the ChemDraw software and imported into the molecular modelling. The energy parameters for the AOT molecule were generated using default values and the AOT conformation minimized. The peptide was then docked to the AOT molecule from different orientations. A subsequent energy minimization of 250 steps of steepest gradient followed by 300 steps of Newton Raphson minimization was performed, allowing both the peptide and AOT molecule to move.

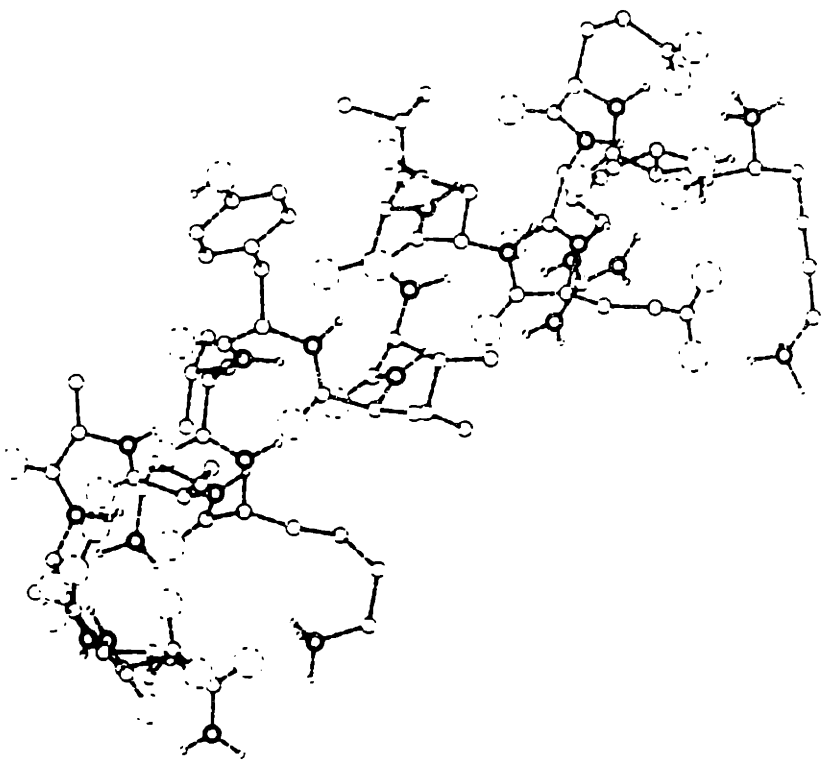

Figure 3.35 α-helical conformer of C-terminal peptide

Extensive rearrangement of the hydrogen bonding, now involving the head group of the surfactant molecule seems to cause destabilization of the helix backbone (Figure 3.36). The hydrogen bonds that stabilize the helix are broken and reformed with the carbonyl oxygen of the AOT head groups. This results in an extension of the helical peptide.

The ionic interactions between the head group of AOT and the peptide can better be simulated by considering a wall of negative charge. An extended poly-glutamic acid chain was docked to the peptide from different orientations. The energy of the complex was then minimized as described before. The first few residues of the C-terminal helix are positively charged and hence attracted towards the interface. The last few residues of this helix are acidic and hence are negatively charged at this pH. The tail of the helix, therefore helix experiences a strong electrostatic repulsion from the micellar wall. This results in the helix being stretched out causing it to unfold. The hydrogen bonds within the helix are completely disrupted (Figure 3.37). As a result, these protons would now exchange much more rapidly.

Molecular modelling studies indicate that the electrostatic forces between the AOT head groups and the charges on the C-terminal peptide are primarily responsible for the structural perturbation. The experimentally observed increase in the amide proton exchange rates lead us to believe that the C-terminal helix is the probable site of interaction of the protein with the AOT interface. Also the amide exchange behavior of the residues in the N-terminal helix indicate that this end of the protein does not interact with the AOT interface as strongly. This provides us with a picture of the overall orientation of the protein inside the reversed micelle. More rigorous calculations would provide little additional information as hydrophobic

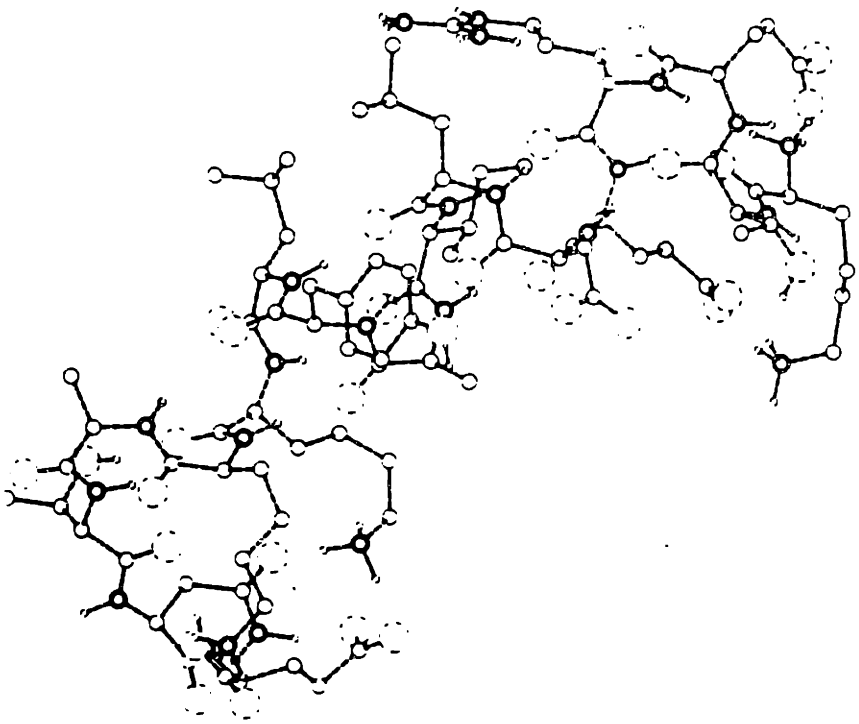

Figure 3.36 C-terminal peptide in presence of AOT
Molecular modelling studies on C-terminal peptide in presence of AOT.

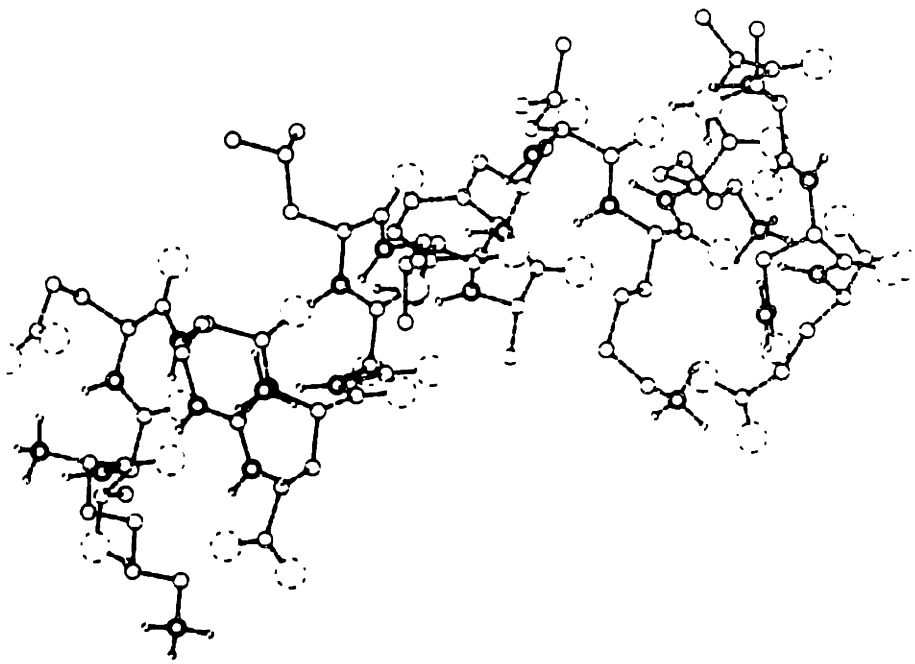

Figure 3.37 C-terminal peptide in presence of Poly-glutamic acid
Molecular modelling studies on C-terminal peptide in presence of poly-glutamic acid to mimic electrostatic interactions.

interactions haven't been accounted for. It is expected that hydrophobic interactions play an important role in the stabilization of protein in the reversed micelle.

3.3 Conclusions

1. Amide proton exchange coupled with 2-D NMR is a powerful technique to determine site-specific changes in the protein structure, as demonstrated here with cytochrome-c in reversed micelle.

2. The structure of cytochrome-c in AOT-isooctane reversed micelles was disrupted, specifically after about 4 hours. Information regarding the effect of the size of the reversed micelle on cytochrome-c structure was lost because of the slow unfolding of the protein molecule inside the reversed micelle.

(i) The amide proton exchange rate at one of the hydrophobic faces of the N-terminal helix seems to be increased dramatically. The solvent accessibility of the N-terminal helical region probably increases in the reversed micellar environment. The hydrogen bonds of this helix, however, seem to be conserved.

(ii) The C-terminal helix of cytochrome-c seems to be completely disrupted in the reversed micelle. The amide proton exchange rate of the residues in the C-terminal helix increases dramatically in the reversed micellar state.

(iii) The protons associated with the ascorbate used for the forward transfer seem to distribute unevenly in the vicinity of the protein molecule, resulting in unusual exchange behaviors.

3. Circular dichroism studies of cytochrome-c in reversed micelles indicates a loss of helical structure in a time range consistent with the amide proton exchange results. The protein retains its helical structure at short times inside the micelle; however, after about 6 hours, the helical structure is almost completely lost. This loss in helical structure is limited for a smaller reversed micelle in the case of cytochrome-c.

4. The absorption of the Soret bands of the heme group clearly confirms the change in the environment in the vicinity of the heme group when cytochrome-c is incorporated in the reversed micelle. The change in the absorption profiles is consistent with the time scales observed with both CD and amide proton exchange experiments. The protein seems to regain its original aqueous solution structure when back extracted to an aqueous phase.

Chapter 4

Protein Proteoglycan Interactions

Heparin, one of nature's most acidic polysaccharide seems to play an important role in modulation of biological events. The interaction of proteins with heparin is investigated. Peptide models for heparin binding regions of two systems - heparinase-I and HBEGF, were used to characterize this interaction. Biochemical and biophysical characterization of the peptides and heparin provide information on heparin-peptide interaction at a molecular level.

4.1 Background

4.1.1 Introduction

Acidic polysaccharides are complex biopolymers which play both a structural and functional role in microorganisms, plants, and animals. In plants, the acidic polysaccharides, pectins and pectates, provide structural basis for the maintenance of physical shape and also form a protective barrier against the environment. The complex polysaccharides in microbial cells are associated with the cell wall integrity. The animal acidic polysaccharides are found linked to what are called core proteins and hence called proteoglycans. When these long polymeric chains are dissociated from the core protein and fragmented, they are called glycosaminoglycans. Glycosaminoglycans (GAG) constitute a characteristic disaccharide repeating unit - an amino sugar (D-Glucosamine or Galactosamine) and a uronic acid, typically L-iduronic acid or D-glucuronic acid. The disaccharide unit is N- and O-sulfated in a variable manner (Lundbald et al., 1981).

Proteoglycans are predominantly found in the extra cellular matrix (ECM) and cell surface and are involved in the adhesion of the cell to the extracellular matrix (Figure 4.1). Glycosaminoglycans are a part of the structural backbone of the ECMs. GAGs also interact with other key proteins of the extracellular matrix, such as laminin, fibronectin, and collagen, and define the physiological properties of the matrix. They also interact with an array of cytokines, like growth factors, by facilitating their biochemical interaction with the receptors and by protecting them

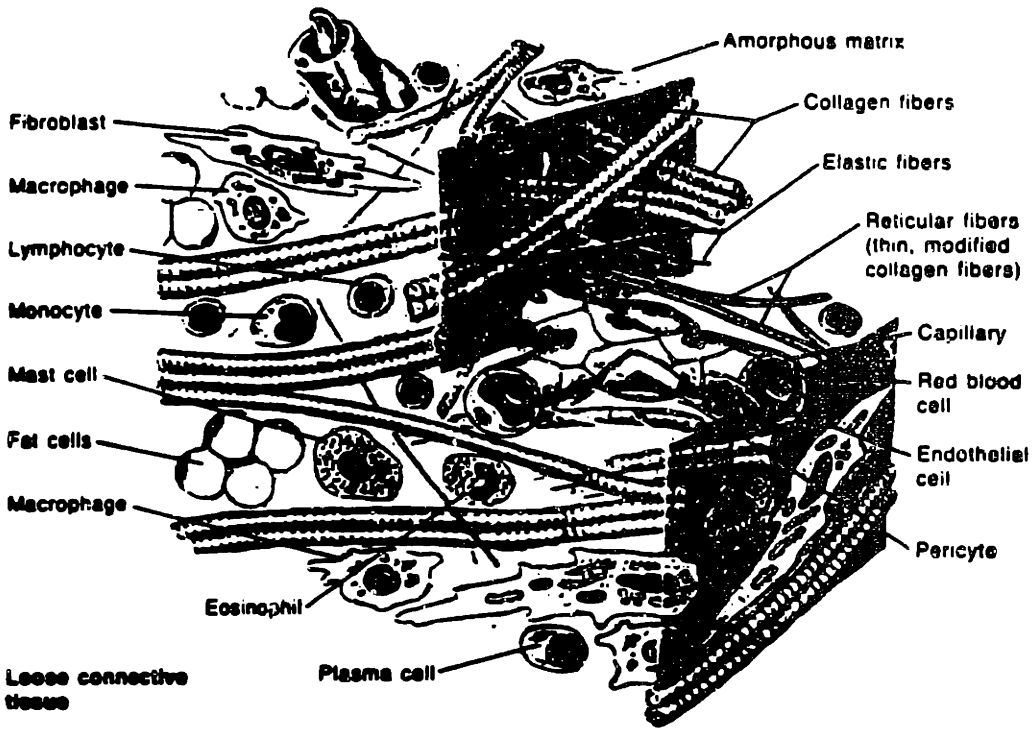

Figure 4.1 Proteoglycans in the extracellular matrix (ECM)

from proteolytic degradation. In addition to the tissue level role, GAGs seem to be involved in the cellular level events like modulation of gene expression. GAGs have been shown to interact with and regulate the function of transcription factors affecting gene regulation in some tissues (Busch, et al., 1991).

The role of GAGs and the mechanism of their interaction with different biological macromolecules is not well understood, partly because the primary sequence of the oligosaccharide is not known. In addition, the sulfation of the backbone does not seem to follow any clear pattern. This heterogeneity of the oligosaccharide chain has often resulted in the belief of a non-specific interaction of GAGs with other biological macromolecules. However, unique heparin oligosaccharides, as small as a pentamer, show structural specificity with regard to the proteins with which they interact (Rosenfeld and Danishefsky, 1986). The proteins appear to bind to these oligosaccharides through certain characteristic amino acid sequences (Cardin et al., 1989).

4.1.2 Structural Properties of Acidic Polysaccharides

The animal acidic polysaccharides, as mentioned earlier, are commonly associated with core proteins and are composed of alternating hexosamine and uronic acid residues. There are three classes of glycosaminoglycans (Sasisekharan, 1991):

Class I is the glucosamine or galactosamine (H), in the β form, linked to iduronic (I) or glucuronic (G) acid through the 3 position of the amino sugar. There are three examples of this class:

Hyaluronic acid [G β (1,3) - H β (1,4) ; Glc A linked to GlcNAc]

Chondrotin sulfate [G β (1,3) - H β (1,4) ; GlcA linked to GalNAc-(4 or 6)-SO_4]

Dermatan sulfate [I α (1,3) - H β (1,4) ; Ido A linked to GalNA-4-SO_4]

Class II GAGs have a glucosamine (H) in the α form, which can either be acylated or sulfated on the amino group and is sometimes sulfated at the 6 position. The glucosamine is linked to an iduronic (I) or glucuronic (G) acid through the 4 position of GlcN. There are two examples in this class: { H is α sugar and the linkage is I α (1,4) - H α (1,4) or G β (1,4) - H α (1,4)}

Heparin : high (IdoA/GlcA) ratio and high degree of sulfation.

Heparan Sulfate: low (IdoA/GlcA) ratio and low degree of sulfation.

Class III GAGs have a galactose linked to a glucosamine (β form), with some degree of sulfation of both the Gal and GlcNAc residues:

Keratan Sulfate: low degree of sulfation on both Gal and GlcNAc residues

Interestingly, the amino sugars of all three classes of GAGs have either GlcN or GalN but never both.

4.1.2.1 Structure of Heparin

The structure of the major disaccharide repeating unit of heparin is α-1,4-linked L-iduronic acid 2-sulfate- D-glucosamine 2,6-sulfate (IdoA-2S - Glc(N,6)S03). This trisulfated disaccharide unit was found to be prevalent in the biosynthesis of heparin. An under-sulfated glucuronic acid residue linked to the hexosamine was

also present in limited amounts. The building blocks of the biopolymer are shown in Figure 4.2. The IdoA-2S-Glc(N,6) SO_3 is the most abundant unit in mammalian heparin (porcine and beef mucosa and beef lung heparin). Clam and whale heparin have higher amounts of GlcA, and three times more of the 3-*O*-sulfation of the hexosamine with no sulfation at the 6 position. Heparin and other GAGs are connected to the core protein through β1,4-D-glucoronic acid-β1,3-D-galacotse-β1,3-D-galacotse-β1,4-D-xylose linked to a serine residue. About 10 to 30 % of commercial heparins contain this 'linkage region' contaminant. The commercial heparin has a MW average of 8000 - 24,000 Daltons and comes from depolymerisation of a core protein precursor having a 60,000 - 100,000 Dalton MW. Because of the structural variation in heparin, it is believed that the cleavage of the core protein by native endoglycosidases in tissues produces heparin chains of different lengths and molecular w ight distribution. Also, given the reproducibility of the gel-filtration profiles of the native heparin, there is compelling reason to believe in a family of heparin sequences rather than in a random distribution of heparin chains of different lengths.

4.1.2.2 Structure of Heparan Sulfate

Earlier, it was difficult to differentiate between heparin and heparan sulfate. Heparan sulfate was classified as a member of the heparin family of acidic oligosaccharides because their structural building units and linkages are similar. Subsequently, they were differentiated based on the core proteins to which they were attached to, their biological activity and their tissue location. The core proteins of heparin and heparan sulfate are quite different due to their cellular origin. Heparin is synthesized and secreted by mast cells, while heparan sulfate is present on the surface of certain cell types like fibroblasts, endothelial cells and the cells of

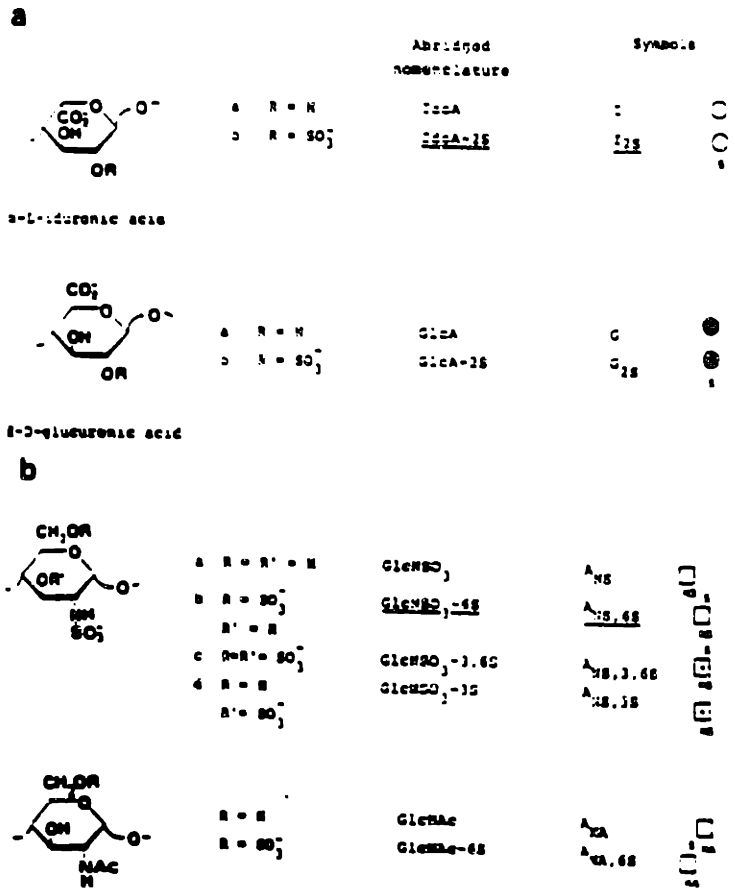

[Adapted from Casu, 1989]

Figure 4.2 Monosaccharide units of heparin and heparan sulfate

the extracellular matrix (ECM). Currently, heparan sulfate is believed to be present on all cell surfaces. This distinction was further supplemented by the difference in biological activities. For example, heparin is more involved in the blood system and the cascade therein, while heparan sulfate is a major component of the ECM regions. This definition was questioned by the observation of heparan sulfate in vascular tissues that have anticoagulant activity (Marcum and Rosenberg, 1984). Also, a large fraction of both polysaccharides are found in nature without their core protein and it is often difficult to distinguish between heparin and heparan sulfate due to the observation of 'heparin like' sequences in heparan sulfate. At this point, the core proteins and the uronic acid component, i.e. the IdoA to GlcA ratio, seem to be the only significant differences between heparin and heparan sulfate structures.

4.1.3 Chemical Properties of GAG

The structure of the major components of GAGs was chemically and enzymatically analysed by cleaving the glycosidic bonds of the chain (Cifonelli, 1968, Shiveley and Conrad, 1969 and Lindahl and Axelsson, 1971). Using NMR (Nuclear Magnetic Resonance) Spectroscopy the composition and the structure of the individual sugar units were established (Perlin et al., 1970).

Heparin and heparan sulfate are degraded chemically using nitrous acid (Shiveley, and Conrad, 1969) and enzymatically (Linker and Hoving, 1979). Nitrous acid degradation results in a disaccharide product, where the original hexosamine is converted to a five membered sugar, 2,5-anhydromannose 6-sulfate (AM $_{6S}$) and the uronic acid remains intact. Enzymatic degradation using heparinase (for heparin) or

hepartinase (for heparan sulfate) results in a disaccharide containing an unsaturated uronic acid (Δ U-2S) linked to a reducing hexosamine (Glc(N,6)SO_3).

The nitrous acid degradation does not cleave the acetylated hexosamine residues and hence results in larger oligosaccharides. Upon deacetylation by hydrazine, the GlcNAc residues are cleaved. Separation and quantification of the different disaccharides produced by exhaustive digestion by nitrous acid, using ion exchange HPLC (High Pressure Liquid Chromatography) is an effective method of characterizing and quantifying the composition of these units in heparin and heparan sulfate (Casu, 1985).

Enzymatic degradation of heparin and heparan sulfate, by the bacterial lyases heparinases I and II respectively, has been a useful method for mapping the two biopolymers. Heparinase cleaves between the hexosamine and the IdoA of a heparin chain while, heparinase II cleaves heparan sulfate between the hexosamine and GlcA. It should be pointed out that HG and HI sequences occur both in heparin and heparan sulfate respectively and hence there is cross-reactivity in both enzymes. Table 4.1 lists heparin disaccharide composition from different sources (Linker and Hoving, 1979).

Table 4.1 *Heparin Disaccharide composition from different sources*

Product yield # of the disaccharide fragments obtained by exhaustive nitrous acid depolymerisation of heparin fragments. Δ is the modified and Δ* is the disulfate hexosamine. I is iduronic and G glucuronic acid residues

Source	I 2S-ΔS	I 2S-Δ	G-ΔS	I-ΔS	G-Δ*S	G 2S-Δ	I-Δ*S
Beef (L)	68	5.7	5.5	3.7	5.0	1.6	n.d
Pork (M)	61	5.1	6.5	2.4	3.2	0.6	n.d
Clam	17	40	28	8.6	1.3	G-Δ; 4.4	1.7

where n.d is not detected
Adapted from Casu B., 1989

4.1.4 Heparin Binding Systems

A wide range of proteins has been purified using heparin sepharose chromatography. The interaction of these proteins with heparin was thought to be a non-specific hydrophilic interaction mediated through salt bridges. However, recently, heparin and other GAGs have been shown to modulate numerous cellular events by very specific interactions. The specificity of the interaction seems to arise from an unique arrangement of the amino acid residues in some domain in the protein and also by a specific orientations of the carboxylic and sulfate groups of the GAG chain.

The heparin binding proteins have been divided into five classes:

Protease Inhibitors (Antithrombin III)

Growth Factors (Basic FGF, Acidic FGF, HB-EGF)

Plasma Lipoproteins (Apolipoprotein B-100, E)

Extracellular Matrix Protein (Laminin, Fibronectin)

Other Proteins (Transcription Factors, Viral Proteins)

4.1.4.1 Serine Protease Inhibitors

Serine protease inhibitors, also known as serpins, are a major component of blood plasma. They form covalent complexes with the target protease. A few of these serpins find GAGs as cofactors to enhance their activity as best evidenced by antithrombin-III and heparin. The physiological phenomenon of AT-III-heparin interaction results in the anticoagulant property of heparin (Damus et al., 1973), which has been exploited in surgery for over fifty years.

The mechanism by which heparin enhances the AT-III-thrombin interaction is still in controversy. The first mechanism proposes a catalytic role for heparin whereby it provides a surface for the AT-III and thrombin to bind. The other hypothesis argues that heparin binds to AT-III and induces a conformational change which directly enhances AT-III binding to thrombin.

The interaction of AT-III and heparin is a tight 1:1 binding with a K_d of 6×10^{-8} M. The importance of basic amino acid residues like lysines in heparin binding was demonstrated (Rosenberg and Damus, 1973). The modification of a single trptophan residue (Trp-49) in AT-III reduced heparin binding (Blackburn et al., 1984). Mutation studies indicate that Arg-47 is directly involved in the initial AT-III binding to heparin. Based on these studies, two regions of AT-III were found to confer heparin binding: a region between 123 and 145 and another in the vicinity of Arg-47. It has been proposed that initial binding of AT-III to heparin, in the vicinity

of Trp-49, results in a conformational change that brings out the second binding site (Carlson et al., 1988).

However, the inhibition of thrombin by AT-III seems to require large heparin fragments (greater than 5kDa), although AT-III is capable of binding specifically to a pentasaccharide fragment of heparin. The AT-III binding fragment of heparin has been shown to be a pentasaccharide unit [GlcNAc, 6S] - [GlcA] - [Glc(N,3,6)S] - [IdoA2S] - [Glc(N,2)S] (Choay et al., 1981, Casu B et al., 1981, Atha et al., 1984). The sulfations at positions 3 and 6 in the second hexosamine are crucial for anti-thrombin binding. The inhibition of thrombin, however, is not achieved by a pentasaccharide-AT-III complex; a large heparin fragment is required. This suggests that heparin might act as a platform that brings AT-III and thrombin together by binding to both molecules in a specific manner.

The interactions between the heparin binding peptide of AT-III and the pentasaccharide have been studied by substituting regions of anti-trypsin sequences with AT-III sequences in the crystal structure of anti-trypsin. A disulfide bond in AT-III between Cys-8 and Cys-128 brings the α-helical peptide 123-145 (A) closer to Arg-47, which happens to be in another α-helix (B). The two helices A and B are orthogonal to each other and are in close proximity to one another. In their model, the 6 O- and the N-sulfates of H_1 make contact with AT-III's Arg 46/47 and Lys-125 respectively. The N- and 3 O- sulfates of the pentasaccharide make contact with AT-III's Arg-129 and Arg-132. The N- sulfation of H_3 interacts with Lys-136 of AT-III according to this model. Figure 4.3 represents a possible mode of AT-III oligosaccharide interaction. It is important to keep in mind that the three dimensional structure of the pentasaccharide and AT-III are not fully known and hence this is only an approximate representation.

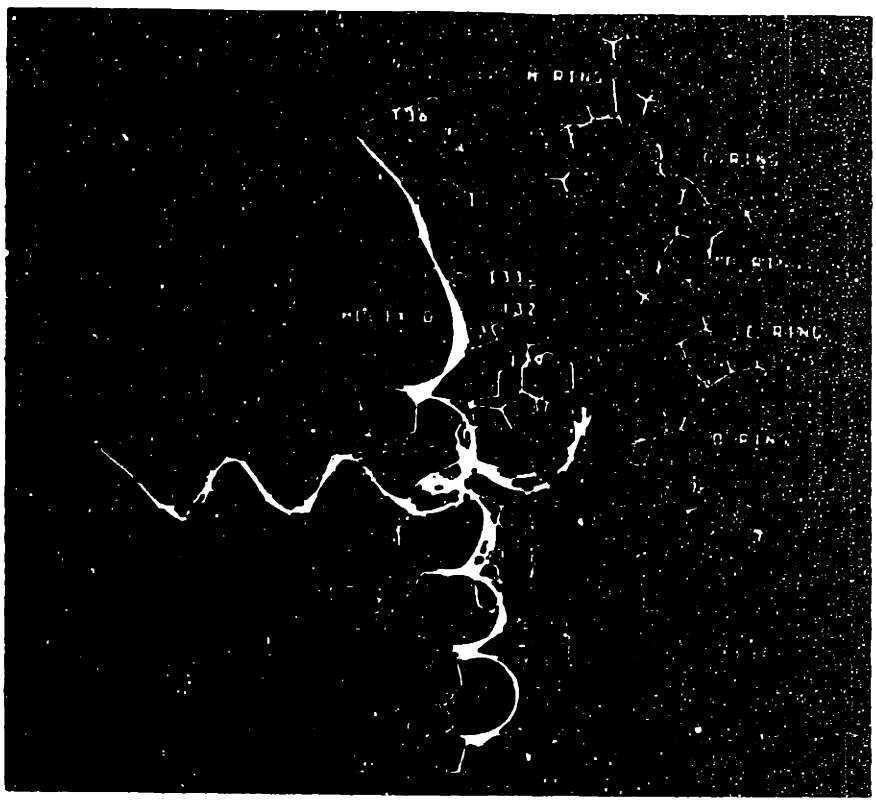

[Adapted from Jackson et al., 1991]

Figure 4.3 Molecular Graphics of AT-III pentasaccharide Interaction

4.1.4.2 Growth Factors

Growth factors are a class of molecules that regulate the growth and differentiation of cells by interacting with the cell surface receptors. The interaction between the growth factors and the receptors is highly regulated and versatile. Heparin sepharose chromatography has been used to purify growth, mitogenic and angiogenic factors from different sources (Shing et al., 1984). On basis of their isoelectric point, they are classified as either basic or acidic growth factors (Folkman and Klagsbrun, 1987).

Basic Fibroblast Growth Factor: bFGF is a 146 amino acid polypeptide which has more than 54% homology to aFGF. The heparin binding region of bFGF was determined to be residues 24 to 68 and 106-120 (Baird et al., 1988). These peptides compete with native FGF binding to cells and also affect FGF induced mitogenic simulation of DNA synthesis. More recently, an additional domain, 18-22, was shown to be important for heparin binding (Gospodarowicz et al., 1987). Different mutants of the three regions were designed by site-directed mutagenesis and their heparin binding capacity and mitogenic property were characterized (Heath et al., 1991). These studies indicated that the heparin binding domain of FGF is a structure formed by the appropriate folding of these three regions. Recent x-ray crystal structure of b-FGF confirmed the binding domain (Eriksson et al., 1991).

Acidic Fibroblast Growth Factor: Acidic FGF is a 154 amino acid polypeptide which was first identified in the brain, potentiating the proliferation of myoblast cultures. Glycosaminoglycan binding to aFGF is poorly understood. Analysis of the carboxy-terminal region reveals a highly basic region- six basic amino acids in the span of 18

residues. Thrombin cleavage of bFGF at Arg-136 and Thr-137 resulted in 136 and 18 amino acid residues (Lobb, 1988). Neither fragments showed heparin binding, indicating that the heparin binding region was possibly centered in the thrombin cleaving site.

4.1.4.3 Lipoproteins

Glycosaminoglycan interaction with the plasma lipoproteins are mediated through the ECM. The lipoproteins include High density (HDL), low density lipoproteins (LDL), coagulation factors, and lipolytic enzymes. The major protein component of the LDL complex is a 4500 residue protein called Apolipoprotein B-100 or Apo-B. The Apo-B protein helps in the transport of cholesterol from the plasma to the cells. The lipoprotein interacts with the surface GAGs of the arterial tissue, resulting in the deposition of cholesterol in the ECM contributing to the pathogenesis of atherosclerosis (Hollander, 1976). The heparin binding domains of Apo-B were identified to be 2016-2151, 3109-3240, 3308-3394, and 3570-3719 amino acid domains (Hirose et al., 1987).

ApoE is a 299 amino acid protein and is associated with LDL, HDL and very low density lipoprotein (VLDL). ApoE binds to heparin in a specific manner, the binding sites in the protein have been mapped to be residues 142-147 and 211-243. The 142 domain of ApoE shows a high degree of sequence homology with the 3359 domain of ApoB. Two synthetic heparin binding peptides corresponding to these regions were further characterized (Cardin et al., 1991).

4.1.4.4 Extracellular Matrix Proteins

ECM is the neighborhood of every cell and mediates or even modulates cell-cell communication, proliferation, migration and adhesion. ECM can be divided into three parts: (i) the structural component which includes the cell adhesion proteins, fibronectin, collagen etc., (ii) the 'filler' component made up of the proteoglycans and GAGs and (iii) the mitogen components, made up of growth factors and other enzymes. The binding of the structural proteins of the ECM to GAGs have been investigated.

4.1.4.4.1 *Fibronectin:*

Fibronectin is made up of two polypeptide domains attached at their carboxyl termini through disulfide bonds. The matrix heparan sulfate proteoglycan binds to fibronectin with a very high affinity. Based on heparin binding consensus sequence proposed by Cardin and Weintraub (section 4.1.5), the sequence, P-R-R-A-R-V was found to be involved in heparin binding by site directed mutation study (Bober-Barkalow and Schwarzbauer, 1991). Two other regions of fibronectin seem to have the heparin binding property, one being the 14kD proteolytic fragment of fibronectin. Differential scanning calorimetry studies of heparin-fibronectin binding indicate that calcium is required for the binding and that fibronectin undergoes a conformational change upon binding to heparin. The conformational change of fibronectin in the ECM brings about cell locomotion through the ECM and hence can have an important bearing on tumor metastasis (Sasisekharan, 1991).

4.1.4.4.2 *Laminin:*

Laminin is a major component of ECM and is involved in cell adhesion. It is made up of three polypeptide chains (A1, B1, and B2), arranged in the form of a asymmetric cross, with three short arms and a long arm. Three heparin binding

domains have been determined based on antibody staining (Martin and Timpl, 1987). Laminin has the capacity to form multimers, especially at low heparin concentrations. This multimer formation is important for its role in cell attachment (Sasisekharan, 1991).

4.1.4.5 Other Proteins

4.1.4.5.1 Transcription Factors

An important mechanism for the control of gene expression is the regulation of transcription. Transcription factors contain a cluster of basic residues in their DNA binding domains. Recently, it was shown that a number of transcription factors bind to heparin through their DNA binding domains (Cardin and Weintraub, 1989). Table 4.2 lists a series of DNA binding proteins and their consensus heparin binding sequences. The heparin binding of these transcription factors has not been characterized extensively.

4.1.5 Heparin Binding Consensus Sequence

The properties of the heparin binding domain in different proteins was investigated by Cardin and Weintraub (1989). The heparin binding regions of vitronectin, apolipoproteins E and B-100, and platelet factor-4 have been characterized. A total of twelve heparin binding sequences from these proteins were used to formulate two search strings for heparin binding regions (Cardin and Weintraub, 1989). A consensus sequence of [-X-B-B-X-B-X-] and [-X-B-B-B-X-X-B-X-], where B is the probability of a basic residue and X is a hydrophobic residue, was identified. These consensus sequences was then found in over 21 heparin binding proteins (Table 4.2). It was found that many of the natural sequences conforming to these consensus

Table Sequence Similarities among Basic Regions in Heparin-binding Proteins*

Consensus*	[X-B-B-B-X-X-B-X]	References
Vn	^{342}RPSLAKKQRFRHRNRKGYRSQRGHSRGRNQNSRR	20
Apo B	^{3359}ALKAGKLKFIIPSPKRPVKLLSGGNTLHLVSTTK	17
Apo B	^{3358}YKLEGTTRLTRLTRKRGLKLATALSLSNKFVEGS	16, 17
Apo E	^{138}ELRVRLASHLRKLRKRLLRDADDLQKRLAVYQAG	18, 19
γ-IP-10	^{54}SQFCPRVEIIATMKKKGEKRCLNPESKAIKNLLK	47
HTGL	^{159}AHVSGFAGSSMGGKRKIGRITGLDPAGPMFEGTS	40, 41
ECGF/aFGF	^{81}ERLEENHYNTYISKKHAEKHWFVGLKKNGRSKLG	42, 43
HRG	^{405}CCHGHGPPPGHLRRRGPGKGPRPFHCRQIGSVYR	48
HRG	^{124}PVLIDFFEDTERYRKQANKALEKYKEENDDFASF	48
Pn	^{29}AVDSFSVKDNFDPKRYAGKWYALAKKDPEGLFLQ	49
β-TG	^{56}GRRICLDPDAPRIKKIVQKKLAGDESAD	50
TS	^{10}NSVFDIFELTGAARKGSGRRLVKGPDPSSPAFRI	37
HTGL	^{284}NCKKGRCNSLGYDIRRIGHAKSKTLFLITRAQSP	40, 41
PF-4	^{47}NGRRICLDLQAPLYKKIIKKLLES	47
LpL	^{133}LGAHAAGIAGSLTNKKVNRITGLDPAGPNFEYAE	39
LpL	^{264}RCNNLGYEINKVRAKRSSKMYLKTRSQMPYKVFH	39
ECGF/aFGF	^{95}ISKKHAEKHWFVGLKKNGRSKLGPRTHFGQKAIL	42, 43
AT-III	^{118}QIHFFFAKLNCRLYRKANKSSKLVSANRLFGDKS	51
HC-II	^{170}ASSKYEITTIHNLFRKLTHRLFRRNFGYTLRSVN	52, 53
Fn	^{2268}QDTRTSYRIGDTWSKKDNRGWLLQCICTGNGRGE	36
Fn	^{1804}AQITGYRLTVGLTRRGQPRQYNVGPSVSKYPLRN	36
bFGF	^{6}GSGAFPPGHFKDPKRLYCKNGGFFLRIHPDGRVD	54
NCAM	^{688}VVNIKQDDGGSPIRHYLIKYKAKHSSEWKPEIRL	45
LPC	^{221}FNTILTTRSYPQLRRVFQKYTKYSKHDMNKVLDL	55
LPC	^{288}EKLHQAMKGVGTRHKALIRIMVSRSEIDMNDIKA	55
THR	^{333}DGKYGFYTHVFRLKKWIQKVIDQFGE	44
GDN	^{104}MVMRYGVNGVGKILKKLNKAIVSKKNKDIVTVAN	46
PCI	^{306}KMQQVENGLSEKTLRKWLKMFKKRQLELYLPKFS	56

Table represents the sequence similarity of basic regions in various heparin-binding proteins. The sequences are compared with the heparin-binding domains of vitronectin, apolipoprotein B-100, apolipoprotein E, and platelet factor 4.

*The consensus sequence [X-B-B-B-X-X-B-X] was derived from the usage frequency of basic (B) and nonbasic (X) residues in the data base (see Table 4).

Vn=vitronectin, γ-IP-10=10 kilodalton gamma-interferon inducible protein, HRG=histidine-rich glycoprotein, Pn=purpurin, β-TG=beta-thromboglobulin, AT-III=antithrombin III, HC-II=heparin cofactor II, bFGF=basic fibroblast growth factor, LPC=lipocortin, PCI=protein C inhibitor. For other abbreviations, see footnote to Table 1.

[from Cardin and Weintraub, 1989]

Table 4.2 Similarity of basic residues of various heparin binding proteins

The consensus sequence of [X-B-B-B-X-X-B-X] where X is a nonbasic amino acid and B is a basic amino acid.

motifs showed prominent amphipathic periodicities having both α-helical and β-sheet conformations, as determined by predictive algorithms and CD studies. A helical wheel diagram of these heparin binding regions indicate the segregation of the basic amino acids to one side of the helical face (Figure 4.4). This high charge density has been thought to mediate interaction with heparin.

Apolipoprotein E is a 299 amino acid protein that is associated with the plasma lipoproteins. The heparin binding site of this protein has been mapped to be between residues 142-147 and 211-243 (Cardin et al., 1991). Two synthetic heparin binding peptides corresponding to these regions were further characterized. Chou-Fasman structure predictions indicate structural similarity between these peptides. CD studies, however, indicate that ApoE forms an amphipathic helix that is stabilized by heparin, while Apo-B peptide forms a β-strand structure upon heparin binding (Weintraub et al., 1990).

Ferran et al. (1992) studied the interaction of an 19-residue peptide with α-helical character with heparin. The peptide was designed based on the heparin binding consensus sequence, so that the basic residues would lie along one face of the helix and interact with heparin. The primary sequence of the peptide is shown below:

Succ-A-E-A-A-A-R-A-A-A-R-R-A-A-R-R-A-A-A-R-NH2

This sequence incorporates many features that promote helix formation and stability. CD studies indicated that the peptide was about 75% helical at neutral pH buffer; the helicity increased to 85% under high ionic strengths and to 100% in the presence of heparin. The binding constant of this peptide to heparin was however, very low. The micromolar K_d value was attributed to the absence of lysine residues

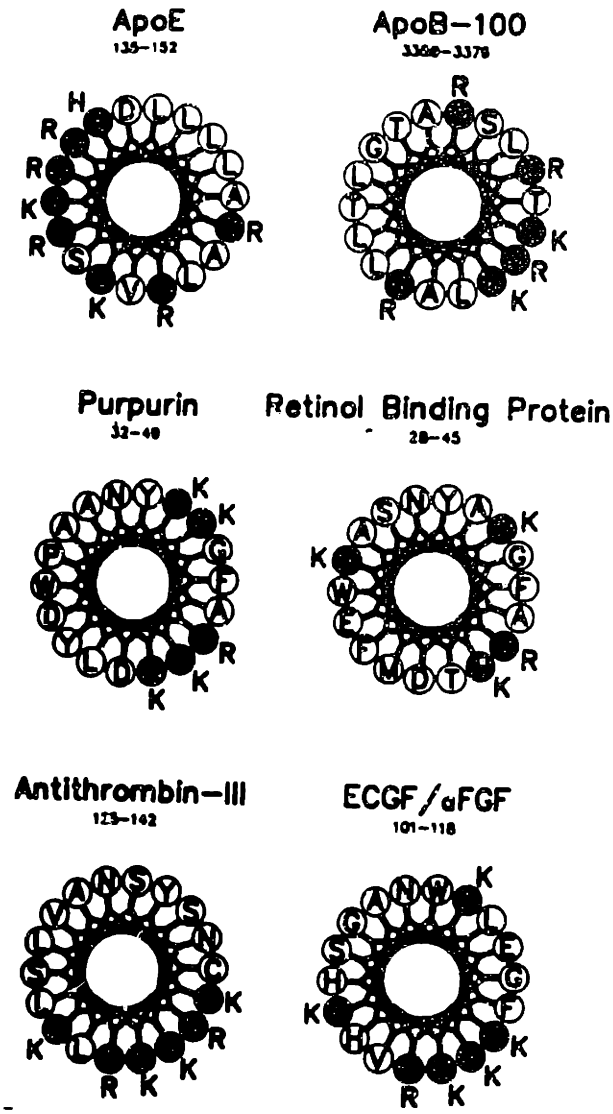

[Adapted from Cardin and Weintraub, 1989]

Figure 4.4 Helical wheel diagram of the consensus sequence regions of various proteins

in the peptide. This however, indicates that the interaction of the peptide to heparin is not mediated by a simple electrostatic interaction between basic residues arranged along one face of a helix. The low binding constant between the peptide and heparin suggests alternate mechanism for the interaction of proteins with heparin. The consensus sequence might therefore be just an indicator of heparin binding homology; the actual secondary structure and conformation that interacts with the protein might depend on the nature of the protein.

Molecular dynamics simulations of the Apo-E peptides with heparin indicate the formation and stabilization of an α-helical structure for the 142 peptide and a β-strand for the 211 peptide in the presence of the oligosaccharides (Cardin et al., 1991). The heparin oligomers considered for the simulation were either tetra or octasaccharides. The repeat unit of heparin was constructed by addition of carboxylate and sulfate groups to cyclohexane and substituting the cyclic methylene groups with oxygen. The structures were then minimized with the parameters provided in the AMPAC program.

The use of cyclohexane as the starting building block for the sugar repeat units might not be appropriate. The pucker in the sugar backbone is one of the key variables that controls heparin conformation and hence, the orientation of the carboxylate and the sulfate functional groups of heparin. This, in turn, determines the interaction of heparin with the peptides and hence the peptide conformation. The parameters that are used for calculating the energies of a molecule in these simulation often fail to adequately represent interactions in a carbohydrate molecule. These energy parameters have been developed predominantly for peptide and protein modeling and capture the atomic interactions in a peptide molecule very effectively. However, ring current stabilization and other steric

effects in a carbohydrate molecule have not been properly quantified in these calculations. Predictions of carbohydrate structures based on these parameters hence, could lead to a non-realistic conformation. Molecular modeling of oligosaccharide conformation in general and heparin conformation in particular have been poorly understood.

The interaction between a protein and a glycosaminoglycan depends on both the conformation of the protein as well as the conformation of the oligosaccharide. Modeling studies with a improper oligosaccharide conformation could lead to erroneous peptide conformations. It is critical, therefore to understand the oligosaccharide conformation in the context of its interaction with the proteins. A more fundamental approach to the modeling of heparin peptide interactions has been addressed in this study.

4.1.6 Scope

The interaction between heparin and proteins is poorly understood. Non-specific charge interactions have been thought to dominate the interaction between heparin and proteins. However, recent investigations provide increasing evidence to a specific nature of these interactions. This study aims at understanding these interactions at a molecular level to gain some insight into how heparin modulates and controls various biological events.

Heparin binding domains of two different systems are isolated and peptides corresponding to the heparin binding regions are characterized by biochemical and biophysical methods. The effect of these peptides on the degradation of heparin by

heparinase I is investigated. The specificity of these peptides to heparin is determined by several chromatographic approaches. The interaction of these peptides with heparin is also studied using capillary electrophoresis and fluorescence measurements.

The relationship between the three dimensional structure of the peptide and the specificity of interaction with heparin is also investigated. The structure of the heparin binding peptides are characterized using spectroscopic techniques like circular dichroism, NMR . Theoretical investigations to understand this interaction focus on using molecular modeling studies of the peptides as well as conformational analysis of heparin chains. Information regarding heparin conformation is critical in understanding the interaction of the peptides with heparin.

Two different heparin binding systems are considered. Heparinase is unique in that it binds and cleaves heparin. The heparin binding region of heparinase is mapped and a 18 amino acid peptide (HBP) is synthesized. HBEGF is a cytokine with a heparin binding domain. Two peptides representing the heparin binding region of HBEGF are characterised in this study.

4.1.6.1 Heparinase

Heparinase I is induced by heparin at the initial stages of heparin catabolism in *F.heparinum* (Hoving and Linker, 1970). Heparinase I is secreted and isolated from the periplasmic space of the *F. Heparinum*. It is a monomeric protein with a apparent molecular weight of 43,000 Daltons and a pI of 9.5. Heparinase I depolymerises heparin in a random endolytic fashion into di-, tetra-, and hexa-

saccharides with a reducing and unsaturated 4,5 end group (Rice and Linhardt, 1989). The enzyme cleaves between the hexosamine and the iduronic acid linkage of heparin. Heparinase I does not cleave the bond between glucosamine and glucuronic acid (heparan sulfate) as effectively. The purified protein has a K_m of 8 x 10^{-6} m and a V_{max} of 4 x 10^{-7} M/min.

Initial studies established that complete enzymatic degradation of heparin by heparinase was sufficient to eliminate the anticoagulation properties of heparin in surgery and this led to the proposal of novel deheparinization post-surgical therapy (Langer et al., 1982). More recently, the cysteines of heparinase and the active site domain were mapped (Sasisekharan et al., 1992). Also a heparin binding domain different from the catalytic region has been identified (section 4.2.1). The heparin binding constant for heparinase I was in the order of 50 nM (Sasisekharan, 1991).

4.1.6.2 Heparin Binding Epidermal Growth Factor

HB-EGF is a recent member of the growth factor family, initially identified in the media of monocytes and macrophages. HB-EGF is a potent smooth muscle cell, epithelial cell and mesothelial cell mitogen, and is a constituent of wound fluid. It is believed that HB-EGF is involved in various inflammatory wound healing processes. Of the EGF family members, HBEGF closely resembles amphiregulin, with about 40% sequence homology (Klagsburn, personal communication). Both, HBEGF and Amphiregulin (AR) have an additional 30-35 amino acids compared to EGF (53 amino acids) or TGF-alpha (50 amino acids). These extra amino acids of HBEGF are found upstream of the EGF like cysteine rich domain (Figure 4.5). The extension region is extremely hydrophilic due to the abundance of lysine and arginine residues. The cationic nature of the extension region might explain the

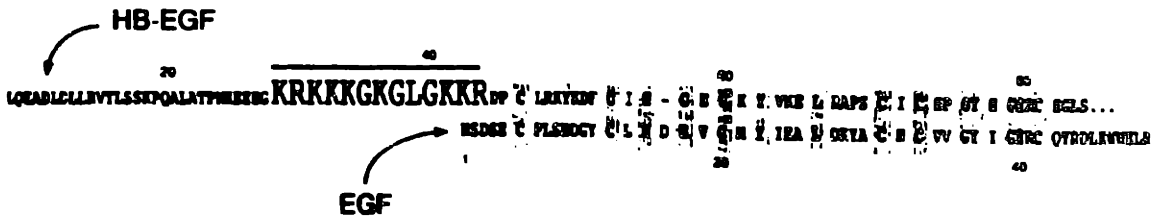

Figure 4.5 Primary sequence of EGF and HBEGF
The extension region is hydrophillic and contains the heparin binding domain of HBEGF

heparin binding property of HBEGF which is not a characteristic of EGF. HBEGF might directly interact with DNA through the localized basic charges in the extension region. HBEGF is also able to compete with the binding of EGF to its receptor. HBEGF has been found to be more than 40 times more potent as a mitogen for smooth muscle cells than EGF or TGF-alpha.

The mitogenic activity of HBEGF seems to depend on its binding to the low affinity glycosaminoglycan on the cell as well as the high affinity cell surface receptor. Heparin is able to block, in a dose dependent manner, the ability of ^{125}I-HBEGF to bind to heparin column. The low affinity GAG binding seems to be mediated through the hydrophilic and positively charged extension region of the HBEGF molecule. It is postulated that inhibition of the low-affinity binding to GAG would be sufficient to mitigate its biological activity. Figure 4.6 is a schematic representation of this model (Klagsburn M., personal communication). Heparin binding peptides designed based on this extension region seem to effectively compete the low affinity binding of HBEGF to the cell surface proteoglycan (section 4.2.1.3).

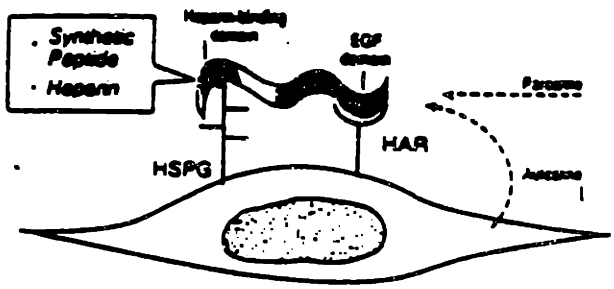

Figure 4.6 Interaction of HBEGF with cell surface GAG
A schematic diagram of interaction of HBEGF with the low-affinity receptor (GAG) on the cell surface.

4.2.1 Isolation of Heparin Binding Sites

4.2.1.1 East - Western Mapping of Heparinase

The heparin binding site on heparinase was identified by an technique that will hence forth be called "East-Western" technique. The prinicple behind this method is the modification of the classical western of south-western technique. In western (protein), biochemical characterization of protein-protein interaction (for example binding of an antibody to a protein) is studied by first separating the protein using electrophoresis (like SDS-PAGE), and then transferring the protein onto a membrane. The protein is then probed using an antibody. In case of south-western, DNA binding to proteins is studied, where the procedure is very similar to western, but the only difference is using DNA as a probe instead of an antibody. This study demonstrates the use of heparin (carbohydrate) as a probe to determine the heparin binding site of a protein, and hence we are using the term east (carbohydrate) -western.

The enzyme was first cleaved at the methionines using cyanogen bromide. The cynaogen bromide digest of heparinase gave about 9 bands, suggesting several incomplete digested bands (there are 5 met residues in heparinase, hence a complete digest by CnBr would give 5 peptide fragments). The peptide fragments from a

complete digest of CNBr would be 21-195 (17.4 kD), 196-272 (8.2 kD), 273-288 (1.6 kD), 289-326 (4.1 kD), and 327-384 (6 kD). The fragments were then separated on a 12% SDS-PAGe, electrophoresed and transferred onto a nitrocellulose membrane (Figure 4.7). The experiment at this stage was performed by two different methods. In the first method, the membrane was blocked using chondroitin sulfate, then probed for 12 hrs using ^{125} I heparin (gift from A. Lander, Dept of Biology, MIT). Following the probing, the membrane was washed with standard heparinase buffer and autoradiographed. In the second method, the transferred membrane was stained using pontso S, a red dye. Different bands were cut out of the membrane and then incubated with chondroitin sulfate and ^{125}I heparin probing cocktail. The membrane strips were washed and counted using a γ counter. It was found that peak 8 bound to radioactive heparin in a specific manner. This peptide migrated between the 6kD and the 14kD molecular weight standards and was in agreement with the predicted molecualar weight of about 8 kD (72 amino acid long). Upon sequencing this peptide, it was found to be "MIFKKNIA...". It was subsequently (HPLC competition and amino acid sequencing) shown that the linear sequence of amino acid which would be important for heparin binding ranged from KKNIAHDKVEKKDKDGKITYVAGK.

4.2.1.2 HPLC Competition Experiments:

Heparinase has been extensively mapped at the amino acid sequence level for cloning and other biochemical characterizations (Sasisekharan, 1991). The enzyme has been digested with trypsin to generate a typtic map as a fingerprinting to establish its cysteines. As trypsin cleaves at lysines and arginines, the basic residues which would be important for heparin binding, the actual heparin binding domain

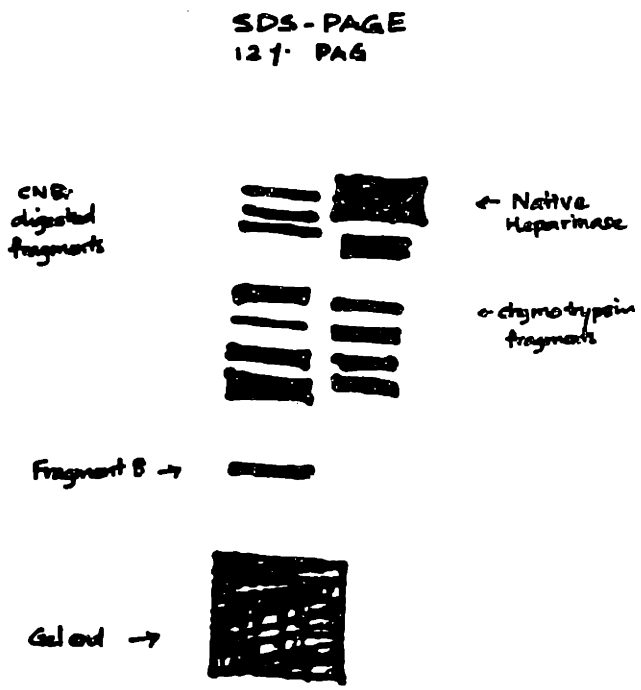

Figure 4.7 East-Western analysis of Heparinase
Fragment 8 of heparinase binds specifically to radioactive heparin

cannot be mapped from a tryptic digest. However, the enzyme fragments flanking the binding site might bind to heparin to reflect a change in the HPLC tryptic profile.

Figure 4.8 shows the reverse phase separation of the peptide fragments of heparinase digested by trypsin. When heparin is added to the fragments before separation, peak td-hbf, td 9, td 22 and td Lx disappear, probably because they come out in the void volume with heparin. Addition of chondroitin sulfate to the tryptic digest fragments of the enzyme seems to indicate that the binding of td 9 and td 22 are non-specific charge interaction. However, peak td-hbf disappears only in the presence of heparin indicating that it binds specifically to heparin. Isolation and sequencing of peak td-hbf indicates that it is the flanking site (KITYVAGK) to the heparin binding domain KKNIAHDKVEKKDKDGKITYVAGK mentioned earlier, confirming the binding site in the enzyme.

The binding site isolated form these different approaches seems to have the sequence of:

MIFKKNIAHDKVEKKDKDGKITYVAGK

A eighteen residue peptide was then synthesized to represent the heparin binding domain of heparinase as shown:

IFKKNIAHDKVEKKDKDG

This peptide seems to bind heparin with a very high (nM range) binding constant Dot blot experiments with radioactive heparin conclusively demonstrate the binding of this peptide to heparin (Sasisekharan, 1991).

4.2.1.3 Heparin Binding Site of HBEGF

The highly hydrophilic extension region of HBEGF (section 4.1.8) seems to play a critical role in its binding to the low affinity heparan sulfate receptor on the cell surface. A 22-mer synthetic peptide derived from this extension region of HBEGF was able to completely block the binding of HBEGF to heparin sepharose. By synthesizing different fragments of the hydrophilic region, a 13 amino acid peptide was found to be capable of competing the binding of HBEGF to heparin (Klagsburn, M. personal communication). This peptide, termed as P13, has the primary sequence of:

KRKKKGKGLGKKR

This peptide, however, did not block the binding of bFGF to heparin suggesting that FGF and HB-EGF bind to different heparin sequences. Site-directed mutagenesis of HBEGF confirms the involvement of residues 32 to 45 in heparin binding (Klagsburn, personal communication). A second peptide that includes residues 31 through 52 was also synthesized to determine the involvement of Arg-51 and Lys-52 in heparin binding. The primary sequence of this peptide, termed as P21 is:

GKRKKKGKGLGKKRDPCLRKY

It can be seen that P21 contains the P13 peptide and an additional 7 amino acids in the end, including a cysteine and a tyrosine. The tyrosine can be used effectively to study the interaction of the peptide with heparin through fluorescence.

Figure 4.9 shows the binding of radioactive HBEGF to heparin. The amount of radioactive HBEGF bound to heparin is not affected by the addition of EGF. EGF molecule does not have a heparin binding domain and hence does not compete with HBEGF to bind to the glycosaminoglycan. However, when peptide P13 is added, it is able displace almost all the radioactive HBEGF from heparin. This indicates that the peptide P13 adequately represents the heparin binding domain of HBEGF. The effect of P21, however, seems to be much more pronounced. P21 is able to completely block the binding of HBEGF to the GAG (Klagsburn, M. personal communication). Dot-Blot experiments with radioactive heparin confirm the binding of these peptides to heparin in a concentration dependent manner (Sasisekharan, R., unpublished results).

4.2.1.4 Consensus Sequence

The primary sequence of the heparin binding peptides form heparinase and HBEGF is shown in Figure 4.10. Both the consensus sequences proposed by Cardin and Weintraub [-X-B-B-X-B-X-] and [-X-B-B-B-X-X-B-X-] are present in the primary sequence of HBP. Moreover, structure prediction algorithms like Chou-Fasman and Rous-Gardner predictions, indicate a very high α-helix forming tendency for this peptide (Figure 4.11). Peptides P13 and P21 conform to the [X-B-B-B-X-X-B-X] consensus sequence but have an excess of basic residues. These peptides are also expected to be in an α-helical structure based on structure prediction algorithms.

The helical-wheel diagram of these peptides are shown in Figure 4.12. It can be seen that there is a high degree of homology in the charge distribution along the helical face between the peptides. Moreover, the relative position of the hydrophobic and the charged residues seem to be conserved in these peptides, although the source of

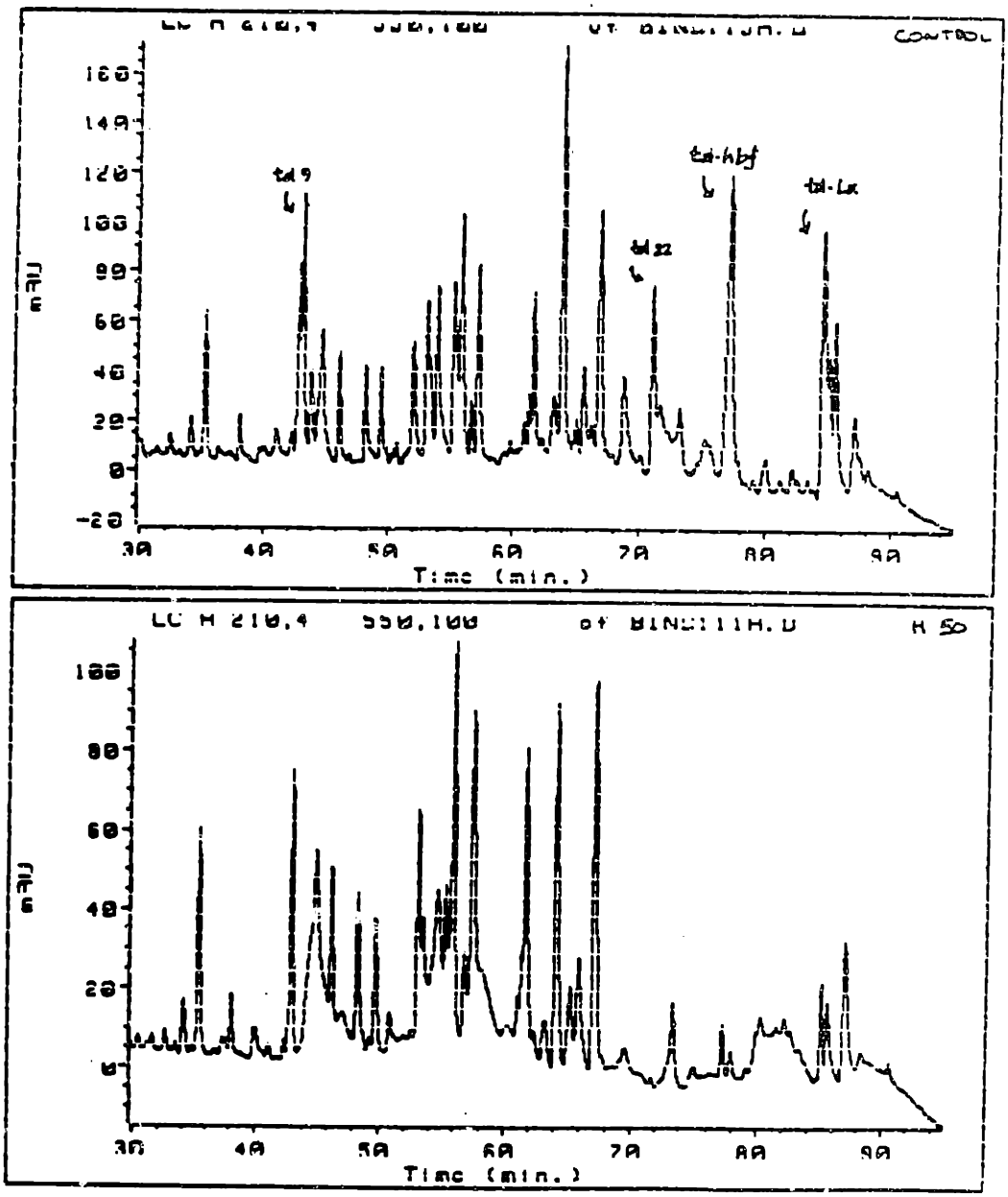

Figure 4.8 Tryptic map of Heparinase

Heparinase fragments after digestion by trypsin separated by reverse phase chromatography. (a) no heparin, (b) heparin added before chromatographic seperation.

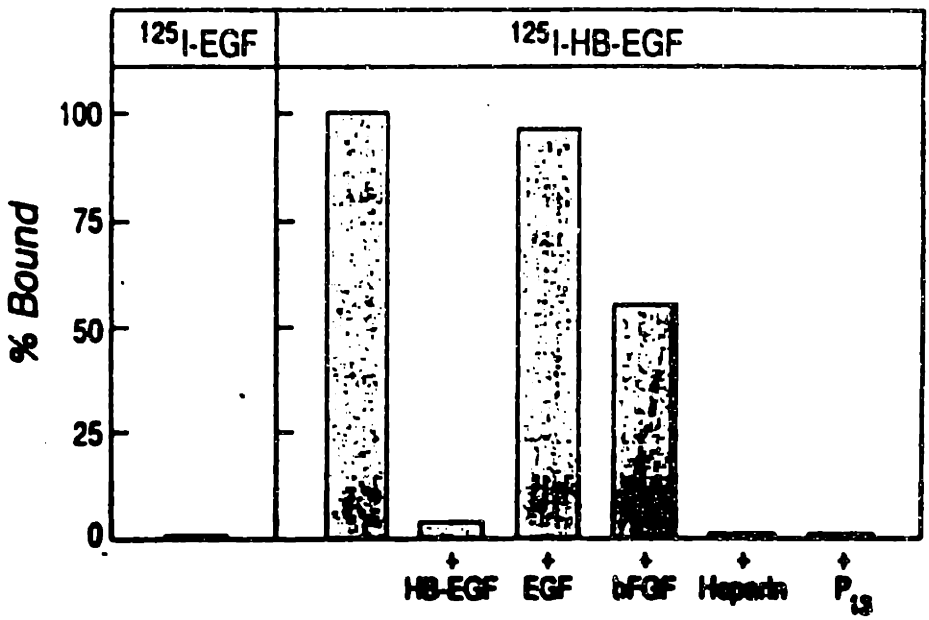

Figure 4.9 Binding of HBEGF to low-affinity receptor (GAG)
Binding of radioactive HBEGF to heparin is not affected by EGF but is completely blocked by addition of P13.

(a) HBP: I-F-K-K-N-I-A-H-D-K-V-E-K-K-D-K-D-G

(b) P21: G-K-R-K-K-K-G-K-G-L-G-K-K-R-D-P-C-L-R-K-Y

(c) P13: K-R-K-K-K-G-K-G-L-G-K-K-R

Figure 4.10 Primary sequence of Heparin Binding Peptides
Amino-acid sequence of (a) HBP, (b) P21 from HBEGF, (c) P13 from HBEGF

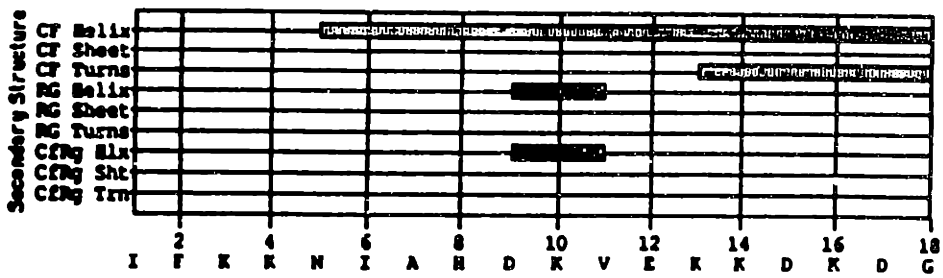

Figure 4.11 Secondary structure predictions for peptides
Chou-Fasman predictions and Rous-Gardner predictions for HBP

the peptides is very different. The following sections detail the study of the interaction between these peptides and heparin.

4.2.2 Characterization of Heparin Binding Peptides

4.2.2.1 Enzyme Reactions

The enzyme heparinase is known to act specifically on heparin, cleaving it at the linkage between the hexosamine and the uronic acid. The lyase action results in an unsaturated bond between the C_4 and C_5 of the uronic acid residue of the heparin chain (Figure 4.13). This double bond absorbs at 232 nm. The formation of degradation products of heparin can hence be followed at 232 nm.

The interaction of the peptides with the heparin molecule would alter the degradation profile. Information on the binding of the peptides to heparin can be obtained based on the nature and extent of the alteration. The initial reaction rate depends on the number and conformation of the available heparin molecules that can be cleaved by the enzyme. In addition, the degradation products formed also gives information on the nature of the interaction between the peptide and heparin. The peptides can, for example, bind tightly to some products, preventing their further degradation by the enzyme. The quantity and the distribution of the products were followed using anion exchange chromatography.

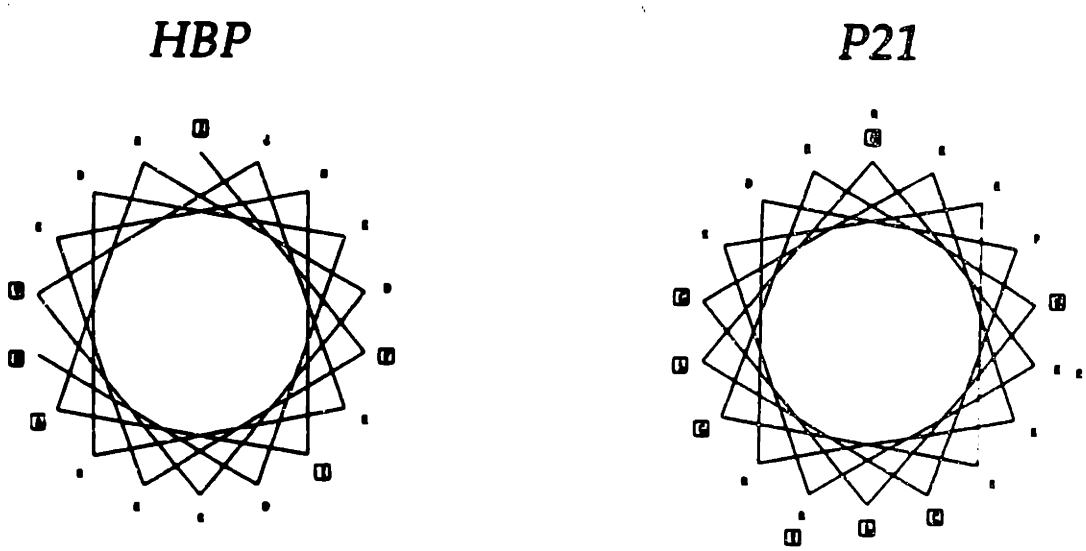

Figure 4.12 Helical Wheel diagram of heparin binding peptides
(a) HBP, (b) P21.

4.2.2.1.1 *Effect of Calcium*

The degradation reaction proceeds only in the presence of calcium ions in the reaction buffer. Figure 4.14 shows the degradation reaction profile with varying amounts of calcium in the buffer. At very low calcium concentrations, the enzyme is almost inactive. The reaction rate, however, levels off after about 5 mM calcium concentration. The calcium is necessary for the catalytic activity of the enzyme, however, the binding is unaffected by calcium ions (Sasisekharan, 1991).

4.2.2.1.2 *Control Reaction*

Figure 4.15 shows the cleavage of heparin by heparinase followed at 232 nm. The absorbance increases sharply at first and then level off after about 8 min. The saturation of the double bond formation indicates that the reaction is almost complete at the end of 8 min. This UV trace will henceforth be referred to as the control reaction profile. The products formed by the reaction are also shown in Figure 4.16. The anion exchange peaks have been earlier assigned using mass spectroscopy. The structure of these peaks are shown in Figure 4.17.

The predominant degradation product is a disaccharide which comprises of about 80% of the total products. Of the three tetrasaccharides, tetrasaccharide 1 and 3 (Figure 4.17) can be further cleaved by the enzyme to a disaccharide, but the rate of cleavage is extremely slow. However, tetrasaccharide 2, with the IHGH sequence, cannot be degraded to the disaccharides as the enzyme is not capable of cleaving at the glucuronic acid bond.

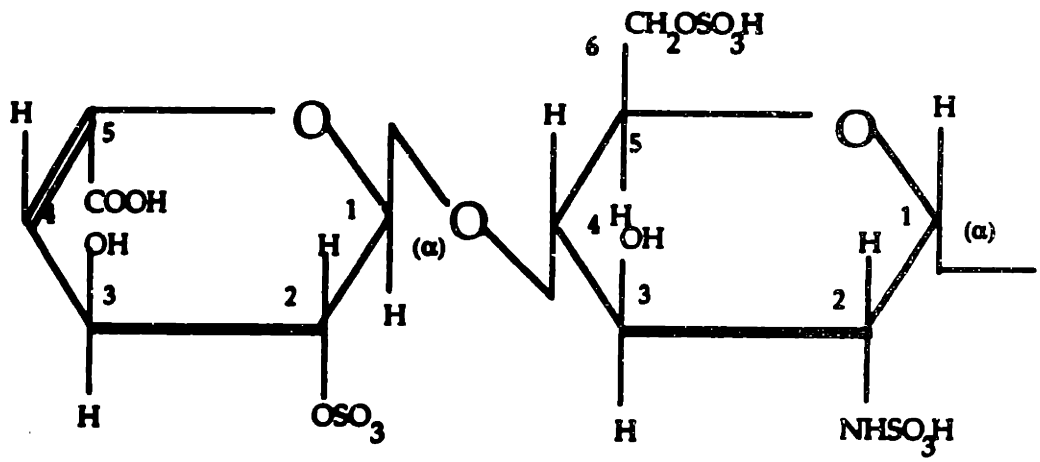

Figure 4.13 Heparinase action on Heparin
The lyase action of heparinase results in an unsaturated bond between the C_4 and C_5 of the uronic acid residue.

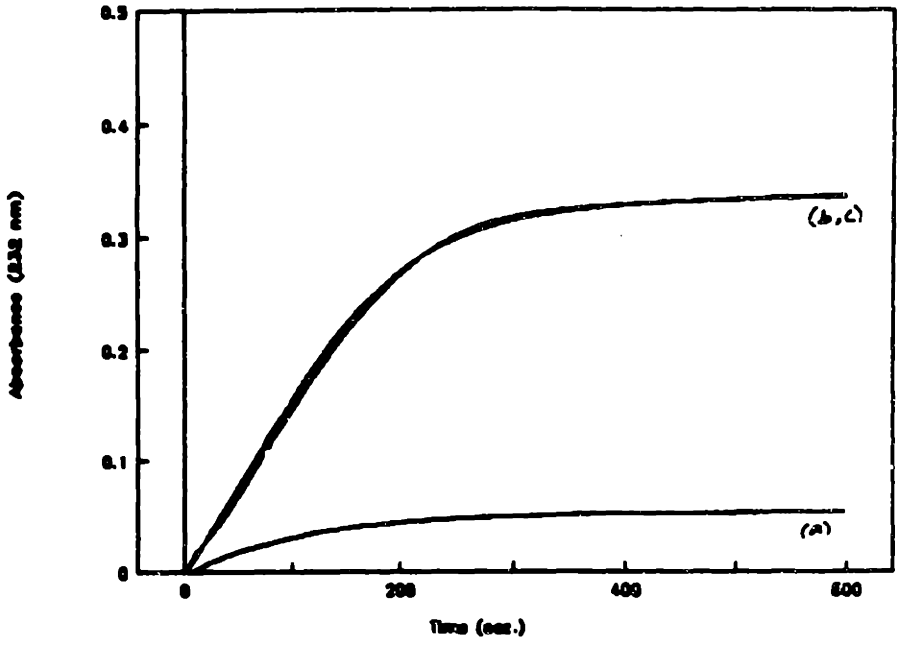

Figure 4.14 Effect of Calcium on heparin degradation
Formation of unsaturated bond is followed by its absorbance at 232nm
(a) 0 mM calcium, (b) 5mM calcium, (c) 10mM calcium

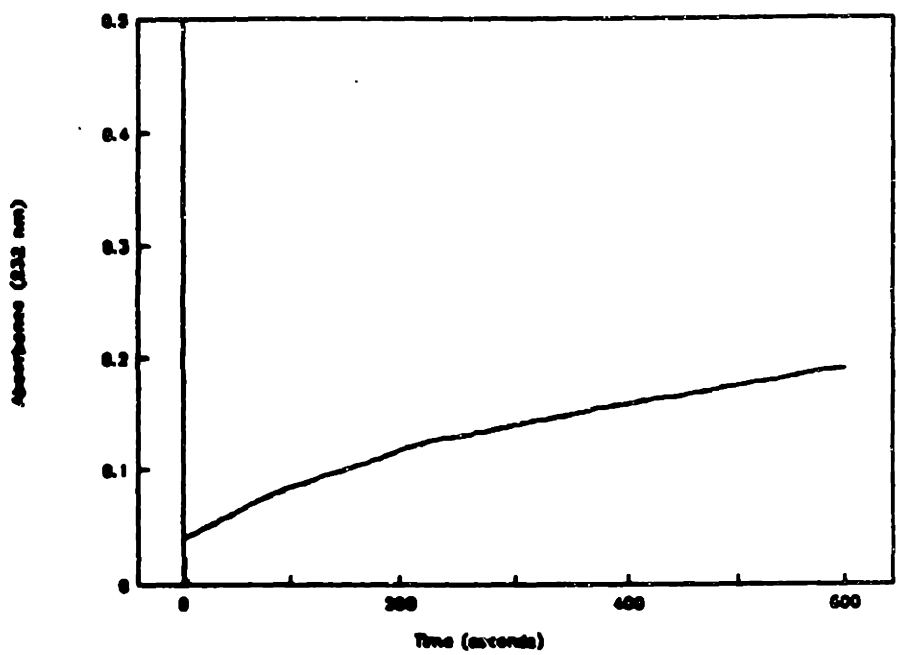

Figure 4.15 Heparin degaradtion by heparinase
Formation of unsaturated bond in heparin followed by absorbance at 232nm.

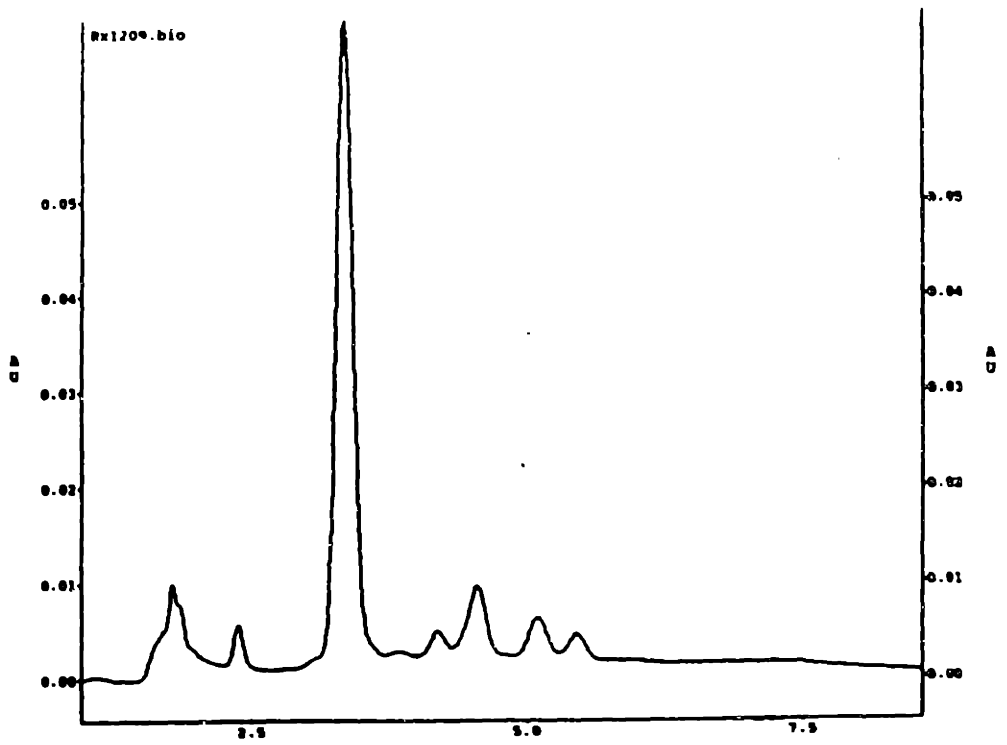

Figure 4.16 Heparin degradation by heparinase
Degradation products analyzed by anion exchange chromatography.

4.2.2.1.3 *Effect of control Peptide - Maxidialin*

Maxidialin has a heparin binding consensus sequence. The heparin binding domain of Maxidialin has been removed by recombinant methods to yield a peptide that does not bind to heparin. This peptide, called as truncated Maxidialin, has been used as a control peptide to study the cleavage of heparin in the presence of the peptides.

Figure 4.18 shows the degradation reaction in the presence of different amounts of truncated Maxidialin. The reaction rate is not altered by the addition of increasing quantities of the peptide, indicating that the heparin and truncated Maxidialin do not interact. In addition, the distribution and the amount of product formed in the presence of increasing amounts of peptide is exactly identical (Figure 4.19), confirming the absence of any interaction between the peptide and heparin.

4.2.2.1.4 *Effect of HBP*

Heparin Binding Peptide (HBP), isolated from heparinase is expected to compete with the enzyme for the binding sites in heparin. As a result, one would expect the reaction rate to be slower in the presence of the peptide. Figure 4.20 shows the reaction trace in the presence of different HBP concentrations. The initial reaction rate seems to be slower than the control profile, especially at high peptide concentrations. This decrease in the initial reaction rate is similar to the one observed in the presence of monoclonal antibody for heparinase. The saturation value of the absorbance, however, seems to be identical to the case in the absence of the peptide (Figure 4.20). This suggests that the binding site for both the enzyme and the peptide in heparin is the same. However, the binding affinity of the enzyme seems to be higher as the enzyme is able to replace the peptide bound to the heparin

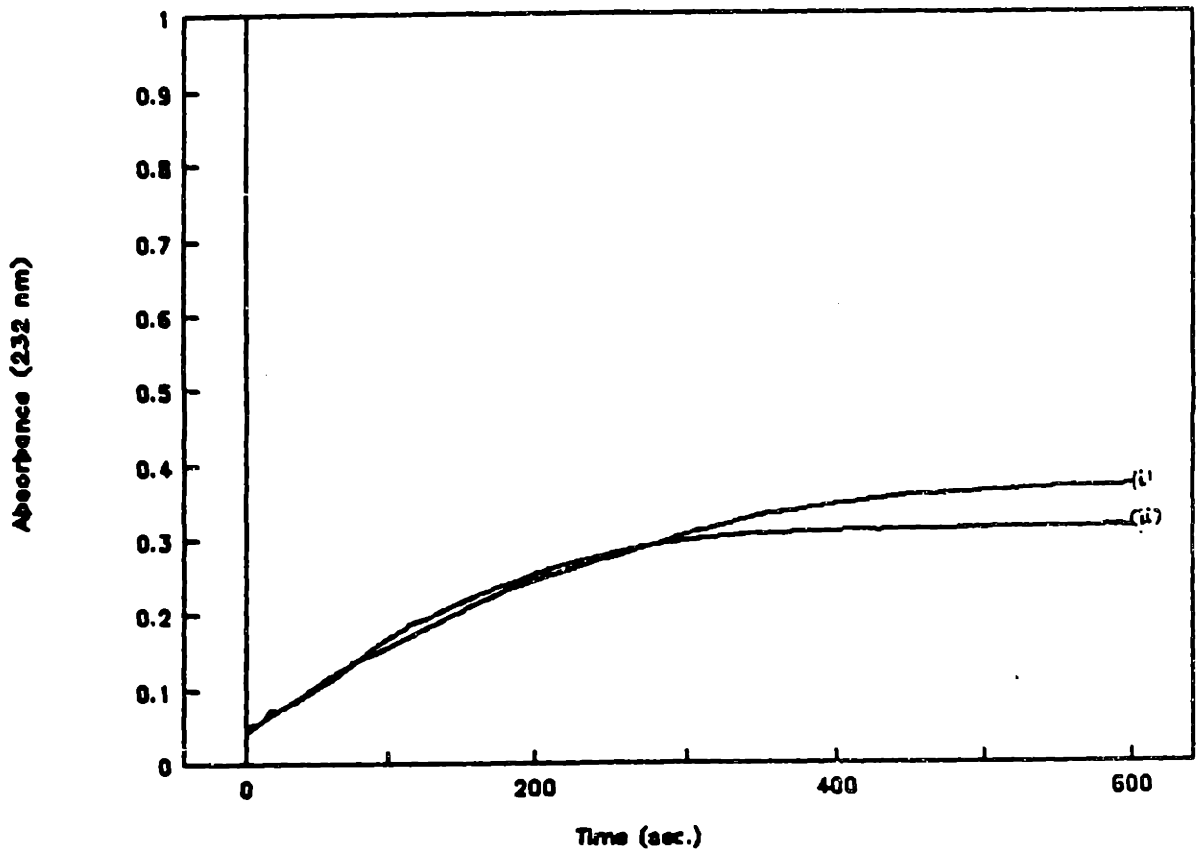

Figure 4.18 Heparin Degradation by Heparinase in presence of truncated maxidialin

Absorbance at 232nm followed as a function of time.
(i) control reaction with no peptide (ii) 10µg trunc. Maxidialin.

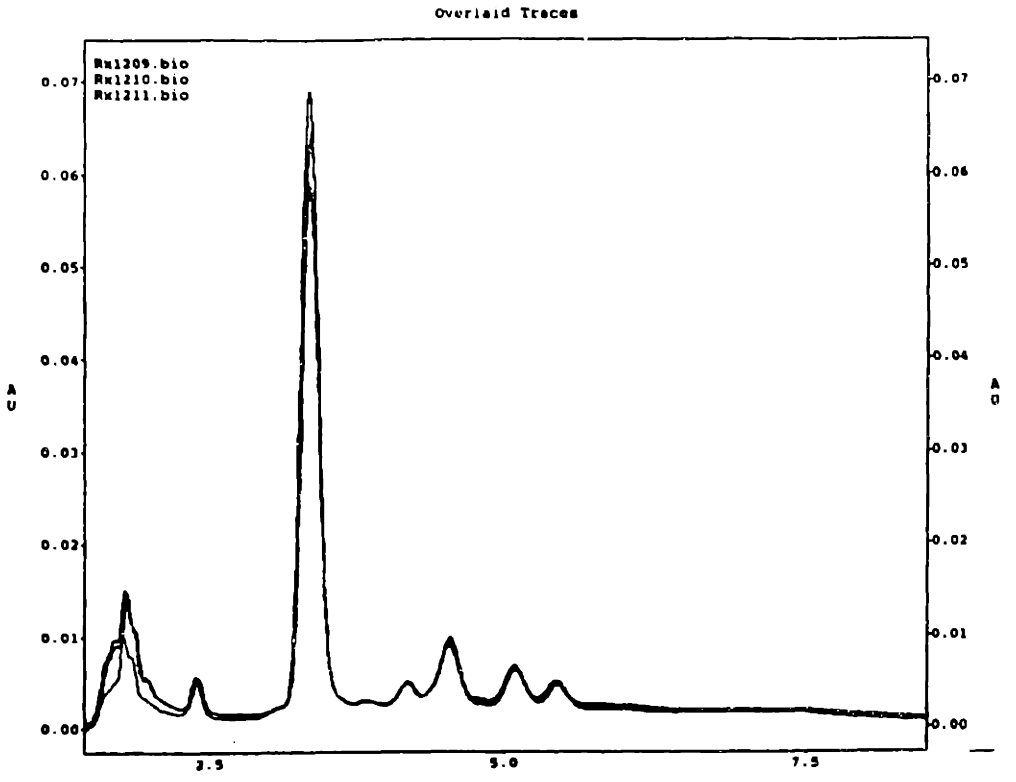

Figure 4.19 Heparin Fragments in presence of trunc. Maxidialin
Anion Exchange Chrometographic separation of heparin fragments obtained by degradation of heparin by heparinase in the presence of no peptide (the control), 10µg and 20µg Maxidialin. The profiles are identical in the presence of the peptide.

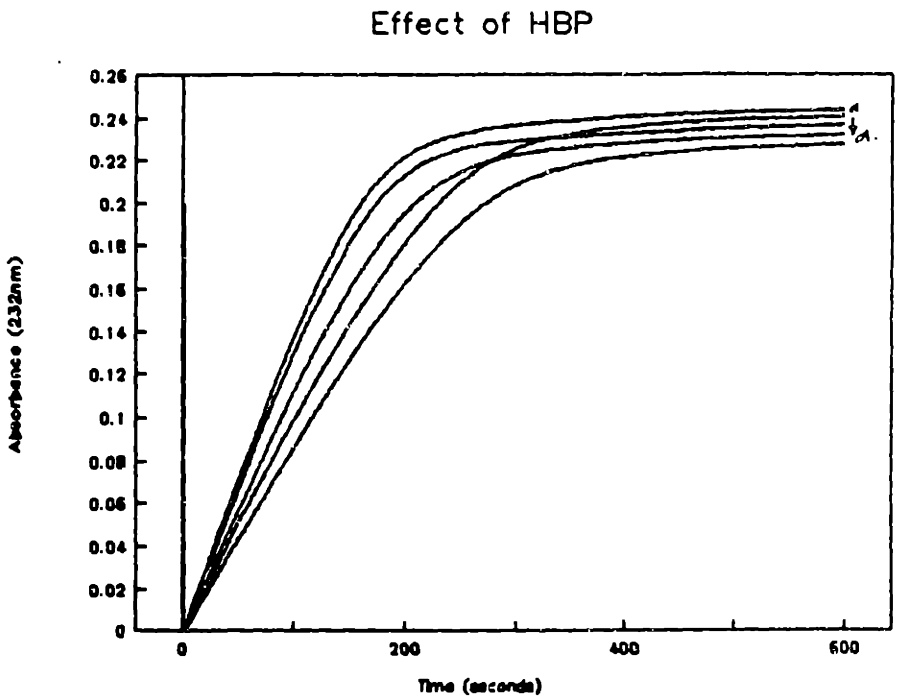

Figure 4.20 Heparin Degradation by Heparinase in the presence of HBP
Absorbance at 232nm followed as a function of time. (a) control reaction with no peptide (b) 5µg HBP, (c) 10µg HBP, (d) 15µg HBP, (e) 20µg HBP.

and digest it. If the binding affinities were equal, the saturation point would be lower in the presence of the peptide.

The degradation product profile in the presence of HBP at short times is identical to the product profile of the control reaction (Figure 4.21). However, when the reaction mixture in the presence of the peptide is incubated overnight, even at room temperature, tetrasaccharide 3 disappears (Figure 4.22). The products of a control reaction, however, does not change after the long incubation with the enzyme, indicating that the peptide makes this tetrasaccharide digestible by the enzyme. Further investigations, where this tetrasaccharide was isolated and incubated with the enzyme confirm that this tetrasaccharide is indeed being cleaved by the enzyme in the presence of the peptide (section 4.2.2.2.7)

4.2.2.1.5 *Effect of P13*

P13, the peptide isolated from HBEGF, has been shown to bind more tightly to heparin than HBP (section 4.2.2.3). However, P13 seems to have no effect on the degradation reaction (Figure 4.23). The absorbance profile in the presence of different concentrations of P13 indicates that the degradation of heparin is not affected by the presence of the peptide. The binding site of P13 on heparin might be far removed from the enzyme binding site. As a result, the binding and hence the degradation of the heparin by the enzyme is not affected by increasing quantities of the peptide P13. The independence of the reaction on the enzyme kinetics can also be due to differences in binding affinities. If the binding constant of the enzyme to heparin is much higher than the binding constant of the peptide to heparin, the enzyme would displace the peptide and the reaction would then be independent of the peptide concentration.

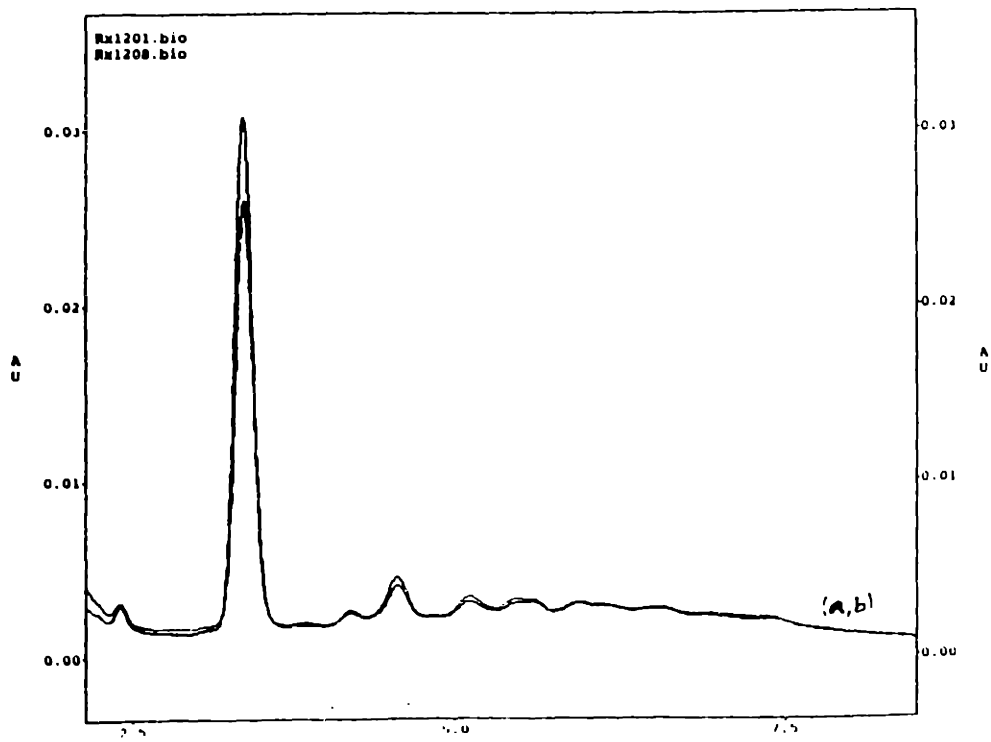

Figure 4.21 Heparin Fragments in presence of HBP (short time)
Anion Exchange Chromatographic separation of heparin fragments obtained by degradation of heparin by heparinase. Degradation quenched after 20min (a) control reaction with no peptide, (b) 20 µg HBP.

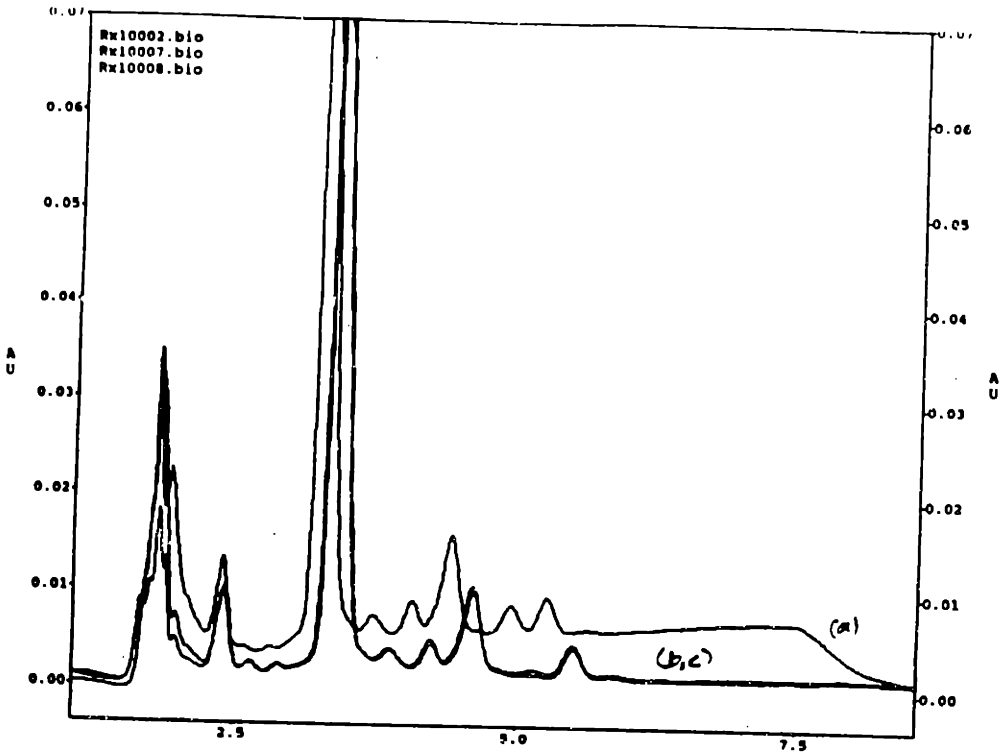

Figure 4.22 Heparin Fragments in presence of HBP (long reaction)
Anion Exchange Chromatographic separation of heparin fragments obtained by incubating heparin with heparinase overnight.
(a) control reaction with no peptide, (b) 10 μg HBP, (c) 20μg HBP.

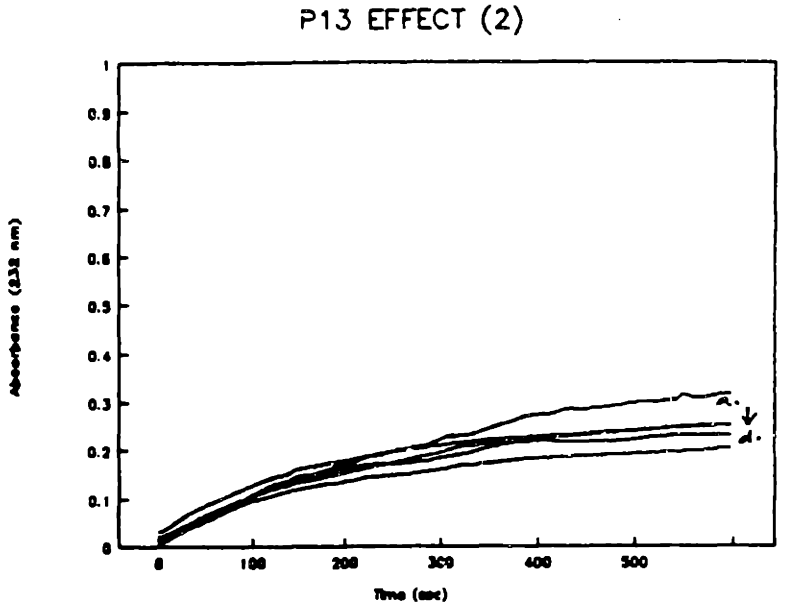

Figure 4.23 Heparin Degradation by Heparinase in the presence of P13
Absorbance at 232nm followed as a function of time. (a) control reaction with no peptide (b) 5μg P13, (c) 10μg P13, (d) 20μg P13

The degraded product profile at the end of the reaction is exactly identical to that of the control reaction (Figure 4.24). However, like HBP, P13 also facilitates he degradation of tetrasaccharide 3 when the reaction mixture is incubated with the enzyme for long time periods.

4.2.2.1.6 *Effect of P21*

P21, on the other hand, seems to increase the reaction rate drastically. Figure 4.25 shows the degradation of heparin in the presence of P21. The absorbance at 232 nm seems to increase with increasing peptide concentrations, suggesting an overall increase in the reaction rate. Also, the saturation value of the absorbance is much higher than the control runs. This indicates a larger number of double bonds formed in the reaction. The amount of product formed seems to be much higher in the presence of P21. This also implies that the saturation observed in the control runs is probably not because non-availability of heparin chains but some other mechanism that stops the reaction. Product analysis of the reaction in the presence of P21 confirms that the amount of product formed is much higher than in the control reaction (Figure 4.26). There is also no differentiation in the kind of product formed in the presence of P21 as the product distribution is exactly identical to the control reaction. The amount of long heparin fragments that elute at high salt concentrations (more than .7M) are lower in the presence of the peptide. Like the other peptides, P21 also facilitates the degradation of tetrasaccharide 3 by the enzyme at long reaction times.

4.2.2.1.7 *Degradation of Heparin Fragments*

These results suggest that at the end of 10 minutes of a control reaction, there are large chains of heparin molecule that are not broken down. The saturation could be a result of enzyme inactivation with time, rather than a non-availability of heparin

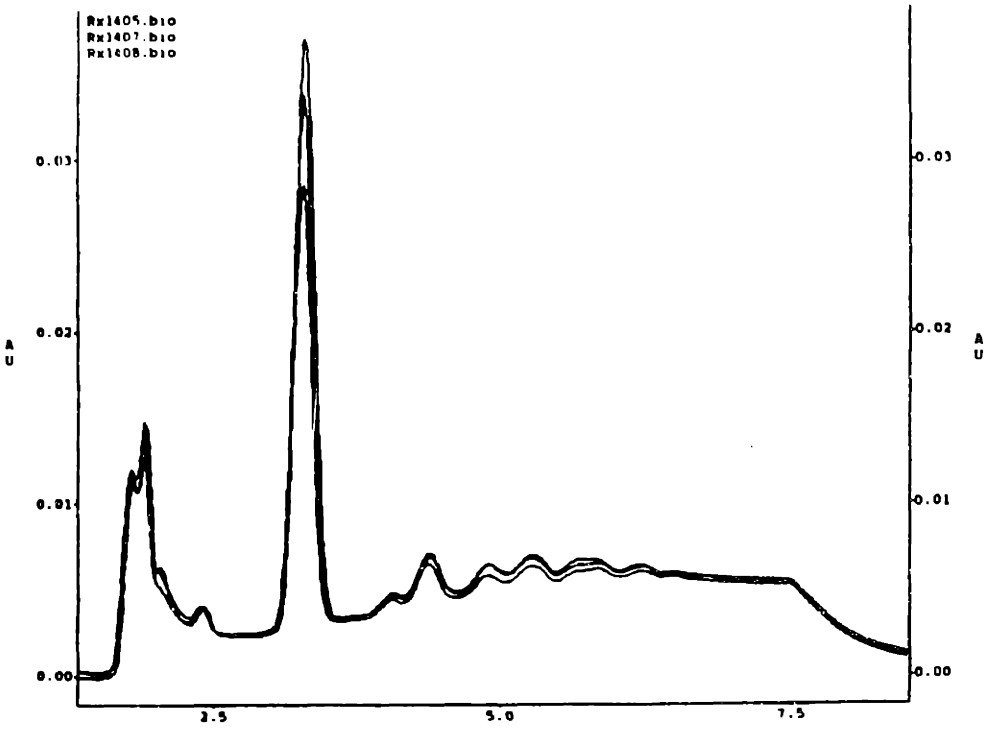

Figure 4.24 Heparin Fragments in the presence of P13
Anion Exchange Chromatographic separation of heparin fragments obtained by degradation of heparin by heparinase in the presence of no peptide (the control), 10μg and 20μg P13. Addition of P13 does not alter the product profile.

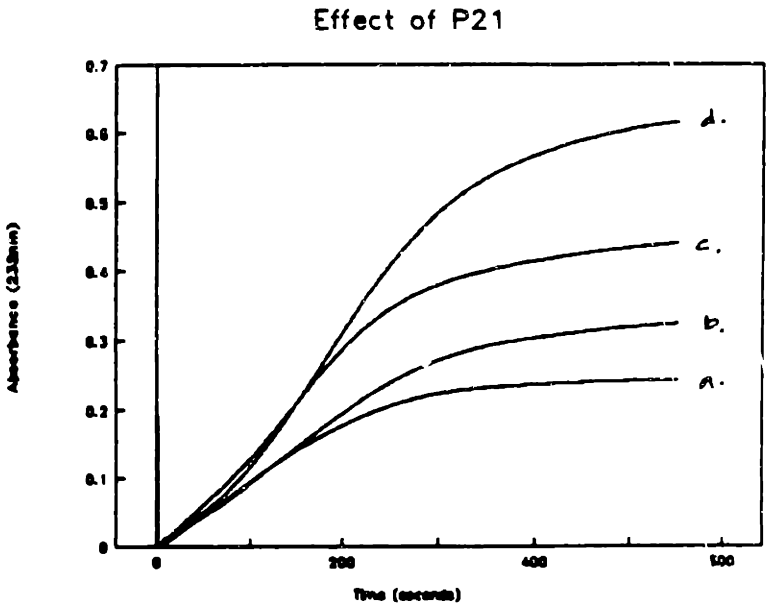

Figure 4.25 Heparin Degradation by Heparinase in the presence of P21
Absorbance at 232nm followed as a function of time. (a) control reaction with no peptide (b) 5µg P21, (c) 10µg P21, (d) 15µg P21.

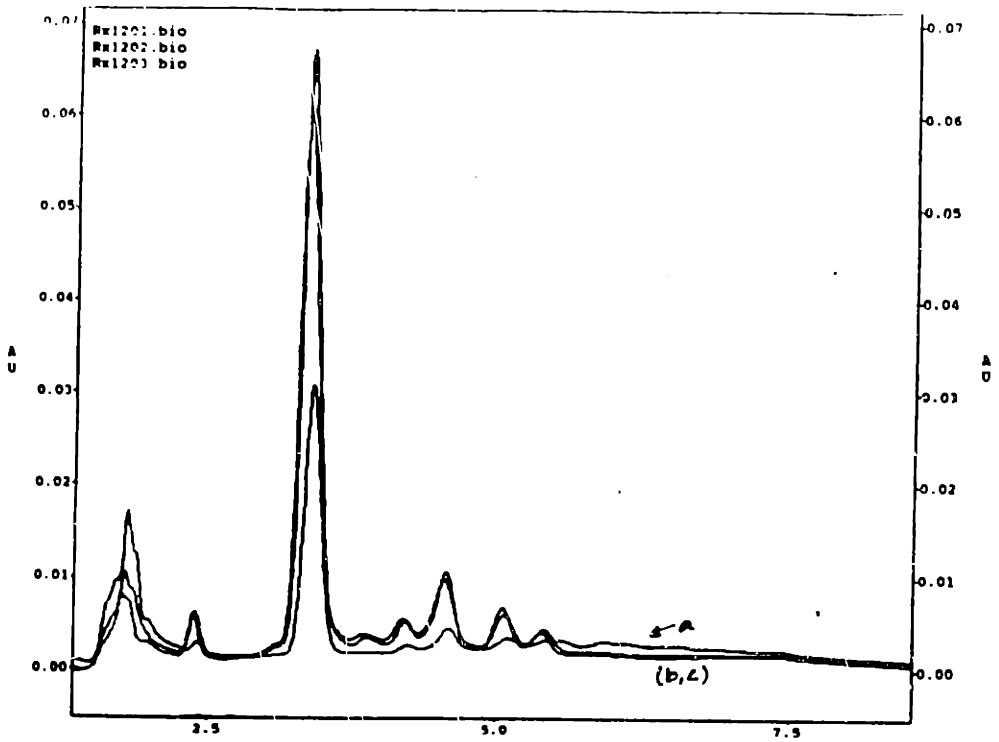

Figure 4.26 Heparin Fragments in the presence of P21
Anion Exchange Chromatographic separation of heparin fragments obtained by degradation of heparin by heparinase (a) control reaction- no peptide, (b) 10μg P21, (c) 15 μg P21

molecules. Addition of more enzyme after the saturation point (10 minutes) does not affect the amount of products formed (Figure 4.27). Also, addition of more heparin after 10 minutes of digestion clearly shows that the enzyme is still active (Figure 4.28). These experiments indicate that the enzymatic degradation stops within 10 minutes although the enzyme is still active at this time. Reactions in the presence of P21 indicate a much higher amount of product formed, suggesting that the undigested heparin chains, in the presence of P21 are rendered easily degradable by the enzyme. The addition of P21 after the saturation (10 min.) causes the same increase in the absorbance and the amount of products formed (Figure 4.29). This clearly indicates that the unreacted heparin chains after the saturation of absorbance are made digestible by P21. HBP and P13, however, do not cause this additional degradation.

The inability of the enzyme to completely degrade all the heparin molecules could be due to inactivation of the enzyme by the products formed. It is likely that the products, e.g., tetrasaccharides, bind very tightly to the enzyme thereby preventing other longer heparin chains to be digested. The addition of a peptide like P21, could compete with binding of the tetrasaccharide to the enzyme, making the enzyme free to bind to undigested heparin chains. This suggests that the relative affinity of the products to the peptide P21 is much higher than its affinity to the enzyme.

However, the binding of the peptide to the tetrasaccharides seems to make the saccharides more vulnerable for enzymatic degradation. As mentioned earlier, tetrasaccharides 1 and 3 can be further cleaved by the enzyme to form disaccharides. However, the rate of this cleavage is extremely slow. Figure 4.30 shows the enzymatic degradation of tetrasaccharide 3 in the presence of the different peptides. The degradation of the saccharides in the absence of the peptides is also plotted in

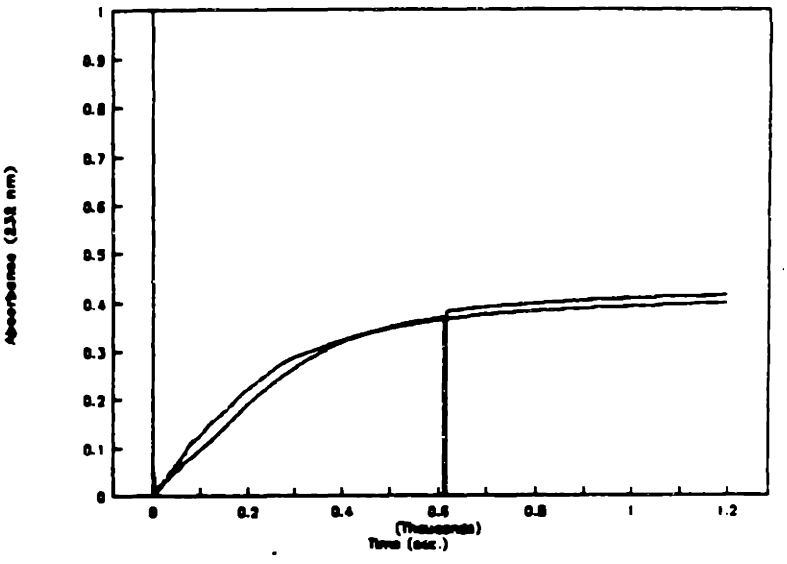

Figure 4.27 Heparin degradation by heparinase - enzyme activity
Addition of fresh enzyme after the saturation (10 min.) does not increase the absorbance at 232nm. No addtional product is formed by addition of more enzyme.

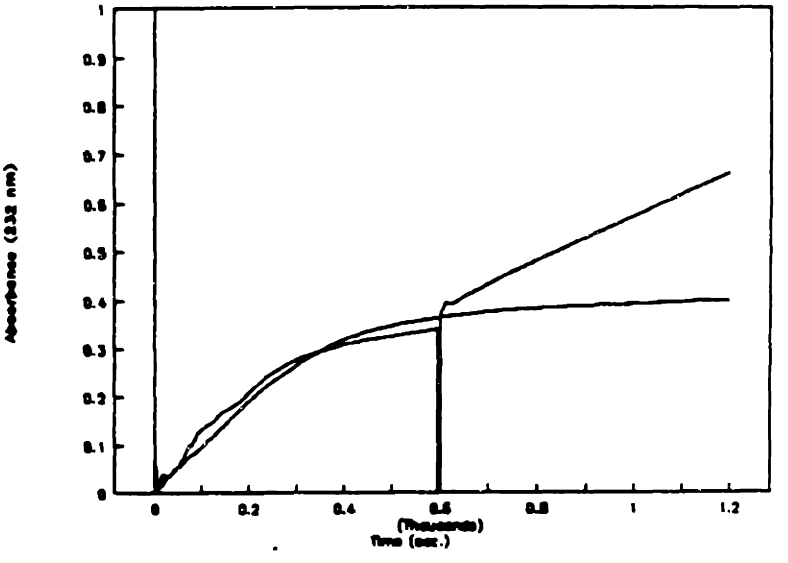

Figure 4.28 Heparin degradation by heparinase - enzyme activity
Addition of fresh heparin after the saturation (10 min.) increases the absorbance at 232nm. The enzyme seems to be still active.

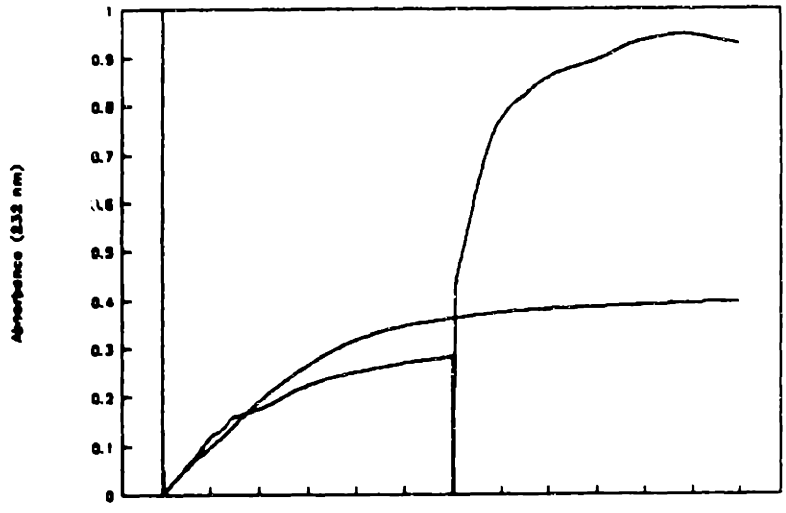

Figure 4.29 Heparin degradation by heparinase - Addition of P21
Addition of peptide P21 after the saturation (10 min.) dramatically increases absorbance at 232nm. Peptide P21 seems to facilitate the enzyme to degrade heparin fragments.

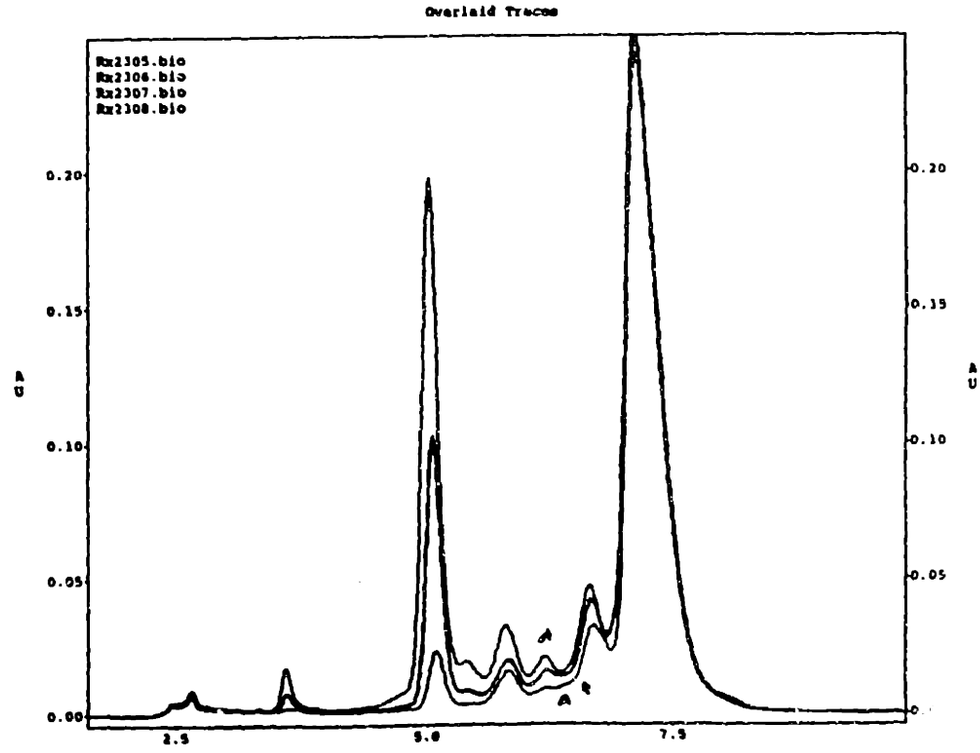

Figure 4.30 Degradation of Tetrasaccharide-3 by Heparinase-I
Tetrasaccharide-3 (ΔUHIH) purified by anion exchnage chromatography and incubated with heparinase-I. (a) control reaction with no peptides, (b) 10μg HBP, (c) 10μg P13, (d) 10μg P21.

the same graph. There is a dramatic increase in the rate of disaccharide formation in the presence of the peptides. The increase is more pronounced for P21 than for P13 and HBP, consistent with earlier observations. The binding of the peptide to the tetrasaccharide 3 seems to facilitate the cleavage of the saccharides. This could be due to a more rigid conformer of the tetrasaccharide in the presence of the peptides, facilitating easy binding by the enzyme. This implies that the binding site on the tetrasaccharide for the peptide and the enzyme are different. The saccharide can, at any instant of time, be bound to both the enzyme and the peptide, the peptide inducing the rigidity, while the enzyme cleaves the linkage.

The bond between the hexosamine and the glucuronic acid residue in tetrasaccharide 2 (Figure 4.17) cannot be cleaved by the enzyme. The binding of peptides to this saccharide does not make this bond any more susceptible to cleavage (Figure 4.31). The addition of different amounts of peptide does not aid the digestion of this tetrasaccharide.

Isolation of large amounts of hexasaccharide and incubating with the enzyme displayed a increase in the amount of smaller oligosaccharides (Di- and Tetrasaccharides). Addition of peptides enhanced this digestion, as seen with the other saccharides (Figure 4.32).

The analyses has considered heparin molecules to be a linear chain and the enzyme acting at the iduronic acid residue. Heparin, however, shows a strong circular dichroic activity, in the far-UV region (Figure 4.33), indicating the presence of some tertiary structure. Heparinase might therefore, not just recognize the primary sequence of heparin and cleave it but bind to a certain spatial arrangement of saccharides. Glucuronic acid might disrupt this secondary structure of the heparin

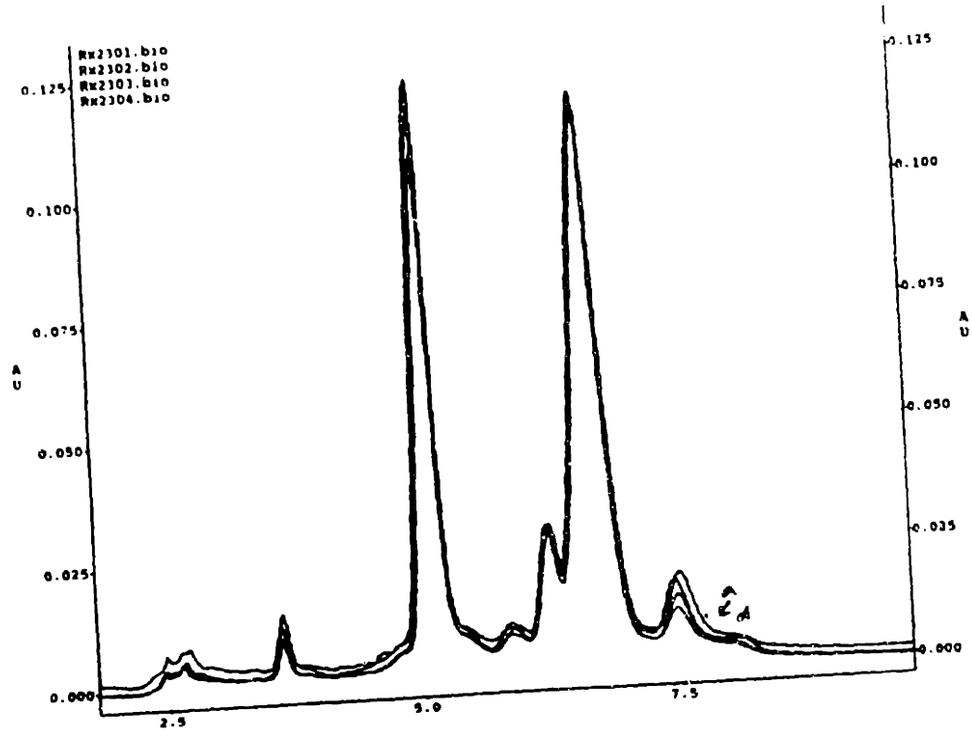

Figure 4.31 Degradation of Tetrasaccharide-2 by Heparinase-I
Tetrasaccharide-2 (ΔUHGH) purified by anion exchnage chromatography and incubated with heparinase-I. (a) control reaction with no peptides, (b) 10μg HBP, (c) 10μg P13, (d) 10μg P21.

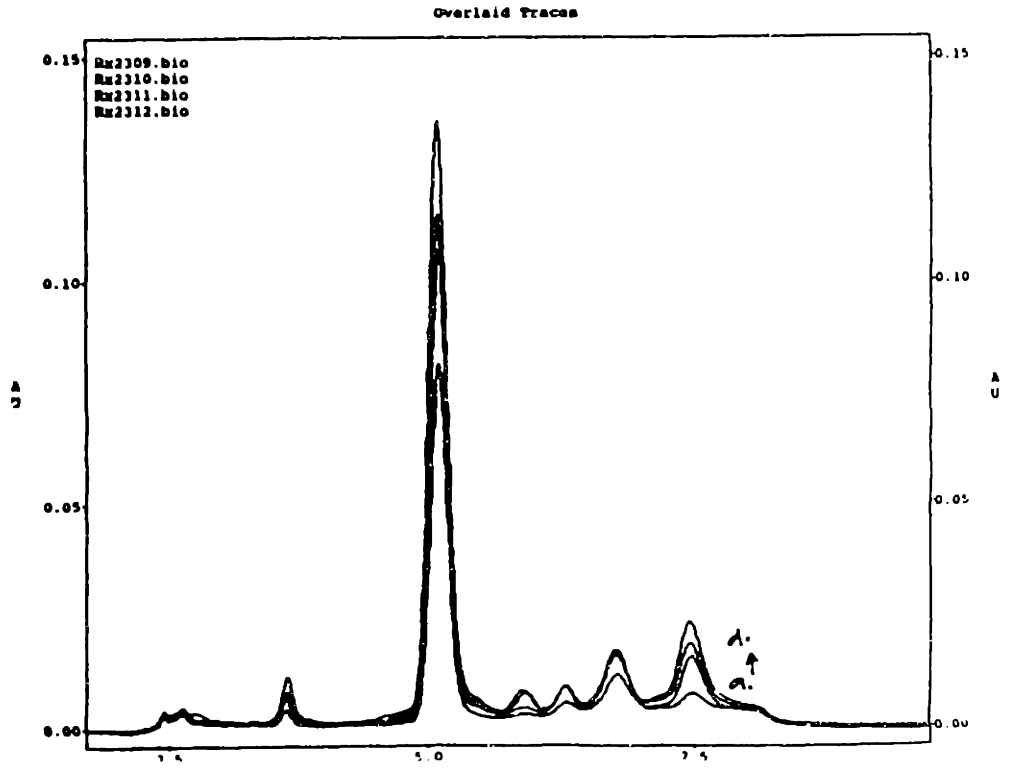

Figure 4.32 Degradation of Hexasaccharide by Heparinase-I
Hexasaccharide (ΔUHIIHGH) purified by anion exchnage chromatography and incubated with heparinase-I. (a) control reaction with no peptides, (b) 10μg HBP, (c) 10μg P13, (d) 10μg P21.

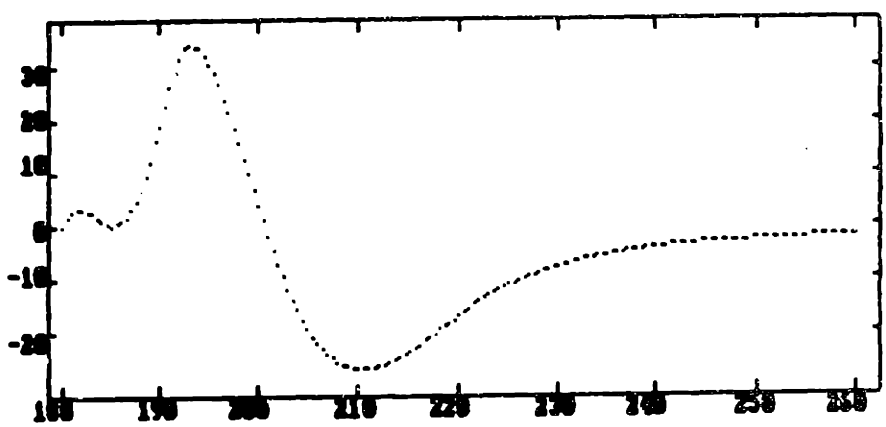

Figure 4.33 Secondary Structure of Heparin
Circular dichroism spectrum of Heparin chains in water

molecule, thereby making it non-cleavable by the enzyme. Also, a critical number of disaccharides would be required for the formation of secondary structure in the heparin chains. The random endolytic cleavage of heparin by heparinase possibly leaves behind chains of heparin that are not capable of forming the secondary structure and hence, are not capable of being cleaved. This could explain the saturation of the absorbance values after a certain time, although large heparin chains still exist in the reaction mixture.

The addition of peptides, especially P21, aid the enzymatic digestion of these heparin fragments. The peptides, might induce certain secondary structure to these heparin chains, thereby making it degradable by the enzyme. This induction of secondary structure has been observed by CD studies earlier, but has been attributed to changes in the conformation of the peptide rather than the heparin molecule. The interaction of the peptides with heparin fragments, as small as tetrasaccharides, induces a conformation to these oligosaccharides that makes it digestible by the enzyme. These results open an important variable in the study of heparin-protein interactions - the conformation of heparin. The oligosaccharide conformations have been ignored mostly in earlier studies. Conformational studies on heparin chains might hence provide valuable information that aid in our understanding these interactions.

Cardin and Weintraub (1989) suggest that the heparin interaction is mediated through simple charge interactions between regions of the protein and the sulfate and carboxylic groups of heparin. The consensus heparin binding sequence requires the arrangement of basic amino acids separated by spacers. All the peptides systems considered in this study confirm to the consensus sequence proposed by Cardin and Weintraub. However, the binding characteristics of these peptides to heparin seem

to be quite different. Peptides P13 and P21, isolated from the same parent molecule, exhibit vastly different properties. The results clearly indicate that in addition to the arrangement of basic amino acids according to the consensus sequence, other factors are important in heparin binding. The conformation of the molecule and the arrangement of hydrophobic residues in the primary sequence could be a few of the factors that influence heparin binding.

4.2.2.2 Chromatographic Characterization

The acceleration of the enzymatic reaction in the presence of P21 is interesting, especially because P13, which is 8 amino acids lesser than P21, seems to have no significant effect on the degradation rate. The additional eight amino acids seem to confer a unique structure of the peptide whereby it interacts differently with the heparin. The formation of multimers of P21 through disulfide linkages could lead to higher order conformers interacting more specifically with regions in heparin chain, making the heparin more easily digestible by the enzyme. P13, however, is not capable of forming multimeric aggregates due to the lack of cysteines (Figure 4.10).

Figure 4.34 shows the chromatographic separation of P21 in reversed phase (C18) column. The predominant peak is the monomeric form of the peptide (peak 1), while the higher order structures elute as three different peaks in this gradient (peaks 2, 3, and 4). Reduction and derivatization of the cysteine using Iodo-acetic acid disrupts the disulfide bond formation. Chromatographic analysis of the reduced P21 indeed confirms that there is a significant amount of multimeric aggregates of P21, stabilized by disulfide linkages. The different peaks could be different orientations of the disulfide linkage leading to dimers with slightly

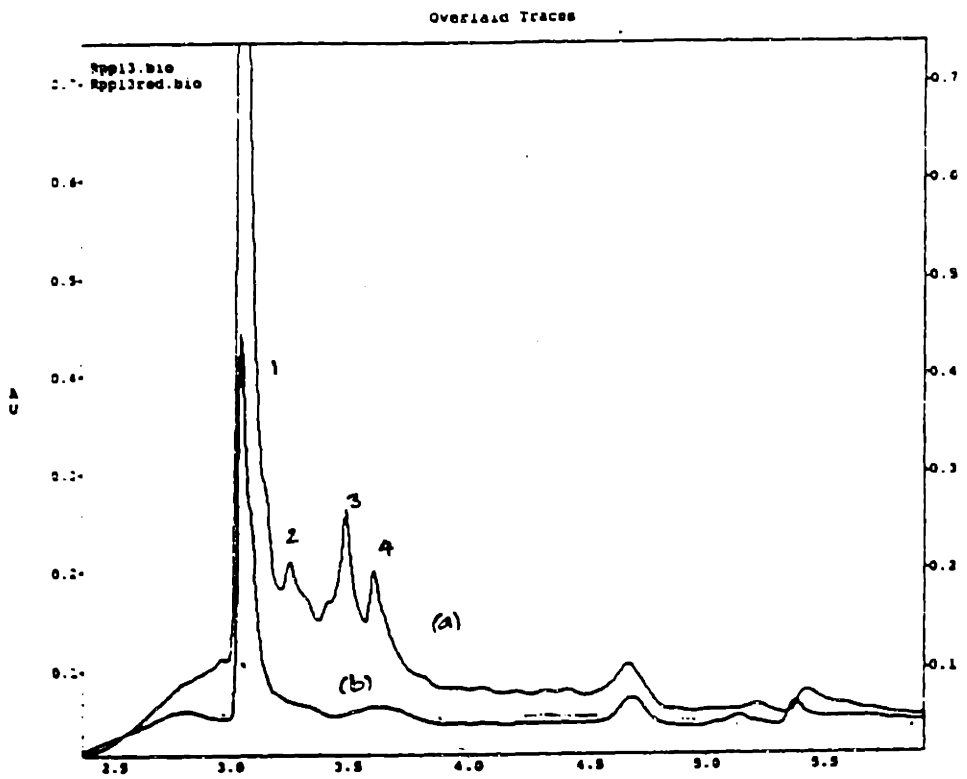

Figure 4.34 Chromatographic Characterization of P21
Reverse Phase Chromatogram of P21 in POROS C-18 column.
(a) crude P21; peak 1 represents monomeric P21, peaks 2, 3, and 4 represent mutimeric forms
(b) Cysteine-17 of P21 reduced and derivatized with iodo-acetic acid.

different properties. Formation of multimers through a more complex interactions between the dimers or the monomeric units is also possible.

The affinities of multimeric P21 molecules to heparin might explain unusual effects on the enzyme kinetics. The binding strength is estimated from the amount of salt required to disrupt the interaction between the peptide molecules and heparin. Figure 4.35 shows the chromatographic trace of a P21 on a heparin POROS column. The appearance of two peaks in the salt gradient elution confirms the presence of a peptide population with higher heparin affinity. Analysis of the peaks separately on the heparin column indicates that peak 2 exhibits a higher affinity to heparin than peaks 1, 3, and 4 (Figure 4.35). Moreover, the higher affinity peak on the heparin column disappears when the Cysteine is derivatized. This clearly demonstrates that the higher affinity to heparin is a result of a more complex multimer formation. A SDS-PAGE analysis of the multimers of P21 indicates that peak 2 is about twice the size of peak 1, indicating peak 2 is a dimer of peak 1.

4.2.3 Binding Affinities

4.2.3.1 Specificity Studies

The disaccharide building units of chondroitin sulfate A and C are structurally very similar to heparin (Figure 4.36). The difference between these acidic polysaccharides lies in the type of linkage between the saccharides and the nature of the sugar backbone. Both, chondroitin sulfate A and C, have a 1-3 linkage of uronic acid to galactosamine, while in heparin, the uronic acid is linked by 1-4 α linkage. Chondroitin sulfate A is sulfated at the 4 position of the galactosamine, while

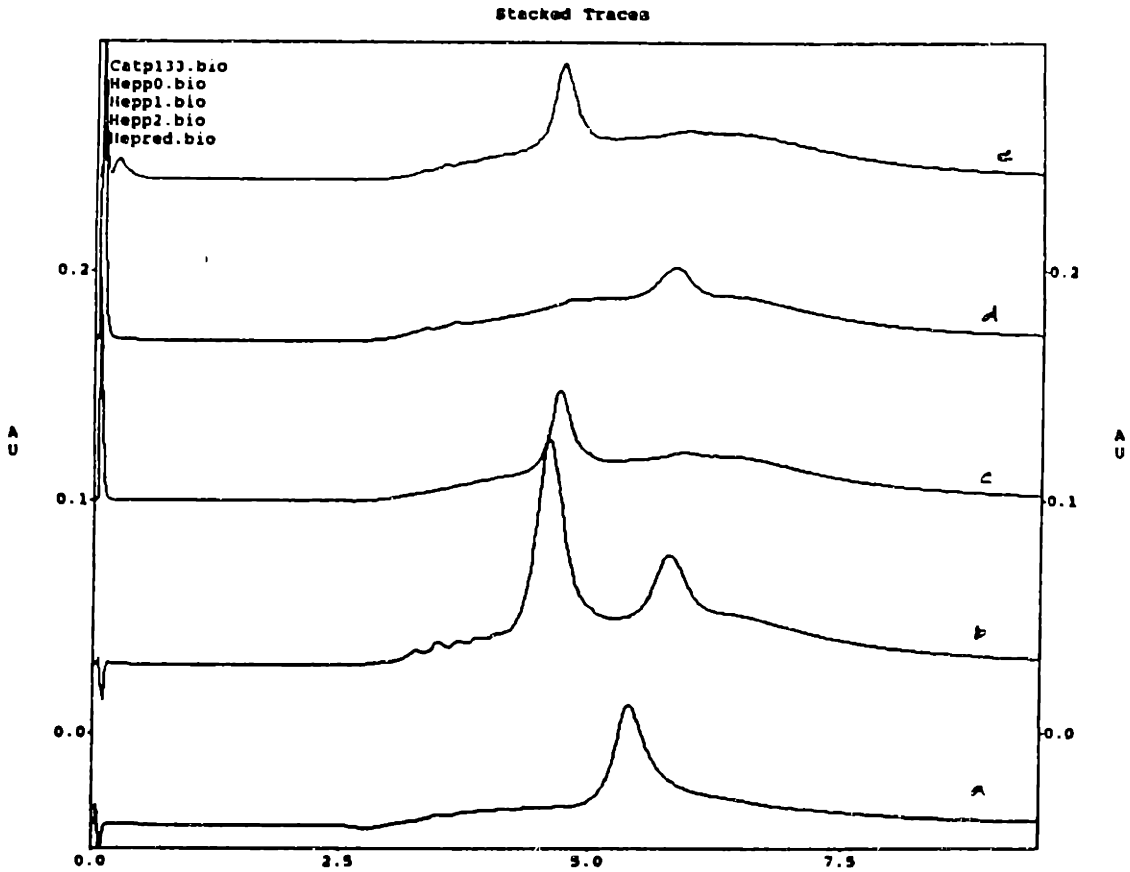

Figure 4.35 Chromatographic Characterization of P21
(a) P21 crude on a POROS cation exchange column, gradient of 0-1M Nacl in 5 min.
(b) P21 crude on a Heparin POROS, same gradient as (a).
(c) Monomer P21 (peak 1 of Figure 4.34) and multimer P21 (peaks 3, 4 of Figure 4.34) on Heparin POROS
(d) Dimer P21 (peak 2 of Figure 4.34) on Heparin POROS.
(e) P21's cysteine-17 reduced and derivatized, on Heparin POROS.

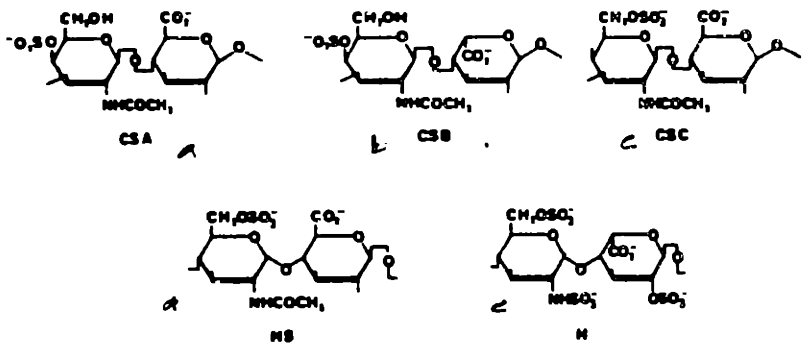

Figure 4.36 Basic Disachharide units of GAGs
(a) Chondroitin sulfate A, (b) Chondroitin sulfate B
(c) Chondroitin sulfate C (d) Heparin (e) Heparan sulfate

chondroitin sulfate C is sulfated at the 6 position of the same residue. The binding of peptides to these acidic polysaccharides, like other protein-ligand interactions, depends both on the structure of the peptide and the carbohydrate. The binding affinities of these peptides to the different oligosaccharide is expected to be different. In addition, binding of the peptides to the highly charged dextran sulfate is also considered as a control.

The difference in the binding affinity of the peptides was studied by competing the binding of the peptide to a heparin column using chondroitin sulfate A and C and dextran sulfate. If the peptide binds more strongly to the oligosaccharide in solution than the immobilized heparin, it would elute in the void volume along with the oligosaccharide. Conversely, if the binding affinity of the peptide to heparin is higher, the amount of peptide bound to the column will not be affected by increasing amount of oligosaccharides in the solution.

Figure 4.37 shows the chromatographic trace of HBP incubated with the different oligosaccharides, and loaded onto a heparin POROS column. Figure 4.37a shows that the amount of peptide bound to the heparin column decreases up to a heparin concentration of about 50µg. At higher heparin concentrations, there is still a small amount of peptide that binds to the immobilized heparin. Binding constant between the peptide and heparin can be estimated using these competition experiments.

Figure 4.37b and c shows that HBP binds to chondroitin sulfate A and C with a slightly lower affinity than to heparin. The amount of peptide bound to the immobilized heparin decreases with increasing chondroitin sulfate C concentration, suggesting that the binding affinities are similar. The effect is less pronounced with

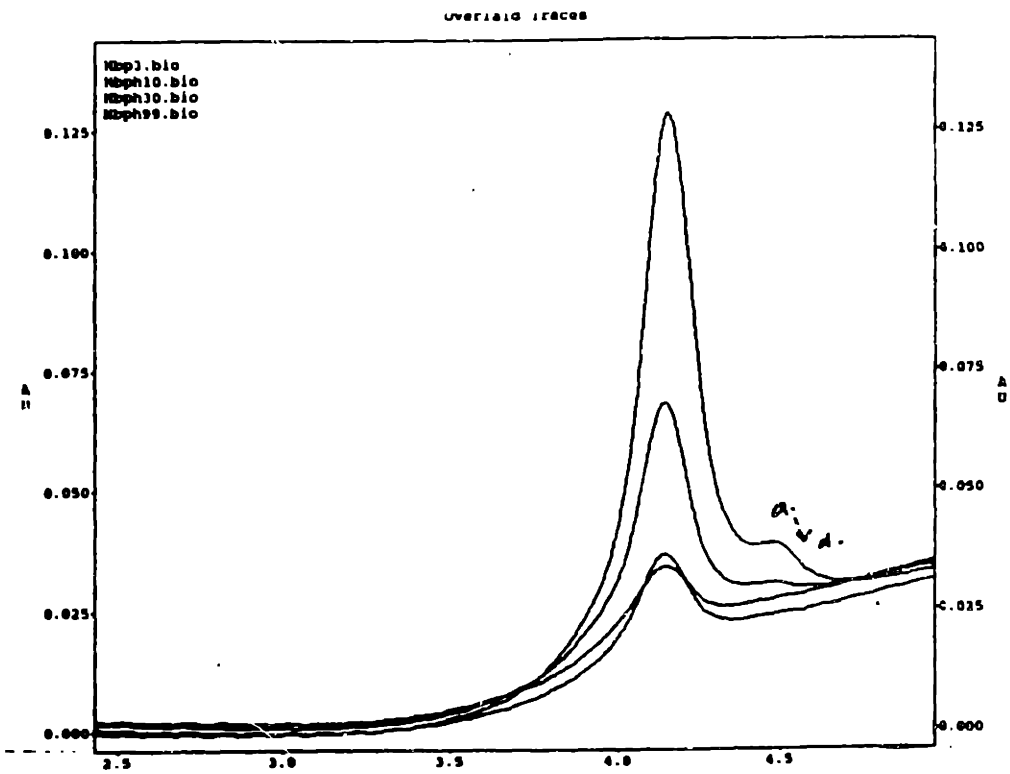

Figure 4.37a Specificity Study of HBP
100 µg of HBP loaded to heparin POROS column along with
(a) 0 µg heparin,(b) 10 µg heparin, (c) 50 µg heparin, (d) 100 µg heparin

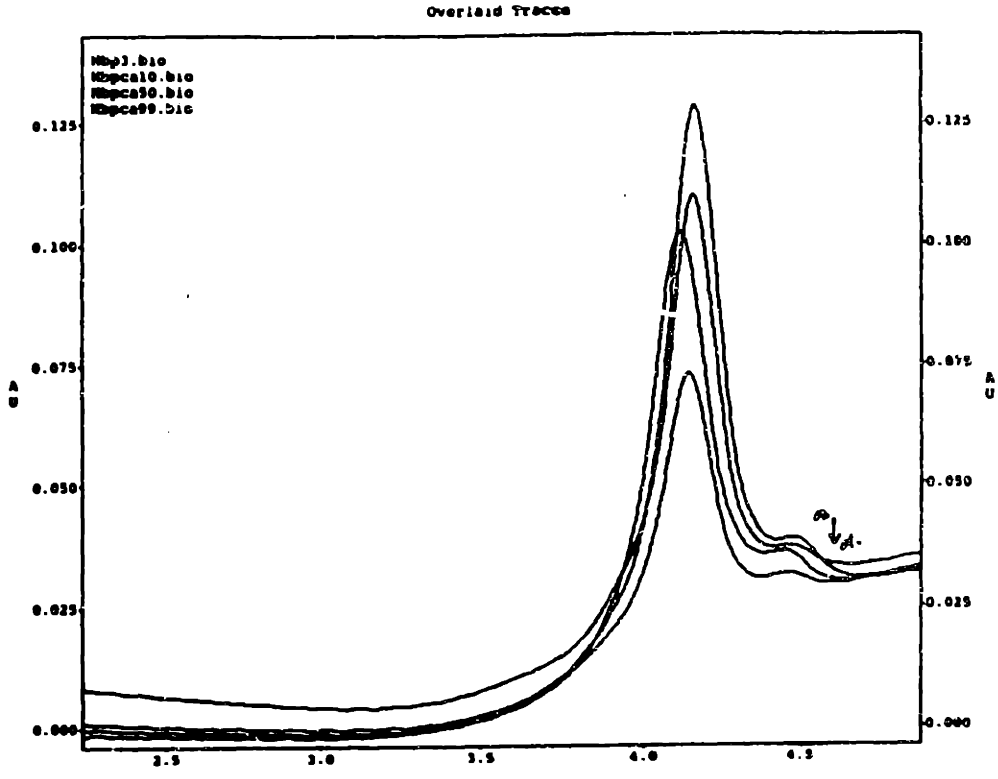

Figure 4.37b Specificity Study of HBP
100 µg of HBP loaded to heparin POROS column along with varying amounts of chondroitin sulfate A: (a) 0 µg, (b) 10µg, (c) 50 µg, (d) 100 µg.

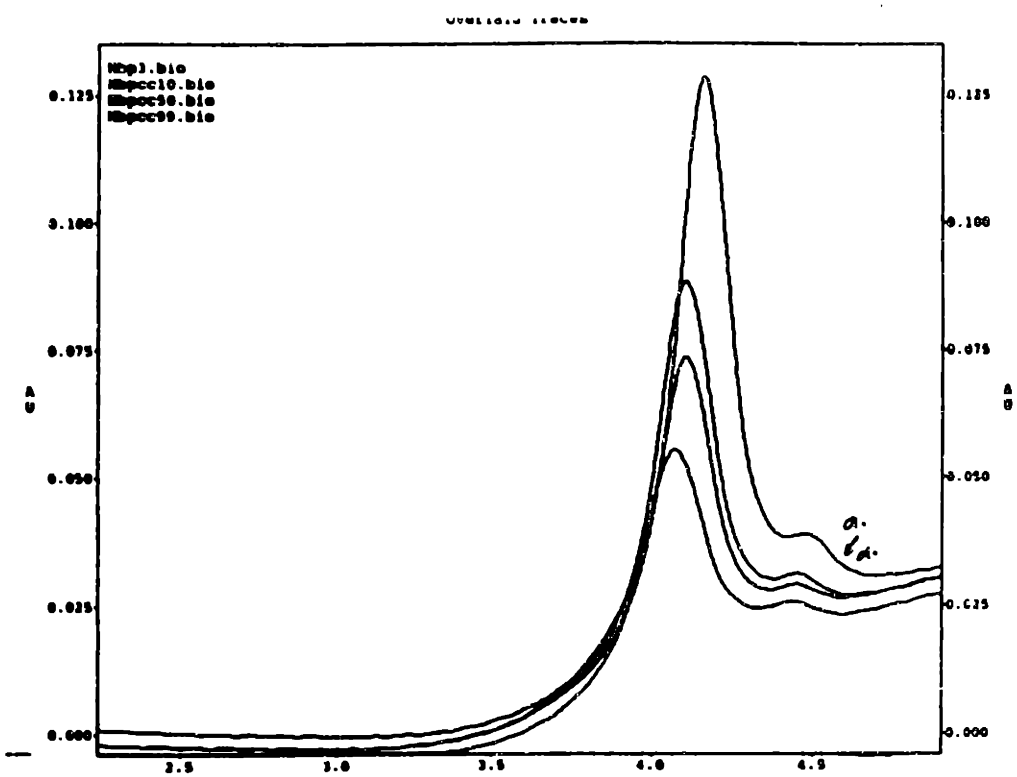

Figure 4.37c Specificity Study of HBP
100 µg of HBP loaded to heparin POROS column along with varying amounts of chondroitin sulfate C: (a) 0 µg, (b) 10µg, (c) 50 µg, (d) 100 µg.

chondroitin sulfate A, indicating a lower binding affinity to this proteoglycan. This indicates that sulfation in position 6 of the galactosamine is important for the higher binding affinity of HBP to chondroitin sulfate. Addition of dextran sulfate, however, is able completely compete the heparin binding of HBP, probably due to the highly anionic nature of this oligosaccharide (Figure 4.37d).

The peptide P13 seems to bind with higher affinity to heparin than chondroitin sulfate A or C (Figure 4.38). Addition of increasing amounts of chondroitin sulfate A or C does not alter the amount of peptide bound to an heparin column. This indicates that the peptide specifically binds to heparin immobilized in the column. The binding, however, is competed by the addition of increasing amounts of heparin to P13 before loading on the column. P13 is able to specifically recognize the oligosaccharides linked with an α 1-4 linkage as in heparin. The position of sulfation in the 1-3 linked chondroitin sulfate does not seem to affect the binding of P13. Also, P13 binds to dextran sulfate with an comparable affinity, as evidenced by the amount of peptide retained on the heparin column (Figure 4.38c).

The amount of P21 bound to the heparin column seems to decrease with increasing chondroitin sulfate C (Figure 4.39a). However, DP21 seems to be relatively insensitive to the added proteoglycan in solution indicating that the preferential binding of DP21 to heparin. This difference in the binding specificity might be a result of the conformational orientation of the charged and the hydrophobic residues of the peptides. Addition of dextran sulfate, however, seems to affect both P21 and DP21 to the same extent. The peptides seem to bind to dextran sulfate with the same affinity as to heparin (Figure 4.39b). The decrease in the amount of peptide bound to the column is the same when heparin or dextran sulfate is added.

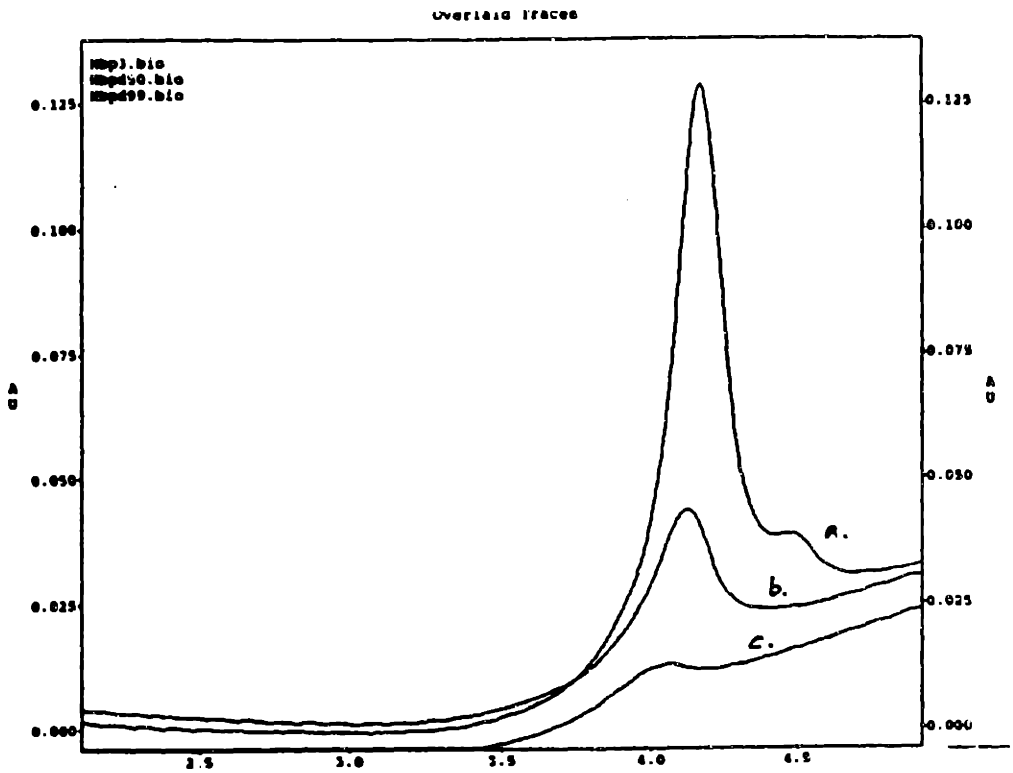

Figure 4.37d Specificity Study of HBP
100 µg of HBP loaded to heparin POROS column along with varying amounts of Dextran sulfate: (a) 0 µg, (b) 10µg, (c) 50 µg.

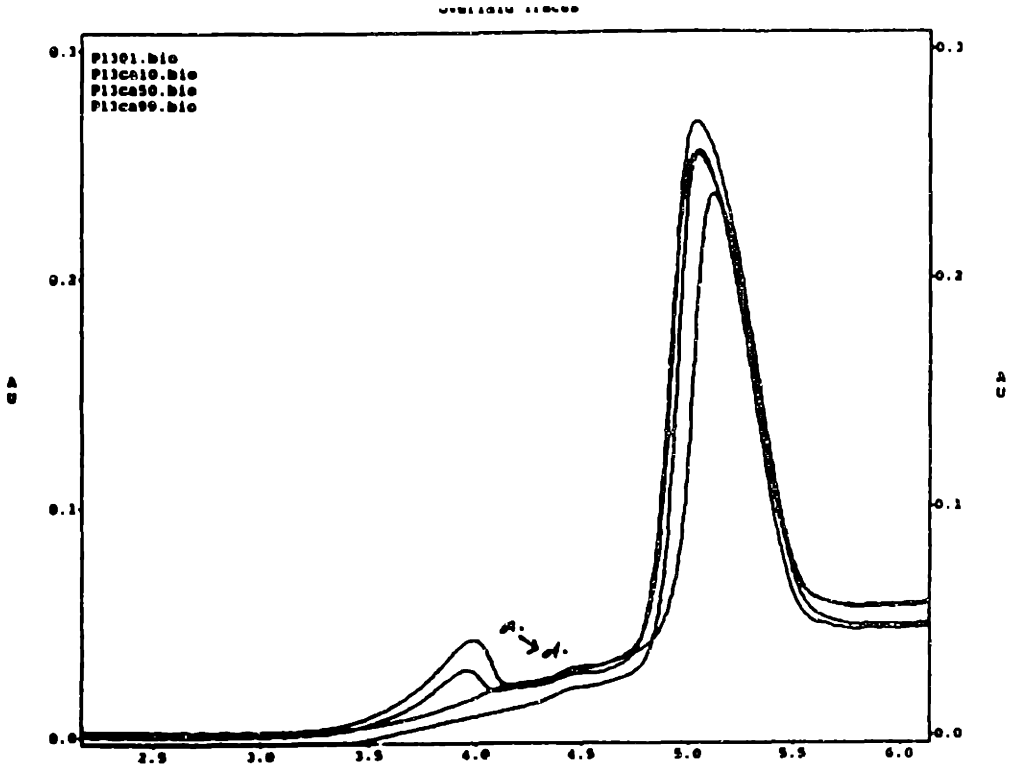

Figure 4.38a Specificity Study of P13
100 µg of P13 loaded on a heparin POROS column along with varying amounts of Chondroitin sulfate A: (a) 0 µg, (b) 10 µg, (c) 50 µg, (d) 100 µg.

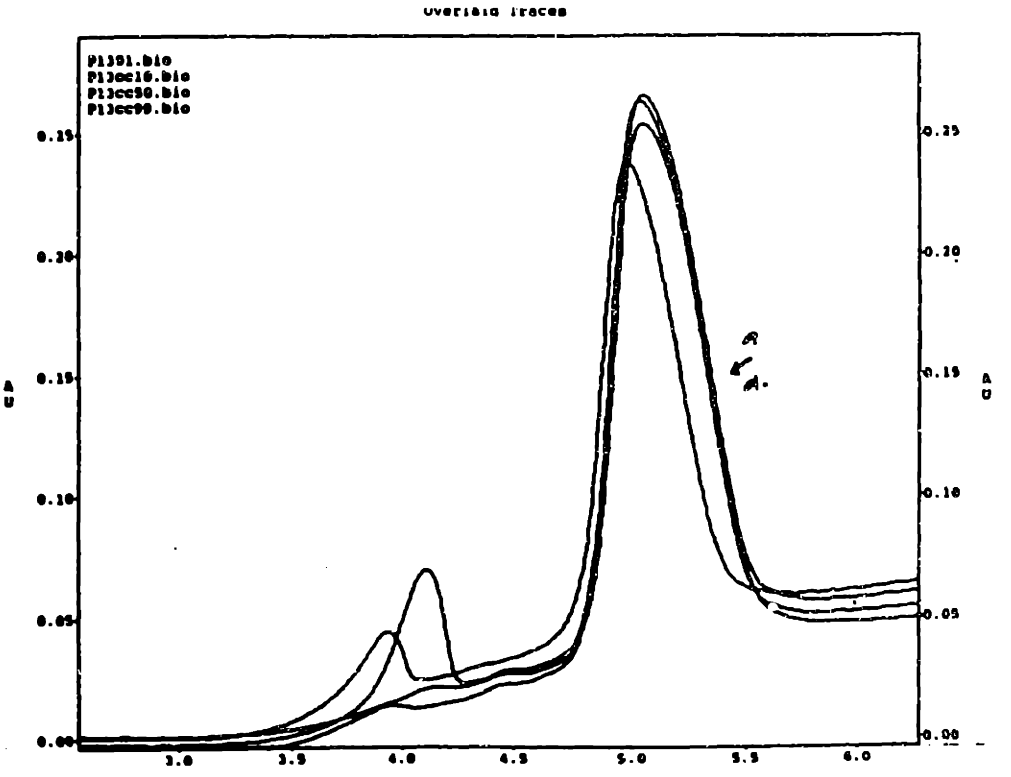

Figure 4.38b Specificity Study of P13
100 µg of P13 loaded on a heparin POROS column along with varying amounts of Chondroitin sulfate C: (a) 0 µg, (b) 10µg, (c) 50 µg, (d) 100 µg.

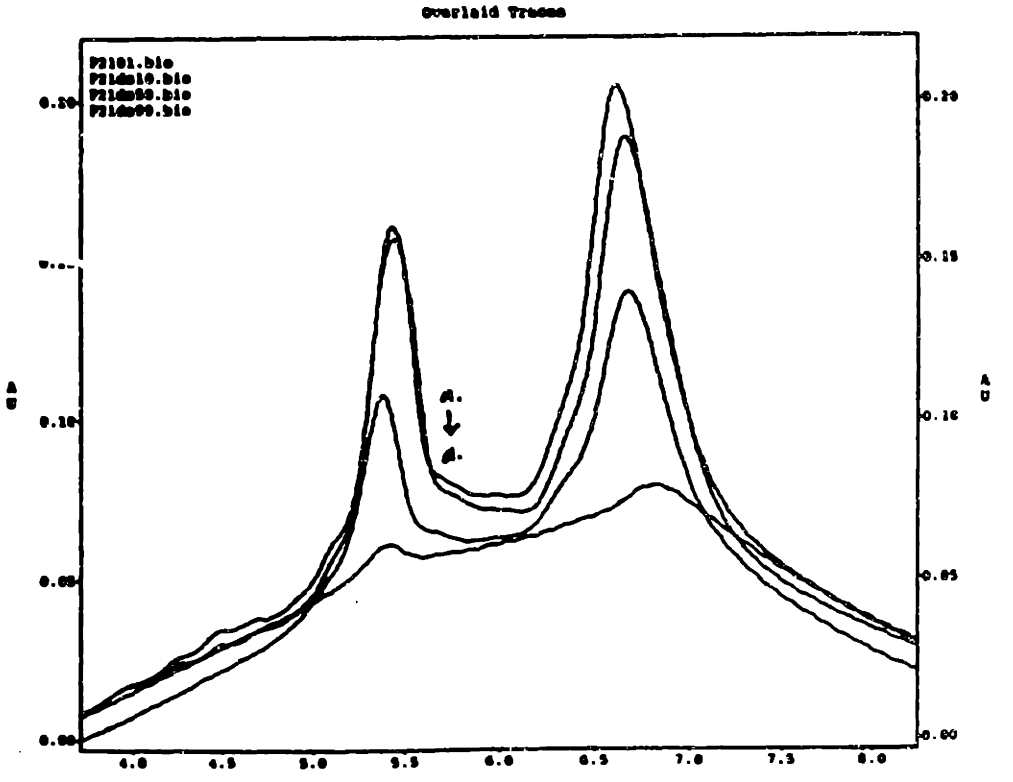

Figure 4.39b Specificity Study of P21
100 µg of P21 loaded on a heparin POROS column along with varying amounts of Dextran sulfate: (a) 0 µg, (b) 10µg, (c) 50 µg, (d) 100 µg.

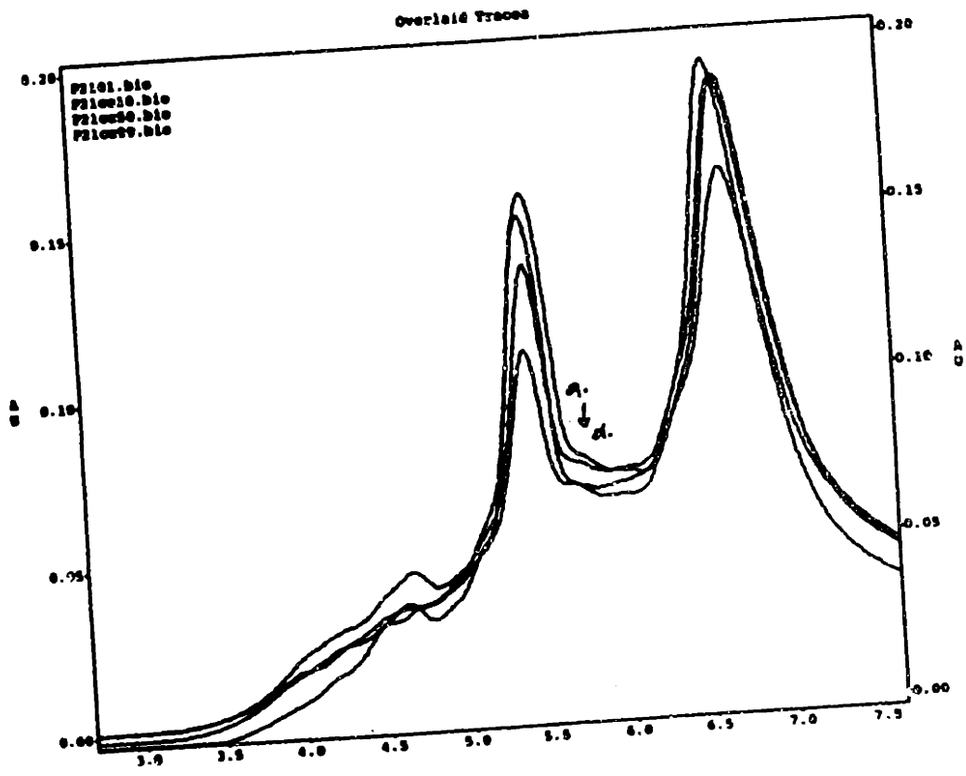

Figure 4.39a Specificity Study of P21
100 µg of P21 loaded on a heparin POROS column along with varying amounts of Chondroitin sulfate A: (a) 0 µg, (b) 10µg, (c) 50 µg, (d) 100 µg.

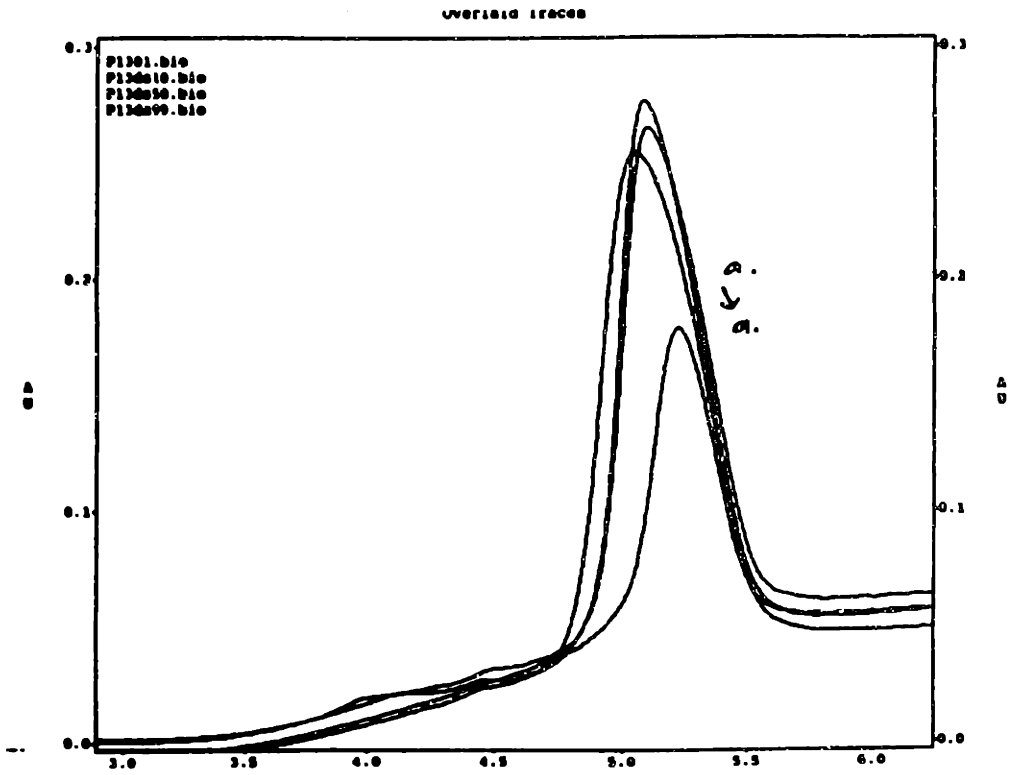

Figure 4.38c Specificity Study of P13
100 µg of P13 loaded on a heparin POROS column along with varying amounts of Dextran sulfate: (a) 0 µg, (b) 10µg, (c) 50 µg, (d) 100 µg.

These results indicate the peptides are able to specifically recognize certain oligosaccharide linkages, and hence certain structures of the acidic polysaccharides. Conformational analyses of these structures could lead to a better understanding of the nature of these interactions and the reasons for the specificity of the peptides to heparin. Peptide P13 and P21 seem to specifically recognize heparin chains even in the presence of related GAGs.

4.2.3.2 Capillary Electrophoresis

The mobility of a peptide through a glass capillary under an electrostatic field is dependent on the mass and the net charge of the peptide. In addition, the retention time of the peptide is also dependent on adsorption of the peptide on the negatively charged silica groups of the capillary wall. In order to calculate binding constants between a peptide and a ligand, it is important that the components do not absorb on the wall of the capillary.

Figure 4.40 shows the mobility of a neutral marker through a glass capillary 25cm long, when a field strength of 600V/cm is applied across the ends of the capillary. The retention time of the neutral marker is a measure of the endo-osmotic flow, as it does not interact with either the capillary wall or the applied electrostatic field. HBP, at a pH of 7.0, is positively charged and elutes before the neutral marker. There is a small amount of broadening of the peptide peak, probably due to the interaction of the peptide with the capillary wall.

The addition of the ligand, heparin, alters the mobility of the peptide-ligand complex. This change in the electrophoretic mobility comes about because of a change in the charge and the mass of the peptide-heparin complex. Heparin does

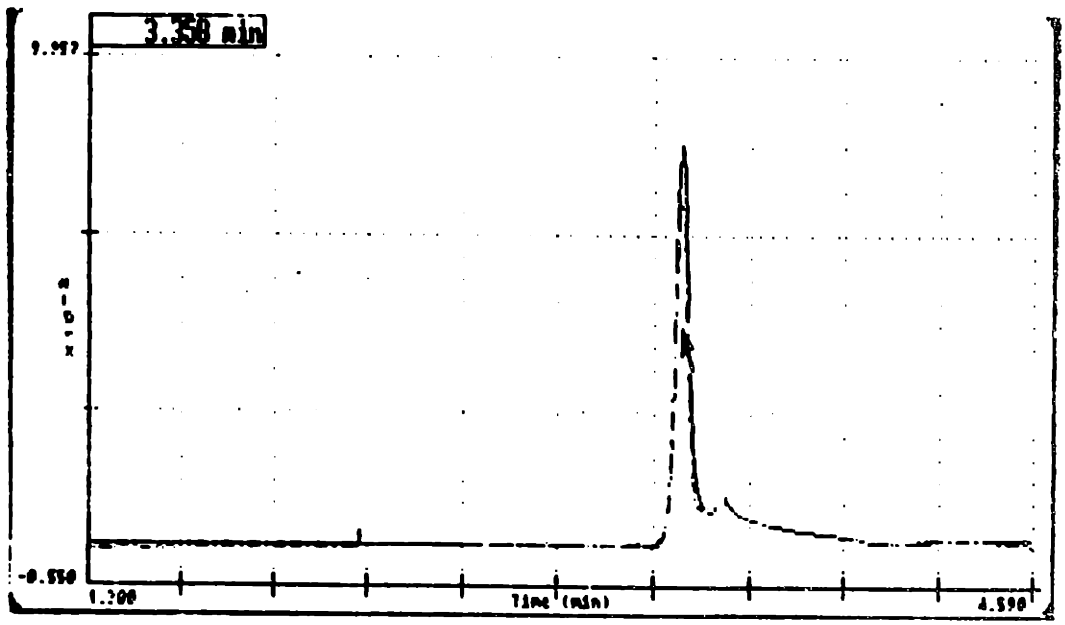

Figure 4.40 Endoosmotic flow in capillary electrophoresis
Mobility of the neutral marker (Mesityl oxide) in a 50μm ID capillary when 600V/cm is applied.

not absorb UV light, and hence cannot be detected by spectroscopic techniques. If the on-off rate for the binding is extremely low compared to the experimental time scales, one would observe two peaks - one corresponding to the bound peptide and the other to the free peptide. However, if the on-off rate for the binding is very high compared to the experimental time scales, a single peak with an altered electrophoretic mobility is observed. The change in the retention time of the peptide is correlated to the binding constant between the peptide and the heparin.

Figure 4.41 shows the increase in retention time of the peptide upon addition of increasing amounts of heparin in the electrophoretic buffer. The addition of heparin changes the ionic strength of the buffer and hence affects the endo-osmotic flow. This change in the endo-osmotic flow is reflected in the retention time of the neutral marker. Therefore, comparison of the retention time of the peptide peak relative to the neutral marker peak would be appropriate. The difference in retention time upon addition of heparin is expected to saturate at high heparin concentrations. However, in this experiment, the peptide-heparin complex was so highly negatively charged that the endo-osmotic flow was not sufficient to overcome the electrostatic force and hence the peptide heparin complex did not migrate through the capillary.

A Scatchard's analysis of the data should provide the binding constant, provided the approximations involved are valid. The binding constant between HBP and heparin is expected to be in the order of few nanomolar (Sasisekharan, 1991). In order to use Scatchard's analysis, the concentrations of the peptide and the heparin must also be in the same order of magnitude as the expected binding constant. However, the detection system of UV absorption through the capillary wall

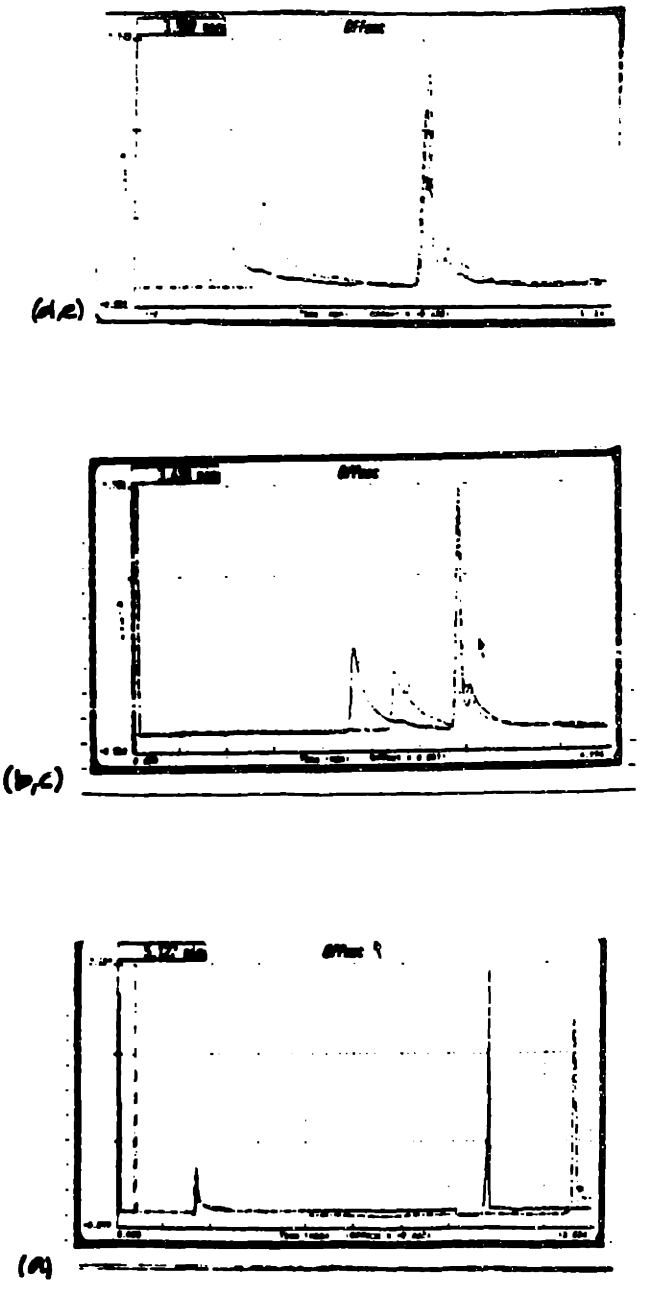

Figure 4.41 Capillary Electrophoresis of HBP with heparin
Mobility of the peptide in a 50μm ID capillary when 600V/cm is applied.
(a) HBP, (b) HBP + 0.25mg heparin, (c) HBP + 5mg heparin
(d) HBP + 10 mg heparin, (e) HBP + 60 mg heparin.

sensitive only in the order of few micrograms. As a result, a binding constant could not be calculated.

Efforts to increase the sensitivity of the detection focus currently on using field amplification techniques for sample concentration and also using fluorescence detectors and tyramine labeled heparin. It will be interesting to calculate the binding constant between the peptides and different heparin fragments using capillary electrophoresis. The attractive feature of this technique is the binding constant can be estimated very rapidly. The electrophoresis runs last about 10 min. and hence binding constants can be estimated within a few hours.

4.2.3.3 Fluorescence Spectroscopy

The fluorescence emission intensity and the wavelength depends on the electronic environment in the viscinity of the fluorescing moiety. Heparin binding in the proximity of the tryosines or tryptophan of a peptide would alter the fluorescing properties of the peptide. Figure 4.42 shows the fluorescence emission of AT-III in the presence of increasing quantities of heparin. The emission intensity increases upon addition of heparin, although the wavelength of emission does not change. This increase in the quantum yield with heparin concentration can be used to determine a binding constant between AT-III and heparin (Jordan et al., 1989).

Peptide P21 and DP21 have a tyrosine which fluoresces at about 300nm. The emission intensity of these peptides is altered upon heparin binding. Figure 4.43 shows the fluorescence spectrum of P21, excited at 270nm. The Tyr-21 of the P21 molecule emits at 300nm. Changes in the fluorescence spectrum of P21 would directly reflect on the changes in the environment at the tail end of the peptide.

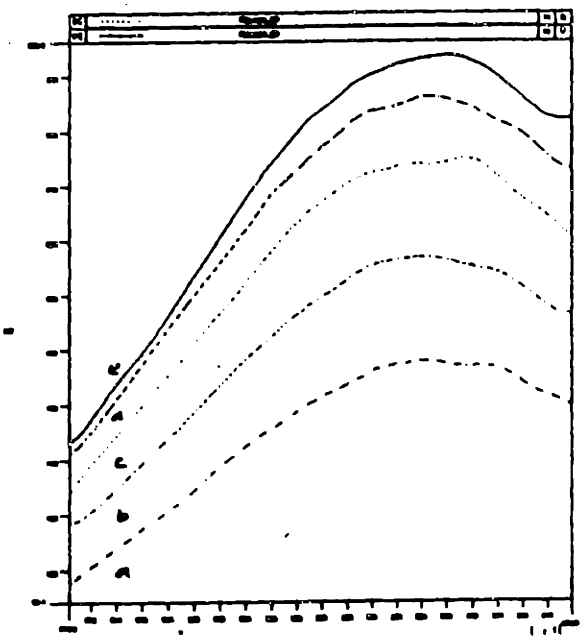

Figure 4.42 Change in Antithrombin-III fluorescence with heparin
Fluorescence of AT-III (1.2mM) measured by exciting at 280nm.
The emission intensity at 340nm is recorded for heparin concentrations of:
(a) 0 mM, (b) 0.1 mM, (c) 0.2mM, (d) 0.5mM, (e) 1mM.

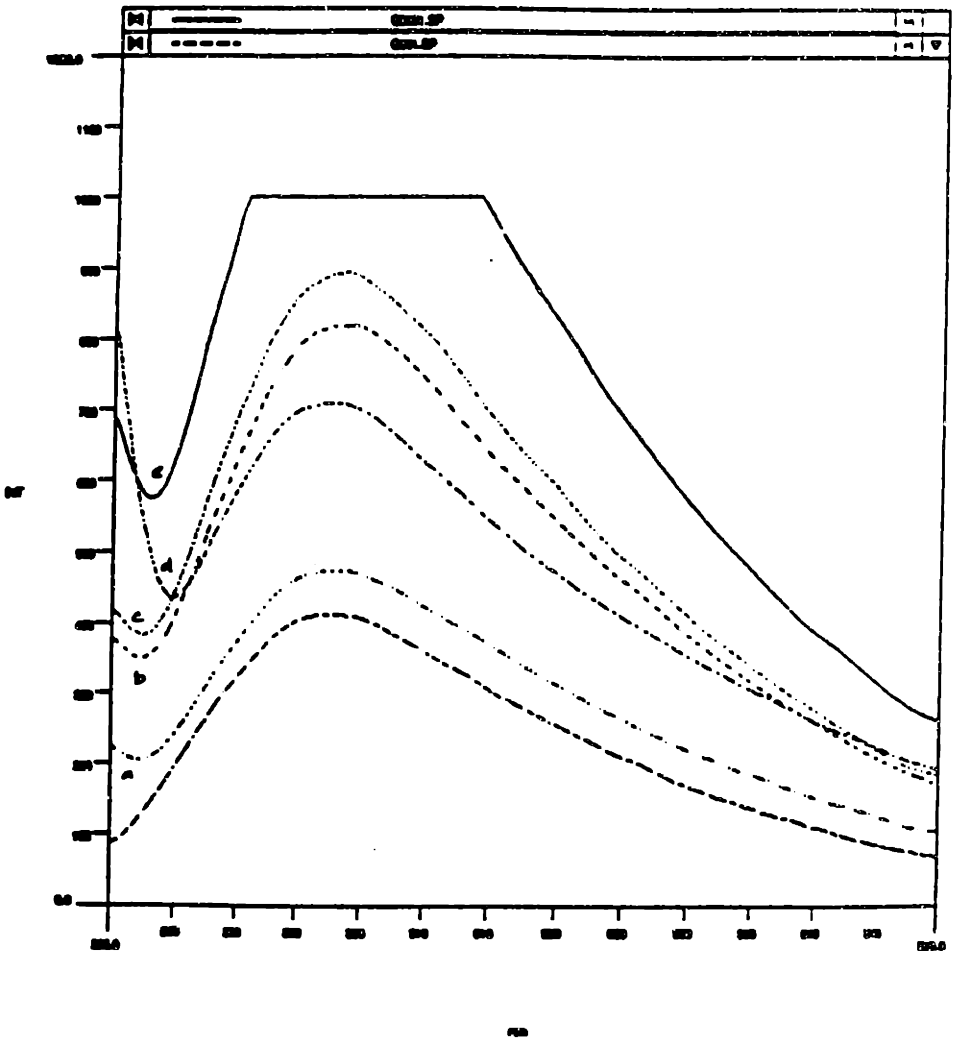

Figure 4.43 Change in P21 fluorescence with heparin
Fluorescence of P21 (25μM) measured by exciting at 280nm.
The emission intensity is recorded for heparin concentrations of:
(a) 0 mM, (b) 0.5 mM, (c) 1mM, (d) 5mM, (e) 10mM.

Addition of small amounts of heparin increases the emission intensity at 300nm (Figure 4.43), clearly demonstrating that P21 binds to heparin. This binding alters the environment around the tyrosine, thereby increasing the quantum yield. The increase in fluorescence is, however, not as dramatic because, the tyrosine, being the last residue of the peptide, might not be directly involved in heparin binding. The heparin concentration ranged from 10nM to 10mM, while the peptide concentration was held constant at 25μM. The emission intensity increases sharply at very low heparin concentrations and then levels off at high heparin concentrations.

The increase in the emission intensity of DP21 upon heparin addition is much more compared to that of P21 (Figure 4.44). The heparin concentrations used here was the same as before, while the peptide concentration was half that of the P21 experiment in order to maintain the same molar binding ratio. The increase in the quantum yield of DP21 is much more compared to that of P21, for a particular heparin concentration. This indicates that the interaction of heparin with the tyrosines in the case of DP21 is significantly more than that of P21 case. Preliminary calculations of the binding constant from these data indicate the K_d to be in the high nm to μM range for these peptides. Calculation of binding constants form fluorescence data might be inaccurate especially if the fluorescing tyrosine is far-removed from the actual interaction site.

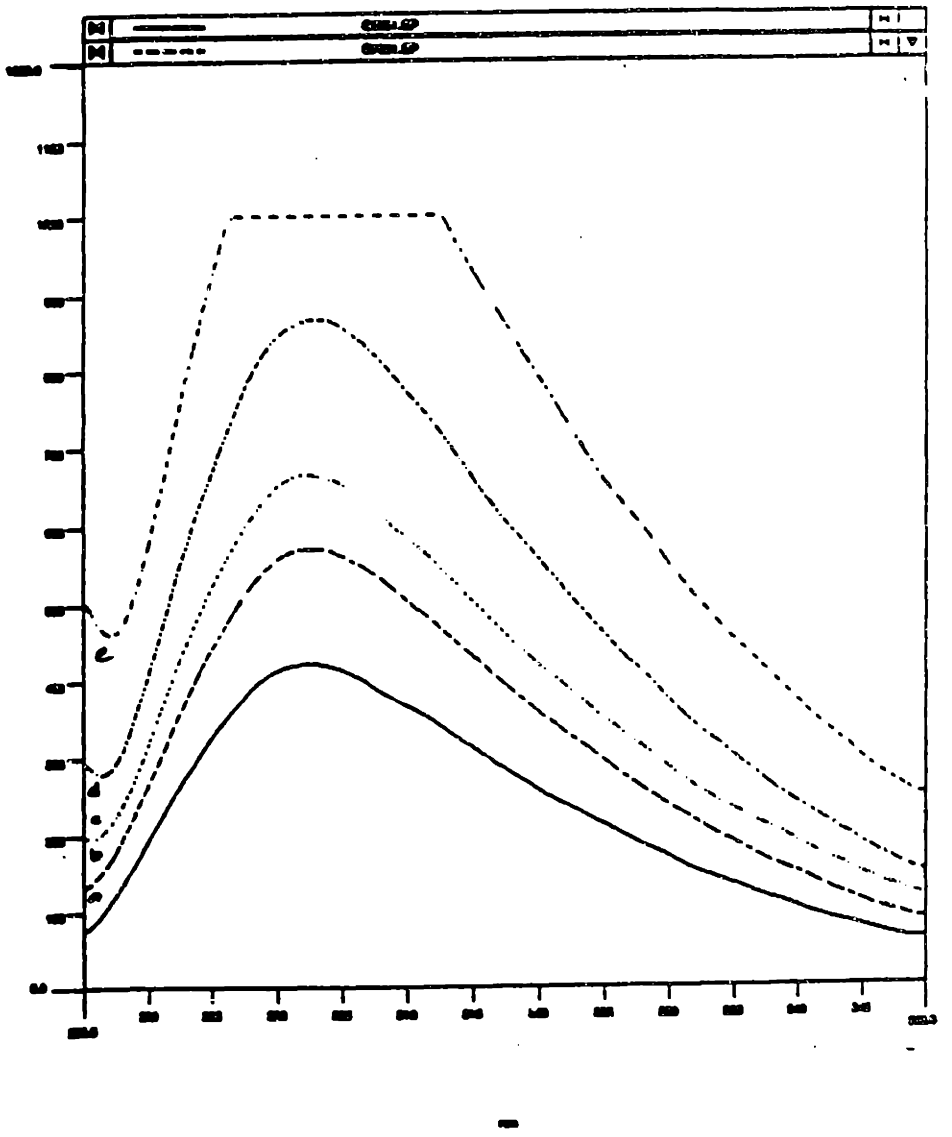

Figure 4.44 Change in DP21 fluorescence with heparin
Fluorescence of DP21 measured by exciting at 280nm.
The emission intensity is recorded for heparin concentrations of:
(a) 0 mM, (b) 0.5 mM, (c) 1mM, (d) 5mM, (e) 10mM.

4.2.4 Structural Characterization of the Peptides

4.2.4.1 Circular Dichroism

Specific interactions between a peptide and a ligand are mediated through their secondary structure. The three dimensional structure of the peptide is a result of a balance between the various forces acting on the residues. Hydrophobic interactions of the side chains result in some residues of the peptide buried away from the solvent, leaving the more polar side chains on the surface. The interaction of the peptide with other molecules is dependent on the correct orientation of the charged and hydrophobic areas, which in turn depends on the secondary structure.

A qualitative measure of the overall secondary structure can be obtained using circular dichroism studies. The optical rotation of a circularly polarized light at a particular wavelength depends on the periodicity of the repeating structure. The UV region of the circular dichroism spectrum reflects on the protein's secondary structure. Random coils, α-helices and β sheets have characteristic CD spectra in the UV region. The difference between these spectra is quite significant in the far-UV region (180-200 nm). Secondary structure in a protein can be determined using CD spectra and deconvoluting the individual contributions from the various secondary structures.

The circular dichroism spectrum of HBP in aqueous solution (Figure 4.45) clearly indicates that HBP exists predominantly as a random coil. There is a small amount of negative optical rotation at about 232, indicative of a small percentage of α-helical structure. However, the peptide is far from a complete α-helix, or any regular

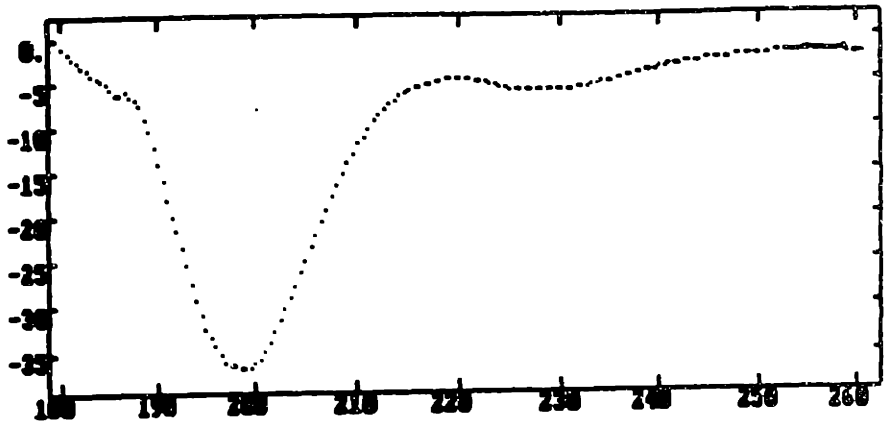

Figure 4.45 Circular Dichroism of HBP
CD spectrum of 200μM HBP in water.

secondary structure. Statistical structure prediction algorithms like Chou-Fasman and Rous-Gardner predict an α-helix for the HBP sequence. Also, based on free energy calculations, the residue sequence of HBP is likely to be in a a-helical structure (Zhu, 1991). However, these structure prediction algorithms are probabilistic. They do not account for electrostatic interactions between the side chains. The highly charged residues of HBP, may therefore, destabilize the helical structure in solution.

The charges on the side chains depend on the pH of the solution. The net charge of the peptide and the electrostatic interactions within the peptide can be screened to a certain extent by adjusting the pH of the solution. The CD profile of HBP in pH 3.0 and at pH 11.0 seem to be almost identical to that in neutral solution (Figure 4.46). At a pH of 3.0, one would expect the acidic residues of the peptide to be protonated and hence electrostatic repulsion between these negatively charged residues disappear. However, the lysines and arginine side chains would now be fully protonated and hence might disrupt the secondary structure. At he high pH, the situation is reversed with the acidic residues being fully charged. In effect, HBP in aqueous solution does not seem to have any secondary structure.

The peptide derived from HBEGF, P21, also seems to exist mostly as a random coil in aqueous solution (Figure 4.47). Since the number of acidic residues in this peptide are much lower compared to HBP (Figure 4.10), at a high pH, one can expect complete screening of electrostatic repulsions. However, the CD profile indicates that the amount of helical structure does not increase at high pH (Figure 4.48). This suggests that peptide secondary structure is not determined entirely based on electrostatic interactions.

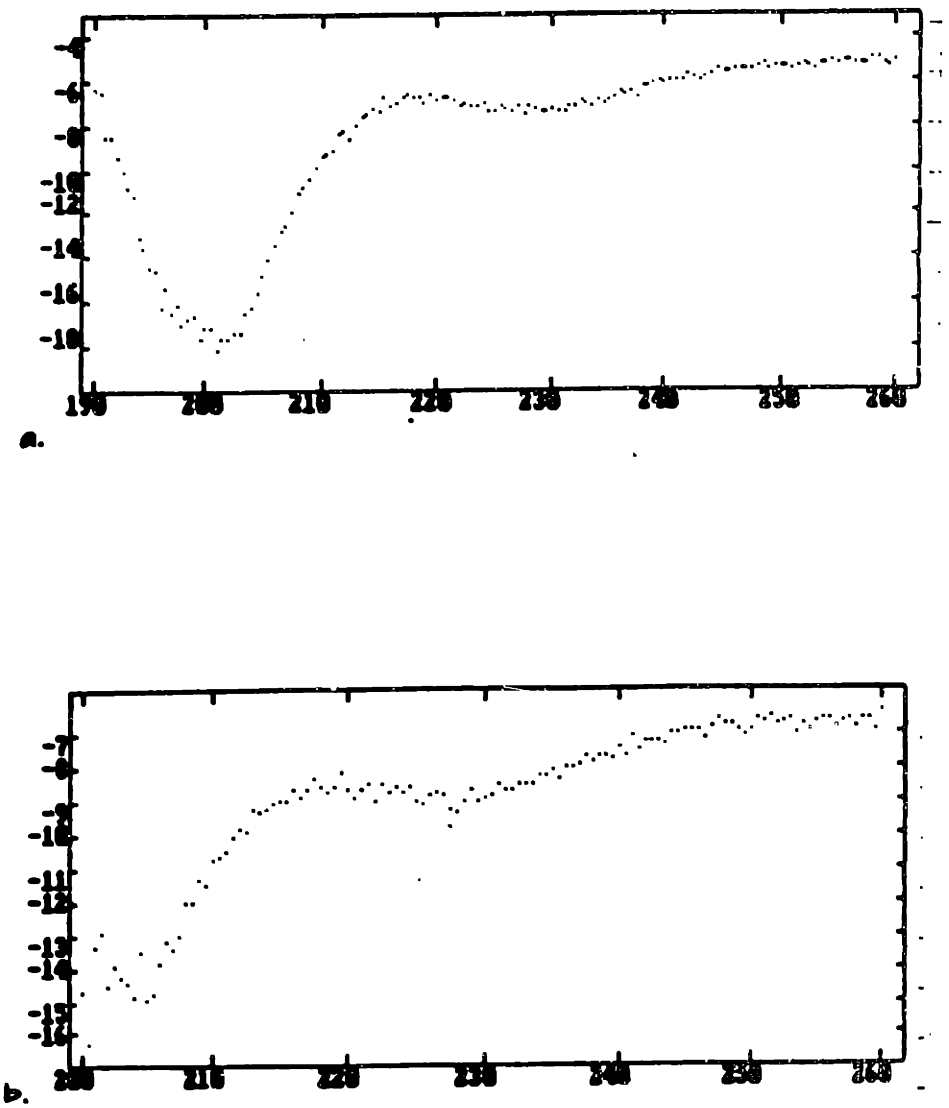

Figure 4.46 Circular Dichroism of HBP - pH effect
CD spectrum of 200μM HBP in water (a) pH 3.0, (b) pH 11.0

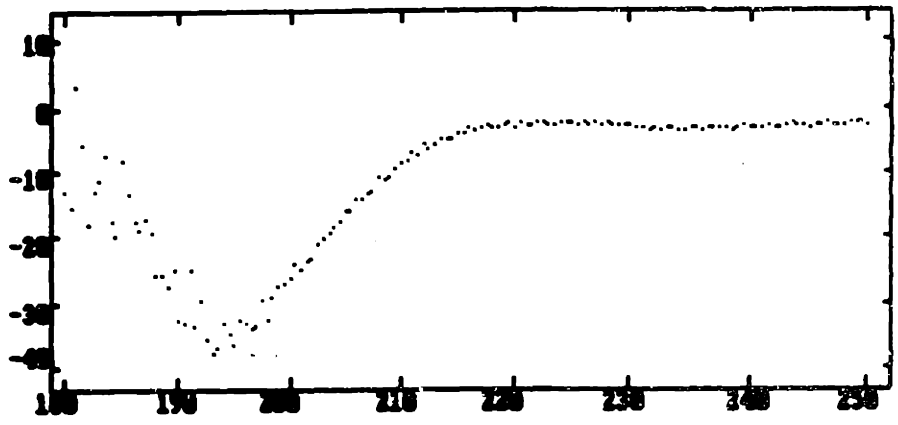

Figure 4.47 Circular Dichroism of P21
CD spectrum of 200μM P21 in water

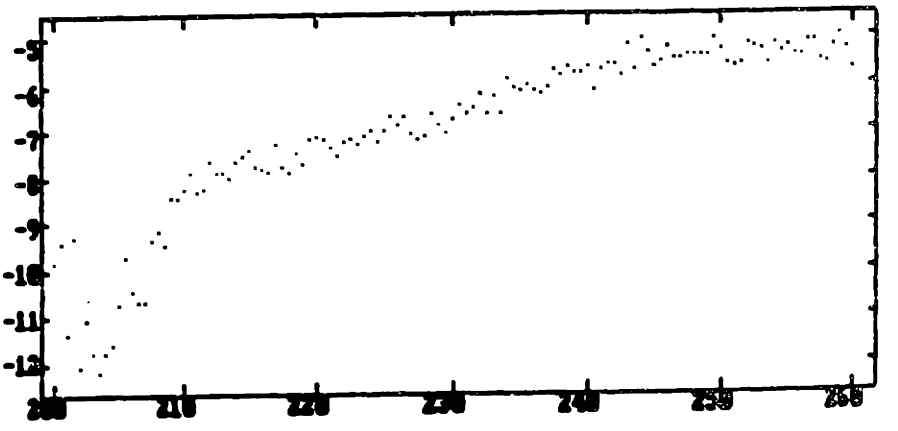

Figure 4.48 Circular Dichroism of P21 - pH effect
CD spectrum of 200μM P21 in water at pH 11.0

The CD profile of P13 exactly resembles that of a random coil. The small amount of secondary structure exhibited by the other peptides is not present in P13 (Figure 4.49). These data indicate that the peptide exists as a random coil in aqueous solution. The peptides, however, failed to exhibit any secondary structure in organic solvents as well. The CD profile of the peptides in 89% TFE indicate that the peptides exist as random coils. The organic solvents usually strengthen the hydrogen bonding between the residues. This indicates that the peptides seem to exist in some stable structure, but not a regular secondary structure.

If the residues from the heparin binding consensus sequence are arranged along an α-helix, the lysines and arginines of the peptides align along one face of the helix. This charged helical surface has been believed to interact with the negatively charged surface groups of heparin in a specific manner. Circular dichroism studies of the peptides, however, indicates lack of any secondary structure in these peptides.

The stabilization of the secondary structure by addition of heparin has been observed previously for other heparin binding peptide models (Koffman and Lansbury, 1991). Figure 4.50 shows the circular dichroism trace of the peptides in the presence of 2mM heparin. The CD profile of the peptides in the absence of heparin is also shown in the same spectrum for comparison. Heparin added does not seem to induce any secondary structure on any of these peptides at these concentrations. The heparin concentration used here represents a equimolar ratio of heparin chains to the peptide. Increasing the number of heparin chains is limited by the dichroic activity of heparin at high concentrations. Figure 4.51 shows the strong optical rotation exhibited by the heparin chain at a concentration of about 10mM. Hence, interaction of the peptides with higher heparin concentrations cannot be studied using this technique.

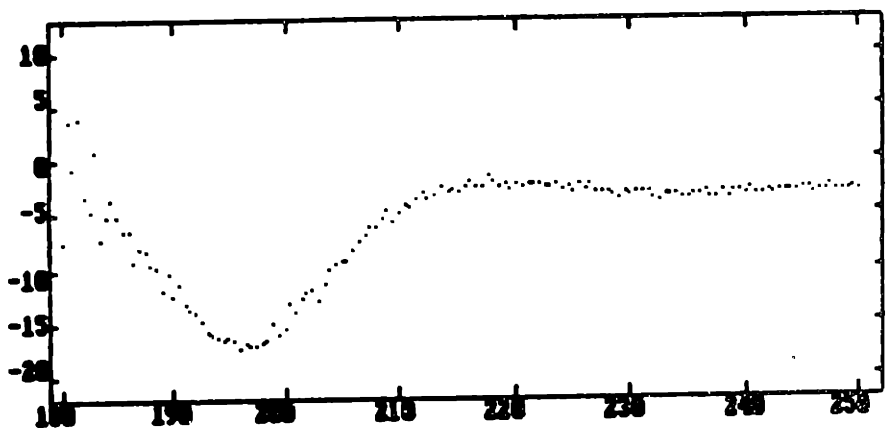

Figure 4.49 Circular Dichroism of P13
CD spectrum of 200μM P13 in water, pH 7.0

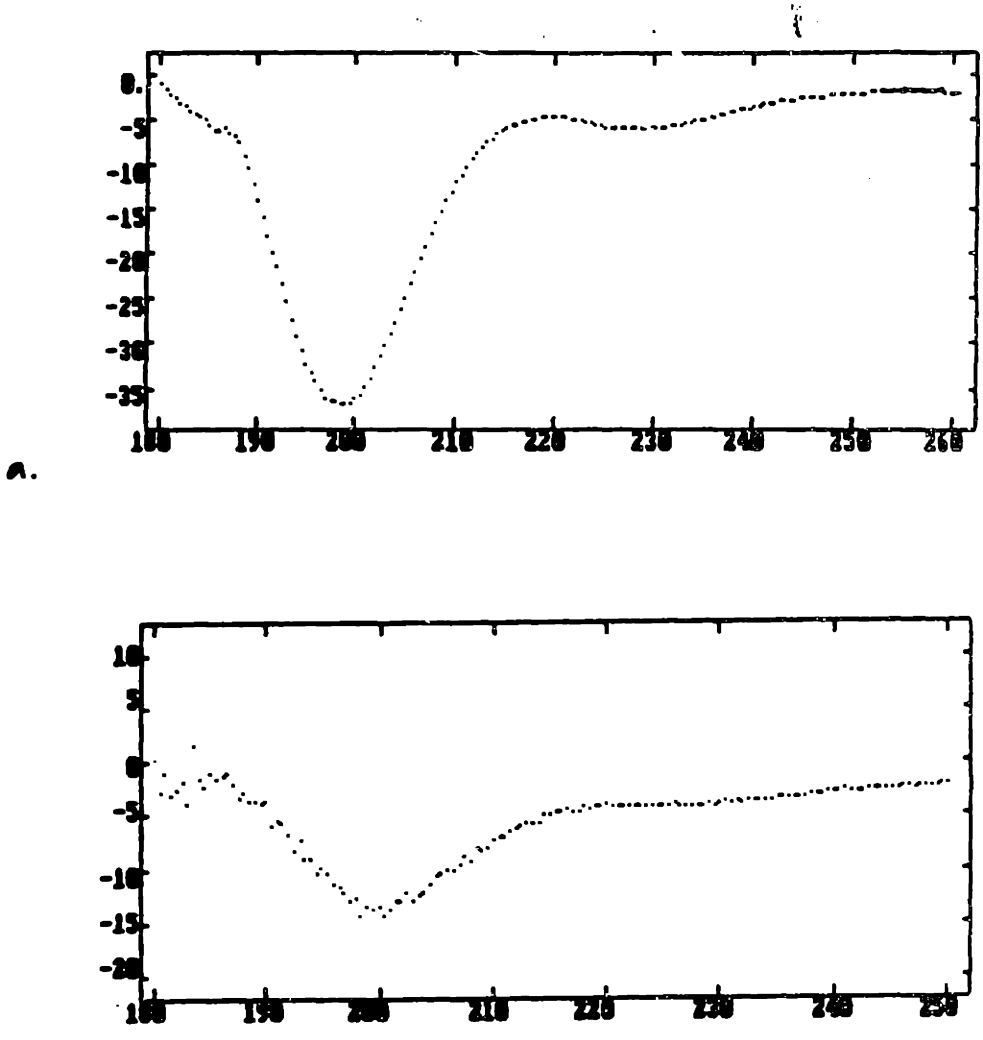

Figure 4.50a Circular Dichroism of HBP in presence of heparin
CD spectrum of 200μM HBP with (a) no heparin (b) 2mM heparin

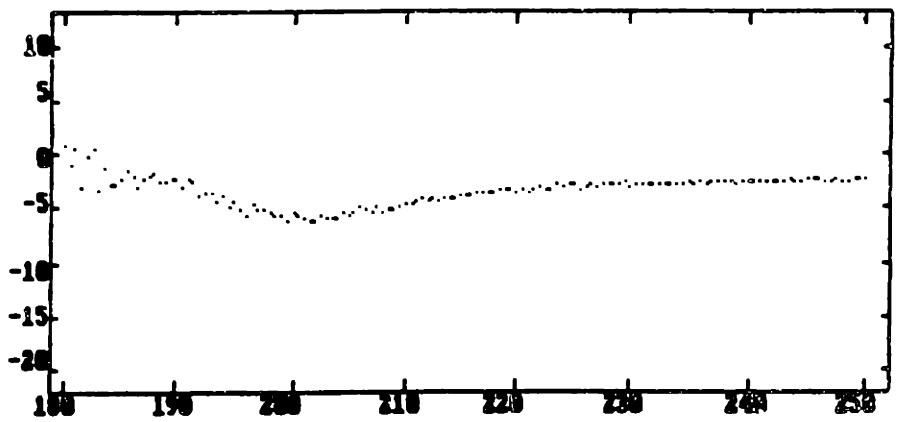

a.

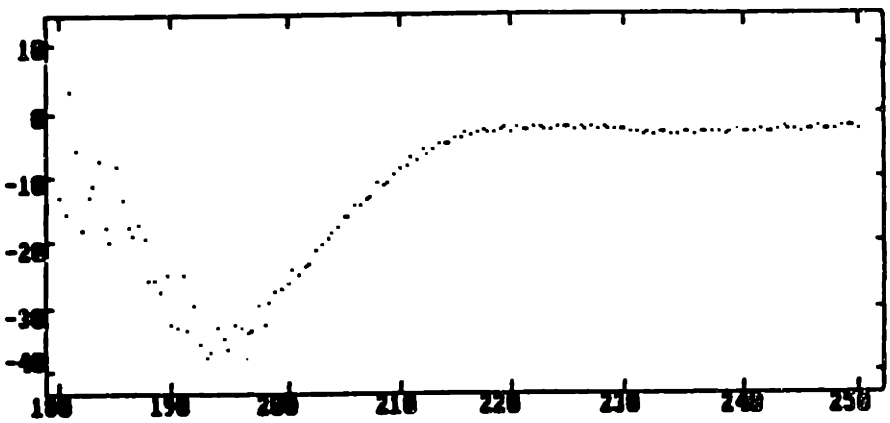

b.

Figure 4.50b Circular Dichroism of P21 in presence of heparin
CD spectrum of 200μM P21 with (a) no heparin (b) 2mM heparin

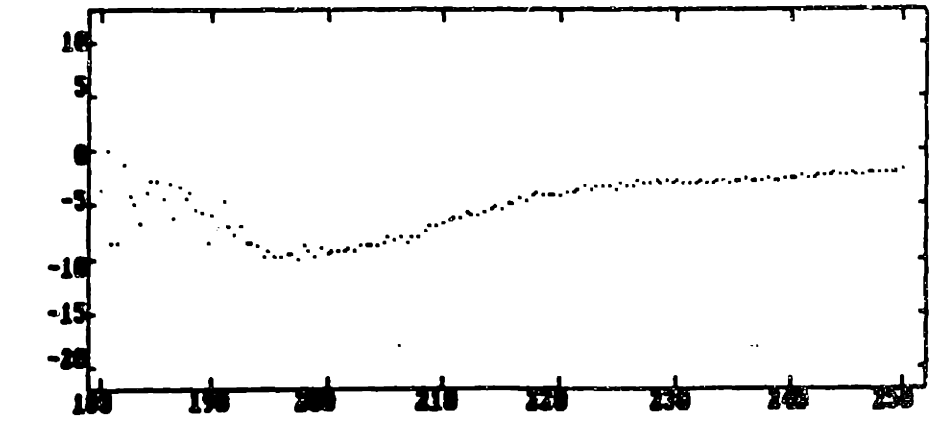

a.

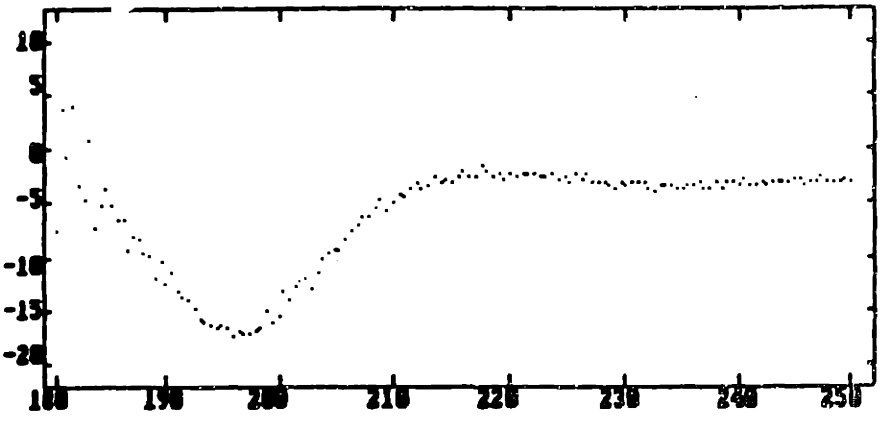

b.

Figure 4.50c Circular Dichroism of P13 in presence of heparin
CD spectrum of 200μM P13 with (a) no heparin (b) 2mM heparin

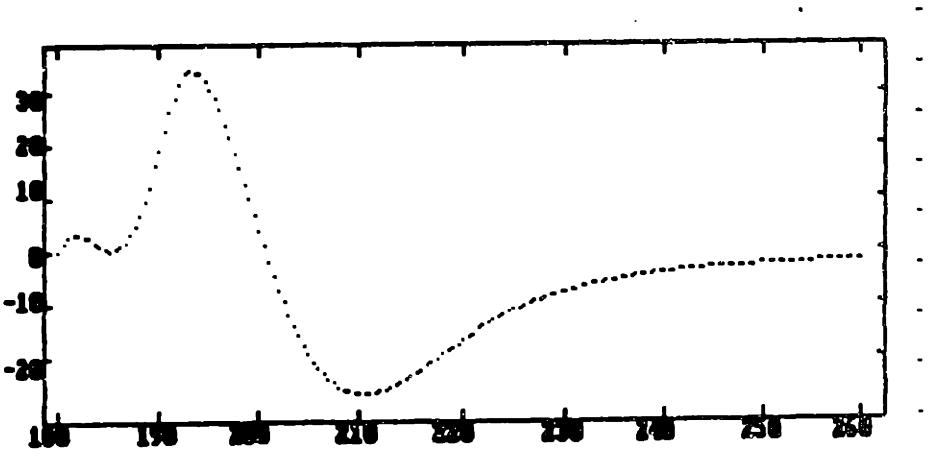

Figure 4.51 Circular Dichroism of heparin
CD spectrum of 20mM heparin in water

The circular dichroism spectra of heparin fragments obtained by digestion of heparin using heparinase also seems to display optical rotation. This contribution probably comes from the undigested heparin fragments left behind by the enzyme (section 4.2.2.2.7). Addition of peptides to a diluted mixture of heparin fragments did not induce any helical structure in the peptide.

Heparin fragments were isolated and their interaction with the peptides studied. Figure 4.52 shows the CD profile of HBP with tetrasaccharide 1, 3 and hexasaccharide. These heparin fragments clearly do not alter the secondary structure content in the peptides. The same behavior is observed for P21 as well (Figure 4.53). However, in the case of P13, there is a slight introduction of secondary structure in the presence of the tetrasaccharides. The CD profile of P13 in aqueous solution resembles that of a random coil. However, there is a small amount of secondary structure that seems to be introduced upon addition of heparin fragments (Figure 4.54). The final CD profile, resembles the CD spectra of HBP and P21. This indicates that the interaction between heparin and the peptides is not entirely random. This interaction is governed by a small amount of regular secondary structure along with a predominant irregular coiled conformation. Specific solution conformation of this heparin binding structure could provide the key to understanding the interaction between these peptides and heparin. 2-D Nuclear Magnetic Resonance studies has been used to determine the solution structure of the peptides (section 4.2.4.2).

Calcium ions in the buffer have been shown to affect the degradation of heparin by the enzyme. Although calcium has been shown not to affect the binding of the enzyme to heparin, the effect of calcium on the structure of the peptides was

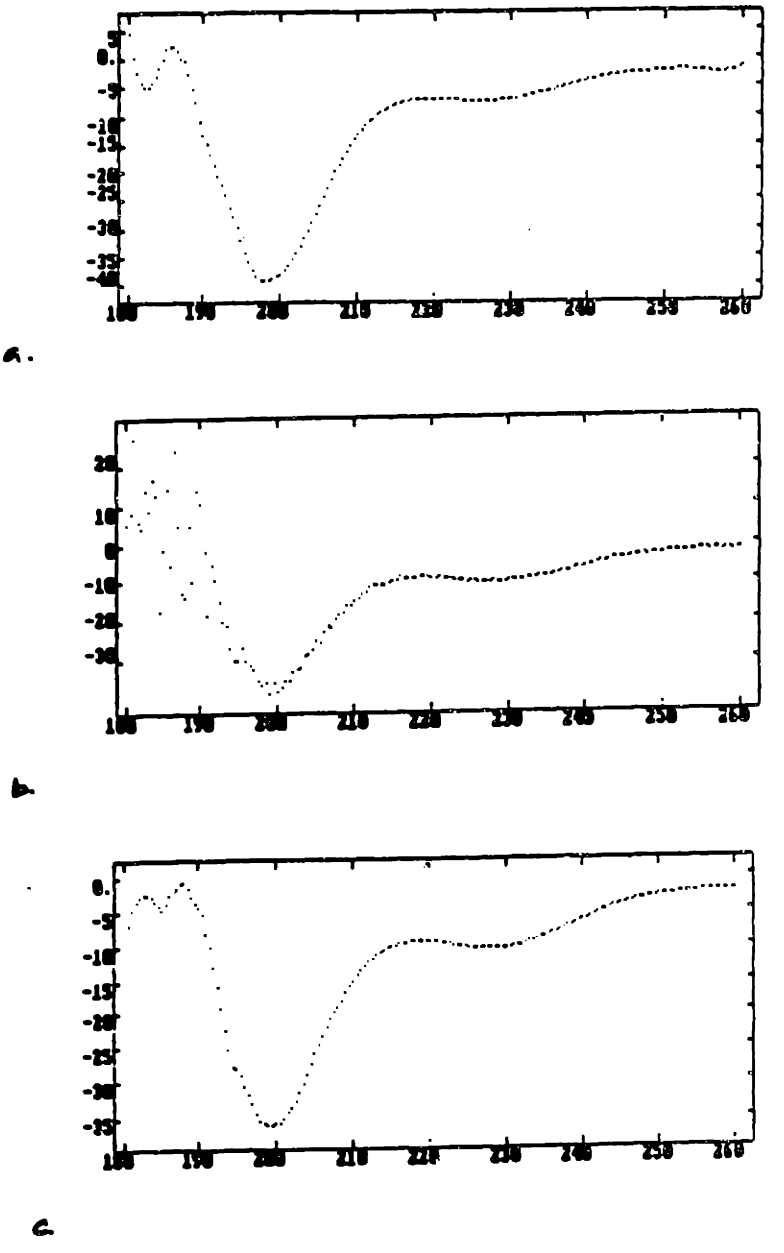

Figure 4.52 Circular Dichroism of HBP in the presence of heparin fragments
CD spectrum of 200μM HBP in the presence of (a)800μg tetrasaccharide-1,
(b) 800μg tetrasaccharide-3, (c) 1mg hexasaccharide

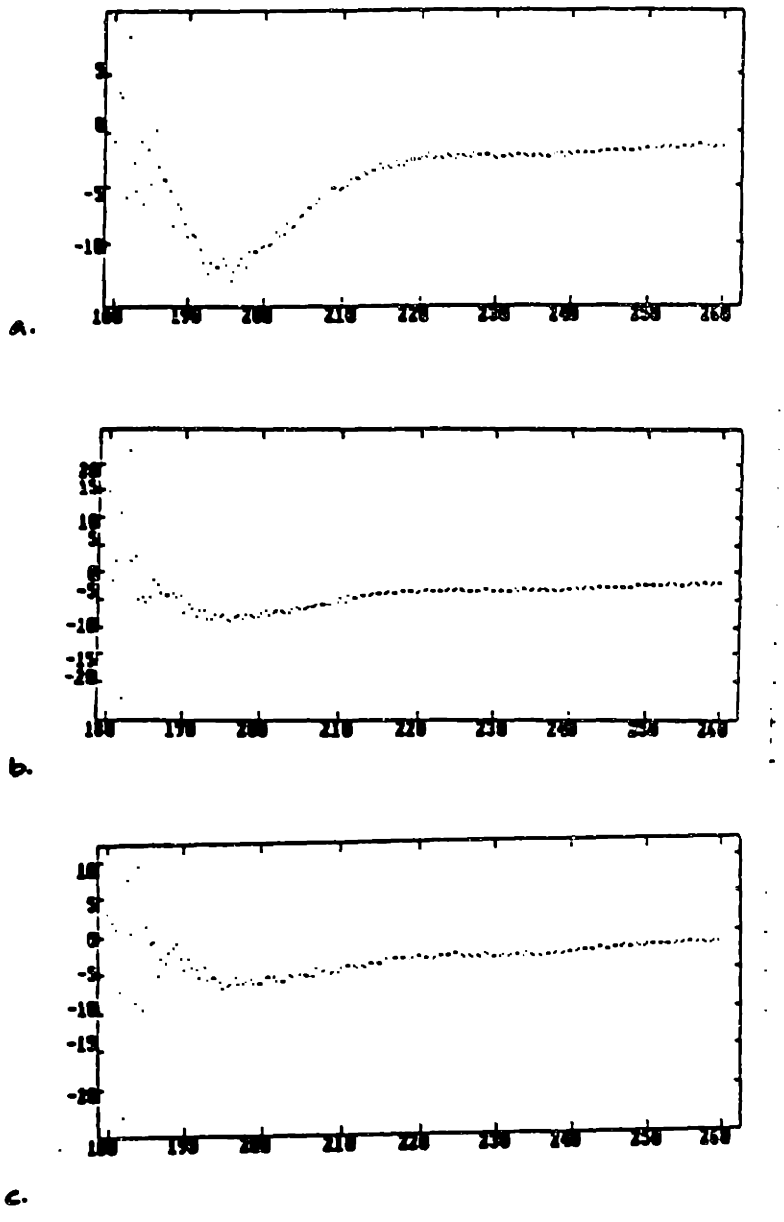

Figure 4.53 Circular Dichroism of P21 in the presence of heparin fragments
CD spectrum of 200μM P21 in the presence of (a) 800μg tetrasaccharide-1, (b) 800μg tetrasaccharide-3, (c) 1mg hexasaccharide

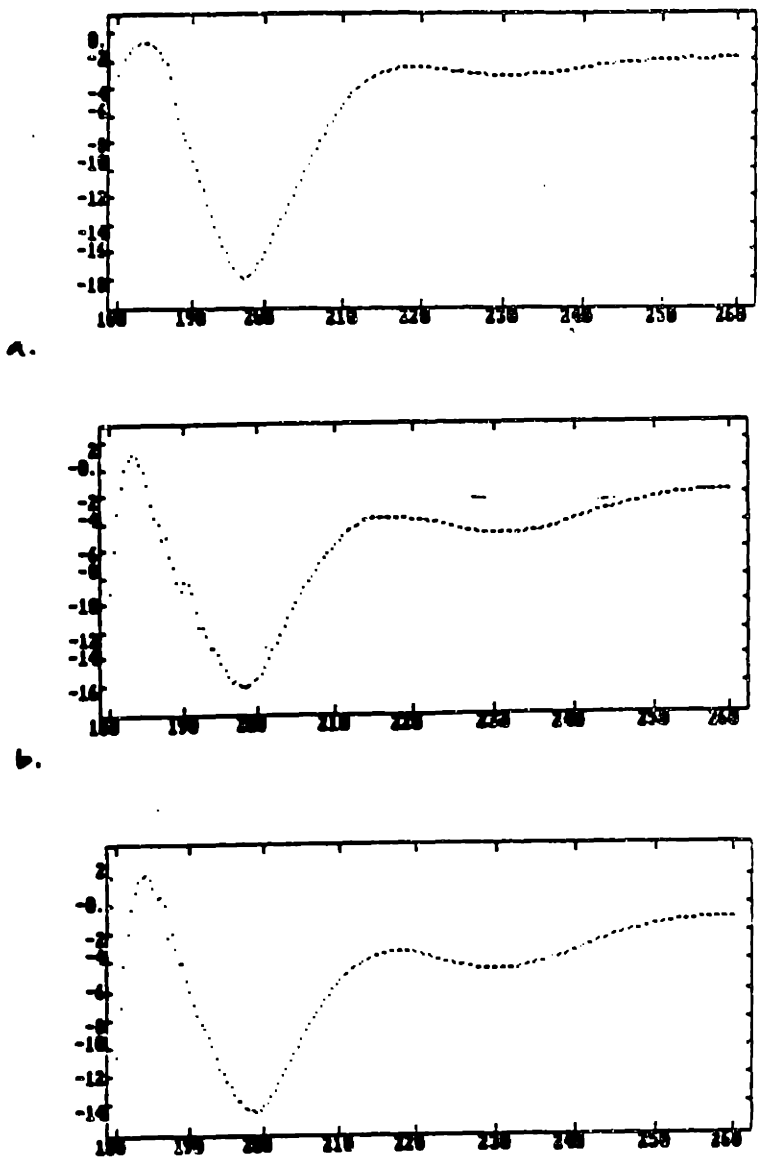

Figure 4.54 Circular Dichroism of P13 in the presence of heparin fragments
CD spectrum of 200μM P13 in the presence of (a) 800μg tetrasaccharide-1, (b) 800μg tetrasaccharide-3, (c) 1mg hexasaccharide

investigated. Figure 4.55 shows the CD profile of the peptides in the presence of heparin and calcium. the secondary structure of the peptide does not seem to be affected by the addition of calcium ions to the buffer. This also signifies that he interaction between the heparin and the peptide is not altered by addition of calcium ions.

4.2.4.2 NMR

The solution structure of the peptide can provide useful information on the orientation of the functional groups that could interact with the heparin. CD studies show that the interaction of the peptide with heparin does not change its structure appreciably. However, the peptide does not exhibit any regular secondary structure in solution, and hence could be very flexible in aqueous solution. The dynamic nature of the peptide backbone would then make it difficult to determine distance constraints for secondary structure predictions. The number of constraints obtainable from a typical experiment would be far lower because of the lack of a regular secondary structure.

The interaction between the peptide and heparin fragments can be studied by looking at the changes in proton resonances. The electronic nature around the protons of the residues that interact with the peptide changes leading to shifts in the resonance peaks. If the resonance peaks are assigned and if the shifts are localized to small regions of the peptide, specific interaction sites could be isolated. However, overlap of the proton resonances from the saccharide could make data interpretation more complex.

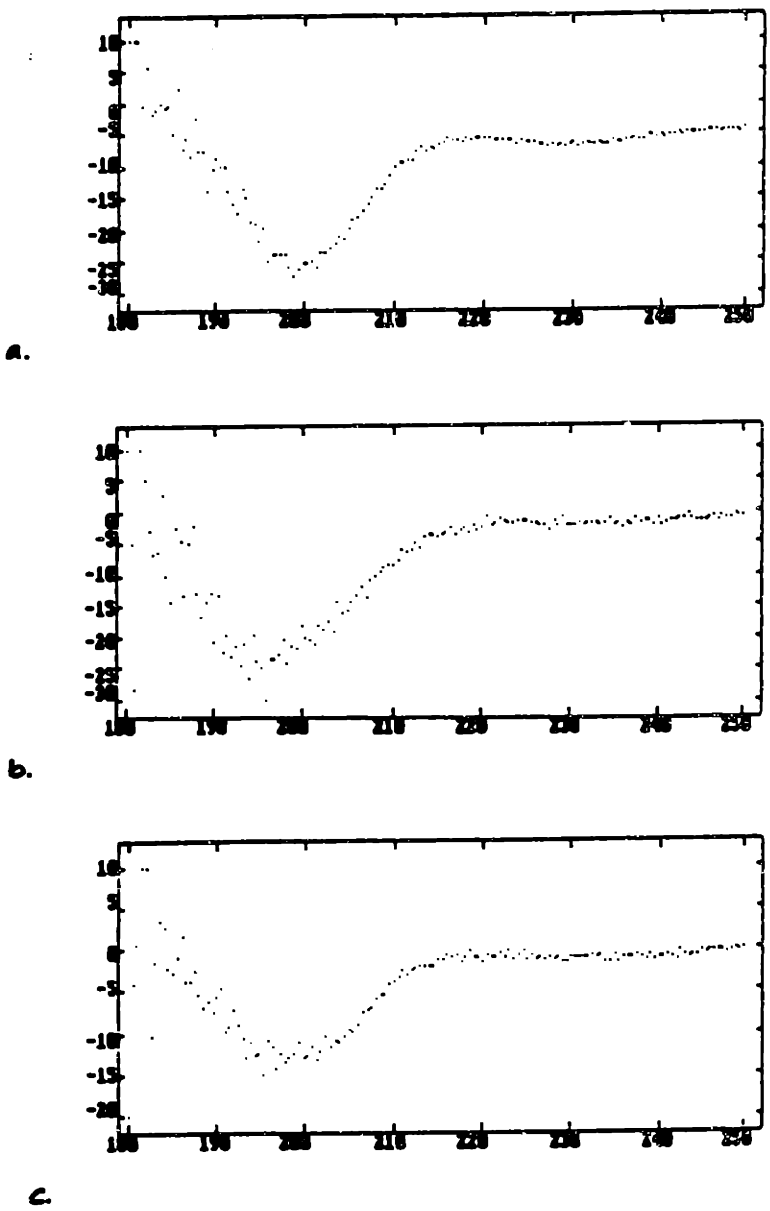

Figure 4.55 Circular Dichroism of Peptides with Calcium
CD spectrum of Heparin Binding Peptides in the presence of 5mM calcium.
(a) 200μM HBP, (b) 200μM P21, (c) 200μM P13

The first step towards the assignment of the peptide resonances was a phase-sensitive COSY spectrum of the peptide in D_2O (Figure 4.56). The amide protons of the peptide are fully exchanged out confirming a lack of any tightly hydrogen bonded structure in the peptide. However, the cross peaks between the C_α protons and the amide protons (Figure 4.57) will be used to assign the amide proton resonances. The side chain connectivities can be used to identify certain characteristic spin systems.

Phase sensitive COSY spectrum of the peptide in 90% H_2O shows clearly the amide proton resonances (Figure 4.58). The Cα protons close to the water peak are however, lost in the suppression of the water peak. A TOCSY spectrum with 80 ms mixing time in 90% H_2O indicates the complete spin systems of the residues. The TOCSY information, coupled with the COSY data, help in identifying the side chain resonances of most of the residues. ROESY experiments with different mixing times (20, 50, 120, 200 msec), however, yielded only a minimal number of through space connectivities. As a result sequence specific assignment of the peptide is not possible.

Figure 4.56 shows the 2-D COSY spectrum of the peptide in D_2O. The amide protons are fully exchanged with deuterium extremely rapidly, indicating lack of any tight hydrogen bonded structure in the peptide. An α-helical structure would imply tight hydrogen bonding between the amide protons and the carbonyl oxygens, thereby reducing the rate of amide proton exchange (chapter 3). The COSY experiments, as well as the ROESY data clearly indicates that HBP does not posses a regular secondary structure in solution.

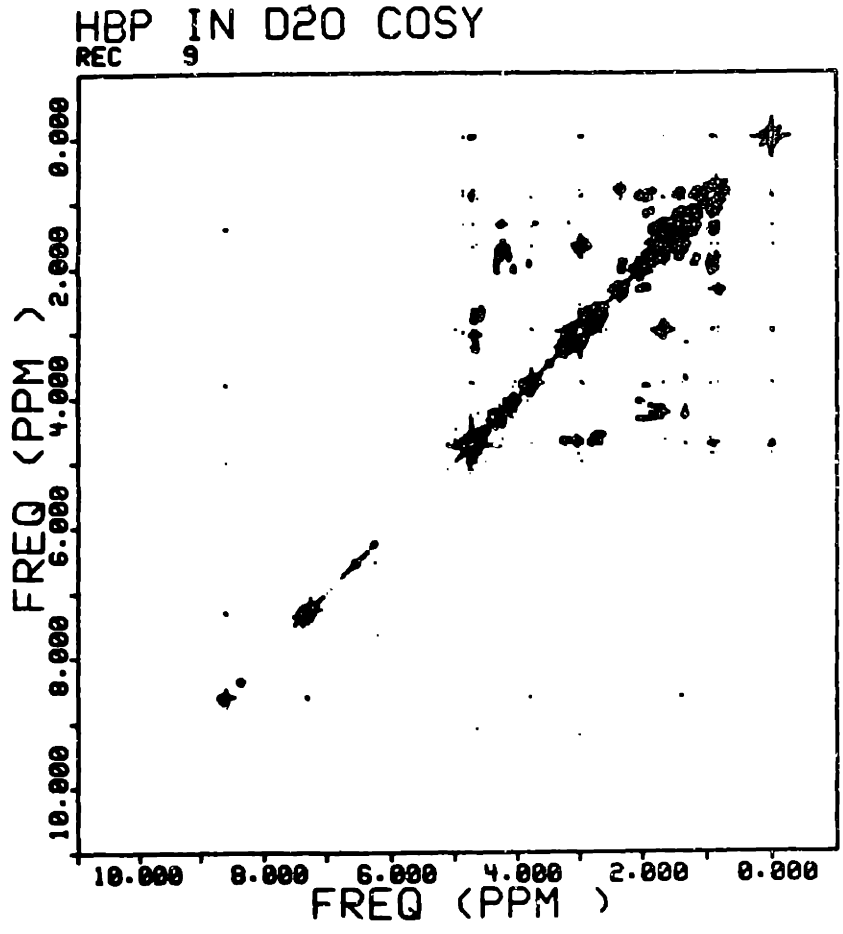

Figure 4.56 Phase-sensitive COSY spectrum of HBP in D_2O

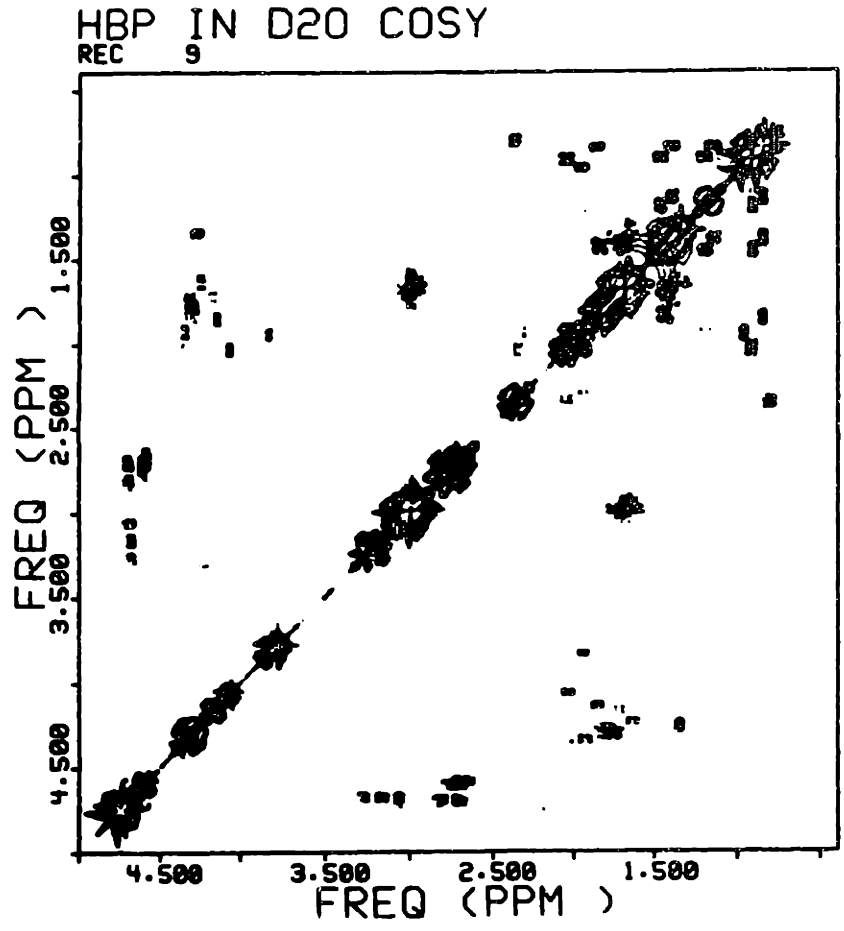

Figure 4.57 C_α-C_β and Side chain connectivities of HBP in D_2O
The region between 0 to 5 ppm on t1 and t2 of a phase sensitive COSY exhibits the side chain connectivities

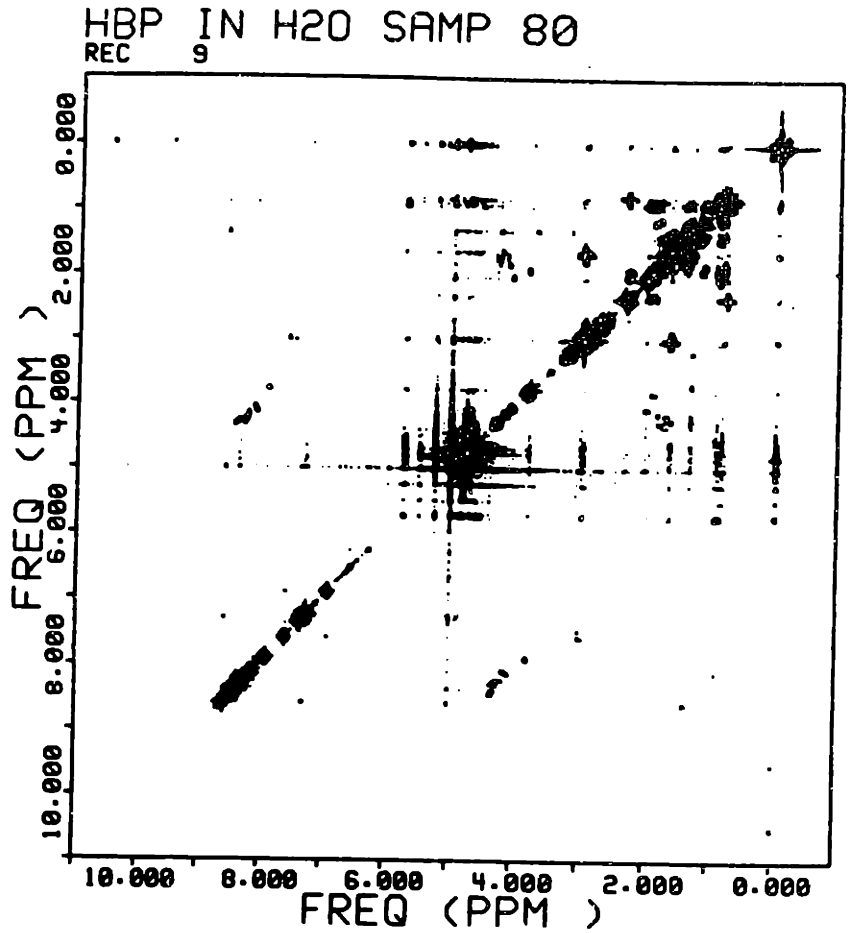

Figure 4.58 Phase-sensitive COSY spectrum of HBP in H_2O
The amide protons are can be seen in addition to the side chain protons.

The heparin binding domain of proteins that interact with heparin has been believed to be in an α-helix. The separation of the basic amino-acids by spacers, according to the consensus sequence, would orient the charged groups along one face of the α-helix. It is believed that this charged interaction of the peptides side-chains with the sulfates and carboxyl groups of heparin mediate the binding between heparin and peptides. Helix forming peptides that comply with the consensus heparin binding sequence have been designed (Ferran et al., 1992); however, the binding constant of the α-helical peptides to heparin is quite low (in the μm range). Data on HBP clearly indicates that the peptide does not exist as an α-helix, indicating that the interaction between these peptides and heparin might be more than just an salt-bridge type of electrostatic interaction.

4.2.5 Molecular Modeling:

The interaction between a peptide and a ligand depends critically on the three dimensional structure of the peptide and the ligand. The conformation of the molecules, in turn is a result of the balance between the various forces acting on the molecules. The energy of the molecule can be calculated as a sum of the internal energies and the electrostatic and van der Waals energies (Chapter 2). The most likely structure of the molecule is the lowest energy conformer.

The aprori prediction of a peptide structure from molecular modeling studies sometimes fails either because the physically existing structure is a pseudo-low energy state or due to additional terms in the energy that are to be accounted (e.g. hydrophobic forces). However, molecular modeling can be used in conjunction with experiments to better understand the experimental results and to devise more

appropriate experiments. In addition, the graphical representation of the molecules help visualize the orientation of the side chains in the structure and hence the importance of the various functional groups in the interaction.

Conventional structure prediction algorithms like Chou-Fasman and Rous-Gardner predict the HBP sequence to be in an α-helical structure. When the peptide is constrained to an α-helix, the lysines and arginines that form a part of the consensus sequence, align along one of the faces of the helix. It has been proposed that the charged cylindrical surface of the helix is the site of interaction with the negatively charged sulfate groups of heparin. Based on this hypothesis, peptides confirming to the consensus sequence with an α-helical structure have been synthesized (Ferran et al., 1992). However, the binding constant of these helical peptides to heparin is in the order of few μM, much lower than the binding constants seen for HBP and P21.

The total computed energy of the helical conformer of HBP is 48.6 KCal/Mol. The individual energy contributions are shown in Figure 4.59. The dihedral energy contributes to a significant penalty for the overall stabilization of the molecule. The van der Waals energy, however seems to compensate for the unfavourable dihedral angles in the helical structure.

Simple energy minimization of the helical structure with 500 steps of Adopted Basis Newton Raphson method (Chapter 2) does not perturb the structure away from the helical conformation. The forces acting on each atom was then computed and the atoms allowed to move in the direction of the force acting on them. A simple dynamics study of 500 steps resulted in a partially unwound helical structure (Figure 4.60). The energy of this conformation was much lower than the starting helical

Energy	KCal / Mol
Bond	8.70
Angle	32.80
Dihedral	44.64
Improper	4.42
Leonard-Jones	-41.95
Total	**48.62**

Figure 4.59 Energy contributions to HBP in α-helical structure
The energy was computed using energy parametrs from CHARMM. The mathematical forms for the energy calculations are outlined in chapter 2.

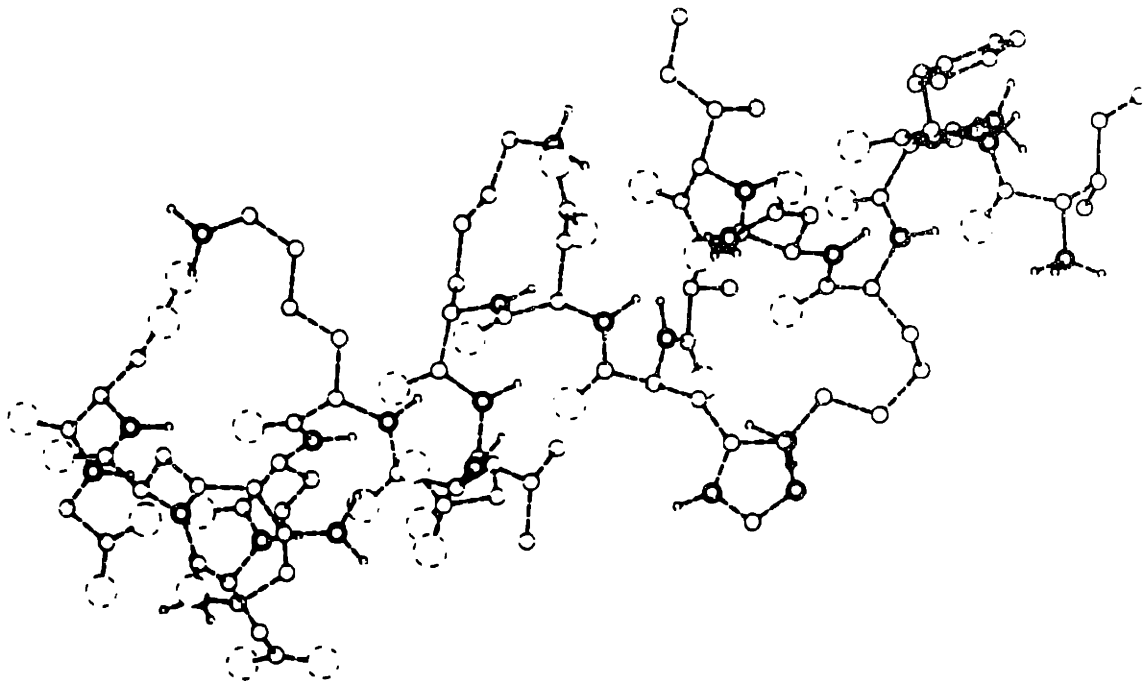

Figure 4.60 HBP conformation after Energy minimization
The energy was computed using energy parametrs from CHARMM. 500 steps of Adopted Basis Newton Raphson method was used to minimize HBP from an starting a-helical conformation.

structure. This, however, might not be the conformation with the lowest energy, but just a local minimum structure that the molecule is trapped into.

Thermal energy was imparted to the molecule to aid its crossing the local energy barriers. A complete annealed dynamics simulation to search for the lowest energy state was performed on HBP. The starting structure of α-helix was first minimized and a simple dynamics was performed. The dynamics consisted of three steps - heating, equilibration and simulation. During the heating step, the temperature of the system is incremented from 0K to 300K at 0.1° per step. The energy imparted is in the form of kinetic energy of the molecules (Figure 4.61a), and hence the velocity of the atoms also increases. The equilibration step involves an adiabatic enclosure around the molecule allowing the imparted energy to be redistributed among the atoms. The velocities and the potential energy of the molecule is calculated every 0.001picosecond, until the temperature of the system does not change any further (Figure 4.61b).

After the energy of the molecule has been equilibrated, dynamics simulation of 80,000 to 100,000 steps is performed. At each step, the force on the atom is calculated and Newton's laws of motion are solved to determine the displacement vector. The atom is then allowed to move in the direction of the force and the energy of the molecule in its new conformation is calculated. It is critical that this calculation be performed at a time scale smaller than bond vibrations. The lowest time scale of atomic motion is the vibration of the C-H bond, which is in the order of 0.0005 picoseconds. The computational intensity was reduced by constraining the C-H bond vibrations, allowing us to use a 0.001picosecond step size.

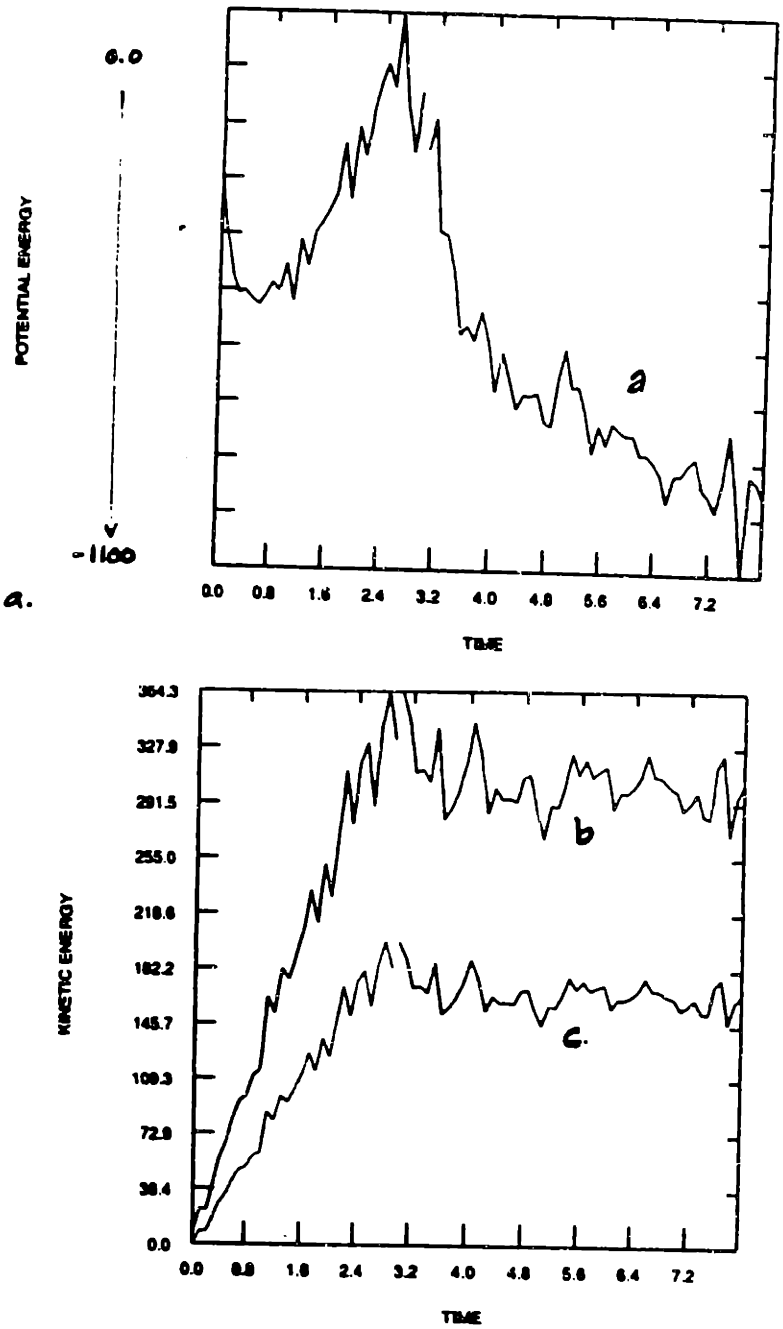

Figure 4.61 Dynamics of HBP - Heating and Equilibration
Heating (3 ps) followed by 5 ps of equilibration in steps of 0.001ps.
(a) Potential Energy trace, (b) Temperature, (c) Kinetic Energy

The trace of the potential energy of the molecule during the dynamics simulation is shown in Figure 4.62. The temperature of the system during this time is also plotted in the same graph. The potential energy monotonically decreases and then levels off after about 50 picoseconds of dynamics. The conformation of the molecule after the dynamics simulation is significantly different from the starting helical structure (Figure 4.63). The molecule seems to have unwound to a coiled structure, retaining only a small amount of the helical nature. This conformation is most likely to be the global minimum conformation. Dynamics simulation with a different starting structure should lead to the same final conformation if this represents the global minimum conformation.

Figure 4.64 shows the low energy conformer after dynamics simulation of a linear HBP molecule. The extended HBP chain was first minimized and a simple dynamics was performed. Dynamics simulation of 80,000 steps was then performed as described earlier. This minimum energy conformer is very similar to the peptide in Figure 4.63, indicating that the same low energy is reached from a different starting point. Similar studies with an initial β-sheet structure confirm that the peptide structure shown in Figure-4.63 is close to the global minimum structure.

The results of the molecular modeling studies are in complete agreement with the experimental data. CD data as well as 2-D NMR measurements indicate that he conformation of the peptide in solution is predominantly a random coil (sections 4.2.4.1 and 4.2.4.2) with very small amounts of secondary structure. Figure 4.63 shows a small amount of helical structure in the beginning of the molecule, with a large loop. A predicted CD profile of this molecule would resemble the CD profile of HBP in solution. Additionally, the lack of tight hydrogen bonding of the amide

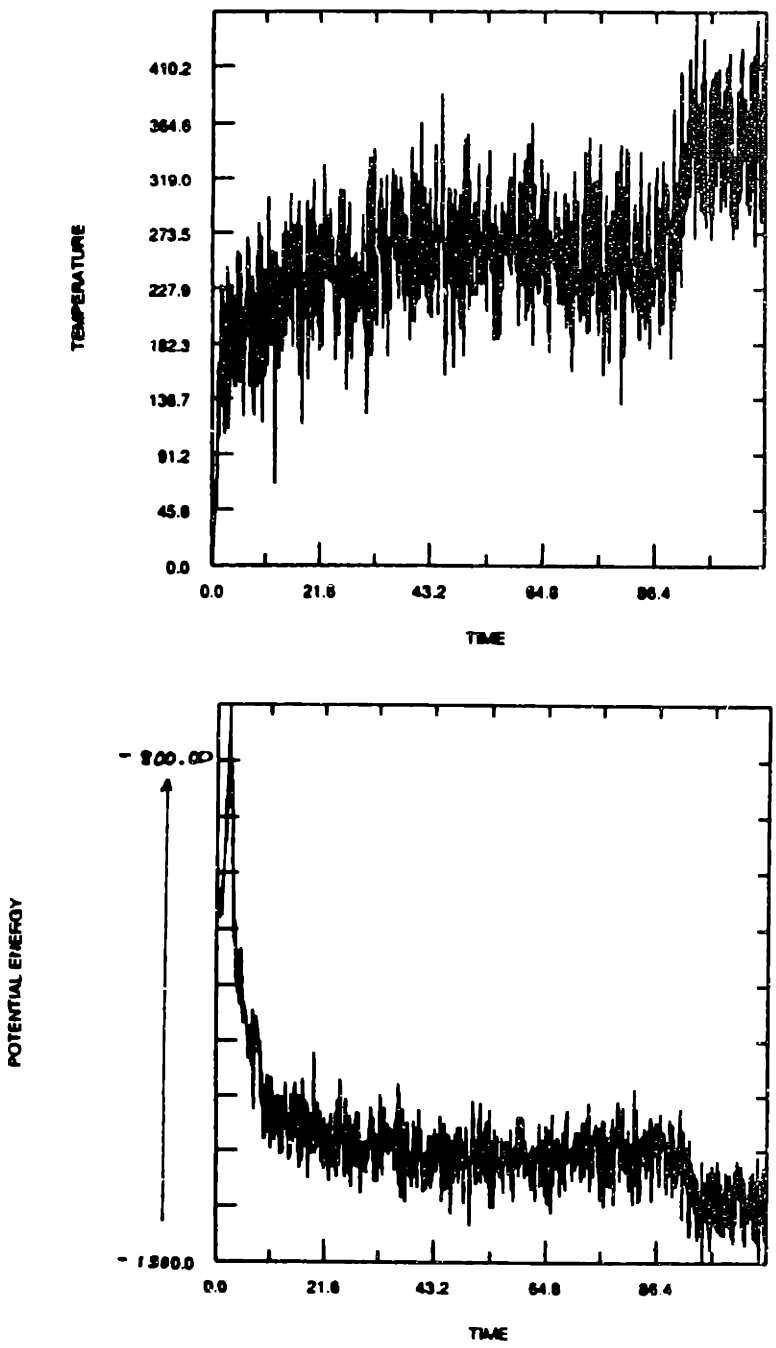

Figure 4.62 Dynamics of HBP.
The temperature and potential energy trace of HBP during dynamics.

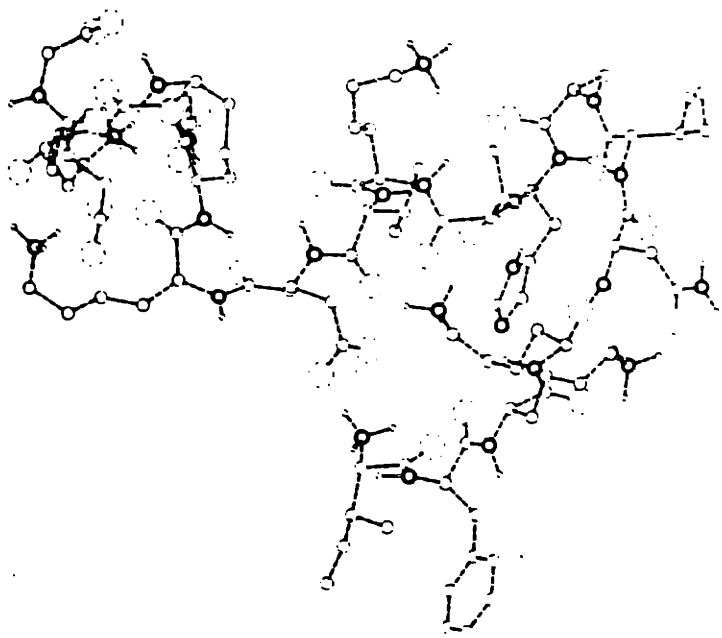

Figure 4.63 Conformation of HBP after dynamics simulation.
Starting structure for dynamics study: α-helix

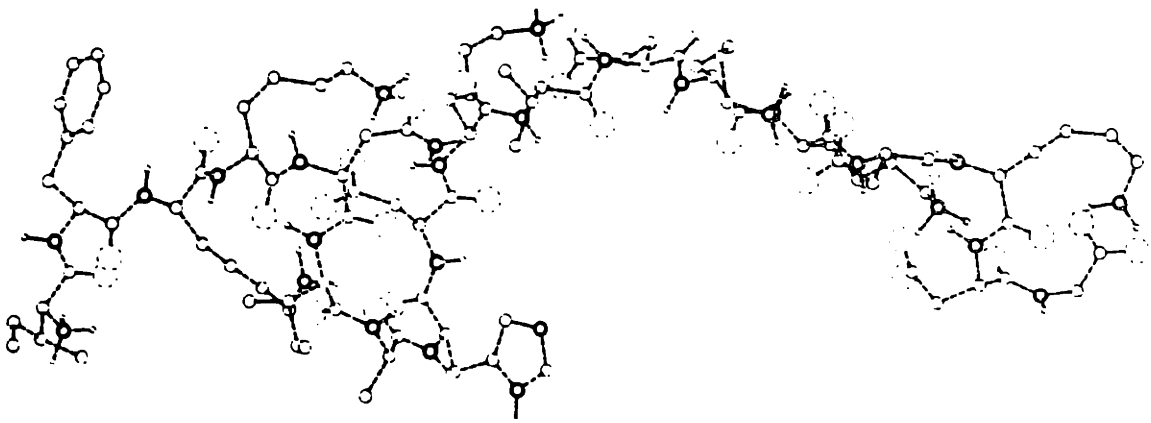

Figure 4.64 Conformation of HBP after dynamics simulation.
Starting structure for dynamics study: extended chain

protons exhibited by this structure would confirm the rapid exchange of these protons in D_2O.

Molecular modeling of the interaction between HBP and heparin is complicated by the absence of energy parameters for the carbohydrates. As a first order approximation, the parameters used for peptides were used to build the 3 different tetrasaccharides and minimize their energy. Figure 4.65 shows the structure of these three tetrasaccharides.

The tetrasaccharides were then docked to HBP and the energy of the bound complex was minimized. Both, the saccharide and the peptide were allowed to move during the minimization process. The final minimum energy of tetrasaccharide 3 with HBP was much lower than the energy of the other two tetrasaccharide-peptide complex. This suggests a very strong and specific interaction between HBP and tetrasaccharide 3. Experimental data shows that HBP specifically binds to tetrasaccharide 3 and facilitates its cleavage by the enzyme (section 4.2.2.2.7). Rigorous analysis of the binding sites in the peptide and the saccharide must be interpreted with caution as the structure of the tetrasaccharides used here might be far from realistic.

The structure of heparin has been very poorly investigated. The heterogeneity of heparin, combined with the lack of proper energy parameters for complex sugars, make it difficult to use molecular modeling techniques to determine likely heparin structures. The two key parameters that determine the orientation of the side chains in a proteoglycan are the structure of the sugar backbone and the linkage between the sugars.

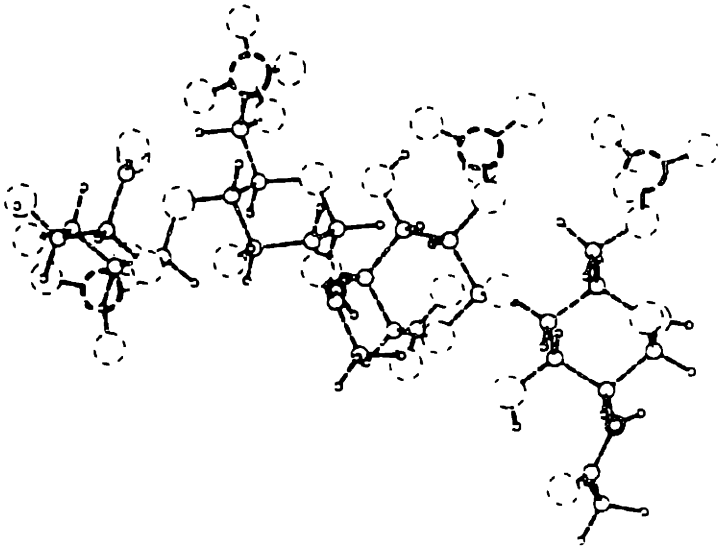

a.

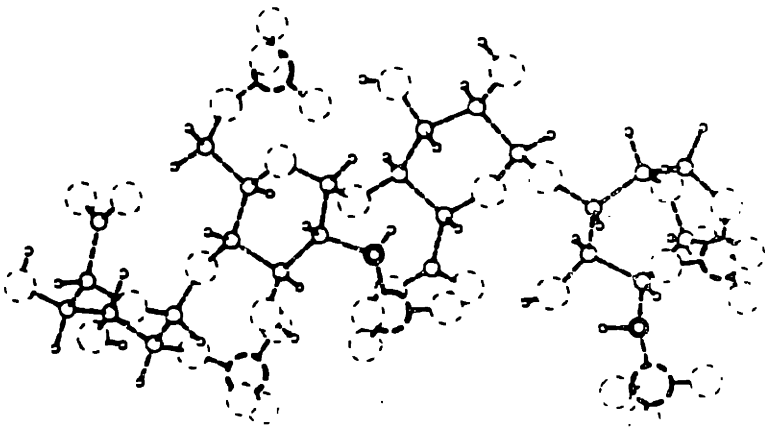

b.

Figure 4.65 Structure of Heparin fragments.
Energy minimized structures of (a) Tetrasaccharide 3 (ΔUHIH), and (b) Tetrasaccharide 2 (ΔUHGH).

The basic structural unit of a heparin chain consists of a repeating uronic acid and a hexosamine (Figure 4.66). The uronic acid is either glucuronic acid (D form, predominant in heparan sulfate) or Iduronic acid (L form, predominant in Heparin). The linkage between the sugars has been shown to be an α,1-4 linkage. Theoretical conformation analysis indicate that the sugar pucker of the hexosamine is in the $^4C_1$ chair conformation shown in Figure 4.67 (Nagarajan and Rao, 1979). NMR and fiber diffraction data confirm the backbone pucker of the glucosamine to be $^4C_1$ chair conformation . The backbone structure of the glucuronic acid residue also seems to be in the $^4C_1$ chair conformation. However, the conformational energies of a $^4C_1$ chair and a $^1C_4$ chair of Iduronic acid are almost equal. Experimental data suggests a skewed boat conformation for the iduronic acid. Based on NMR and Fiber diffraction distance constraints, a $^2S_0$ or an $^1S_3$ conformation for the iduronic acid backbone has been proposed (Casu et al., 1981, Atkins et al., 1975).

It is likely that in solution, the structure of the iduronic acid is in equilibrium between the $^4C_1$ and the $^1C_4$ chair conformations. The rapid switching between these two conformations in an experimental time scale might result in NMR peaks that reflect the statistical average of the structures. The structure that fits the NMR information, might not have any relation to the solution structure of the sugar backbone but a mere average of the two conformations. the proposed skewed boat conformations are energetically unfavorable and hence unlikely to exist in solution.

The linkage between the sugar residues determines the secondary structure of the polysaccharide chain. The ϕ and ψ angles of the linkage (Figure 4.68) determine the orientation of the adjacent sugar residues. Although the possible values for these angles vary from -180 to 180, molecular overlap prohibits some of these allowed

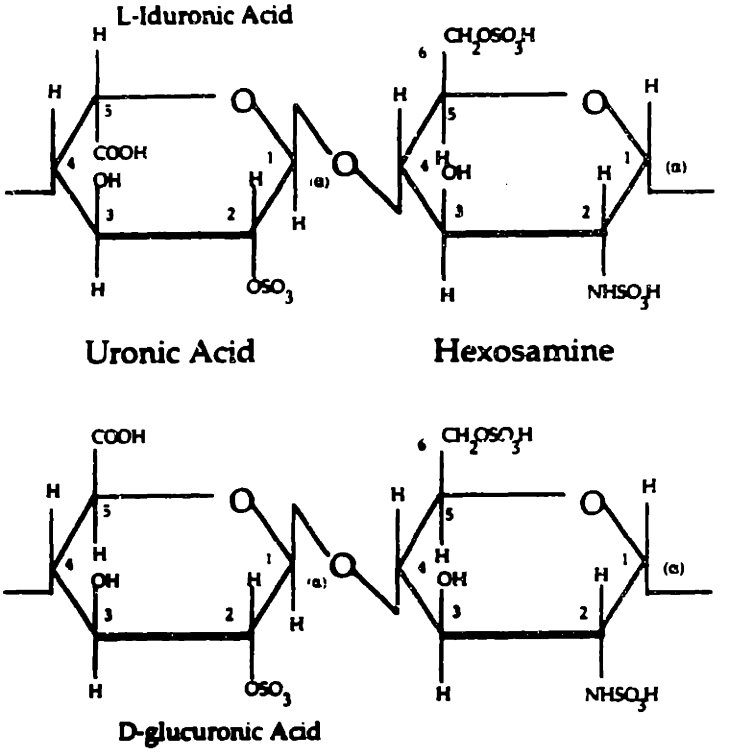

Figure 4.66 Basic Disaccharide units of Heparin.

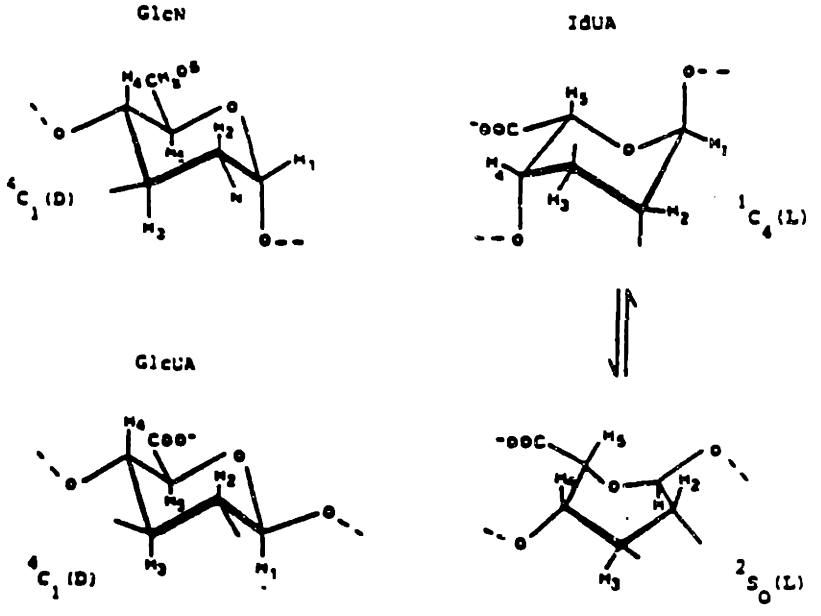

[Adapted from Casu,1989]

Figure 4.67 Conformation of major sugar units of heparin
(a) Glucosamine, (b) Glucuronic acid, (c) Iduronic acid

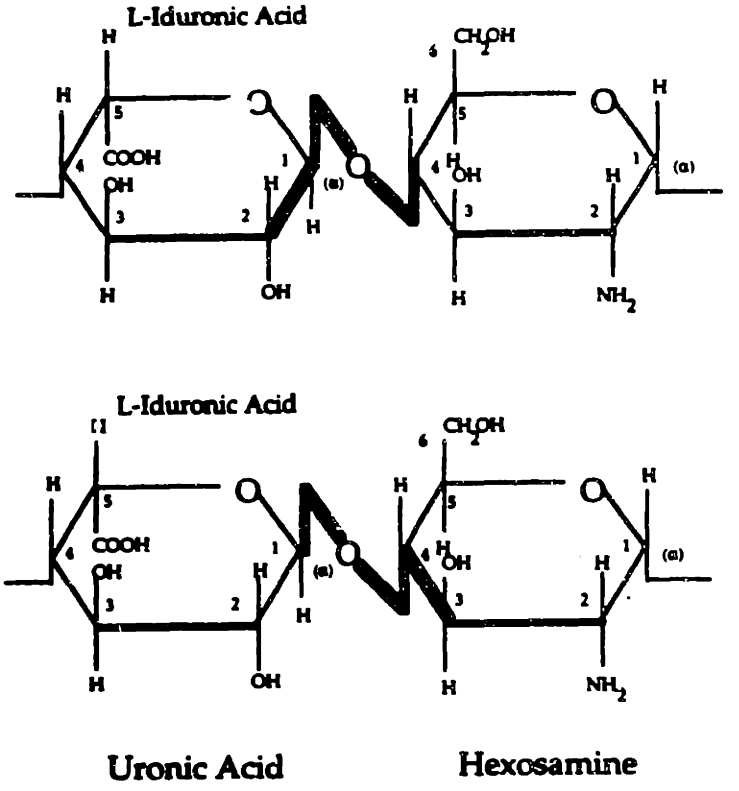

Figure 4.68 ϕ and ψ angles in heparin disaccharide

angles. As a result, the allowed values of ϕ and ψ are a small subset of the entire conformational space.

The ϕ - ψ map of a basic disaccharide of heparin is shown in Figure 4.69. The functional groups (sulfates and acetates) have not been included in the calculation of the allowed region. The minimum energy contour of this ϕ - ψ map represents the allowed conformations. Points in the disallowed regions indicate very high conformational energies, due to overlap of atoms. The allowed region of the ϕ - ψ map is less than 10% of the total conformational space.

The addition of functional groups to the disaccharides further reduces the allowed area (Figure 4.70). The number of possible torsion values reduces because of the space occupied by the bulky functional groups. The orientation of the carboxyl group of the iduronic acid also affects the allowed conformations significantly. Figure 4.71 shows the ϕ - ψ plot of an glucuronic acid glucosamine disaccharide. The allowed conformations in this case are slightly more than the glucuronic case. The effect of sulfation of the glucuronic acid glucosamine disaccharide are similar to those discussed earlier.

The number of possible disaccharide structures are therefore limited. However, for a longer polysaccharide chains, the degrees of freedom increases exponentially increasing the possible structure to a very large number. Experimental data can then help in choosing a few or one of these possible structures to be the structure in reality. Future work in this area should develop parameters for carbohydrate energies and use these starting allowed conformations to determine a low energy conformer. The low energy conformer should then be validated using NMR or other experimental data.

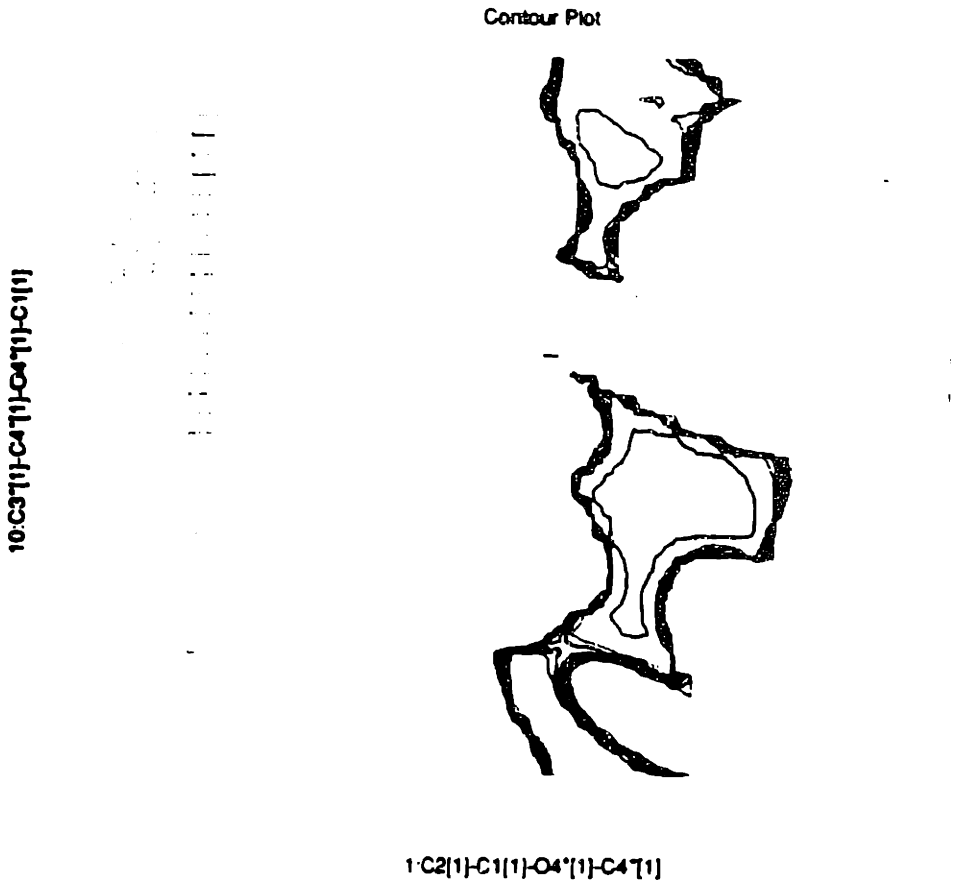

Figure 4.69 ϕ - ψ plot of heparin disaccharide
Allowed energy regions of a iduronic acid-glucosamine disaccharide without sulfates.

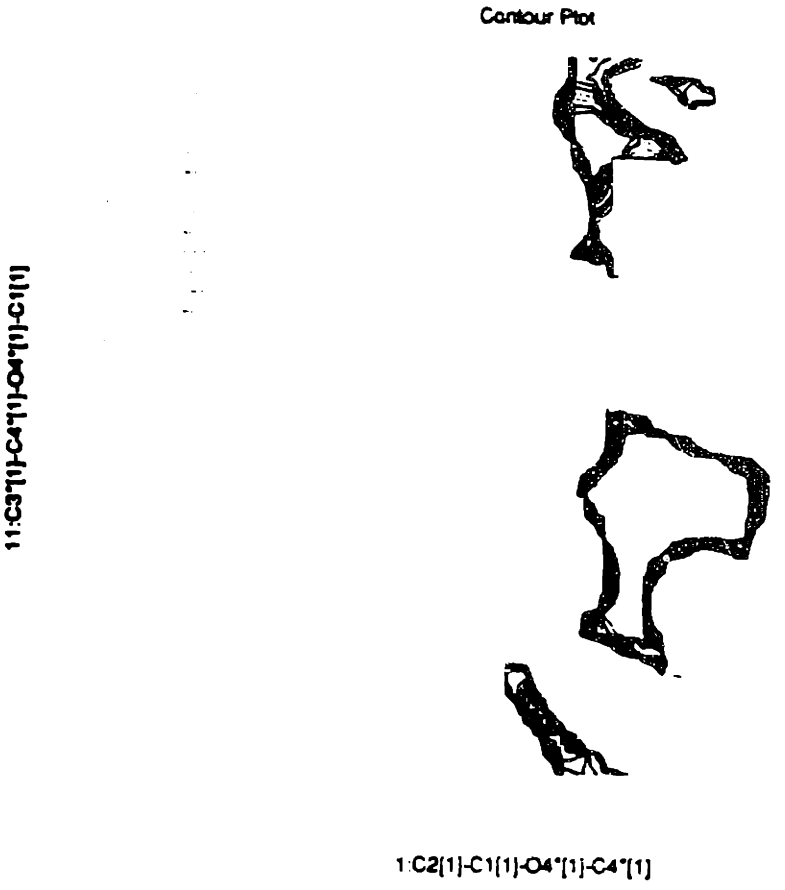

Figure 4.70 ϕ - ψ plot of heparin disaccharide with functional groups
Allowed energy regions of a iduronic acid glucosamine disaccharide
with N sulfation on glucosamine and 2 and 6 sulfations on the uronic acid.

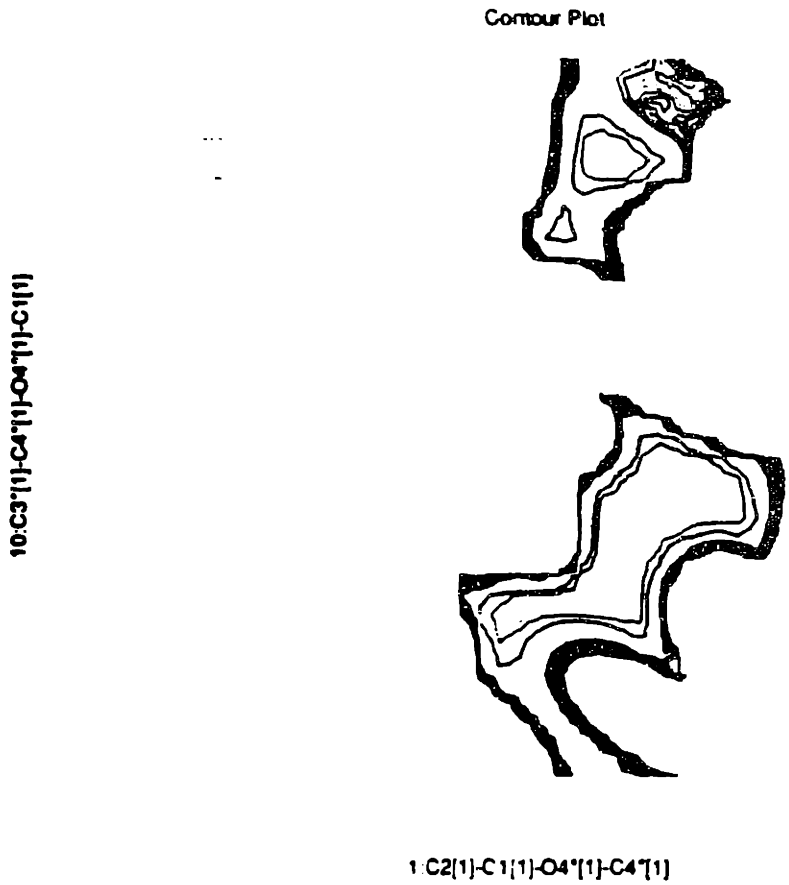

Figure 4.71 ϕ - ψ plot of heparin disaccharide (GH)
Allowed energy regions of a glucuronic acid-glucosamine disaccharide without functional groups

The elucidation of heparin structure can then lead to a better understanding of issues regarding the specificity of the different peptides. This would then pave the way for rational peptides that bind to different proteoglycans in a very specific manner. The biological implications of such a peptide are numerous.

4.2 Conclusions

1. The heparin binding domains of heparinase was identified and mapped. The synthetic peptides corresponding to the heparin binding domains of heparinase and HBEGF conform to the heparin binding consensus sequence proposed by Cardin and Weintraub. Secondary structure predictions indicate α-helical structure for these peptides.

2. In spite of the high degree of homology in charge and hydrophobic residue distribution among these peptides, the effect of the peptides on the degradation of heparin by heparinase is different.

i. The peptide 'truncated maxidialin' does not affect the reaction rate or the amount, or distribution of products formed as compared to the control case of no peptide. This peptide does not interact with heparin.

ii. In the presence of HBP, the initial reaction rate is slower, but the final saturation absorbance and the product distribution are unaffected.

iii. P13 does not affect the reaction rate or the product profile.

iv. Peptide P21 dramatically increases the degradation rate of heparin. The amount of products formed with P21 is also much more than in the case of control reaction. The formation of dimers and higher order structures

in P21 molecule through the involvement of cysteine seems to significantly influence heparin binding.

3. The peptides facilitate the degradation of tetrasaccharide 3 by the enzyme. In the absence of the peptides, this degradation proceeds very slowly. However, in the presence of peptides, the degradation rate is significantly enhanced, the enhancement more pronounced for P21 than P13 and HBP.

4. The peptides derived from HBEGF, P13 and P21, seem to be very specific towards heparin compared to chondroitin sulfate A or C. HBP, however, seems to bind to chondroitin sulfate A with almost an equal affinity as heparin and to chondroitin sulfate C with a lower affinity.

5. Circular Dichroism studies confirm the absence of any secondary structure in these peptides in solution. Addition of heparin or heparin fragments do not induce any secondary structure to these peptides.

6. NMR studies confirm the absence of any hydrogen bonded structure in HBP. ROESY studies indicate the absence of any regular secondary structure in HBP in aqueous solution.

7. Molecular modeling studies of the peptide indicate the low energy conformer of HBP is not an α-helical structure. Instead, a large loop with a small helical end seems to be the most favorable conformation for the peptide.

8. The conformation of heparin depends both on the backbone sugar pucker and the ϕ and ψ torsion angles. An allowed region of the ϕ - ψ map was used to narrow

down the possible heparin disaccharide conformations. Addition of sulfate and other functional groups reduce the allowed conformational space significantly.

Chapter 5

Significance

Nenjil uramuminri nermai thiramuminri
vanjanai seivaradi, kiliye', vaichollil veeraradi ...

Subramaniya Bharathi

Proteins in different micro-environments has been the theme for this thesis. Proteins are highly dynamic molecules constantly in tune with their surroundings. The ability of a protein to change and adapt to its environment is important for its biological function.

In the study of cytochrome-c in AOT-isooctane system, the objective was to mimic the proteins natural micro-environment and examine site specific effects on protein structure. Biophysical techniques used to study subtle changes in cytochrome-c conformation revealed information that was consistent with the biochemical properties of this molecule. Conformational changes of cytochrome-c in a membrane-like environment can help us understand its electron transport properties and give us insights into protein folding. The distribution of the surface lysines in cytochrome-c, especially in the vicinity of the C-terminal helix, can be exploited to design affinity ligands for cytochrome-c. The micro-environment provided by the reversed micelle does not affect the protein structure over short time intervals and can be effectively used as a preliminary purification step for other similar hydrophobic proteins. This has particular implications in recombinant protein isolation and recovery. Protein conformation studies can therefore be used to understand structure-function relationships and to design specific schemes for protein purification.

The heparin-peptide interaction was studied by classical biochemical techniques. The heparin system is important in the tissue level organization of biological systems. Understanding the nature of heparin-protein interaction is crucial to several physiological processes, ranging from embryonic development to tissue regeneration in wound healing. In a pathological condition, heparin regulates the destruction of the extra-cellular matrix and hence influences abnormal

situations like infections or diseases such as tumor metastasis. This thesis demonstrates that peptides having similar heparin binding consensus sequence differ significantly in their heparin binding properties. One could speculate that the mode of peptide-heparin interaction depends on the class of heparin binding protein in addition to the consensus sequence. For example, heparin binding serum proteases (molecules that regulate the coagulation pathway) that Cardin and Weintraub (1989) have characterized bind to heparin through an α helical structure. It is very clear from this study that heparinase and HB-EGF do not interact in the same manner as the serum proteases. It is possible that growth factors and cytokines that bind heparin may *see* heparin differently. The interaction of transcription factors with heparin is not characterized. Further it is that possible that this interaction is different from both the serum proteases and the cytokines.

Advances in Polymer science, Biochemical engineering, and most importantly, our understanding of the extra-cellular matrix have brought Tissue engineering to the forefront of modern Biotechnology. Tissue engineering has several important clinical applications which include wound healing and organ regeneration.

As we march to the end of the Millennium, the interplay of Polymer science, Tissue culture technology, and the engineering of glycosaminoglycans in the extracellular matrix is bound to have significant impact in the progress of modern medicine.

5 References

Atha, D. H., A. H. Stephens, A. Rimon, and R. D. Rosenberg., *Biochemistry*, **23**, 5801, 1984

Atkins E. D. T and I. A. Nieduszynski., In *Heparin Structure, Function and Clinical Implications*. Eds: R. A. Bradshaw and S. Weeser, Plenum N. Y., 1975.

Aveyard, R., Binks, B. P., Clark, S., and J. Mead, *J. Chem. Soc. Faraday Trans. I*, **82**, 125, 1986.

Baird, A., D. Shubert, N. Ling, and R. Guillemin.,*Proc. Natl. Acad. Sci. USA*, **85**, 2324, 1988.

Barbaric, S., and P. L. Luisi, *J. Am. Chem. Soc.*, **103**, 4239, 1981

Belonogova, O. V., Likhtenshtein, G. I., Levashov, A. V., Khmel'nitskii, Y. L., Klyachko, N. L., and K. Martinek, *Biokhimiia*, **48**, 379, 1983.

Blackburn, M. N., R. L. Smith, J. Carson and C. C. Sibley, *J. Biol. Chem.*, **259**, 939-941, 1984.

Bober-Barkalow, F. J. and J. E. Schwarzbauer, *J. Biol. Chem.*,**266**, 7812, 1991

Brochette P., Petit C., and M. P. Pileni, *J. Phys. Chem.*, **92**, 3505, 1988.

Brown, L. R., and K. Wuthrich, *Biochim. Biophys. Acta*, **602**, 477, 1980.

Busch, S. J. G., R. L. Jackson and P.Sassone-Corosi, *Trans. Assoc. Am. Physician*. 1991.

Cardin, A. D. and H. J. R. Weintraub, *Arteriosclerosis*, **9**, 21-32, 1989.

Cardin, A. D., R. L. Jackson, B. Elledge and D. Feldhake., *Int. J. Biol. Macromol.*, **11**, 59, 1989b.

Cardin, A. D., Demeter, D. A., Weintraub, H. J. R. and R. L. Jackson, *Methods Enzymol.*, 1991.

Carlson, T. H., T. Babcock, A. C. Atencio, C. Levioson, and H. R. Mora., *Biol. Chem.*, **263**, 2187, 1988.

Casu, B., P. Oreste, G. Torri, G. Zoppetti, J. Choay, J. C. Lormeau, M. Petitou and P. Sinay., *Biochem. J.* **197**, 599, 1981.

Casu, B. Structure and biological activity of heparin. *Adv. Carbohydr. Chem. Biochem* **43**, 51, 1985.

Craik, C. S., Buchman, S. R., and S. Beychok, *Proc. Natl. Acad. Sci. USA*, **77**, 1384, 1980

Choay, J., J. C. Lormeau, M. Petitou, P. Sinay and J. Fareed., *Ann. N.Y. Acad. Sci.*, **370**, 644, 1981.

Cifonelli, J. A., *Carbohydrate Res.* **8**, 233-242, 1968.

Damus, P. S., Hicks, M. and R. D. Rosenberg, *Nature Lond.*, **246**, 355-357, 1973.

Day, R. A., Robinson, B. H., Clarke, J. H. R., and J. V. Doherty, *J. Chem. Soc. Faraday Trans. 1*, **75**, 132, 1978.

Delahodde, A., M. Vacher, C. Nicot, and M. Waks, *FEBS Lett.*, **172**, 343, 1984

De Marco, A., Zetta, L., Menegatti, E., and P. L. Luisi, *J. Biochem. Biophys. Meth.*, **12**, 335, 1986.

Demel, R. A., Jordi, W., Lambrechts, H., van Damme, H., Hovius, R., and B. de Kruijff, *J. Biol. Chem.*, **264**, 3988, 1989.

Dickerson, R. E., and R. Timkovich, in The Enzymes, (Boyer P. D. ed.), Vol. XIA, Academic Press, New York, 1975.

Englander, S. W., N. W. Downer and H. Teitelbaum, *Annu. Rev. Biochem.*, **41**, 903, 1972.

Eriksson , A. E., L. S. Cousens, L. H. Weaver and B. W. Matthews.,*Proc. Natl. Acad. Sci., U. S. A.*, **88**, 3441, 1991

Erjomin, A. N., and D. I. Metelitza, *Biochem. Biophys. Acta.*, **732**, 377, 1983.

Erjomin, A. N., and D. I. Metelitza, Biokhymia, **49**, 1947, 1984.

Feng, Y., H. Roder, and S. W. Englander, *Biochemistry*, **28**, 195, 1989.

Ferran, D. S., M. Sobel and R. H. Harris, *Biochemistry*, **31**, 5010, 1992.

Fletcher, P. D. I., Robinson, B. H., and J. Tabony, *J. Chem. Soc. Faraday Trans. 1*, **82**, 2311, 1986.

Folkman, J and M. Klagsbrun., *Science*, 235, 442, 1987.

Gierasch L. M., Lacy E. J., Thompson K. F., Rockwell A. L., and P. I. Watnick, *Biophys. J.* 37, 275-284, 1982.

Gospodarowicz, D., N. Ferrara, L. Schweigerer and Neufield, G., *Endocr. Rev.*, 8, 95, 1987.

Grandi, C., Smith R. E. and P. L. Luisi, *J. Biol. Chem.*, 256, 837-843, 1981

Heath., W. F., A. S. Cantrell, N. G. Mayne and S. R. Jaskunas., *Biochem.*, 30, 5608, 1991.

Hirose, N. D. T. Blankenship, M. A. Krivanek, R. L. Jackson and A. D. Cardin., *Biochemistry*, 26, 5505, 1987.

Hollander, W., *Expt. Mol. Pathol.*, 25, 106, 1976.

Hoving, P. and A. Linker, *J. Biol. Chem.*, 245, 6170, 1970.

Imre, V. E., and P. L. Luisi, *Biochem. Biophys. Res. Commun.*, 107, 538, 1987.

Jackson R. L., S. J. Busch and A. D. Cardin, *Physiol. Rev.*, 71, 481-539, 1991.

Jordan, R., D. Beeler and R. Rosenberg, *J. Biol. Chem*, 254, 2902, 1979

Kinberberg, H. K. and C. P. Lee, *J. Membr. Biol.*, 2, 252, 1970

Kumar C., and D. Balasubramanium, in "Solution behavior of Surfactants", (K. L. Mittal and E. J. Fendler eds.), Vol.2, p1207, Plenum, New York, 1982.

Langer, R., Linhardt, R. J., Klien, M., Galliher, P. M., Cooney, C. L. and M. M. Flannagan, *Biomaterials: Inter-facial Phenomenon and Applications, Adv. in Chem. Symposium Series*, Chap. 31, Cooper, S., Hoffman, A., Pepas, N. and B. Ratner, eds., Washington DC, pp 493-509, 1982.

Laursen, R. A., Samiullah, M., and M. B. Lees, *Proc. Natl. Acad. Sci. USA*, 81, 2912, 1984.

Leodidis, E. B., and T. A. Hatton, *Langmuir*, 5, 741, 1989.

Lindahl, U. and O. Axelsson., *J. Biol. Chem.* 246, 74, 1971.

Linker, A. and P. Hoving., *In heparin: Structure, Cellular Function and Clinical Applications* N. M. McDuffie, Ed.: 3 Academic, New York.,19?9.

Lobb. B. R., *Biochemistry*, 27, 2572, 1988.

Luisi, P. L., *Angew. Chem. Int. Ed. Engl.*, 24, 439, 1985.

Luisi, P. L., and L. J. Majid, *Crit. Rev. Biochem.*, 20, 409, 1986.

Luisi, P. L., Giomini, M., Pileni, M. P., and B. H. Robinson, *Biochem. Biophys. Acta*,947, 209, 1988.

Luisi P. L., Meier P., Imre V. E., and A. Pande, in "*Reversed Micelles*", (P. L. Luisi and B. E. Straubs eds.), p332, Plenum, New York, 1984.

Lundblad, R. L., W. V. Brown, K. G. Mann and H. R. Roberts, eds., *Chemistry and Biology of Heparin*, Elsevier/North Holland, NY, 1981.

Marcum, J. A and R. D. Rosenberg,. *Biochemistry*, 23, 1730, 1984.

Martin, G. R. and R. Timpl., *Annu. Rev. Cell Biol.* 3, 57, 1987

Marsh, D., and G. L. Powell, *Bioelectrochem. Bioenerg.* 20, 73, 1988.

Martinek, K., Levashov, A. V., Klyachko, N. L., Pantin, V. I., and I. V. Berezin, *Biochem. Biophys. Acta*, 657, 277, 1981.

Masson, A., and K. Wuthrich, *FEBS Lett.*, 31, 114, 1973.

Meier, P. and P. L. Luisi, *J. Solid-Phase Biochem.*, 5, 269, 1980.

Menger, F. M., and K. Yamada, *J. Am. Chem. Soc.*, 101, 6731, 1979.

Nagarajan, M. and V. S. R. Rao., *Biopolymers* , 18, 1407, 1979.

Nicot, C., Vacher, M., Gallay, J., and M. Waks, *Biochemistry*, 24, 7024, 1985.

Patel, D. J., and L. L. Canuel, *Proc. Natl. Acad. Sci. U. S. A.*, 73, 1398, 1976.

Paterson, Y., S. W. Englander and H. Roder, *Science*, 249, 755, 1990.

Perrin, C. L., T. J. Dwyer, J. Rebek Jr. and R. J. Duff, *J. Am. Chem. Soc.*, 112, 3122, 1990.

Rahaman, R. S., Ph. D. Thesis, MIT.

Rice, K.G and R. J. Lindhardt., *Carbohydrate Research*, 190, 219-233, 1989

Rosenberg, R. D. and P. S. Damus, *J. Biol. Chem.*, **248**, 6490-6505, 1973

Rosenfeld, L. and I. Danishefsky, *Biochem. J.*, **237**, 639-646, 1986.

Sasisekharan, R., Ph.D Thesis, Harvard Medical School, 1991.

Sasisekharan, R., Personal Communication, 1992.

Sasisekharan, V., Personal Communication, 1992.

Schomaecker R., Robinson B. H., and P. D. I. Fletcher, *J. Chem. Soc. Faraday Trans.*, **84**, 4203, 1988.

Seno, M., Noritomi, H., Kuroyanagi, Y., Iwamoto, K., and G. Ebert, *Colloid Polymer Sci.*, **262**, 727, 1984.

Shing, Y., J. Folkman, R. Sullivan, C. Butterfield, J. Murry and M. Klagsbrun., *Science*, **223**, 1296, 1984.

Shiveley, J. E. and H. E. Conrad, *Biochemistry* **9**, 33, 1969.

Spooner, P. J. R., and A. Watts, *Biochemistry*, **30**, 3871, 1991

Thompson, K. F. and L. M. Gierasch, *J. Am. Chem. Soc.*, **106**, 3648, 1984

Vik, S. B., Georgevich, G., and R. A. Capaldi, *Proc. Natl. Acad. Sci. U. S. A.*, **78**, 1456, 1981.

Vincent, J. S., and I. W. Levin, *J. Am. Chem. Soc.*, **108**, 13, 1986.

Vos, K., Laane, C., Weijers, S. R., Van Hoek, A., Veegar, C., and A. J. W. G. Wisser, *Eur. J. Biochem.*, **169**, 259, 1987.

Waks, M, *PROTEINS: Structure, Function and Genetics*, **1**, 4, 1986.

Walde P., Peng Q., Fadnavis N. W., Battistel E., and P. L. Luisi, *Eur. J. Biochem*, **173**, 401-409, 1988.

Weintraub, H. J. R., D. A. Demeter, A. D. Cardin and R. L. Jackson., In; *Molecular Description of Biological Membranes by Computer Aided Analysis*, Ed. R. Brasseur, CRC, Vol II, 161, 1990.

Wolf R., and P. L. Luisi, *Biochem Biophys Res. Commun.*, **89**, 209, 1979.

Woll, J. M., Hatton T. A., and M. L. Yarmush, *Biotech. Prog.*, **5**, 57, 1989.

Wong, M., Thomas, J. K., and M. Gratzel, *J. Am. Chem. Soc.*, **98**, 2391, 1976.

Wong, M., Thomas, J. K., and T. Nowak, *J. Am. Chem. Soc.*, **99**, 4730, 1977.

Zhu, Yizu., Ph.D. Thesis , Department of Chemical Engineering, MIT., 1991